

京 都 大 学
エ ネ ル ギ ー 科 学 研 究

第 1 集

自 平成 8 年 1 月
至 平成 9 年 3 月

Research Activities
in Graduate School of Energy Science
Kyoto University

1996/1 ~ 1997/3

Vol. 1

Graduate School of Energy Science
Kyoto University

1997.12

平成 9 年 12 月
京都大学エネルギー科学研究科

This issue is edited with the aim to introduce our research activities from January 1996 to March 1997, under the four categories.

- A. Current Research Fields
- B. Original Articles
- C. Review Articles
- D. Books

本誌はエネルギー科学研究科における研究活動の紹介をおもな目的とし、次のA、B、CおよびDに分けて編集されたものである。

- A. 研究現況(テーマ)
- B. 研究発表
- C. 総説
- D. 著書(学術図書)

Contents

目次

Contents

1	Current Research Fields	1
I	Department of Socio-Environmental Energy Science	1
II	Department of Fundamental Energy Science	3
III	Department of Energy Conversion Science	8
IV	Department of Energy Science and Technology	11
2	Original Articles	15
I	Department of Socio-Environmental Energy Science	15
1:	* Study of magnetoresistance in nano-structured Co-Ag alloy produced by mechanical alloying	15
2:	* Nano-scale Metal Multilayers Produced by Repeated Press-Rolling	15
3:	* Solid Solution Formation in the Al_2O_3 - Cr_2O_3 System Assisted by Ball Milling	16
4:	* Structural changes during low energy ball milling in the Al-Ni system	16
5:	* Solid state reaction between powders and foils by low-energy ball milling	16
6:	* Nanocrystalline metals prepared by low energy ball milling	17
7:	* Structure Change of Graphite by Ball Milling	17
8:	* Amorphous Fe-Al Alloys Obtained by Mechanical Alloying	18
9:	* Stored Energy and Electromotive-force of Mechanically Milled Copper	18
10:	* Wood-Inorganic Composites Prepared by Sol-Gel Process V. Fire-resisting properties of the SiO_2 - P_2O_5 - B_2O_3 wood-inorganic composites.	18
11:	* Wood-Inorganic Composites Prepared by Sol-Gel Process VI. Effects of a property-enhancer on fire-resistance in SiO_2 - P_2O_5 and SiO_2 - B_2O_3 wood-inorganic composites.	19
12:	* Thermal Properties of Cellulose Triacetate as Prepared from Low-grade Dissolving Pulp.	19
13:	O-Benzoylation of Phloroglucinol via Phloroglucinol Triacetate	20
14:	Stoichiometric Studies of Tannin-Protein Co-Precipitation	20
15:	Convenient Synthesis of Galloylglucoses	20
16:	Experimental Study on the Operators' Cognitive Behavior Analysis for the Plant Anomaly Diagnosis	21
17:	Cognitive Process in Plant Diagnosis Using an Operator Cognitive Model	21
18:	Development of Simulation Based Evaluation Support System for Man-Machine Interface Design: SEAMAID System	22

19:	Validating Physiological Measures for the Cognitive Behavior Analysis Using Neural Network	22
20:	Simulation Based MMI Evaluation Support System; SEAMAID System	23
21:	Virtual Environment for Integrated Design Support (VINDS) for Conceptual Design of Advanced Reactor System	23
22:	Study on Methodology of Evaluating Man-Machine System	24
23:	Analysis of Operator's Diagnostic Behavior and its Application to the Human Modeling	24
24:	A New VR-based CSCW Environment for Conceptual Design of A Space Power Reactor	25
25:	Development of Machine-Maintenance Training System using Petri Net and Virtual Environment	25
26:	Simulation based evaluation of Man-Machine Interface in power plants	26
27:	Virtual Environment for Integrated Design Support (VINDS) for Conceptual Design of a Space Power Reactor Core	26
28:	* Evaluation of the Relationship between Energy Supply-Demand System and Information Technology,	26
29:	* A Study on the Optimal Power Plant Planning with Photovoltaic Generation and Heat Storage	27
30:	* Methods of Determining the Introduction Limits of Dispersed Generation Systems in a Distribution System	27
31:	* Development of an Analysis Support System for Man-Machine System Design Information	28
32:	* The Size Distribution and Composition of the Atmospheric Aerosol at a Rural and nearby Urban Location	28
33:	* Characterization of Atmospheric Aerosols Separated by Particle Size and Water Solubility Using PIXE Analysis	29
34:	* Soluble and Insoluble Components of Air Pollutants Scavenged by Rain Water	29
35:	Ion Nucleation and Growth of Sulfuric Acid Water Aerosol Particles: Application of general dynamic equation	30
36:	Data Reduction on the Measurement of the Size Distribution of Atmospheric Aerosols by a Low-Pressure Cascade Impactor	30
37:	Production of Contact-Free Nanoparticles by Aerosol Process: Dependence of particle size on gas pressure	31
38:	Growth of Nanophase Particles in Free-Molecular Regime and Its Dependence on Medium Gas Pressure	31
39:	Production of Binary Nanoparticles (BiCu, BiTe and CdS) by Aerosol Process: Treatment for isolation and concentration	31
40:	EXAFS Study on the Noncrystalline Structure of Binary Component (BiCu, BiTe) Nanophase Particles	32
41:	Two-Layer Box Model for Dense Gas Spill Considering Evaporation Effect	32
42:	* Application of NR for Research in Electrochemical Systems	33

43:	* Human Melanoma Treated by Boron Neutron Capture Therapy : Comparison of the Clinical Response with the Predicted Response	33
44:	* Studies on the Lithium Ion Conduction in $\text{Ca}_{0.95}\text{Li}_{0.10}\text{WO}_4$ using Cold Neutron Radiography	34
45:	* Characteristics of the Kyoto University Lead Slowing-down Spectrometer (KULS) coupled to an Electron Linac	34
46:	* A system for correlation measurement of fission fragments and prompt neutrons for thermal neutron induced fission	35
47:	Bayesian Analysis of the Public Reliance on the Nuclear Development	35
48:	Procedures for the Medical Application of Research Reactors.	36
49:	Reply to Matoba's Comment on "Mean Reaction Length of Destruction and Production of Neutron"	36
50:	Neutron Activation Analysis of Ivory of African Elephants	36
51:	Reactor Laboratory Course for Students Majoring in Nuclear Engineering with the Kyoto University Critical Assembly (KUCA)	37
52:	Influence of Photovoltaic Power Generation on Required Capacity for Load Frequency Control	37
53:	Japan's Strategy in Technology Development for Mitigating Global Warming	37
54:	Japanese Strategy for Mitigating Global Warming	38
55:	Natural Gas for Electricity and Cogeneration	38
56:	Development of a Three-Dimensional Core Dynamics Analysis Program for Commercial Boiling Water Reactors	39
II	Department of Fundamental Energy Science	40
57:	* Hydrogen Electrode Reaction in Molten Fluoride System	40
58:	* Hydrogen Electrode Reaction in Molten LiCl-KCl-LiH System	40
59:	* Electrochemical Behavior of Nitrogen Gas and Nitride Ion in Molten Chloride System	40
60:	Graphite Intercalation Compounds of Lanthanide Metals Prepared in Molten Chlorides	41
61:	The Electric Properties of Sintered Cermet as a Continuum Percolation Medium	41
62:	* A Quenching Effect on the Grain Boundary in Sintered Ag-BPSCCO	42
63:	Thermal Conductivity of Pr Doped $\text{YBa}_2\text{Cu}_3\text{O}_y$ and a Quasiparticle Contribution	42
64:	* Percolative Behavior of Cuprate Grains in the Ag-BPSCCO Composite System	43
65:	Quantitative SIMS Analysis of Mo in Ti-Dilute Mo Alloys Using Isotopic Abundance	43
66:	Structural change of the LiMn_2O_4 spinel structure induced by extraction of lithium	44
67:	Crystal Structure and Metal-Insulator Transition of $\text{La}_{1-x}\text{Sr}_x\text{CoO}_3$	44
68:	Layered structures of hydrated vanadium oxides. Part 5. - Single-crystal structure of $\text{Rb}_{0.5}\text{V}_2\text{O}_5$ and phase changes of rubidium intercalate	45
69:	* Synthesis and Crystal Structure of $\sigma\text{-Zn}_{0.25}\text{V}_2\text{O}_5 \cdot \text{H}_2\text{O}$ with a Novel Type of V_2O_5 Layer	45
70:	Novel Method for Zirconium Oxide Synthesis from Aqueous Solution	46

71:	Hydrothermal Synthesis of Hydrrous Vanadium Oxide Bronzes $M_xV_3O_8(VO)_y \cdot nH_2O$ ($M = K, Rb, Ba$)	46
72:	Preparation and Characterization of $LaMnO_3$ Thin Film Electrode on YSZ	46
73:	Preparation and Characteristics of Ni/YSZ Cermet Anodes by Vapor-phase Deposition	47
74:	Preparation of Functionally Gradient Fluorocarbon Polymer Films by Plasma Polymerization of NF_3 and Propylene	47
75:	* Suppression of nonlinear interchange mode by zonal counterstreaming flow generation	48
76:	* ELM modelling based on the nonlinear interchange mode in edge plasma	48
77:	* An optimized plasma shape for magnetic confinement	48
78:	* High Ion Temperature Mode in Heliotron-E	49
79:	* Dipole Moment of the Pfirsch Schluter Current in a Finite Beta Stellarator Plasma on Heliotron E	49
80:	Magnetic Equilibrium Diagnostics in a Finite-Beta Toroidal Helical Plasma on Heliotron E	50
81:	D-D Fusion Neutron Measurements in the Beam-Heated Stellarator Deuterium Plasmas on Heliotron E	50
82:	Operation of Thin Metal Foil Bolometer for Radiation Loss Measurement in a Toroidal Plasma on Heliotron E	51
83:	Effect of radial electric field and bulk plasma velocity shear on ion thermal transport in Heliotron-E	51
84:	Enhancement and suppression of density fluctuations around electron drift frequency in Heliotron E plasmas measured using CO2 laser phase contrast method	52
85:	Impurity behavior in Heliotron E plasmas	53
86:	Radial profiles of 2p-1s heliumlike oxygen lines measured from the compact helical system using a vacuum crystal spectrometer	53
87:	Comparison of the Calculations of the Stability Properties of a Specific Stellarator Equilibrium with Different MHD Stability Codes	54
88:	MHD Instabilities in Current Carrying Toroidal Heliotron/Torsatron Plasmas	54
89:	Improvement of Collisionless Particle Confinement in L=1 Helical Systems	55
90:	* Control of Mode Locking of Tearing Mode by Lower Hybrid Current Drive and Electron Cyclotron Heating in WT-3	55
91:	* Observation of Sawtooth Crashes Associated with $m=2/n=1$ and $m=3/n=2$ Precursors	56
92:	* Localized Plasma Heating Experiments using a Quasi-optical ECH System on the WT-3 Tokamak	56
93:	* Polarization of Impurity Emission Lines from a Tokamak Plasma	57
94:	* Experiments on Nonneutral Electron and Positron Plasmas in a Potential Well Formed with Multi-Ring-Electrodes	57
95:	* Effects of ECH on NBI Plasma in Heliotron-E	58
96:	Dynamics of Ion Temperature in Heliotron-E	58

97:	* Effect of Radial Electric Field and Bulk Plasma Velocity Shear on Ion Thermal Transport in Heliotron-E	58
98:	* Parameter Study of 106GHz Second Harmonic ECH Plasma in Heliotron-E	59
99:	Study of the Core Particle Confinement during the Transition Phenomenon in the Edge Heating Experiment in Heliotron-E	60
100:	Ion Transport Analysis of NBI heated Plasma in Heliotron-E	60
101:	Electron Thermal Transport Analysis for ECH and NBI Plasmas in Heliotron-E . .	60
102:	Non-local Response of the Electron Temperature and Longitudinal Propagation of the Plasmoid during Pellet Injection on Heliotron-E	61
103:	Effects of ECH on Ion Heating during NBI in Heliotron-E	61
104:	Li pellet Injection Experiment on Heliotron-E	62
105:	TV Thomson Scattering Measurement in Heliotron-E	62
106:	Field line measurements in the divertor of Heliotron-E under boronized conditions	63
107:	Energy confinement scaling from the international stellarator database	63
108:	Study of high energy particles produced by ICRF heating in Heliotron-E	64
109:	Impurity behaviour in Heliotron E plasmas	64
110:	Boiling Point of Tetrahalomethanes	65
111:	Diffusion through a Multilayer and Its Application to Hydrogen Permeation through Nickel Coated Iron	65
112:	* Mechanism of Protein Solubilization in Sodium Bis(2-ethylhexyl) Sulfosuccinate Water-in-Oil Microemulsion	65
113:	* Model for Geometry of Surfactant Assemblies in the Oil-Rich Phase of Winsor II Microemulsions	66
114:	Analysis of the Bulk and Surface-Induced Structure of Electrolyte Solutions Using Integral Equation Theories	67
115:	* Control of Microstructure Formed by Spinodal Decomposition	67
116:	* Growth Mechanism of Cadmium Sulfide Ultrafine Particles in Water-in-Oil Microemulsion	68
117:	* Dynamic Behavior and Structure of Concentrated Water-in-Oil Microemulsions in the Sodium Bis(2-ethylhexyl)sulfosuccinate Systems	68
118:	* X-ray and Light Scattering from Oil-Rich Microemulsions Containing Sodium Bis(2-ethylhexyl) Phosphate	69
119:	* Bioaffinity Separation of Concanavalin A in Reverse Micellar System Composed of AOT/Butanol or Non-ionic Surfactant	69
120:	Application of the Reference Interaction Site Model Theory to Analysis on Surface-Induced Structure of Water	70
121:	Interaction between Macroparticles in Aqueous Electrolytes	70
122:	Interaction between Macroparticles in Lennard-Jones Fluids or in Hard-Sphere Mixtures	71
123:	Interaction between Macroparticles in a Simple Model System of a Non-Polar Liquid Containing Trace Amounts of Water	71
124:	* Microemulsions as Liquid Media for Materials Separation	72

125:	* Selective Separation of Concanavalin A Using Bioaffinity in Reverse Micellar System	72
126:	* Protein Extraction in Polyoxyethylene Alkyl Ether/AOT Microemulsion Systems	73
127:	* Catalytic activity of a novel water-soluble cross-linked polymer imprinting by a transition-state analogue for the stereoselective hydrolysis of enantiomeric amino acid esters	73
128:	* The Role of the membrane-assisted hydrophobic interaction between di-, tri-, or tetrapeptide catalysts and amino acid esters in the enhancement of stereoselective hydrolysis reactions.	74
129:	* Novel Photocatalytic Asymmetric-Synthesis of Δ (or Λ)-[Co(acac) ₃] (Hacac = Pentane-2,4-dione) from [Co(acac) ₂ (H ₂ O) ₂] and Hacac with Helical Ruthenium(II) Complexes.	74
130:	* Extremely high stereoselectivity of novel ruthenium(II) complexes for photoinduced reduction of racemic-[Co(acac) ₃] (Hacac = Pentane-2,4-dione).	74
131:	* Tryptophan Dioxygenase-like Catalysis of Achiral and Chiral Manganese(II) Porphyrins for Dioxygen-inserted Indole-Ring Opening Reactions.	75
132:	Electrochemical behavior of glassy carbon and some metals in a ZnCl ₂ -NaCl melt	75
133:	* Study on Reactivity Worth of Beryllium by (n,2n) and (γ , n) Reactions	75
134:	* Design Study of Spectrum Shifter Region in Research Reactor by Using the Kyoto University Critical Assembly (KUCA)	76
135:	Analysis of Experiment on Temperature Coefficient of Reactivity in Light-Water-Moderated and Heavy-Water-Reflected Cylindrical Core Loaded with Highly-Enriched-Uranium or Medium-Enriched-Uranium Fuel	76
136:	* Measurement and Analysis of Reaction Rate Distributions in Cores with Spectrum Shifter Region	77
137:	* Calculation of Void Coefficient in HCLWR Cells	77
138:	Measurements of First-Harmonic Eigenvalue Separation in Loosely Coupled-Core Reactor	78
139:	* Study on Reactivity Measurement by the Feynman- α Method	78
140:	* Feasibility of High Frame-Rate Neutron Radiography by Using a Steady Thermal Neutron Beam with 10 ⁶ n/cm ² s Flux	79
141:	* Visualization and Measurements of Two-Phase Flow in Metallic Ducts Using Neutrons as Microscopic Probes – (2nd Report, Measurements of Some Flow Characteristics by Image Processing Techniques)	79
142:	* Visualization and Measurement of Two-Phase Flows in Metallic Ducts Using Neutrons as Microscopic Probes – (3rd Report, Quantitative Measurement of Neutron Radiography Image)	80
143:	* Visualization and Measurements of Two-Phase Flows in Metallic Ducts Using Neutrons as Microscopic Probes – (4th Report, Effect of Image Gray Scale and Pixel Number on Image Quantification)	80
144:	* Quantitative Limits of Thermal and Fluid Phenomena Measurements Using the Neutron Attenuation Characteristics of Materials	81

145:	* Some Characteristics of Air-Water Two-Phase Flow in Small Diameter Vertical Tubes	81
146:	* Quantitative Limits of Thermal and Fluid Phenomena Measurements Using the Neutron Attenuation Characteristics of Materials Quantitative Method to Measure Void Fraction of two-Phase Flow Using Electronic Imaging with Neutrons	82
147:	* Approximate Method for Measurement of Phase-Distribution in Multiphase Materials with Small Neutron-Attenuation Using a Neutron Beam as a Probe	82
148:	* Visualization and Measurements of Two-Phase Flows in Metallic Ducts Using Neutrons as Microscopic Probes - (5th Report, Void Distribution Measurement Method for Two-Phase Flow in a Round Tube)	83
149:	* Experimental Study on Critical Heat Flux in Laterally Non-Uniformly Heated Rectangular Channels	83
150:	* High-Frame-Rate Neutron Radioscopy with a Steady Thermal Neutron Beam	84
151:	* Evaluation of Scattered Neutron Component in Thermal Neutron Radiography Image- (-Influence of Scattered Neutrons and Unparallelness of Incident Neutron Beam-)	84
152:	* Verification of Neutron Radioscopic Measurement of Void Fraction by Monte Carlo Simulation	85
153:	Analytical Study of Two-Phase Flow Pressure-Drop Oscillations in a Vertical Heated Tube	85
154:	* Visualization and Measurement of Two-Phase Flow by Using Neutron Radiography	85
155:	* Dryout in a Boiling Channel under Oscillatory Flow Condition	86
156:	Observation of Superstructure on the (0001) Face of C ₇₀ Single Crystals	86
157:	Electrochemical Reduction of CO ₂ with High Current Density in a CO ₂ + Methanol Medium at Various Metal Electrode	87
158:	Electrochromic Behavior of Electrodeposited Tungsten Oxide Thin Films	87
159:	Two-Dimensional Surface-Enhanced Raman Imaging of a Roughened Silver Electrode	88
160:	Strong Magnetocrystalline Anisotropy in MnTPP-TCNE Charge Transfer Complex	88
161:	Photoinduced Magnetization of a Cobalt-Iron Cyanide	89
162:	An Efficient TiO ₂ Thin-Film Photocatalyst: Photocatalytic Properties in Gas-Phase Acetaldehyde Degradation	89
163:	Syntheses and Magnetic Properties of Dye Included Organometallic Magnets: DAMS[MCr(ox) ₃]	90
164:	Molecular Arrangement in an Azobenzene-Terminated Self-Assembled Monolayer Film	90
165:	A Film-Type Photocatalyst Incorporating Highly Active TiO ₂ Powder and Fluororesin Binder: Photocatalytic Activity and Long-Term Stability	90
166:	Surface-Enhanced Raman Scattering Imaging of Photopatterned Self-Assembled Monolayers	91

167:	Molecular-Level Design of a Photoinduced Magnetic Spin Coupling System: Nickel Nitroprusside	91
168:	Atomic Force Microscopy and Kelvin Probe Force Microscopy Evidence of Local Structural Inhomogeneity and Nonuniform Dopant Distribution in Conducting Polybithiophene	92
169:	Micropattern Formation on ZnO Films Using a Photodissolution Reaction	92
170:	An Electrochemical Study of Some Spirobenzopyran Derivatives in Dimethylformamide	92
171:	Surface Enhanced Raman Imaging of a Patterned Self-Assembled Monolayer Formed by Microcontact Printing on a Silver Film	93
172:	Electrochemical Syntheses and Electrochromic Properties of Chromium Cyanide Magnetic Thin Films	93
173:	Tuning of Superexchange Couplings in a Molecule-Based Ferro-ferrimagnet: $(\text{Ni}_{1-x}\text{Mn}_x\text{III})1.5[\text{CrIII}(\text{CN})_6]$	94
174:	Photoinduced Magnetic Pole Inversion in a Ferro-ferrimagnet : $(\text{Fe}_{0.40}\text{Mn}_{0.60})1.5\text{CrIII}(\text{CN})_6$	94
175:	Photoelectrorheology of TiO_2 Nanoparticle Suspensions	94
176:	Photoeffects on Electrorheological Properties of TiO_2 Particle Suspensions	95
177:	* Electrochemistry of Diamond	95
178:	Self-Cleaning and Anti-bacterial Functions of Various TiO_2 Coated and Containing Materials	95
179:	* The Kinetic Study of Photocatalysis Using TiO_2 Thin Film Under Weak UV Light	96
180:	* Reaction Mechanism and New Materials for Photocatalysis	96
181:	* Electrochemistry and Photoelectrochemistry of Diamond	96
182:	* TiO_2 Photocatalysis : Reaction Mechanisms and Real Applications	96
183:	* Photoelectropheology of TiO_2 Particle Suspensions	96
184:	* Recent Progresses in TiO_2 Photocatalysis	97
185:	* Photo-Induced Super-Hydrophile Property of TiO_2 Coated Materials : Novel Phenomenon in Photocatalysis	97
186:	* Anti-Fog Glass and Mirror Utilizing Super- Hydrophilic TiO_2 Photocatalysis . .	97
187:	* Dependence of Product Distribution on TiO_2 Surface Characters : Photocatalytic Decomposition of Gaseous Acetaldehyde	97
188:	* Reproducibility of Supported TiO_2 Films on Pyrex and Soda Line Glass in Photocatalytic Degradation of Formic Acid for 50 Days	98
189:	* Self-Cleaning Building Materials Utilizing Super-Hydrophilic TiO_2 Photocatalysis	98
190:	* Water Pulification Using Immobilized Titanium Dioxide : Adsorbent Effect on Photocatalysis	98
191:	* Interfacial Photochemical Reactions	98
192:	* Optically Tunable Molecule-Based Magnets	99
193:	* New Challenges in Photofunctional Systems	99
194:	* The Diamond Surface-A New Type of Electrochemical Reaction Site	99
195:	* New Challenges in Photofunctional Systems	99

196:	* A Drastic Change in Magnetic Hysteresis Loop by Photo-Induced Spin-Flopping in MnTEtOPP-TCNE Charge Transfer Salt	99
197:	* Optical Control of Magnetic Properties in Molecule-Based Magnets	100
198:	* Magnetic Properties of Functional Prussian Blue Derivatives	100
199:	* In Situ Observasion of a Thin Film TiO ₂ Photocatalyst Surface using a Holographic Method	100
200:	* Electrostatic cis-trans Isomerization of Azobenzene Derivatives in Langmuir-Blodgett Films	100
201:	* Photo-Induced Magnetization of Cobalt Iron Cyanide	101
202:	* Band to Band Excitation of p-type Diamond Thin Films by Short-Wavelength UVillumination	101
203:	* Photoelectrorheology of TiO ₂ Particle Suspensions	101
204:	* Electrochemistry of Conducting B-Doped Diamond Electrodes	101
205:	* Photoelectrochemical Studies of P-Type Semiconducting Diamond Electrodes using Excimer Laser Illumination	102
206:	* Scanning Probe Microscopic Study of Diamond Film Surfaces as Organic Electroluminescence(EL)and Electrochemical Electrodes	102
207:	* Electrochemical Responce of Diamonds in Aqueous Electrolytic Solution Containing Ce ³⁺ Ions	102
III	Department of Energy Conversion Science	103
208:	* Analysis of Stability of a Two-Dimensional Jet with Density Variation	103
209:	* Formation of Turbulent Eddies in Jet Diffusion Flames	103
210:	* Reduced Initial Injection Rate and Pilot Injection at a Spool Acceleration Type Injection System	104
211:	* Fuel Injection Rate Shaping and Its Effect on Exhaust Emissions in a Direct-Injection Diesel Engine Using a Spool Acceleration Type Injection System	104
212:	* Effects of Heat Release Rate on NO _x Time History in Diesel Combustion	105
213:	Simultaneous Reduction of Particulates and Nitrogen Oxides in the Unsteady Turbulent Diffusion Combustion	105
214:	* Gas-Flow Measurements in a Jet Using Cross Correlation of Particle Images	105
215:	* Production and Destruction of Nitrogen Oxides in the Dilution Process of Fuel-Rich Burnt Gases	106
216:	Effects of Shock Waves on Living Tissue Cell (Red Blood Cell) (Damage of Red Blood Cell and Mthematical Analysis of Deformation Model Using Spherical Shell Filled with Liquid)	106
217:	* Predction of Hemolysis Tendency by Shear Stress in a Pipe Orifice Blood Flow	107
218:	Experimental and Mathematical Model of Living Tissue Cell Damage Induced by Plane Shock Waves	107
219:	* Predction of Hemolysis by Shear Orifice Flow	108
220:	* Effects of Shock Waves on Living Tissues (Numerical Analysis of a Propagating Pressure Wave toward Living Tissue)	108

221:	* Coupled Solid-Liquid Analysis for Viscoplastic Body with Moving Boundary Caused by Melting/Solidification (1st Report, Modeling and Fundamental/Finite Element Equations)	109
222:	* Coupled Solid-Liquid Analysis for Viscoplastic Body with Moving Boundary Caused by Melting/Solidification (2nd Report, Application to the Simulation of Welding Process)	109
223:	Metallo-Thermo-Mechanical Simulation of Quenching-Tempering Process Based on Metallo-Thermo-Mechanics	109
224:	Computer Simulation of Residual Stresses, Distortion and Structural Change in the Course of Scanning Induction Hardening	110
225:	Simulation and Experimental Verification of Induction Hardening Process for Some Kinds of Steel	110
226:	Development Strategy of CAE System HEARTS and Some Results of Heat Treatment Simulation of Steel	111
227:	Identification of Heat Transfer Coefficient of Quenching Media	111
228:	Metallo-Thermo-Mechanical Simulation of Centrifugal Casting Process of Multi-layer Roll	112
229:	Simulation of Damaging Interface between Matrix and Reinforcement in Metal Matrix Composite	112
230:	Finite Element Analysis of Solidification Process Based on Integral Penalty Method	113
231:	Investigation on Variation of Drawability of Laminated Sheet Metals Using FEM Simulations	113
232:	* Effect of Strain Rate on Compaction Characteristics of Iron Powders	113
233:	Generation of Various Curves and Slitting of Aluminium Thin Sheet along the Curves	114
234:	* On the Use of Piezoelectric Films for Determination of Plane Stress Distribution	114
235:	* Inversion Scattering in Finite Space Domain	115
236:	* Analysis of Bias-Type Actuator Using Shape Memory Alloy Based on Its Thermomechanical Constitutive Description	115
237:	* Rate-Dependence in One-Dimensional Magnetization	116
238:	* Determination of Plane Stress Distribution by Potential Measurements of Surface-Mounted Piezoelectric Film	116
239:	* Magnetostriction and Magnetoacoustic Emission of Ferromagnetic Material under Stress	116
240:	* Mechanical Properties of Borosilicate Glass Coated with Alumina by Sputtering Process	117
241:	Fatigue Life Evaluation of Notched Components under Combined Axial-Torsional Loading	117
242:	* Cost Analysis of IDLT Reactors Using the ARIES Code	118
243:	An Equilibrium in Negative Hydrogen Ion Production Process Related to the Sheet Plasma Experiment	118
244:	* Preliminary Studies of Inertial-Electrostatic Confinement Fusion Experiments .	119
245:	Direct Energy Conversion from Spent Electron Beam in High-Power CW Klystrons	119

246:	First-Principles Calculation of Oxygen Adsorption on Zr(0001): Possible Site Occupation between the Second and the Third Layer	119
247:	First-Principles Calculation of the Longitudinal Phonon in the Surface Normal Direction of Zirconium(0001) Slab: Localization Mode at the Subsurface	120
248:	Measurements of Young's Modulus and the Modulus of Rigidity of the Solid Solution of Hydrogen in Zirconium between 300 and 1300 K	120
249:	Calculation of Lindgård and Mouritsen's Free Energy Using Recently Measured Moduli of Elasticity for Hydrogen in Zirconium	121
250:	Diffusion of Hydrogen in Titanium, $Ti_{88}Al_{12}$ and Ti_3Al	121
251:	Isotope Effect in the Diffusion of Hydrogen and Deuterium in Titanium, $Ti_{88}Al_{12}$ and Ti_3Al	122
252:	Formation of Singlet Oxygen Photosensitized by Aromatic Amino Acids in Aqueous Solutions	122
253:	Vibrational Properties of a Polycrystalline Titanium Surface Studied by Electron Energy-Loss Fine Structure (EELFS) Analysis	123
IV	Department of Energy Science and Technology	124
254:	* First Principles Molecular Orbital Calculation of Electron Energy Loss Near Edge Structures of α -quartz	124
255:	* Chemical Bonding of Transition Metal Disilicides	124
256:	* Electronic States of F-Centers in Alkali Halide Crystals	125
257:	* Structure and Chemistry of Intergranular Films in Ca-doped Si_3N_4	125
258:	* Electronic Structures of $Ln^{3+}\alpha$ -Sialons with Correlations to Solubility and Solution Effects	126
259:	* Calculation of Core-Hole Excitonic Features on Al- L_{23} edge X-Ray Absorption Spectra of α - Al_2O_3	126
260:	* Electronic States and Chemical Bondings of an Interstitial Cation in Ionic Compounds AgCl and NaCl	126
261:	* Growth Mechanism of $BaTiO_3$ Thin Film by Theoretical Calculation of Electronic Structure	127
262:	* Effects of Solute Atoms on the Chemical Bonding of Fe_3C (cementites)	127
263:	* Dopant modified local chemical bonding at a grain boundary in $SrTiO_3$	128
264:	Estimation of Kapitza Conductance Effect on Steady and Transient Boiling Heat Transfer in He I based on Kapitza Conductance Results in He II	128
265:	Boiling Phenomena due to Quasi-steadily and Rapidly Increasing Heat Inputs in LN_2 and LHe I	129
266:	* Transient Heat Transfer from a Horizontal Wire in Subcooled He II at Atmospheric Pressure for a Wide Range of Wire Diameter	129
267:	Incipient Boiling Superheats and Critical Heat Fluxes due to Increasing Heat Inputs in Subcooled He I at Various Pressures	130
268:	Pool Boiling Critical Heat Flux on a Horizontal Cylinder in Subcooled Water for Wide Ranges of Subcooling and Pressure and Its Mechanism	130
269:	Experimental Study on Measurement of Damping Coefficient of Power System by Use of SMES	131

270:	A Method of Simulation for Power System Characteristics including Superconducting Generator with High Response Excitation	131
271:	Evaluation of Steady State Stability of Electric Power System by Use of Superconducting Magnet Energy Storage	132
272:	On-line Measurement of Eigen-Frequencies of Power Systems by Use of SMES . .	133
273:	A New Power Supply for Superconducting Pulse Magnet by Use of Energy Transfer Circuit	133
274:	* Removal of Antimony by Volatilization from Industrial Copper Matte and White Metal	133
275:	Elimination of Copper from Molten Steel by Ammonia Gas Blowing	134
276:	Quantitative SIMS Analysis of Trace Metallic Impurities in High Purity Copper .	134
277:	Quantitative SIMS Analysis of Mo in Ti-Dilute Mo Alloys Using Isotopic Abundance	135
278:	Electrochemical deoxidation of yttrium-oxygen solid solutions	135
279:	Removal of copper from steel scraps by NH_3 gas	136
280:	Thermodynamic Properties of Oxygen in Yttrium-Oxygen Solid Solutions	136
281:	* Removal of Antimony by Volatilization from Industrial Copper Matte and White Metal	136
282:	Iron-Based Element for Low Temperature Thermoelectric Generator	137
283:	Removal of oxygen and nitrogen from niobium by external gettering	137
284:	* Chemical potentials of the components in the system $\text{CaO} + \text{P}_2\text{O}_5 + \text{FeO}$. . .	138
285:	Oxidation-reduction equilibrium of $\text{Cu}^{2+}/\text{Cu}^+$ in binary alkaline sulfate melts . .	138
286:	* Chemical potentials of oxygen for mixtures of $\text{CaO} + \text{Ca}_4\text{P}_2\text{O}_9 + (\text{CaO} + \text{P}_2\text{O}_5 + \text{FeO})$ melts and $\text{Ca}_4\text{P}_2\text{O}_9 + \text{Ca}_3\text{P}_2\text{O}_8 + (\text{CaO} + \text{P}_2\text{O}_5 + \text{FeO})$ melts	138
287:	* An automatic equipment for determinations of the FeO activity - laboratory and in-plant applications	139
288:	Depression of vaporization of melts formed during the immobilization of high level nuclear waste by the addition of P_2O_5	139
289:	A Thermodynamic study of the system $\text{CaO} + \text{Al}_2\text{O}_3 + \text{FeO}$ at 1673 K	140
290:	Activity of phosphorous in liquid Ni + P alloys saturated with solid nickel	140
291:	Solubilities of CO_2 in candidate glasses for nuclear waste immobilization part 2, a summary for binary alkali silicate and borates	140
292:	Solubility of molybdenum in liquid tin	140
293:	New nitriding technologies of steel utilizing thermal decomposition of CaCN_2 and its characteristics	141
294:	* Thermodynamics of oxygen behaviour in cobalt-nickel alloys	141
295:	A Solid State Sensor for The Determination of Silicon in High-Carbon Ferro FerroChromium Melts	141
296:	* Refining of ferrous scrap intermingled with copper by using molten aluminium .	142
297:	* Distribution equilibria of the metallic elements and boron between Si based liquid alloys and $\text{CaO-Al}_2\text{O}_3\text{-SiO}_2$ fluxes	142
298:	* Reducing Removal of Phosphorous from Calcium Containing Silicon Alloys . . .	143
299:	Application of a Florescent Technique to the Study of the Weathering Process .	143

300:	Pre processing Using Fluorescent Paint in Visual Recognition and Image Analysis - Extraction and Evaluation of the Vein by Image Processing -	144
301:	Trends and Short-Term Prospects for Copper Demand	144
302:	The Borehole Television System by the Fluorescent Method	144
303:	* An Application of Computer Graphic Simulation of Changes at Stone-Quarrying Sites	145
304:	* Theoretical Analysis for Non- Equilibrium Flow Fields with Transitional Process from Two-Phase to Three-Phase Mixtures by Injecting Air Halfway into a Lifting Pipe - (-Fundamental study on lifting system for mining marine mineral resources (3rd Report)-)	145
305:	* Deformation and Rebounding Processes of a Water Droplet Impinging on a Flat Surface Above Leidenfrost Temperature	146
306:	* Nonsteady Behaviour of a Free Surface Configuration and Velocity Distribution in a Flow Field of Molten Steel in a Mold	146
307:	* Prediction of Forming Limit in Axisymmetric Deep Drawing of Steel/Aluminium Alloy Laminated Sheets Using a Simple Criterion for Ductile Fracture	147
308:	* Prediction of Forming Limit in Deep Drawing by Combination of Finite Element Simulation and Criterion for Ductile Fracture	147
309:	* Prediction of Forming Limit in Deep Drawing of Fe/Al Laminated Composite Sheets Using Ductile Fracture Criterion	148
310:	* Finite Element Simulation of Redrawing Processes with Ductile Fracture Criterion	148
311:	* Experimental Study of Deformation Process of a Water Droplet Impinging on Polished and Rough Surfaces Heated to above the Leidenfrost Temperature	149
312:	* Deformation Process of a Droplet Impinging on a Hot Oxide-Scaled Surface above the Leidenfrost Temperature	149
313:	* Effect of Pressure Drop Owing to Friction between Pipe Inner Wall and Water on Non-equilibrium Flow Fields in an Air-lifting Pipe - (-Fundamental study on lifting system for mining marine mineral resources-)	150
314:	* A Study on Recycling of Disposal Consumer Electronic Goods	150
315:	A Study on Recovery of Valuable Metals from Auto Shredded Dust	151
316:	* The Role of Hydrolyzed Metal Cations in the Liquid-Liquid Extraction of Ultra-fine Silica with Dodecyl Sulfate	151
317:	Flotation Separation of Plastics Using Selective Depressants	152
318:	* Mass Transfer Rate in Powder Injection	152
319:	Electrodeposition of Copper under Microgravity	153
320:	Ionic Mass Transfer Rate Associated with Electrodeposition of CdTe Film	153
321:	Observation of Electrochemical Interfacial Phenomena under Microgravity	154
322:	* Adsorption of Inorganic Depressants on Synthesized Diamond and Graphite . .	154
323:	* $S=1/2$ quantum spin-gap in 1-D antiferromagnet with bond alternation: NMR study of $\text{CuCl}_2(\gamma\text{-picoline})_2$	155
324:	* Effect of Spin Correlation on ^{133}Cs Nuclear Magnetic Relaxation in Singlet Ground State System CsFeCl_3	155
325:	* ^{59}Co NMR in Stacked Triangular Lattice Antiferromagnet CsCoBr_3	155

326:	* Reports on Quantum Spin Effect Contributed to LT21: NMR Study on Quantum Spin-Gap and Magnetic Frustration	156
327:	Materials Studies for Fusion Reactors - with the Emphasis on Radiation Damage Studies-	156
328:	A modeling of radiation induced microstructural evolution under applied stress in austenitic alloys	157
329:	Elastic FEM Analysis of Fiber Push-Out Test for C/C Composites	157
330:	NIFS Information Network for Fusion Engineering Research in Japanese Universities	158
331:	* Temperature Dependence of Young's Modulus And Internal Friction on SiC/SiC Composites	158
332:	* In-Situ Observation Fracture Process and Microstructural Analysis of SiC/SiC Composites	159
333:	Preparation of High-Purity SiCf/SiC Composites	159
334:	Tandem Electron Beam Welding for Maintenance of Nuclear Fusion and Fission Reactors	160
335:	A Modeling of Radiation Induced Microstructural Evolution Under Applied Stress in Austenitic Alloys	160
336:	Effect of Heat Treatment Temperature on Interfacial Mechanical Properties of C/C Composites by means of Micro-Indentation Test	161
337:	Blanket Design Using FLiBe in Helical-type Fusion Reactor FFHR	161
338:	Effect of Heat Treatment Temperature on Young's Modulus and Microstructure of C/C Composites	162
339:	Design Assessment of Heliotron Reactor	162
340:	Low Activation Ferritic and Martensitic Steels Development for Fusion Reactors	163
341:	Current Status of Materials Research for Nuclear Fusion Reactors	164
342:	Status of Silicon Carbide Composites for Fusion	164
343:	Rate Theory Modeling of Defect Evolution Under Cascade Damage Conditions: The Influences of Vacancy-type Cascade Remnants on Defect Evolution	165
344:	NIFS Information Network for Fusion Engineering Research in Japanese Universities	165
345:	Effect of Heat Treatment Temperature on Young ' s Modulus and Microstructure of C/C Composites	165
346:	Evaluation of Interfacial Shear Strength of C/C Composites by means of Micro-Indentation Test	166
347:	In-situ Observation of Compressive Fracture Processes in Flat Woven Carbon Fabric Reinforced Carbon Composite Materials	166
3	Review Articles	169
I	Department of Socio-Environmental Energy Science	169
1:	Pursuit of Happiness	169
2:	The Problem of Energy and Environment -Pursuit of Happiness-	169
3:	Application of Virtual Reality for Nuclear Engineering	169

4:	Chemical Composition of Atmospheric Aerosols, and Their Sources and Generation Mechanism	170
5:	Current Status and Key Issues of Nuclear Liability Regime	170
6:	Reforming the Social Regulation of Japan	171
7:	Current Topics of BWR Nuclear Thermal Hydraulic Stability: Regional stability and activities in design and operation	171
II	Department of Fundamental Energy Science	172
8:	Crystal Chemistry on the Cation Sites of Oxide Spinel	172
9:	Overview of Heliotron E results	172
10:	Infrared spectroscopy of hydrogen in porous silicon	173
11:	Present Status and Future Prospect of Research Reactors	173
12:	Development of High Frame-Rate Neutron Radiography and Its Application to Fluid Measurement	173
13:	Electrochemistry and Photoelectrochemistry of Diamond	174
14:	TiO ₂ Photocatalysis : Reaction Mechanisms and Real Applications	174
15:	Photoelectrochemistry of TiO ₂ Particle Suspensions	174
16:	Recent Progresses in TiO ₂ Photocatalysis	174
17:	Photo-Induced Super-Hydrophile Property of TiO ₂ Coated Materials : Novel Phenomenon in Photocatalysis	175
18:	TiO ₂ Photocatalysis in Action	175
19:	Photocatalytic Ceramic Tile	175
20:	Techniques for Ultra Thin Film Using Ultrafine Particles	175
21:	Self-Cleaning Material Using Light – A New Application of TiO ₂ –	175
22:	New Trends in TiO ₂ Photocatalysis	176
23:	Frontiers in Photocatalytic Materials	176
24:	Role of Oxygen for Photocatalysis	176
25:	Semiconductor Photoelectrode and Photocatalysis	176
26:	Photocatalysis for Self-Cleaning and Sterilizing Effects	177
27:	TiO ₂ Photocatalysis Remarkable for Antibacterial and Self-Cleaning Effects	177
28:	Water Treatment Using TiO ₂ Photocatalyst	177
29:	Electrorheology and Photoelectrochemistry	177
III	Department of Energy Conversion Science	178
30:	Problems of Diesel Engine Combustion	178
31:	Current Status of Automotive Technology and Environmental Protection	178
32:	Role of Turbulence in Diesel Combustion	178
33:	Scientific Exchange Programme on Integrated Engineering	179
34:	Simulation of Engine Combustion	179
35:	Sheet Metal Forming Simulation System Using Finite Element Method	179
36:	Speed Change of Waves Due to Stress and Damage in High-Polymer Composite	180
37:	Strength Characteristics of Structural Ceramics	180
IV	Department of Energy Science and Technology	181
38:	Electron Energy Loss Spectroscopy	181
39:	Electronic structures of metal-oxides by DV-X α cluster calculations	181

40:	Ferrors scrap - an overview with a particular emphasis on the removal of copper	182
41:	Development of Deep Sea Minerals from the Viepoint of Social Engineering of Resources	182
42:	Hydrodynamic Examinations and Problems on Lifting Characteristics of Manganese Nodules by Air-Lift Pump System	182
43:	Summary and Conclusions of the Discussion Session (ch. A.Kohyama) on "Joining SiC/SiC Composites"	183
44:	Dedign Studies of Helical Reactor FFHR (1) - Overview of FFHR Dedign	183
45:	Dedign Studies of Helical Reactor FFHR (6) - Overview of FFHR Dedign	183
4	Books	185
1:	Challenges to Japan	185
2:	Wood-Plastic Combination, in "The Handbook of New Woody Materials"	185
3:	Wood-Inorganic Composites, in "The Handbook of New Woody Materials" . . .	186
4:	Butterflies and Environments	186
5:	Wood Is Environmentally Friendly	186
6:	Proceedings of Cognitive Systems Engineering in Process Control: CSEPC 96 . .	187
7:	Energy-Resources Handbook: 7-1 A Survey of Energy System Models - Their Roles in Energy-Systems Study-	188
8:	Cancer Neutron Capture Therapy	188
9:	Electrochemical Technology (-Inovation and New Developments-)	189
10:	Intoroduction to Fluorine Chemistry(-Fundamentals and Experiments-) Inorganic, Chapter 3 1.3.2 S ₂ O ₆ F ₂	189
11:	Intoroduction to Fluorine Chemistry(-Fundamentals and Experiments-) Inorganic, Chapter 3 2.1 Fluorides and fluorocomplexes of silver	189
12:	Microstructures and Functions of Matter	190
13:	Microstructures and Functions of Matter	190
14:	Photocatarysts for unti-pollution and sterilization	190
15:	Corrosion of iron	191
16:	Photo Clean Revolution	191
17:	Corrosion of Iron	191
18:	Photo Clean Revolution	191
19:	Combustion in Internal Combustion Engines	192
20:	Metals Resources, Smelting and Recycling	192
21:	"Infrared Semiconductor Laser by Means of J x H Force Excitation of Holeds" Elec (Amazing Light, A Volume Dedicated to Charles Hard Townes on His 80th Birthday, ed. R. Y. Chiao, Springer, New York, 1996) pp.497-505.	192
5	List of Academic Staff	193

A. Current Research Fields

A. 研究現況

Chapter 1

Current Research Fields

I Department of Socio-Environmental Energy Science

a1-1	Pursuit of happiness	幸福論
a1-2	New material for energy saving	低環境負荷材料の開発
a1-3	Recycle process	リサイクルプロセス
a2-1	Analysis of Energy Supply and Demand in Japan	日本のエネルギー需給分析
a2-2	Analysis of Optimal Generation Mix under Uncertainty	不確実性を考慮した最適電源構成の分析
a2-3	Life Cycle Analysis of Electric Vehicle	電気自動車のライフサイクル分析
a2-4	Economic Analysis of Energy Efficient Technologies	省エネルギー技術の経済性分析
a3-1	Chemical conversions of biomass and plastics wastes to their liquified fuels by the supercritical fluids	超臨界流体によるバイオマスおよび廃プラスチックの液体燃料化に関する研究
a3-2	Bioconversion of lignocellulosics to ethanol by the supercritical water	超臨界水によるリグノセルロースのエタノールへの酵素変換に関する研究
a3-3	Pyrolysis of lignocellulosics to value-added chemicals	リグノセルロースの熱分解による有用物質への変換
a3-4	Topochemistry of biocarbon-inorganic composites for their property-enhancement	無機質複合化バイオカーボンの諸機能発現に関するトポ化学
a3-5	Long-living of wood enhanced by antimicrobial treatments	防菌・防黴性付与による木材のロングライフ化に関する研究

a3-6	Forest soil and carbon cycling in earth ecology	地球生態系での炭素循環と森林土壌に関する研究
a4-1	Development of Mutual Adaptive Interface with Eye-Sensing HMD	アイセンシングHMDによる相互協調型インタフェースの開発
a4-2	A Study on a Human Model based on Artificial Intelligence	AIによるヒューマンモデルの構築
a4-3	Adaptive Interface based on Recognition of Facial Expression and Verbal Protocol	顔表情・発話認識を用いた適応型インタフェース
a4-4	A Study on Integrated CAI system	統合型教育支援システムの構築
a4-5	Development of Maintenance Training System based on Networked Virtual Environment	共有仮想空間を用いた保修訓練システムの構築
a4-6	Optimal Planning of Autonomous Decentralized Energy System	自律分散型エネルギーシステムの計画
a5-1	Characterization of Physical and Chemical Properties of Atmospheric Aerosols	大気エアロゾルの物理・化学的性状の特性化
a5-2	Application of PIXE Analysis to Atmospheric Sciences	PIXE分析法の大気環境科学への応用
a5-3	Analysis and Modelling of Deposition of Air Pollutants	大気汚染物質の沈着機構の解析とモデル化
a5-4	Long-Range Transport of Gaseous and Particulate Air Pollutants Combined with Chemical Transformation and Removal	沈着、変質を伴う大気汚染物質の長距離輸送モデルの開発
a5-5	Assessment of Atmospheric Environmental Impacts Connected with Cars by Life Cycle Analysis	ライフサイクル分析による自動車の大気環境負荷の評価
a6-1	Scientific consideration about best mixture of electricity sources in future	将来における電力源のベストミックス（最適組合せ）に関する科学的考察
a6-2	Investigation on nuclear subjects including non-proliferation, safeguards, physical protection, transportation, criticality safety, radioactive waste management, etc.	核不拡散、保障措置、核物質防護、核燃料輸送、臨界安全、放射性廃棄物管理などの核問題に関する研究
a6-3	Study on application of reactor neutrons to medicine	原子炉中性子の医学への利用に関する研究
a6-4	Neutron radiography	中性子ラジオグラフィ

a6-5	Experimental study on neutron-induced fission	中性子核分裂に関する実験的研究
a6-6	Evaluation of fluence and absorbed dose for neutrons and gamma-rays	中性子、ガンマ線のフルエンス及び吸収線量の評価
a7-1	Formation and evolution of nuclear-safety culture	原子力安全文化の醸成
a7-2	Transmission of information and public relations on energy problems	エネルギー問題に関する情報伝達と広報
a7-3	Formation of public attitudes on nuclear energy or radioactivity issues	原子力・放射線/放射能問題に関する社会の態度形成
a7-4	Neutron Activation Analysis of Ivory of African Elephants	アフリカ象の象牙の中性子放射化分析
a7-5	Physical Interpretation of Adjoint Flux in Reactor Physics	原子炉物理における随伴中性子束の物理的意味
a8-1	Japanese Strategy for Mitigating Global Environmental Issues (Global Warming)	地球環境問題、地球温暖化に対する日本の政策
a8-2	Technology Development for Mitigating Global Environmental Issues (Global Warming) (1) -Photovoltaic Power Generation System	地球環境、温暖化に対する技術開発 (1) -太陽光発電システム
a8-3	Technology Development for Mitigating Global Environmental Issues (Global Warming) (2) -Natural Gas for Electricity and Cogeneration	地球環境、温暖化に対する技術 (2) -天然ガスによる発電とコジェネ
a8-4	Effective Use of Uranium	ウラン資源の有効活用
a8-5	Plutonium Use in Light Water Reactors	プルトニウムの軽水炉利用

II Department of Fundamental Energy Science

b1-1	Electrochemical Energy Conversion by Fuel Cells and Hydrogen Systems	燃料電池、水素エネルギーシステムによる電気化学的エネルギー変換
b1-2	Physical Chemistry of Molten Salts and Applications to Energy Conversion Processes	熔融塩の物性・化学とエネルギー変換プロセスへの応用

b1-3	New Functional Materials and Their Applications	マテリアル・テーラリングによる新規な機能材料の創製と応用
b1-4	Development of Interdisciplinary Fields of Electrochemistry and Plasmas/Ion Beams	プラズマ、イオンビームなどと電気化学の境界領域の開拓
b1-5	Determination of Molecular and Solid Structures by Vibrational Spectroscopies and Diffractions	ラマン分光、中性子回折などによる物質構造の解明
b1-6	Inorganic Halgen Chemistry and Applications to Energy Processes	フッ化物、塩化物の化学とエネルギープロセスへの応用
b2-1	Dynamics of photo-induced electrons in amorphous chalcogenide semiconductors	アモルファスなカルコゲン化合物半導体における分光特性と電子の動的挙動
b2-2	Critical phenomena and the transport processes in structurally complicated media	複雑系における臨界現象と輸送物性
b2-3	Superconducting characteristics of structurally disordered high- T_c cuprates	乱れた構造を持つ高温超伝導体の超伝導特性
b2-4	Thermoelectric and galvanomagnetic effects in semimetals and semiconductors	半金属と半導体における熱電効果と低温強磁場電流磁気効果
b2-5	Synthesis of High Performance Materials by DC Arc Plasma	DC アークプラズマによる高機能材料の合成
b2-6	Micro-Characterization at the Interface of High Performance Materials	高機能材料界面のマイクロキャラクタリゼーション
b3-1	Analysis and Design of Ceramic Energy Materials	セラミックスエネルギー材料の解析と設計
b3-2	Studies on Rechargeable Lithium Battery Materials	リチウム2次電池の材料開発
b3-3	Development of Solid Oxide Fuel Cell Systems	固体酸化物型燃料電池の開発
b3-4	Synthesis of Functional Ceramic Thin Film from Aqueous Solution	水溶液からの機能性セラミックス薄膜の合成
b3-5	Design and Analysis of Novel Optical Energy Materials	新規光エネルギー材料の設計と解析
b3-6	Development of X-ray Diffraction and X-ray Absorption System for Material Analysis	X線回折及びX線吸収による材料解析システムの開発
b4-1	fusion plasma	核融合プラズマ

b4-2	magnetic confinement	磁気閉じ込め
b4-3	MHD theory	MHD理論
b4-4	plasma transport theory	プラズマ輸送理論
b4-5	optimization of stellarator field	ステラレータ磁場の最適化
b5-1	Studies on multiply-ionized impurity ions in high temperature plasmas.	高温プラズマ中の多価電離不純物イオンの研究
b5-2	Theoretical studies on equilibrium and stability in the 3-dimensional non-axis symmetric torus plasmas.	3次元非軸対称トーラスプラズマの平衡と安定性の理論的研究
b5-3	Studies on magnetohydrodynamic(MHD) equilibrium and plasma current in non-uniform magnetic field.	磁場測定による不均一磁場中の超高温プラズマの平衡および内部電流の研究
b5-4	Studies on radiation by bolometric and spectroscopic diagnostics from high temperature plasmas.	ボロメーターおよび分光による高温プラズマからの輻射の研究
b5-5	Studies on neutron energy spectrum by D-D reaction.	高温プラズマ中のD-D反応による中性子のエネルギースペクトルの研究
b6-1	Electron cyclotron heating and current drive	プラズマの電子サイクロトロン加熱・電流駆動
b6-2	Control of MHD instabilities by LHCD	低域混成電流駆動による磁気流体不安定性の制御
b6-3	Control of MHD instabilities by ECH	電子サイクロトロン加熱による磁気流体不安定性の制御
b6-4	Plasma diagnostics (soft X-ray CT and ECE)	プラズマ診断法の開発(軟X線トモグラフィと電子サイクロトロン輻射計測)
b6-5	Confinement and nonlinear waves in non-neutral plasmas	非中性プラズマの閉じ込めと非線形波動
b7-1	Confinement Study of High Temperature Plasma in Helical System	ヘリオトロン装置による高温プラズマの閉じ込め制御
b7-2	Study of Helical Magnetic Configuration	ヘリカル磁場構造の研究
b7-3	Control of Edge Plasma	プラズマ閉じ込め領域周辺部におけるプラズマ制御

b7-4	Divertor Study	ダイバータ基礎研究
b7-5	Study of Plasma Production and Heating by Electron Cyclotron Wave	電子サイクロトロン波によるプラズマ生成・加熱の研究
b7-6	Study of Plasma Heating by Neutral Beam Injection	高速中性粒子によるプラズマ加熱の研究
b8-1	Study on High Temperature Plasma Heating and Confinement	超高温プラズマの加熱・閉じ込めに関する研究
b8-2	Experimental Analysis on Vacuum Magnetic Field Structure	真空磁場配位の実験構造解析
b8-3	Development of Monte Carlo Calculation Scheme for the Simulation of Plasma Transport and Heating	プラズマの輸送と加熱のシミュレーションのための新しいモンテカルロ計算スキームの開発
b8-4	Theoretic Analysis on Charged Particle Orbit in the None-axisymmetrical Torus with Adiabatic Constants	非軸対称トーラスにおける荷電粒子軌道の断熱不変量をもちいた理論解析
b8-5	Study on the Advanced Heliotron Magnetic Field with the Control of Chaotic and Statistic Characteristics	磁力線のカオスや統計的性質の制御に基づいたヘリオトロン磁場の高性能化に関する研究
b8-6	Study on the Optimization of Ion Cyclotron Heating Antenna for Various Heating Modes	イオンサイクロトロン加熱の加熱モードによるアンテナ最適化の研究
b9-1	Confinement Study of High Temperature Plasma in Helical System	ヘリオトロン装置による高温プラズマの閉じ込め制御
b9-2	Study of Helical Magnetic Configuration	ヘリカル磁場構造の研究
b9-3	Control of Edge Plasma	プラズマ閉じ込め領域周辺部におけるプラズマ制御
b9-4	Divertor Study	ダイバータ基礎研究
b9-5	Study of Plasma Production and Heating by Electron Cyclotron Wave	電子サイクロトロン波によるプラズマ生成・加熱の研究
b9-6	Study of Plasma Heating by Neutral Beam Injection	高速中性粒子によるプラズマ加熱の研究

b10-1	Design of Functional Supramolecules Based on Amphiphilic Molecular Assembly and their Utilization for Chemical Reaction and Separation of Substances	両親媒性分子集合体を用いた超分子集合体の構造設計とその反応分離場への応用
b10-2	Construction of Advanced Materials with Nano-Meso Sized Structure Using Amphiphilic Molecular Assemblies as Template	両親媒性分子集合体を鋳型として用いたナノメゾ材料の構築
b10-3	Method to Integrate the Processes for Obtaining Materials with Hierarchal Structures	階層構造を持つ材料作成プロセスのインテグレート手法
b10-4	Interaction between Solutes in Aqueous and Nonaqueous Solvents	水溶液中及び非水溶媒中における溶質間相互作用
b10-5	Prediction of Ternary Structures of Proteins in Aqueous Solutions	水溶液中におけるタンパク質の3次構造予測
b11-1	Molecular design of plastic enzymes	プラスチック酵素の分子設計
b11-2	Molecular design of asymmetric photocatalysts	不斉光触媒の分子設計
b11-3	Molecular design of pepetide enzymes	ペプチド酵素の分子設計
b11-4	Creation of artificially evolved enzymes and cells	人工進化酵素及び細胞の創製
b12-1	Research on high-temperature batteries for energy storage	エネルギー貯蔵用高温二次電池の研究
b12-2	Elucidation of electrochemical behavior of sulfur dioxide and nitrogen oxides as the environmental pollutants	二酸化硫黄や窒素酸化物などの環境汚染物質の電気化学的挙動の解明
b12-3	Electrodeposition of refractory metals in molten salts	熔融塩電解によるリフラクトリーメタルの析出
b12-4	Analysis of current and potential distributions in electrochemical cells	電気化学セルにおける電流・電位分布の解析
b13-1	Study on nuclear characteristics of high performance reactors in next-generation	次世代の高性能新型原子炉の核特性研究
b13-2	Development of High performance advanced research reactor as neutron source	高性能研究用中性子源炉の開発
b13-3	Nuclear reactors utilizing thorium-uranium fuel cycle	トリウム・ウラン燃料サイクル原子炉

b13-4	Hybrid reactor system of accelerator driven fission reactor	加速器と核分裂炉のハイブリッド炉
b13-5	Transmutation and incineration of high level nuclear waste	高レベル放射性廃棄物の消滅処理
b13-6	Criticality safety study of nuclear fuel facility	核燃料施設の臨界安全性研究
b14-1	Study on target cooling of a spallation neutron source	スポレーション中性子源のターゲット冷却に関する研究
b14-2	Flow and heat transfer characteristics of gas-liquid two-phase flow in narrow channels	狭小流路における気液二相流の流動と伝熱
b14-3	Characteristics of two-phase flow with a large liquid/gas density ratio	高密度比気液二相流の特性
b14-4	Basic study of steam explosion	水蒸気爆発に関する基礎研究
b14-5	Study on basic phenomena in post-CHF heat transfer	ポスト限界熱流束熱伝達の基礎的現象に関する研究
b14-6	Visualization and measurement of multiphase phenomena by neutron radiography	中性子ラジオグラフィによる混相流現象の可視化と計測
b15-1	Studies on TiO ₂ thin film photocatalysts under weak UV light illumination.	酸化チタン光触媒反応の研究
b15-2	Applications and coating of fine particles	微粒子で構成される薄膜の作成と応用
b15-3	Studies on conductive diamond electrodes	導電性ダイヤモンド薄膜電極の研究

III Department of Energy Conversion Science

c1-1	Mitigation of Pollutants in Thermal Energy Conversion Systems	熱エネルギー変換システムにおける汚染物質低減
c1-2	Mixture Formation and Combustion in Diesel and Spark-Ignition Engines	ディーゼル機関および火花点火機関の混合気形成と燃焼
c1-3	Spray Characteristics and Their Effects on Combustion	噴霧特性ならびにその燃焼への作用
c1-4	Prediction of Combustion Processes in Internal Combustion Engines	内燃機関内燃焼過程の予測

c1-5	Alternative Fuels in Combustion Systems	燃焼システムにおける代替燃料
c1-6	Optimum Design of Power Plants	動力プラントの最適設計
c2-1	Ignition and Combustion of Homogeneous and Heterogeneous Mixtures	均一および不均一混合気の着火と燃焼
c2-2	Chemical Reaction Kinetics of Pollutant Formation	汚染物質生成の化学反応動力学
c2-3	Structure of Turbulent Diffusion Flames	乱流拡散火炎の構造
c2-4	Laser Diagnosis and Picture Analysis for Combustion Research	レーザ計測および画像処理による燃焼診断
c2-5	Numerical Simulation of Turbulent Flows and Combustion	乱流および燃焼の数値シミュレーション
c2-6	Biological Effects of Fluid Energy on Bio-Tissues and Cells	生体組織および細胞に及ぼす流体エネルギーの生物学的作用
c3-1	Inelastic Constitutive Equation of High Temperature Materials and Construction of the Data Base	高温における非弾性構成式とそのデータベース化
c3-2	Foundation of Materio-Thermo-Mechanics and Computer Simulation of Some Processes Incorporating Phase Transformation	変態・熱・力学の基礎と相変態を伴う工学過程のコンピューターシミュレーション
c3-3	Analysis of Plastic Forming Process under Large Deformation Depending on Microstructural Evolution	大変形を伴う塑性加工過程の解析とそれに及ぼす組織の効果
c3-4	Development of Sheet Metal Bending Process by Line Heating Technology	線状加熱による板材の曲げ加工機の試作開発
c3-5	Molecular Dynamics Simulation of Thermo-Mechanical Fields under Phase Transformation	分子動力学による相変態過程とそれに伴う熱・力学場のシミュレーション
c4-1	Mechanics of Electromagnetic Materials	電磁気材料の力学
c4-2	Mechanics and Application of Functional Materials	機能材料の力学と応用
c4-3	Nondestructive Evaluation of Stress, Damage and Inhomogeneity by Ultrasonic Waves and Electromagnetic Phenomena	超音波と電磁気現象による応力、損傷、非均質の非破壊評価

c4-4	Processing of Ceramic-Coated Materials and Analysis of Their Structure and Deformation	セラミックス・コーティング材料の創成とその構造および変形の解析
c4-5	Strength Evaluation of Advanced Ceramics and Its Numerical Simulation	先進セラミックスの強度評価とその数値シミュレーション
c4-6	Computer Simulation of Fatigue Strength in Metallic Materials	金属材料の疲労強度コンピュータ・シミュレーション
c5-1	Design of Intense 14 MeV Volumetric Neutron Source	強力 14 MeV 体積中性子源のデザイン
c5-2	Magnetic Confinement of Ultra-Cold Neutrons	超冷中性子の磁気閉じこめ
c5-3	Study of the Production Mechanism of Negative Hydrogen Ion in Plasmas	プラズマ中での負イオン生成メカニズムの解明
c6-1	Free Electron Laser	自由電子レーザーの研究
c6-2	Particle Simulation for Advanced Klystron Tube and RF Guns	クライストン及びRFガンの高性能化のための粒子シミュレーション研究
c6-3	D - ³ He Advanced Fuel Fusion	D - ³ He 先進燃料核融合炉の研究
c6-4	Beam-Beam Colliding Fusion (IECF)	ビーム衝突型核融合の研究 (慣性静電閉じ込め方式核融合)
c6-5	Spherical Plasma Generation and Application	球状プラズマの生成及び応用の研究
c7-1	Electronic Structures and Properties of Transition-Metal Hydrides	遷移金属の水素化物, 酸化物, 窒化物の電子構造と物性
c7-2	Mechanism of Absorption of Hydrogen Isotopes in Transition Metals and Intermetallic Compounds	遷移金属および金属間化合物の水素同位体吸収の機構
c7-3	First-Principles Calculation of the Total-Energy and the Interatomic Force of Solid and Its Surface	固体, 固体表面の全エネルギー, 原子間力の第一原理計算
c7-4	Surface Science of the Transition Metal-Light Element System	軽元素-遷移金属系の表面科学
c7-5	Theoretical Studies on the High Temperature Properties of Condensed Matter Using Semi-Empirical Model Potentials	半経験的モデルポテンシャルを用いた凝縮体の高温物性の理論計算

IV Department of Energy Science and Technology

d1-1	Study on structure and process of VLSI	超L S I のデバイスプロセスに関する研究
d1-2	Study on electrical characteristics of scaled-down MOS devices	サブミクロンM O S デバイスに関する研究
d1-3	Study on reliability physics and modeling on carrier transport in insulating films	M O S 界面の信頼性物理とモデリングに関する研究
d1-4	Investigation of local chemical bondings of ceramics by EELS	高空間分解能 EELS 法による局所化学結合状態の解明
d1-5	Material design of new functional ceramics through electronic calculations	新しい機能性セラミックス材料の量子設計
d1-6	Electronic states of ceramic interfaces	セラミックス界面の機能と電子状態
d2-1	Heat transfer characteristics of cryogenic liquids (LN ₂ , LHe, HeII) in relation to the cooling of superconducting magnets.	超伝導マグネット冷却に関連した極低温流体 (LN ₂ , LHe, 超流動 He) の熱伝達特性
d2-2	High density heat removal from plasma facing devices in nuclear fusion systems.	核融合装置プラズマ対向壁からの高密度除熱
d2-3	Non-boiling and boiling heat transfer in liquid metals.	液体金属の非沸騰及び沸騰熱伝達
d2-4	Superconducting magnet energy storage system in electrical power system.	超伝導エネルギー貯蔵装置の電力系統特性に関する研究
d2-5	Power system characteristics of superconducting fault current limiter.	超伝導故障電流限流器の電力系統特性に関する研究
d2-6	Energy transfer between superconducting magnets.	超伝導マグネット間のエネルギー転送に関する研究
d3-1	Development of Iron-Based Device for Low Temperature Thermoelectric Generator.	低温用鉄基熱電素子の開発
d3-2	New Continuous Process for Production of Titanium Metal.	金属チタンの新しい連続精錬プロセスの開発
d3-3	Ammounium Gas Steel Making.	アンモニアガス製鋼法
d3-4	Production of Functional Materials by Ozone Gas.	オゾンガスによる機能材料創製
d3-5	Thermodynamics of Superconductive Oxides.	酸化物超伝導材料の熱力学

d3-6	Process for Zinc Recovery from Steel Making Dust.	製鋼ダストからの亜鉛の回収プロセス
d4-1	Physical Chemistry of Radioactive Nuclear Waste Management	放射性廃棄物処理の物理化学
d4-2	Thermochemistry of steelmaking	製鋼プロセスの熱化学
d4-3	Chemical sensors for metallurgical processes	材料プロセス用化学センサ
d4-4	Oxidation-reduction equilibrium in molten slags, fluxes and salts.	熔融スラグ、フラックス、ソルト中の酸化還元平衡
d4-5	Recovery of iron unit from waste generated at steel works	製鉄所起源の廃棄物からの鉄資源回収
d4-6	Thermochemistry of zirconium-based alloys	ジルコニウム系合金の熱化学
d5-1	The Earth Energy and Mineral Resources	地球エネルギーと鉱物資源
d5-2	Trends and Forecasts for the Supply and Demand of Resources and Energy	資源エネルギーの需給動向と予測
d5-3	Geological Studies of Radioactive Waste Disposal	放射性廃棄物の地層処分
d5-4	Resources Development and Environmental Protection	資源開発と環境保全
d6-1	Theoretical Analysis of Air-Lift Pump System for Conveying Marine Mineral Resources from Deep-Sea Bed	深海底鉱物資源の揚鉱理論
d6-2	Analysis of Heat Transfer by Impinging Jet	衝突噴流による熱伝達解析
d6-3	Numerical Simulation of Working Processes	数値加工プロセス
d6-4	Behaviour of Liquid Droplets on Super-High Temperature Metal Surface	超高温金属表面における液滴の挙動
d6-5	Combined Simulation of Fluid Flow and Heat Transfer	流動・伝熱複合シミュレーション
d6-6	Prediction of Forming Limit in Sheet Metal Forming Processes	板材成形における成形限界予測
d7-1	Hydrometallurgical Treatment of Rare Earth Magnet Scrap	希土類磁石スクラップの湿式処理

d7-2	Liquid-liquid Extraction of Oxide Fines in Metal Salts Solutions	液-液抽出法による金属酸化物微粒子の回収に及ぼす金属イオンの影響
d7-3	Adsorption of Inorganic Depressants on Inherently Hydrophobic Mineral Surfaces	疎水性鉱物表面への無機抑制剤の吸着に関する研究
d7-4	Injection Smelting Operation for Environmentally Friendly Process	地球環境調和型吹き込み溶錬プロセスに関する基礎的研究
d7-5	Electrochemical Processing for Compound Semiconductor Solar Cell	化合物半導体太陽電池の電気化学プロセッシング
d7-6	Non-equilibrium Electrochemical Interfacial Phenomena in Space Station	宇宙ステーションにおける非平衡電気化学界面現象に関する基礎的研究
d8-1	NMR study of quantum spin-gap in low dimensional spin system	低次元スピン系における量子スピギャップの核磁気共鳴
d8-2	NMR Study of Magnetic Frustration	フラストレートするスピン系における核磁気共鳴
d9-1	R&D of Advanced Reduced-Activation Materials	先進低放射化材料の開発及び基礎研究
d9-2	Ceramic Composite Materials for Advanced Energy Systems	セラミクス系複合材料の開発と先進エネルギーシステムへの応用
d9-3	Physics and Irradiation Effects in Energy Conversion Materials	エネルギー変換材料の照射効果と物理
d9-4	Small Specimen Testing Technologies for Energy Materials Research	微小試験片による材料強度特性評価法の研究
d9-5	Joining of Materials for Nuclear Energy Systems	先進核融合・原子力材料等の接合の科学
d9-6	Fundamental Processes of Irradiation Creep	粒子線場における静的塑性変形挙動基礎過程の研究

B. Original Articles

The mark (*) indicates that the work was financially supported by Grant-in-Aid for Scientific Research, Ministry of Education, Science, Sports and Culture, Japan.

B. 研究発表

題目左肩の*印は、文部省科学研究費補助金による研究であることを示す。

Chapter 2

Original Articles

I Department of Socio-Environmental Energy Science

(エネルギー社会・環境科学専攻)

- 1: * **Study of magnetoresistance in nano-structured Co-Ag alloy produced by mechanical alloying**

K.Yasuna, A.Otsuki, K.N.Ishihara, and P.H.Shingu

Materials Science Forum Vols.235-238 (1997) pp.823-830

Nan-structures of Co-Ag alloys produced by mechanical alloying(MA) have been investigated by using magnetoresistance measurements and transmission electron microscopy(TEM). Nanometer-ordered mixtures of Co and Ag crystalline have been produced by means of a vibratory ball milling. For $\text{Co}_{30}\text{Ag}_{70}$ at the applied field of 14kOe at 77K, resistivity change, $\Delta\rho$ is $1.6\mu\Omega\text{cm}$, which results in $\Delta\rho/\rho$ of 7 %. Subsequent annealing at 523-673K increases $\Delta\rho/\rho$ to 12 % because of the decrease in the sample resistivity, ρ . TEM observation and magnetization measurement show the mechanically alloyed Co-Ag to consist of nanometer-size Co particles embedded in Ag matrix.

- 2: * **Nano-scale Metal Multilayers Produced by Repeated Press-Rolling**

P.H.Shingu, K.Yasuna, K.N.Ishihara, A.Otsuki, and M.Terauchi

Materials Science Forum Vol.235-238 (1997) pp.35-40

Multilayer structured alloys which have the layer thickness less than 10nm have been produced by the application of repeated pressing and rolling to the initially macroscopically thick layered sample. The

TEM observation of a Ag/Fe sample revealed a regular alternate lamination of Ag and Fe with the later thickness in the range of 10nm. The measured electrical resistivity showed a large dependence on the applied magnetic field which is characteristic to the composite structure of magnetic and non-magnetic metal in the thickness range of nanometers.

3: * Solid Solution Formation in the $\text{Al}_2\text{O}_3\text{-Cr}_2\text{O}_3$ System Assisted by Ball Milling

S.D.de la Torre, K.N.Ishihara, P.H.Shingu

Ceramic Transactions, Vol.79, 1996, 155-162

Complete solid solubility in the alumina-chromia system can only be reached thermodynamically by heating up both oxides to temperatures near their melting points, immediately followed by its quenching. In this work their partial solid solution is obtained at room temperature by means of high energy ball milling.

4: * Structural changes during low energy ball milling in the Al-Ni system

R.Maric, K.N.Ishihara, P.H.Shingu

Journal of Materials Science Letters, Vols.15 (1996) pp.1180-1183

We have shown that the formation of NiAl during ball milling mechanical alloying of the elemental powders occurred either by an explosive reaction, when all the particles reacted at the same time, or by a gradual explosion in individual grains. The interrupted milling in the early stage of the milling process and the easy oxidation that occurred just after the lamellar structure formation led to the first kind of reaction. In the second case, continuous milling after the formation of lamellae and the later interruption of the milling process did not lead to an abrupt explosion, and a reaction occurred by an explosion in individual grains when the lamellae reached the critical lamellar thickness of about 100nm. The magnetization measurement showed that in this case the rate of NiAl formation was not affected by the milling atmosphere or by the performing temperature.

5: * Solid state reaction between powders and foils by low-energy ball milling

Kwang-Min Lee, P.H.Shingu

Journal of Alloys and Compounds 241 (1996) 153-159

Thin metallic titanium foil was used instead of titanium powders in Al-Ti alloy to check the possibility whether bulk materials could be applied to mechanical alloying (MA) processing for overcoming material limitations. On the basis of the results of microstructural evolution and structure examination by X-ray analysis, the final MA powders in the powder-foil system of an Al-Ti alloy exhibit structures almost identical to those in the powder-powder systems. The low-energy ball milling processing needed to produce an ultrafine dispersion of fractured titanium particles in aluminum powder particles was found to be reached after a milling time of 200 h.

6: * Nanocrystalline metals prepared by low energy ball milling

Oleszak, D.; Shingu, P.H.

Journal of Applied Physics, Vol.79 (1996) pp.2975-80

The influence of low energy ball milling on the crystallite size, lattice strain, and storage of deformation energies of elemental metal powders is studied. The formation of nanosized grains (5-25 nm) and enhancement of lattice strain up to 0.4% is found. Excess enthalpies of up to 25% of the heat of fusion are reached.

7: * Structure Change of Graphite by Ball Milling

ミリングによる黒鉛の構造変化

Tanaka Takeo, Hiromi Yoshikawa, Takahiro Kaneyoshi, Myneyuki Motoyama, Keiichi N. Ishihara and Paul Hideo Shingu

Journal of the Japan Society of Powder and Powder Metallurgy, Vol.43 (1996) pp.742-747

粉体および粉末冶金、第43巻 (1996) pp.742-747

Ball-milling of graphite powder was performed by the use of a stainless steel ball-mill and an agate ball-mill. The crystal structure of the ground graphite was studied by transmission electron microscopy and X-ray diffractometry. A spectrometric approach to the change of structure during the milling process was also carried out by the carbon $K\alpha$ X-ray-emission band spectroscopy (XES). The carbon $K\alpha$ XES spectra were compared with those of carbon materials such as ball-milled diamond powder, *i*-diamond film and amorphous carbon powder. In the case of the stainless steel ball milling, microcrystalline and/or onion-like structure were formed. The XES spectra suggested that sp^3 hybrid orbital was formed after 2000h of milling. While, in the case of an agate ball-milling, it was suggested that the $2p$ orbital became narrower as a result of further finely-ground pulverization of graphite crystallite after 1750h of milling.

8: * Amorphous Fe-Al Alloys Obtained by Mechanical Alloying**OLESZAK D; SHINGU PH**

MATERIALS SCIENCE FORUM, Vol.235-8 (1997) p.91-96

The amorphization processes by mechanical alloying in the Fe-Al system have been studied for several compositions, including the ones corresponding to equilibrium FeAl_2 , $\text{Fe}_2\text{Al}_{15}$ and FeAl_3 intermetallic compounds. Mixtures of pure crystalline metal powders containing from 60 to 85 at.% Al and low energy ball milling have been applied for alloys synthesis. X-ray diffraction, differential scanning calorimetry and transmission electron microscopy were utilized to monitor the structural and phase transformations through different stages of milling. For all alloys studied mechanical alloying resulted in an amorphous structure formation. In equilibrium conditions the stable intermetallic compounds exist in this composition range, however, their formation by solid state reaction has been kinetically suppressed and an amorphous phase appeared. Heating the samples in the DSC resulted in the crystallization of the synthesised amorphous alloys and equilibrium intermetallic compounds appeared. However, for Fe- 60 and 75 at.% Al alloys, the phases corresponding to a lower Al content were only detected, i.e. FeAl and $\text{Fe}_2\text{Al}_{15}$, respectively. The formation of metastable FeAl_6 compound at the first stage of the crystallization process of Fe-85 at.% Al alloy has been observed.

9: * Stored Energy and Electromotive-force of Mechanically Milled Copper**A.Otsuki, P.H.Shingu and K.N.Ishihara**

Material Science Forum, Vol.235-238 (1997) pp.929-953

The electromotive-force (EMF) of mechanically milled copper relative to the annealed copper was measured by using a solid state super ionic conductive cell at 30 degrees C. The measured EMF values reached -19mV after 100 h milling. This value corresponds to an excess free energy of 1.8 kJ/mol for the milled Cu powders relative to well annealed Cu. The enthalpy released from stored energy due to annealing measured by DSC was larger than the free energy change with the same annealing measured by EMF.

10: * Wood-Inorganic Composites Prepared by Sol-Gel Process V. Fire-resisting properties of the $\text{SiO}_2\text{-P}_2\text{O}_5\text{-B}_2\text{O}_3$ wood-inorganic composites.**Hisashi Miyafuji, Shiro Saka**

Mokuzai Gakkaishi 42(1) 74-80, 1996

A study on the wood-inorganic composites prepared by the sol-gel process indicated that an inorganic modification of wood with SiO₂ gels from tetraethoxysilane (TEOS) can improve its properties. However, the SiO₂ composites still have the potential to be improved further. The binary and ternary systems to prepare the SiO₂ composites were thus studied by adding trimethylphosphite or/and trimethylborate to a reaction system of TEOS/ EtOH/ acetic acid. The obtained SiO₂-P₂O₅, SiO₂-B₂O₃, and SiO₂-P₂O₅-B₂O₃ wood-inorganic composites clearly indicated enhanced fire-resistant properties with relatively low weight percent gain, compared with SiO₂ composites.

11: * Wood-Inorganic Composites Prepared by Sol-Gel Process VI. Effects of a property-enhancer on fire-resistance in SiO₂-P₂O₅ and SiO₂-B₂O₃ wood-inorganic composites.

Shiro Saka, Fumie Tanno

Mokuzai Gakkaishi 42(1) 81-86, 1996

The SiO₂-P₂O₅ and SiO₂-B₂O₃ wood- inorganic composites prepared with trimethylphosphite or trimethylborate in a reaction system of tetraethoxysilane/EtOH/ acetic acid were evaluated on their thermal properties, and their stability of the gels was tested against weathering. Resultingly, P₂O₅ and B₂O₃ gels were found to have leached out from the composites. A property-enhancers, such as 2-heptadecafluorooctylethyltrimethoxysilane (HFOETMOS) and decyltrimethoxysilane (DTMOS) could, however, maintain the fire-resisting properties, particularly in the SiO₂-P₂O₅ composites, due to their water-repellent properties. Additionally, the property-enhancer containing fluorine, as in HFOETMOS could even improve the fire-resisting properties of the binary composites.

12: * Thermal Properties of Cellulose Triacetate as Prepared from Low-grade Dissolving Pulp.

低純度溶解パルプより調製した三酢酸セルロースの熱特性

Shiro Saka, Kosuke Ohmae

J. Appl. Polm. Sci. 62, 1003-1010, 1996

As cellulose triacetate is prepared from low-grade dissolving pulp, a considerable amount of the insoluble residue was present in the acetylation medium of the acetic acid/ acetic anhydride/ sulfuric acid system. To reduce the insoluble residues, a solvent, such as nitromethane, nitroethane, or dichloroacetic acid, added to the acetylation medium was found to be very effective for its reduction. By exploring the optimum conditions for acetylation with these solvents, nitromethane added and dichloroacetic acid

added systems with solvent/acetic acid = 3/7(v/v) were found to have a particularly high transmittance at $\lambda = 670\text{nm}$ in their acetylation solution with a low insoluble residue. The obtained acetates revealed good thermal properties similar to that from high-grade dissolving pulps. Therefore, a high quality cellulose triacetate can be manufactured from acetylation systems with even low-grade dissolving pulps with an appropriate solvent added.

13: O-Benzylolation of Phloroglucinol via Phloroglucinol Triacetate

Haruo Kawamoto, Fumiaki Nakatsubo*, Koji Murakami* *(Faculty of Agriculture)

Synthetic Communications, 26(3), pp.531-534, 1996

Benzyl ether is a popular protecting group of phenolic hydroxyl groups in organic synthesis, because this ether is stable under basic or mildly acidic conditions but is readily cleaved by hydrogenolysis. However, benzylation of phenols with high electron-density such as phloroglucinol, gives a mixture of O- and C-benzylated products, which lead to a low yield of the O-benzylated products, and it is difficult to separate them by chromatographic techniques. In this paper, new O-benzylating method of phloroglucinol using phloroglucinol triacetate as an intermediate is presented.

14: Stoichiometric Studies of Tannin-Protein Co-Precipitation

Haruo Kawamoto, Fumiaki Nakatsubo*, Koji Murakami* *(Faculty of Agriculture)

Phytochemistry, 41(5), pp.1427-1431, 1996

Co-precipitation of a series of galloylglucoses (hydrolysable tannin) with bovine serum albumin (BSA) was studied stoichiometrically by determining both galloylglucoses and BSA in the precipitates using high-performance liquid chromatography. The following results were obtained; BSA precipitating ability is effected mainly by the number of the galloyl groups and by the position of the galloyl group in the galloylglucose molecule (penta- > tetra- > 2,3,6-tri- > 2,3,4-tri- >> di- >> monogalloylglucose); precipitated BSA increases linearly with an increase in the number of the galloyl groups bound on BSA in the precipitates; BSA precipitating abilities of the galloylglucoses are closely related to their relative affinity for BSA. These results suggest two stages mechanism, that is, initial complexation of galloylglucose with BSA and subsequent precipitation, as a mechanism of the co-precipitation.

15: Convenient Synthesis of Galloylglucoses

Haruo Kawamoto, Sumi Iwatsuru*, Fumiaki Nakatsubo*, Koji Murakami* *(Faculty of Agriculture)

Mokuzai Gakkaisahi, 42(9), pp.868-874, 1996

A high-yield synthesis of galloylglucoses was made by effective galloylation with tri-O-benzylgalloyl chloride and 4-N,N-dimethylaminopyridine (DMAP). A series of galloylglucoses having one to five galloyl groups in a molecule were prepared by this method with more than a 41.3% overall yield. These compounds are considered to be suitable model compounds for the stoichiometric investigation of tannin properties such as protein-precipitation, interaction with metal ions, and so forth.

16: Experimental Study on the Operators' Cognitive Behavior Analysis for the Plant Anomaly Diagnosis

プラント異常診断に関する運転員の認知挙動の統合的解析に関する実験研究

Makoto TAKAHASHI, Osamu KUBO, Akira YASUTA, Hidekazu YOSHIKAWA, Kazunori SASAKI*, Toru ITOH*, Masayuki MATSUMIYA*, Takeharu SAKAUE*, Kazuhiro KIYOKAWA, Akira HASEGAWA** *(Mitsubishi Elec. Corp.) ** (Nucl. Power Eng. Corp.)**

Journal of Atomic Energy Society of Japan, Vol.38, No.9, pp.776-786. (1996)

日本原子力学会誌、V o l . 3 8 , N o . 9 , 7 7 6 ~ 7 8 6 頁 (1 9 9 6)

In this paper, a method of human cognitive state estimation based on physiological measures has been applied to the analysis of cognitive behavior during anomaly diagnosis observed with nuclear power plant simulator. This method has also been combined with the conventional experimental protocol such as operational sequence and questionnaire results. The simulator experiments have been performed using plant experts and the results demonstrate that the cognitive state estimation method can be an effective way for understanding cognitive behavior during the anomaly diagnosis of the nuclear power plant. It has also been shown from the results that the combined use of the human cognitive state estimation and the conventional experimental protocol can provide effective information in decreasing the ambiguity of the analysis results.(in Japanese)

17: Cognitive Process in Plant Diagnosis Using an Operator Cognitive Model

運転員認知モデルを用いたプラント異常診断認知過程

Kazuo FURUTA*, Makoto TAKAHASHI, Hidekazu YOSHIKAWA, Kazunori SASAKI, Toru ITOH**, Masayuki MATSUMIYA**, Takeharu SAKAUE**, Kazuhiro KIYOKAWA***, Akira HASEGAWA*** *(Univ. of Tokyo), ** (Mitsubishi Elec. Corp.), *** (Nucl. Power Eng. Corp.)**

Journal of Atomic Energy Society of Japan, Vol.38, No.1, pp.65-74. (1996)

日本原子力学会誌、V o l . 3 8 , N o . 1 , 6 5 ~ 7 4 頁 (1 9 9 6)

An operator cognitive model has been constructed referring to Rasmussen's ladder model, and a simulation system of operator performance has been developed. Computer simulation was then performed to investigate subjects' behavior in a cognitive experiment concerning PWR nuclear power plant diagnosis. The knowledge bases used in the simulation were constructed from the interview to the subjects. Confidence on each hypothesis and performance history of operators were compared between the experiment and the simulation, and the simulation could well explain the behavior of the subjects in the results of event identification, confidence on the results, hypothesis conceived during diagnosis, and plant parameters observed, which indicates the validity of the operator model. The order of parameter observation, however, disagreed, and it has been clearly shown that knowledge on system configuration of the plant as well as the physical layout of interface should be considered.(in Japanese)

18: Development of Simulation Based Evaluation Support System for Man-Machine Interface Design: SEAMAID System

Takeshi NAKAGAWA*, **Yoshio NAKATANI***, **Hidekazu YOSHIKAWA**, **Makoto TAKAHASHI**, **Tomihiko FURUTA****, **Akira HASEGAWA**** *(Industrial Electronics & System Laboratory, Mitsubishi Electric Corporation) **(Institute of Human Factors, Nuclear Power Engineering Corporation)

Probabilistic Safety Assessment and Management 96, Volume 2, pp.1185-1190. (1996)

An integrated software system has been under development which aims at analyzing and evaluating the effectiveness of man-machine system design from the viewpoints of various human factors by simulating plant, man-machine interface and operator. In this paper, the configuration of a distributed simulation system is first introduced, followed by an explanation of how the operator simulator model is constructed. Also presented is an example of the operator simulator using the Petri net model. We have developed a prototype of the distributed simulation system, and the possibility of constructing a total system has been confirmed by a simulation using the developed prototype system.

19: Validating Physiological Measures for the Cognitive Behavior Analysis Using Neural Network

Makoto TAKAHASHI, **Osamu KUBO**, **Akira YASUTA**, **Hidekazu YOSHIKAWA**, **Kazunori SASAKI***, **Toru ITOH***, **Masayuki MATSUMIYA***, **Yoshinobu YAMANAKA***, **Kazuhiro KIYOKAWA****, **Akira HASEGAWA**** *(Research Institute of Industrial Systems, Mitsubishi Electric Co. Ltd.) **(Institute of Human Factors, Nuclear Power Engineering Corporation)

Proceedings NPIC & HMIT*96, Volume 2, pp.1147-1153. (1996)

Experimental study on the operators' cognitive activities was performed using nuclear power plant simulator. The specific feature of the present study is that the cognitive behavior of the operator during the interaction through the man-machine interface has been analyzed based on the diverse information; (1) Estimated cognitive state, (2) Estimated mental work load, (3) Operational sequence history, (4) Questionnaire and (5) Video record. Another point is that the information (1) and (2) were estimated based on the set of physiological measures using neural network as the tool for discrimination. In the present study, in which three subjects (domain experts) participated, it has been shown that the estimated cognitive state can provide useful information on the cognitive behavior during the diagnostic process. It has also been shown that the combined use of the above diverse information can be effective in order to examine the human mental activities.

20: Simulation Based MMI Evaluation Support System; SEAMAID System

Takashi NAKAGAWA*, **Yoshio NAKATANI***, **Hidekazu YOSHIKAWA**, **Makoto TAKAHASHI**, **Tomihiko FURUTA****, **Akira HASEGAWA**** *(Industrial electronics & system Lab. Mitsubishi Electric Corporation) ** (Institute of Human Factors, Nuclear Power Engineering Corporation)

Proceedings NPIC & HMIT 96, Volume 2, pp.1167-1172. (1996)

An integrated software system is under development which aims at analyzing and evaluating the effectiveness of man-machine system design from the viewpoints of various human factors. The scope of the system is control cabinets and operation procedures in nuclear power plants. Since the occurrence of human error depends on situations with interaction between man and machine, our system simulates the plant, man-machine interfaces and operator behavior in real time and creates virtual interaction between them. In this paper, the configuration of a distributed simulation system is first introduced, followed by an explanation of how the operator simulator model is constructed. Also presented is an example of the operator simulator using the Ptri net model. We have developed a prototype of the distributed simulation system, and the possibility of constructing a total system has been confirmed by a simulation using the developed prototype system.

21: Virtual Environment for Integrated Design Support (VINDS) for Conceptual Design of Advanced Reactor System

Hidekazu YOSHIKAWA, **Makoto TAKAHASHI**, **Takashi NAGAMATSU**, **Satoshi TAKEOKA**

Proceedings NPIC & HMIT 96, Volume 2, pp.1511-1518. (1996)

The conceptual design of a new type of reactor system requires a cooperative work by a group of experts from various fields such as neutronics, thermos-hydraulics and so on. In this respect, the integrated design support system on the Virtual Reality Environment (VRE) is proposed. The developed system provides a designer the features that are important for the better understanding of the objective system and for the cooperative work with other designers. Up to now, the developed system has the capability of the two major supporting functions: (i) visualize the objective system from its individual parts and retrieve the design specific information, and (ii) do the related engineering analysis by preparing input data and evaluating the computed output, through the VRE interface. The design target of the present work is space power reactor core as an example of advanced reactor system.

22: Study on Methodology of Evaluating Man-Machine System

Chaogui WANG*, Hidekazu YOSHIKAWA, Huanxing SHENG* *(Nuclear Power Institute of China (NPIC))

Proceedings of Cognitive Systems Engineering in Process Control: CSEPC 96, pp.20-25. (1996)

The analysis and evaluation of Man-Machine System (MMS) of nuclear power plants have been carried out from various viewpoints of human factors. This paper presents a practical approach for the evaluation of MMS with emphasis on the modeling of Man-Machine interaction under the condition of emergency events.

23: Analysis of Operator's Diagnostic Behavior and its Application to the Human Modeling

Makoto TAKAHASHI, Wei WU, Akira YASUTA, Hidekazu YOSHIKAWA, Yoshio NAKATANI*, Takashi NAKAGAWA* *(Industrial Electronics & System Laboratory, Mitsubishi Electric Corporation)

Proceedings of Cognitive Systems Engineering in Process Control: CSEPC 96, pp.26-33. (1996)

The cognitive behavior analysis is quite important to evaluate the effectiveness of the man-machine interface for huge, complex engineering systems. This paper presents a cognitive behavior analysis method based on a laboratory experiment using nuclear power plant simulator and experienced subjects and its application to the human modeling. The analysis is focused on the diagnosis process for plant anomaly. The cognitive behavior analysis was performed based on the Questionnaire Answers(QA) and operational sequence history(OSH) recorded during simulator runs. The results of cognitive behavior analysis of

three subjects using QAs and OSHs showed that diagnosis processes are successfully represented by the proposed analysis methods. The knowledge obtained from the analysis was utilized for the human modeling and represented on the computer. The results of numerical simulation demonstrated that the developed models are capable of representing individual diagnosis behavior properly.

24: A New VR-based CSCW Environment for Conceptual Design of A Space Power Reactor

Hidekazu YOSHIKAWA, Hiroshi SHIMODA, Makoto TAKAHASHI, Takashi NAGAMATSU, Satoshi TAKEOKA

Proceedings of Cognitive Systems Engineering in Process Control: CSEPC 96, pp.130-137. (1996)

The conceptual design of a space power reactor core requires a cooperative work by a group of experts from various fields. It is necessary to implement mechanisms to realize an effective computerized support system for the group activity by different engineers. We aimed at incorporating tasks into a workable human interface system based on virtual reality technology with the full usage of advanced information technology on 3D graphics, numerical calculation and AI processing. We also aimed at developing WWW-based design support system for the same work domain for higher level of flexibility in cooperative work using distributed computer systems.

25: Development of Machine-Maintenance Training System using Petri Net and Virtual Environment

Hirotake ISHII, Ken-ichiro KASHIWA, Tetsuo TEZUKA, Hidekazu YOSHIKAWA

Proceedings of Cognitive Systems Engineering in Process Control: CSEPC 96, pp.138-143. (1996)

In this study, VR-based machine-maintenance training system was developed. The salient feature of this study is the utilization of Petri net for representing the procedures of machine assembly and disassembly in virtual environment. The utilization of the Petri net model realized the environment where the trainee can behave freely, and also made it possible to equip the system with the function that shows the next action to do to the trainee whenever he wants. The size of Petri net, however, usually becomes very large. Therefore, the support system for constructing Petri net was developed so that a large Petri net can be constructed easily. Through the application to a check value, the effectiveness of using Petri net for the VR-based machine-maintenance training system was demonstrated.

26: Simulation based evaluation of Man-Machine Interface in power plants

Takashi NAKAGAWA*, **Yoshio NAKATANI***, **Hidekazu YOSHIKAWA**, **Makoto TAKAHASHI**, **Tomihiko FURUTA****, **Akira HASEGAWA**** *(Industrial Electronics & System Laboratory, Mitsubishi Electric Corp.) ***(Institute of Human Factors, Nuclear Power Engineering Corp.)

Proceedings of Cognitive Systems Engineering in Process Control: CSEPC 96, pp.26-33. (1996)

An integrated software system has been under development which aims at analyzing and evaluating the effectiveness of man-machine system design from the viewpoints of various human factors by simulating plant, man-machine interface and operator. In this paper, the configuration of this software system which is named SEAMAID is first introduced, followed by an explanation of how the operator simulator model is constructed. Also presented is an example of the operator simulator using the Petri net model. We developed a prototype of the SEAMAID system, and the possibility of constructing a total system was confirmed by a simulation using prototype system. A method of human error analysis is also described.

27: Virtual Environment for Integrated Design Support (VINDS) for Conceptual Design of a Space Power Reactor Core

Hidekazu YOSHIKAWA, **Makoto TAKAHASHI**, **Takashi NAGAMATSU**, **Satoshi TAKEOKA**

Proceedings of International Conference on the Physics of Reactors: PHYSOR 96, Volume 1, pp.B-92 - B-101(1996)

The conceptual design of nuclear reactor requires a cooperative work by a group of experts from various fields. It is necessary to implement mechanisms to realize an effective computerized support system for the group activity by different engineers. We aimed at incorporating relevant tasks into a workable human interface system based on virtual reality technology with the full usage of advanced information technology on 3D graphics, numerical calculation and AI processing. To help a designer in performing engineering analysis simulation, the proposed idea by VINDS system will contribute to the cooperative work.

28: * Evaluation of the Relationship between Energy Supply-Demand System and Information Technology,

Tetsuo Tezuka, **Hidekazu Yoshikawa**

Proceedings of IEW/JSER'96 (Joint IEW/JSER International Conference on Energy, Economy and Environment), Osaka, Japan, pp.295-300 (1996)

The future of energy system in the world is quite uncertain due to the limited energy resources and also to the global environmental problems, and, therefore, we need a new concept about energy supply-demand system. The autonomous decentralized system concept has been attracting much attention. This concept can be applied to energy supply-demand system, that is, autonomous decentralized energy system (AUDES), which is supported by the recent technological development in dispersed energy supply. Although one of its disadvantages is that the participants in the system should often get the various sorts of information about the situation of the system, the remarkable development in information technology is expected to change the evaluation of decentralized energy system. This paper shows how the development in information technology improves the behavior of AUDES by using a simulation model approach.

29: * A Study on the Optimal Power Plant Planning with Photovoltaic Generation and Heat Storage

Hajime Kita*, Tetsuo Tezuka, Yoshikazu Nishikawa*
***(Faculty of Engineering, Kyoto University)**

Proceedings of IEW/JSER'96 (Joint IEW/JSER International Conference on Energy, Economy and Environment), Osaka, Japan, pp.395-400 (1996)

Electric power systems are now facing a difficult problem that they have to supply electricity to growing demand under severe constraints on resources and environment. To cope with this problem, it is required to integrate various techniques of generating electricity and controlling the demand. In this paper, the authors discuss impacts of two key devices in future power systems on the optimal power plant planning. One is the photovoltaic (PV) power generation, and the other is utilization of heat storage for air conditioning. These two devices have complicated impacts on the power plant planning. That is, they are mutually substitutive in the sense that the both devices contribute to reduction of the peak loads of the power systems. At the same time, it is also expected that by operating the storage systems cooperatively to absorb the fluctuation of output of the PV power plants, they will work complementarily. In this paper, these impacts are analyzed with an optimal power planning model of a linear programming type taking Kinki District of Japan in 2010 as a studied case.

30: * Methods of Determining the Introduction Limits of Dispersed Generation Systems in a Distribution System

配電システムの電圧管理面から見た分散型電源の導入限界量決定方法

Jae-eon Kim*, Hajime Kita*, Tetsuo Tezuka, Yoshikazu Nishikawa*
***(Faculty of Engineering, Kyoto University)**

Trans. IEE of Japan, Vol.116-B, No.12, pp.1461-1469 (1996)

電気学会論文誌 B, Vol.116-B, No.12, pp.1461-1469 (1996)

Recently, there has been growing interest in utilizing DGS (Dispersed Generation System) to integrate various generation resources and to meet the changing electricity demand. In the long term, as much more introduction of both small and large capacity DGSs into the distribution systems is expected, complete integration of this new technology into the utility system will bring about changes of design strategy and structural facility of the system. Thus, a study is necessary to determine the introduction limit of DGSs into the traditional distribution system without viewpoint of voltage regulation in the distribution system using LRT (Load-Ratio control Transformer) and LDC (Line Drop Compensator) as the control scheme. (in Japanese)

31: * Development of an Analysis Support System for Man-Machine System Design Information

H. YOSHIKAWA T. NAKAGAWA*, Y. NAKATANI*, T. FURUTA, A. HASEGAWA**** *(Industrial Electronics and Systems Development Laboratory, Mitsubishi Electric Corporation) **(Institute of Human Factors, Nuclear Power Engineering Corporation)

Control Engineering Practice, Vol.5, No.3, pp.417-425.

An integrated software system has been under development, aimed at analyzing and evaluating the effectiveness of man-machine system design, by computer simulations from various viewpoints of human factors. The target software system consists of two functional blocks; (i) a distributed simulation system for man-machine interaction at the man-machine interface, and (ii) a man-machine design information evaluation system. In this paper, the configuration of the distributed simulation system is first introduced, followed by an explanation of how the operator simulator model is organized, using a Petri-net model. An example simulation is also presented for the man-machine interaction at a PWR LOCA accident using the developed system.

32: * The Size Distribution and Composition of the Atmospheric Aerosol at a Rural and nearby Urban Location

Helmuth Horvath*, Mikio Kasahara, Peter Pesava*
*(University of Vienna)

J. Aerosol Science, Vol.27, pp.417-435, 1996

At a suburban location near Vienna and in the center of Vienna the aerosol was sampled with a 10 stage rotating cascade impactor classifying of the aerosol particle size between 15nm and 16 μ m. Gravimetric,

light absorption and PIXE analysis have been performed for all samples. The light absorption analysis also gives the concentration of black carbon, the PIXE analysis yielded concentrations of 15 elements such as Si, S, K, Ca, Fe, Zn and Pb. The mass size distribution of the aerosol for most of the elements had two modes. One peak occurred between 0.2 and 0.8 μm , the coarse particles had a slight peak usually above 3 μm . The total mass of the submicrometer particles was more than half of the total mass, except for calcium and iron. Little difference between the mass of the submicrometer particles at the two locations was found, except for Ca, Pb and Black carbon. The particles were generally larger at the suburban location. The light absorbing particles mostly had only one peak at a diameter of 0.2 μm , thus being smaller than other particles. Soot at the suburban location was a factor of 2 less and slightly larger than at the urban site. The similarity of the size distribution for almost all elements between the urban and the suburban location, as well as similarities to the arctic haze and the aerosol in Northern Europe suggests that the aerosol predominately originates from non-local sources and might be considered the central and north European average aerosol. On a day-to-day basis the aerosol shows a very high variability.

33: * Characterization of Atmospheric Aerosols Separated by Particle Size and Water Solubility Using PIXE Analysis

Mikio Kasahara, Jeong Ho Park*, Kouhei Yamamoto
***(Graduate School of Engineering)**

Nuclear Instruments and Methods, Vol.B109/110, pp.471-475, 1996

The elemental characteristics of atmospheric aerosols were investigated as functions of particle size and water solubility. Atmospheric aerosols were sampled with a 8 stage Andersen air sampler permitting classification of the aerosol particles size between aerodynamic diameters of 0.46 and 50 μm . Collected aerosol particles were extracted by ultra pure water and filtered to be separated into soluble and insoluble components. The concentrations of 15 elements in both components were determined by PIXE analysis. In general, the mass size distribution of particulate matter was represented as a bimodal distribution. The mass size distribution of S, Zn and Pb skewed to the smaller size range and those of Si, Ca and Ti skewed to the larger size range. They had roughly one peak in the fine and coarse particle region, respectively. On the other hand, the mass size distribution of K, V, Cr, Mn, Ni, Cu and Br were represented as the bimodal distribution. Fe, Ti and Si in the aerosol particles extracted into pure water are existing in high insoluble state. Conversely, almost the whole of S and Cl is dissolved in water.

34: * Soluble and Insoluble Components of Air Pollutants Scavenged by Rain Water

Mikio Kasahara, Hiroshi Ogiwara*, Kouhei Yamamoto
***(Graduate School of Engineering)**

Nuclear Instruments and Methods, Vol.B118, pp.400-402, 1996

In order to study the scavenging mechanism as a final goal, the characteristics of chemical components in rain water were examined as a function of the amount of rainfall. The rain drops were collected with each 0.1mm rainfall from the beginning of rain. Rain water was separated into the soluble and insoluble components and the concentrations of 15 elements in both components were determined by the PIXE analysis. The elemental concentrations decreased quickly till about 0.5mm of rainfall and then gradually decreased as the rainfall continued. Fe, Ti and Si in the aerosol particles caught in rain water are in high insoluble state. On the contrary, almost all S and Cl are dissolved in rain water.

35: Ion Nucleation and Growth of Sulfuric Acid Water Aerosol Particles: Application of general dynamic equation

Masayuki Itoh*, Susumu Tohno

***(Doshisha University)**

Nucleation and Atmospheric Aerosols 1996, pp38-41, Pergamon Press,1996

The time evolution of size distribution function was calculated with the general dynamic equation regarding ion-induced nucleation of sulfuric-acid water system. The ion-induced nucleation was still effective in low relative humidity, and even after the initial stage of time evolution, the nucleation was dominant process as well as the coagulation process. However, the condensation process was not important in thin vapor condition.

36: Data Reduction on the Measurement of the Size Distribution of Atmospheric Aerosols by a Low-Pressure Cascade Impactor

低圧インパクターを用いた大気エアロゾル粒子の粒度分布測定におけるデータ処理

Susumu Tohno, Jeong-Ho Park*, Mikio Kasahara

***(Graduate School of Engineering)**

J. Aerosol Res., Jpn., Vol.11, No.2, pp.137-144, 1996

エアロゾル研究, Vol.11, No.2, pp. 137-144, 1996

Twomey's nonlinear iteration method was applied to retrieve the size distribution of atmospheric aerosols from data obtained by an Andersen low-pressure impactor. Effects of some factors on the inversion results were investigated using numerically generated data for unimodal and bimodal lognormal functions. The p -th power of response function was adopted as a weighting function and a value of 0.7 was selected for the inversion of data in most cases. Smoothed initial distribution with treatment of the ends of the distribution gave good results in case of the distribution showing a peak near the first stage of the impactor, while uniform initial guess resulted in an oscillatory distribution. We proposed a new stopping criterion based on experimental errors which represent random errors in mass measurement and

sample fluctuation. The criterion is useful for inverting the data involving random errors. The procedure was also applied to estimate the size distribution for ambient aerosol samples. (in Japanese)

37: Production of Contact-Free Nanoparticles by Aerosol Process: Dependence of particle size on gas pressure

Susumu Tohno, Masayuki Itoh*, Shigeo Aono*, Hiroshi Takano*

* (Doshisha University)

J. Colloid Interf. Sci., Vol.180, pp.574-577, 1996

Experiments were made to determine the dependence of the size of contact-free nanoparticles produced by aerosol process on gas pressure. The particles were collected as contact-free dispersoids in hexane with a cationic surfactant, and the geometric mean sizes were below 10nm in diameter. It was found that the size increased linearly as the pressure was raised from 0.04 to 1.43kPa for Ag, Bi, Cu and Te. Similar slopes were obtained for the linear function between size and gas pressure except for Te.

38: Growth of Nanophase Particles in Free-Molecular Regime and Its Dependence on Medium Gas Pressure

Shigeo Aono*, Masayuki Itoh*, Hiroshi Takano*, Susumu Tohno

*(Doshisha University)

Surf. Rev. Lett., Vol.3, No.1, pp.45-47, 1996

A clear linear relationship between the gas pressure and the diameter of nanophase particles generated from the modified gas-flow/cold-trap method was obtained for several kinds of metallic particles. This simple linear relationship was also verified by numerical simulation using a Monte-Carlo method on the diffusion and coagulation of clusters in a free-molecular regime.

39: Production of Binary Nanoparticles (BiCu, BiTe and CdS) by Aerosol Process: Treatment for isolation and concentration

Susumu Tohno, Masayuki Itoh*, Keisaku Kimura**

*(Doshisha University), **(Himeji Institute of Technology)

Surf. Rev. Lett., Vol.3, No.1, pp.63-69, 1996

We extended the modified gas-flow/cold-trap method to produce high-density and contact-free binary nanoparticles containing bismuth (BiCu, BiTe) and CdS particles. Binary nanoparticles were collected as stable dispersoids in hexane with a cationic surfactant. The electron micrographs showed individual clusters were separated from each other by surfactant thin layer and do not contact directly any other clusters even after the concentration process. The binary particles containing bismuth gave diffuse halo diffraction patterns characteristic of an amorphous state. Optical effects due to size quantization were observed for the CdS particles.

40: EXAFS Study on the Noncrystalline Structure of Binary Component (BiCu, BiTe) Nanophase Particles

Masayuki Itoh*, **Susumu Tohno**, **Motoaki Adachi****, **Keisaku Kimura*****

(Doshisha University)**, * (University of Osaka Prefecture)**, ***** (Himeji Institute of Technology)**

Surf. Rev. Lett., Vol.3, No.1, pp.71-74, 1996

From the viewpoint of the size dependence of the melting point of small particles, the microstructure of nanophase particles were investigated with EXAFS. Two EXAFS spectrum from BiCu and BiTe nanophase particles indicated the specific line shape due to the disorder of atomic structure of the particles, which was not found for corresponding bulk materials. This fact means that a nanophase particle has not only soft surface due to size effect but also a liquid-like structure caused by a thermal fluctuation.

41: Two-Layer Box Model for Dense Gas Spill Considering Evaporation Effect

漏洩した Dense Gas の蒸発の影響を考慮した二層ボックスモデル

Kaoru NISHIDA*, **Eiichirou ITO***, **Koichi TAKAGI***, **Kouhei YAMAMOTO**

***(Graduate School of Engineering)**

J. Jpn. Soc. Atmos. Environ., Vol.31, No.3, pp.111-121, 1996

大気環境学会誌, Vol.31, No.3, pp.111-121, 1996

The main purpose of this study is to examine the phenomena when hazardous dense gases, such as ammonia gas or LNG, are spilled into the atmosphere from a pressurized storage tank. This study is significant to develop an accidental risk assessment method. The characteristics of gases released from the pressurized tank is a mixture cloud of gaseousness and droplets. In previous published papers, the effect of evaporation of liquid droplets has never been examined. In this paper, we propose a two layer box model in order to predict a concentration considering this effect. This model is useful for estimating concentration of dense gas released instantaneously from a pressurized tank. Furthermore, for continuous

dense gas spill, we calculated the average concentration at the downwind distance, treating the two box model like gaussian puff models. Also, we improved it to be able to

42: * Application of NR for Research in Electrochemical Systems

**Masahiro Kamata*, Takao Esaka*, Shigenori Fujine, Kenji Yoneda, Keiji Kanda *(Tot-
tori Univ.)**

Nucl. Instru. and Methods in Phys. Research A, Vol.377, pp.161-165, 1996

The neutron radiography (NR) technique has been applied to high temperature ion conducting materials such as $\text{Li}_{1.33}\text{Ti}_{1.67}\text{O}_4$ and $\text{Ca}_{0.95}\text{Li}_{0.1}\text{WO}_4$ in order to visualize the movement of lithium ions within the material. After electrolysis DC current was passed through these oxides prepared with different isotope ratios ($^6\text{Li}/^7\text{Li}$), a set of NR images was obtained which verified the lithium ion conduction in the oxides. It was also clearly shown that the transport number of lithium ions in such oxides can be accurately determined by digitizing and analyzing the NR images. In addition, some investigation was carried out using the NR technique to see the lithium distribution in a lithium battery before and after discharge. The results indicated that NR can be used to clarify the local discharging efficiency in a battery and/or to investigate the reversibility of lithium rechargeable batteries.

**43: * Human Melanoma Treated by Boron Neutron Capture Therapy : Comparison of
the Clinical Response with the Predicted Response**

Junichi Hiratsuka*, Hiroshi Fukuda, Tooru Kobayashi, Keiji Kanda, Chihiro
Honda***, Masamitsu Ichihashi***, Yutaka Mishima**** *(Kawasaki Medical School)
(Tohoku Univ.) * (Kobe Univ.) **** (Mishima Institute for Dermatological Re-
search)**

Radiation Medicine, Vol.14, pp.257-263, 1996

Purpose: A patient with malignant melanoma on the left foot was treated by thermal neutron capture therapy using ^{10}B -paraboronophenyl- alanine. We compared the actual (clinical) response with the predicted response estimated using our past experimental and clinical data, and discussed some problems to be overcome in the future. Conclusion: We concluded that the outcome of our calculated dose values agreed well with the clinical response and that their compatibility indicated considerable validity for our approach. However, there are still some problems - uncertainty concerning the ^{10}B concentration in tumor and skin, determination of the total absorbed dose, and a single curative dose for malignant melanoma - to be overcome with regard to clinical use of this therapy.

44: * **Studies on the Lithium Ion Conduction in $\text{Ca}_{0.95}\text{Li}_{0.10}\text{WO}_4$ using Cold Neutron Radiography**

Masahiro Kamata*, Takao Esaka*, Kazukuni Takami*, Shigeomi Takai*, Shigenori Fujine, Kenji Yoneda, Keiji Kanda *(Tottori Univ.)

Solid State Ionics, Vol.91, pp.303-306, 1996

Cold neutron radiography (CNR) was applied to study the lithium ion conduction in the substituted scheelite-type oxide of $\text{Ca}_{0.95}\text{Li}_{0.10}\text{WO}_4$. The lithium ion distribution profiles were obtained from a set of neutron radiography (NR) images of the electrolyzed oxides having different $^6\text{Li}/^7\text{Li}$ ratios. They showed that the lithium ion transport number of the oxide is 0.99, which coincided with the value derived from the EMF measurement of an oxygen gas concentration cell. Furthermore, they denoted that the lithium ion conduction was preferably ascribed to lithium ions in the interstitial sites.

45: * **Characteristics of the Kyoto University Lead Slowing-down Spectrometer (KULS) coupled to an Electron Linac**

Katsuhei Kobayashi, Shuji Yamamoto, Akihiro Yamanaka*, Yoshihiro Nakagome, Yoshiaki Fujita, Satoshi Kanazawa*, Itsuro Kimura* *(Dept.Nucl.Eng., Kyoto Univ.)

Nucl. Instru. and Methods in Phys. Research A, Vol.385, pp.145-156, 1997

A lead slowing-down spectrometer coupled to a 46 MeV electron linear accelerator (linac) was installed at Research Reactor Institute, Kyoto University(KURRI). The size of this Kyoto University Lead Slowing-down Spectrometer (KULS) is $1.5 \times 1.5 \times 1.5 \text{m}^3$, and it is covered with Cd sheets 0.5mm thick. One of the eleven experimental holes in the KULS is covered with 10 to 15cm thick bismuth layers to suppress high energy capture gamma-rays from lead. The characteristics of this KULS have been experimentally obtained and the results are compared with the predicted values by Monte Carlo calculations using the MCNP code. 1)The slowing-down constant K in the relation $E = K/t^2$ between the neutron slowing-down time t and energy E is $190 \pm 2 (\text{keV} \mu\text{s}^2)$ for the bismuth hole and $156 \pm 2 (\text{keV} \mu\text{s}^2)$ for an ordinary lead hole, respectively. The K values agree with the calculated ones. 2)The measured energy resolution $\Delta E/E$ at full-width-at-half-maximum (FWHM) was about 40% for both holes, while the calculated values were lower by about 10% than the measured ones in the relevant energy region. 3)The neutron energy spectrum from 0.01eV to 20MeV and the spatial distribution of neutrons in the KULS were measured by the foil activation method.

46: * A system for correlation measurement of fission fragments and prompt neutrons for thermal neutron induced fission

Katsuhisa Nishio*, Hideki Yamamoto*, Ikuo Kanno*, Itsuro Kimura*, Yoshihiro Nakagome *(Dept.Nucl.Eng., Kyoto Univ.)

Nucl. Instru. and Methods in Phys. Research A, Vol.385, pp.171-178, 1997

For the purpose of the correlation measurement of fission fragments and prompt neutrons for thermal neutron induced fission, a system consisting of two fragment detectors and a neutron detector was developed. In this system, one fission fragment was detected with a silicon surface barrier detector (SSBD) and the other with a specially designed parallel plate avalanche counter (PPAC). The PPAC had double structures, one for fast timing and the other for position detection. A prompt neutron emitted from a fragment with a specified mass was detected with an organic liquid scintillator (NE213) in this system. The SSBD supplied not only the energy signal of one fragment but also the start timing signal to the time-of-flight (TOF) measurements of the other fragment and the prompt neutron. We tried to carry out the fragment-neutron correlation measurement for $^{235}\text{U}(n_{th}, f)$ with this system, and succeeded in obtaining the neutron energy spectrum in the center-of-mass system and the neutron multiplicity depending on the fragment mass.

47: Bayesian Analysis of the Public Reliance on the Nuclear Development

原子力開発における信頼形成過程に関するベイズ的考察

Hiroshi Yamagata*, Keiji Kanda *(MITI)

J. At. Energy Soc. Japan, Vol.38, pp.683-688, 1996

日本原子力学会誌、第38号、第8巻、683頁-688頁、1996年

The sodium leak accident of MONJU, a fast breeder reactor that Power Reactor and Nuclear Fuel Development Corporation (PNC) has operated since 1995 in Japan, and PNC's management of the accident have been created the public distrust not only in the safety of MONJU but also in the nuclear development policy of Japan. In order to learn a lesson from these and to establish a relationship of mutual trust with the public, this paper simulates process of the public reliance in cases of an accident, no accident, a cover-up, and so on. In this paper the public reliance is defined as the conditional probability that the nuclear reactor is safe given the state of information that the public has. The conditional probability is estimated by using the Bayes' Theorem. The simulation shows that (1) we lose the public reliance by only one accident, recover it by a many-year safe operation, but never by a cover-up, and (2) the more information we open to the public, the better relationship of mutual trust with the public we would establish, especially in an early stage of operation. (in Japanese)

48: Procedures for the Medical Application of Research Reactors.**H. Nishihara, K. Kanda**

Cancer Neutron Capture Therapy, Plenum Press, New York. pp.257-260. 1996

Taking the Kyoto University Research Reactor (KUR) as an example, legal and other procedures for using research reactors for boron neutron capture therapy (BNCT) are discussed. At the Research Reactor Institute, Kyoto University, clinical trials are practiced in accordance with the "Provisional guideline Pertaining to Medical Irradiation by Accelerators and/or Reactors, Other than Defined by the Medical Service Act" of the Science Council of Japan.

49: Reply to Matoba's Comment on "Mean Reaction Length of Destruction and Production of Neutron"

中性子の消滅と生成の平均反応距離に関する的場氏の指摘に対して

Masatoshi Hayashi

J. At. Energy Soc. Jpn. Vol. 39, pp. 72-73, 1997

日本原子力学会誌 39巻、1号、72-73

The confusion for conventional mean fission length is discussed. The new understanding of mean fission length is proposed. (in Japanese)

50: Neutron Activation Analysis of Ivory of African Elephants**Takayuki Takeuchi, Yukihiro Nakano, Hiroko Koike* *(Kyushu Univ.)**

J. Radioanalytical and Nuclear Chemistry, Articles, Vol. 205, pp.301-309, 1996

Instrumental neutron analysis was applied to 61 ivory samples of which origin countries are known. 12 elements such as Br, Ca, Cl, Co, Cs, Fe, Mg, Mn, Na, Sc, Sr and Zn, were determined in all samples. The factor score of each sample was calculated for each factor by making use of principal component analysis in order to determine their origins. The results were compared with those by stable isotope analysis (C-13 and N-15).

51: Reactor Laboratory Course for Students Majoring in Nuclear Engineering with the Kyoto University Critical Assembly (KUCA)

Hideaki Nishihara, Seiji Shiroya, Keiji Kanda

Proceedings of the 10th Pacific Basin Nuclear Conference, Kobe, Japan October 20-25, 1996

With the use of the Kyoto University Critical Assembly (KUCA), joint reactor laboratory courses at graduate level are offered every summer since 1975 for nuclear engineering students of nine associated Japanese universities, in addition to a reactor laboratory course for Kyoto University undergraduate students. These are given for three weeks in summer (two weeks for the joint course and one week for the undergraduate course), and a total of 1,360 students have participated over the last 21 years. The joint course has been institutionalized with the background that it is extremely difficult for a single university in Japan to have her own research or training reactor. By their effort, the united faculty team of the joint course have been successful in giving effective, unique one-week courses. The result of a recent survey is given, which revealed and clarified the needs for these and similar reactor laboratory courses.

52: Influence of Photovoltaic Power Generation on Required Capacity for Load Frequency Control

H. Asano, K. Yajima, Y. Kaya

IEEE Trans. on Energy Conversion, Vol. 11, No. 1, pp188-193, 1996.

We developed a mathematical model to evaluate the impact of small (rooftop) photovoltaic (PV) power-generating stations on economic and performance factors for a larger scale power system, and applied to the Tokyo metropolitan area. We used solar radiation data from five local meteorological stations to estimate both the individual and aggregate contributions of the projected PV stations to the local power grid. We found that an electrical power system containing a 10% contribution from PV station would require a 2.5% increase in load frequency control (LFC) capacity over a conventional system. The break-even cost for PV power generation was found to be relatively high for contribution levels of less than 10%. Higher proportions of PV power generation gave lower break-even cost, but economic and LFC considerations imposed an upper limit of about 10% on PV contributions to the overall power systems.

53: Japan's Strategy in Technology Development for Mitigating Global Warming

Yoichi Kaya et al.

Energy Conversion Management, Vol.37, Nos.6-8, pp.679-684, 1996

Japan is a country much concerned with global environmental issues. This paper describes Japan's prospect on energy and CO₂ emission together with prosperity of other developed countries. Then the needs for developing long term innovative technologies are demonstrated with a few examples of technologies developed under MITI R&D program.

54: Japanese Strategy for Mitigating Global Warming

Yoichi Kaya

Keynote Speech at International Conference on Carbon Dioxide Removal -3, Boston, USA, Sept., 1996

This paper illustrates first what the government of Japan intends to do with a few official pledges on mitigating global warming, such as the action plan and the famous idea of New Earth 21 program, toward long term stabilization of CO₂ concentration in the air. In practice, however, there are a number of factors which may disturb realization of the targets envisaged in these plans. Limitation to advancement of further energy conservation, not only in industrial sectors but also in other sectors where individual consumers play key roles, is certainly serious. Another crucial factor is the nuclear power. Recent accident at the experimental FBR, Monju, has influenced the public acceptance of nuclear power very seriously, and the government is now at the stage of re-designing the future scenario of nuclear power, taking into account both the options in favor of nuclear and those of anti-nuclear. Nevertheless most of energy experts believe that nuclear power is safe and also economical enough to be maintained for the intermediate future at least in Japan so that strong policy measures are to be introduced to improve public acceptance of nuclear power. The second part of this paper describes the future of so called "new energy" which the government of Japan is eager to develop and also the limits to development of these "new energy". The third part is contributed to description of R&D of long term technological options and also difficulties in realizing these options. It is also worth noting that Japan, both government and industries, has much interest in CO₂ removal from flue gas of power plants and its disposal.

55: Natural Gas for Electricity and Cogeneration

Yoichi Kaya

IEA 3rd Gas Technology Conference, Berlin, Germany, Sept., 1996

The role of natural gas in electric power generation has been increasingly important due to its environmentally clean character and high flexibility in handling. This paper tries first of all to overview the

present status of natural gas use in power generation. The second part then deals with the status of cogeneration which differs widely in the world due to different climatic conditions. In some countries in Europe where large heat demand exists large scale cogeneration plants are used as essential part of electric power supply and main sources of heat supply in residential areas, while in Japan where plants are installed for providing power and heat to specific customers such as hotels and hospitals. There is a discussion in Japan about the role of cogeneration in comparison with that of the combination of large scale power plants and heat pumps. This paper tries to identify essential points of the discussion and suggest ways for cogeneration to improve its position in power and heat supplies. The final part intends to stress the importance of R&D and touch upon a few key technologies to be developed for better use of natural gas for power generation and cogeneration.

56: Development of a Three-Dimensional Core Dynamics Analysis Program for Commercial Boiling Water Reactors

Yasunori Bessho, Yuichiro Yoshimoto*, Osamu Yokomizo*, Ryutaro Yamashita,
Masami Ishikawa***, Akio Toba******

***(Hitachi, Ltd.), **(Hitachi Engineering Co., Ltd.), ***(Tokyo Electric Power Co.),
****(Toden Software, Inc.)**

Nuclear Technology, Vol.117, pp.281-292, 1996

Development and qualification results are described for a three-dimensional, time-domain core dynamics analysis program for commercial boiling water reactors (BWRs). The program allows analysis of the reactor core with a detailed mesh division, which eliminates calculational ambiguity in the nuclear-thermal-hydraulic stability analysis caused by reactor core division. During development, emphasis was placed on high calculational speed and large memory size as attained by the latest supercomputer technology. The program was verified to provide satisfactory results within reasonable computational time based on application analysis of stability and scram phenomena in a BWR-5 type plant.

II Department of Fundamental Energy Science

(エネルギー基礎科学専攻)

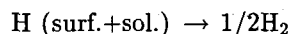
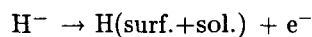
57: * Hydrogen Electrode Reaction in Molten Fluoride System

H. Qiao, T. Nohira* and Y. Ito

*(Graduate School of Engineering)

Proc. 6th Japan-China Bilateral Conference on Molten Salt Chemistry and Technology, 51-54(1996)

The electrode reaction of hydride ion on a molybdenum electrode in LiF-KF-NaF eutectic (Flinak) at 773 K was studied by gas analysis, cyclic voltammetry and chronopotentiometry. It was found that hydride ion is anodically oxidized around 0.5 V(vs. M^+/M) and pure hydrogen gas is generated according to the following reactions:



The diffusion coefficient, D^{H^-} , was estimated from the results of the cyclic voltammetry and chronopotentiometry as between 6×10^{-6} and $8 \times 10^{-6} \text{ cm}^2 \text{ s}^{-1}$.

58: * Hydrogen Electrode Reaction in Molten LiCl-KCl-LiH System

T. Nohira* and Y. Ito

*(Graduate School of Engineering)

Proc. 6th Japan-China Bilateral Conference on Molten Salt Chemistry and Technology, 55-58(1996)

By cyclic voltammetry, anodic oxidation reaction of hydride ion was found to be a reversible and a diffusion controlled process in molten LiCl-KCl-LiH systems. Anodic oxidation product was shown not to be completely soluble in the melt. The cyclic voltammograms for Ni showed that hydrogen was absorbed into the electrode. Diffusion coefficient of hydride ion was estimated as $5 \times 10^{-6} \text{ cm}^2 \text{ s}^{-1}$ by using cyclic voltammetry. Polarization characteristics for Mo and Ni showed that Ni has higher electrocatalytic activity than Mo for anodic reaction. Cathodic polarization curves for Mo and Ni gas electrodes showed that Ni is superior to Mo in cathodic reduction of hydrogen gas.

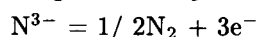
59: * Electrochemical Behavior of Nitrogen Gas and Nitride Ion in Molten Chloride System

T. Goto* and Y. Ito

***(Graduate School of Engineering)**

Proc. 6th Japan-China Bilateral Conference on Molten Salt Chemistry and Technology, 63-66(1996)

The electrochemical behavior of nitrogen gas and nitride ion in molten chloride system have been studied by cyclic voltammetry, chronopotentiometry, chronoamperometry and gas analysis. N₂ gas is cathodically reduced almost quantitatively to form N³⁻ ions. N³⁻ ions is anodically oxidized to form N₂ gas almost quantitatively on nickel electrode according to the following reaction:



This is a reversible one-step three-electron reaction governed by a simple diffusion-controlled charge transfer process. The diffusion coefficient of N³⁻ ions was estimated to be around $1 \times 10^{-5} \text{ cm}^2 \text{ s}^{-1}$ at 470 C.

60: Graphite Intercalation Compounds of Lanthanide Metals Prepared in Molten Chlorides

R. Hagiwara, M. Ito*, Y. Ito

***(Department of Nuclear Engineering)**

Carbon, Vol.34, No.12, pp.1591-1593, 1996

Graphite intercalation compounds of several lanthanide metal donors (Nd, Sm, Dy, Er and Yb) have been prepared by interacting graphite and metals in molten chlorides. These lanthanide metals are suspended in molten chlorides at lower than 400 C in the presence of their trichlorides via disproportionation equilibrium; $3\text{Ln(II)} = \text{Ln(0)} + 2\text{Ln(III)}$. In this condition, one can avoid the formation of carbides in the reaction product. The x-ray powder diffraction patterns for all the lanthanide GIC's prepared suggest they belong to the hexagonal EuC_6 -structure type.

61: The Electric Properties of Sintered Cermet as a Continuum Percolation Medium

Katsukuni Yoshida

Fractals, Vol. 4, pp. 175-180, 1996

The percolation process of the cluster structure in the sintered metal-insulator cermet fabricated by sintering has been investigated by observing the statistical behavior of the clusters of the constituent phase and the critical behavior of the electric conductivity and the dielectric constant. The percolation

threshold in terms of the volume fraction (f) of the metal phase is found to be $f_c=0.16$ and the critical exponents for the conductivity and the dielectric constant are determined as $t = 2$ for $f > f_c$ and $s = 0.6$ for $f < f_c$. Those values are extremely close to those obtained by computer simulation for the lattice percolation system. The relationship between the anisotropy of the cluster-structure and the directional anisotropy of the conductivity is well explained by the links-nodes-blobs model, which is originally based on the discrete percolation system. It follows from those results that the sintered media like the present composites realize a percolation system substantially equivalent to that of the discrete lattice systems.

62: * A Quenching Effect on the Grain Boundary in Sintered Ag-BPSCCO

Katsukuni Yoshida

Physica Status Solidi, Vol. (a)153, pp. K5-K7, 1996

To elucidate the impeding character of the grain boundary against the superconductivity in the bismuth-based high- T_c cuprates, we have investigated the effect of the quenching from the sintering temperature on the grain boundary in Ag-added and unadded Bi-Pb-Sr-Ca-Cu-O sintered samples consisting of 2223 phase of $T_c \approx 110\text{K}$. The quenching from the sintering temperature gives rise to considerable degradation of the superconductivity at the grain boundary in particular for the Ag-added case, as demonstrated by a large shift of the second stage appearing on the temperature-dependence curves of the resistivity and the diamagnetic susceptibility. This degradation is found to be more strongly affected by the impurity phases when quenched than by the oxygen deficiency, although the affection of the latter is not entirely ruled out.

63: Thermal Conductivity of Pr Doped $\text{YBa}_2\text{Cu}_3\text{O}_y$ and a Quasiparticle Contribution

Michiaki Matsukawa*, **H. Suzuki***, **Kimisuke Iwasaki***, **Hiromitsu Ogasawara***,
Koshichi Noto*, **Katsukuni Yoshida**

*(Iwate Univ.)

Czechoslovak Journal of Physics, Vol. 46, pp. 1159-1160, 1996

The thermal conductivity κ of Pr-doped $\text{YBa}_2\text{Cu}_3\text{O}_y(\text{Y}_{1-x}\text{Pr}_x\text{Ba}_2\text{Cu}_3\text{O}_y)$ polycrystals has been investigated as a function of temperature(T) from 10K up to 150K. A pure YBCO crystal exhibits a clear enhancement in κ below T_c , but for highly Pr-doped samples($x > 0.2$) the temperature dependence of κ monotonically decreases when T is lowered. Furthermore, the value of κ of insulating PBCO($x = 1.0$) is strongly suppressed compared with that of superconducting YBCO. Such behavior is not explained by the electron-phonon interaction model proposed by Badeen, Rickayzen and Teword, but suggests a

picture in which an observed peak below T_c in κ of the pure YBCO sample is ascribable to a quasiparticle contribution.

64: * Percolative Behavior of Cuprate Grains in the Ag-BPSCCO Composite System

Katsukuni Yoshida, Michiaki Matsukawa*, Koshichi Noto*

***(Iwate Univ.)**

Czechoslovak Journal of Physics, Vol. 46, pp. 1283-1284, 1996

Clustering of the cuprate grains in sintered composites of Ag-added (Bi, Pb)-Sr-Ca-Cu-O ($T_c \approx 110\text{K}$) has been investigated in particular reference to the percolation process when the volume fraction (f_n) of Ag phase is varied. Although the Ag-phase cluster undergoes a normal percolation process, the cuprate-phase cluster (superconducting) behaves in a different way. The resistivity ρ at 77 K is a decreasing function of f_n , the contribution from the superconducting clusters being concealed. However, when the temperature is lowered to 35K or below, ρ changes into an increasing function, showing an explicit contribution from the superconducting clusters. This transition of the ρ - f_n curve is realized when the superconducting weak-link is enhanced by lowering the temperature, and is ascribable also to the two dimensional character of the percolation process of the cuprate phase.

65: Quantitative SIMS Analysis of Mo in Ti-Dilute Mo Alloys Using Isotopic Abundance

同位体分離法による Ti-希薄 Mo 合金中の Mo の SIMS 定量分析

Yuichiro Sudo, Hiroyuki T. Takeshita, Ryosuke O. Suzuki, Yoichi Tomii, Katsutoshi Ono

J. Japan Inst. Metals, Vol. 60, No.4, pp. 406-411, 1996

日本金属学会誌, 60 卷, 4 号, 406-411 頁, 1996 年

For the application of SIMS (Secondary Ion Mass Spectrometry) to quantitative analysis for the dilute element in metallic alloys, it is indispensable to eliminate the disturbance which is counted with the secondary ions of the dilute element. Ti_2^+ ions from the Ti matrix overlap the Mo^+ ions from the Ti-dilute Mo alloys. However, a conventional SIMS could not be applied to separate Ti_2^+ ions either by its high resolution mass analysis or by the separation based on the energy profiles. Since the secondary ion intensities of Mo^+ and Ti_2^+ are proportional to their isotopic abundances, the secondary ion intensity of Mo^+ can be calculated and separated from the measured intensity. Using the ion intensity of $^{92}\text{Mo}^+$ or $^{100}\text{Mo}^+$ after the disturbance elimination and the normalization, a good linear relationship for the quantitative Mo analysis was obtained in the range of 766 mass ppm to 2.31 mass% Mo. The lower quantitative limit is evaluated to be 80 mass ppm due to the improved preciseness.

66: Structural change of the $\text{Li}_x\text{Mn}_2\text{O}_4$ spinel structure induced by extraction of lithium

Kiyoshi Kanamura*, Hidetoshi Naito*, Takeshi Yao, Zen-ichiro Takehara*

*(Graduate School of Engineering)

Journal of Material Chemistry, Vol. 6, pp.33-36, 1996.

A structural change of the $\text{Li}_x\text{Mn}_2\text{O}_4$ spinel induced by extraction of lithium was investigated using the Rietveld refinement method for its X-ray diffraction pattern change. Two cubic phases of the spinel $\text{Li}_x\text{Mn}_2\text{O}_4$ were observed in the range $0.5 > x > 0.13$ and their lattice parameters were found to decrease with decreasing x . If both phases were thermodynamically stable, the lattice parameters should not change during the extraction of lithium. Therefore, our X-ray diffraction (XRD) patterns suggest the destruction of the rigid $\text{Li}_x\text{Mn}_2\text{O}_4$ spinel structure which provides a high reversibility for the insertion and extraction of lithium. The possible mechanisms corresponding to this structural degradation are the compositional change of Mn or O atoms in $\text{Li}_x\text{Mn}_2\text{O}_4$ through the extraction of lithium. On the other hand, the separation of Mn^{2+} ions from $\text{Li}_x\text{Mn}_2\text{O}_4$ ($0.5 > x > 0.13$) was detected by electron paramagnetic resonance (EPR). From these results, it is concluded that $\text{Li}_x\text{Mn}_2\text{O}_4$ decomposes through the extraction of lithium to form Mn^{2+} compounds as a separate phase.

67: Crystal Structure and Metal-Insulator Transition of $\text{La}_{1-x}\text{Sr}_x\text{CoO}_3$

Atsushi Mineshige*, Minoru Inaba*, Takeshi Yao, Zempachi Ogumi*, Kenji Kikuchi
, Masaya Kawase*

*(Graduate School of Engineering) ** (University of Shiga Prefecture) *** (Kagawa
University)

Journal of Solid State Chemistry, Vol. 121, pp.423-429, 1996

Crystal structure of perovskite $\text{La}_{1-x}\text{Sr}_x\text{CoO}_3$ ($0.0 \leq x \leq 0.7$) was precisely determined by powder X-ray Rietveld analysis, and its correlation with the electrical properties was discussed. The space group was assigned to rhombohedral $R\bar{3}c$ in the range $0.0 \leq x \leq 0.5$ and to cubic $Pm\bar{3}m$ in the range $0.55 \leq x \leq 0.7$. At $x \sim 0.25$ the Co-O distance and Co-O-Co angle of this system showed an abrupt decrease and increase with increasing x , respectively, and the conductivity behavior changed from semiconducting to metallic. The abrupt changes in crystal structure were attributed to a change in the band structure at the transition from semiconducting to metallic, that is, an increase in the overlap between the valence band and doped hole states.

68: Layered structures of hydrated vanadium oxides. Part 5. - Single-crystal structure of $\text{Rb}_{0.5}\text{V}_2\text{O}_5$ and phase changes of rubidium intercalate**Takeshi Yao, Yoshio Oka*, Naoichi Yamamoto*******(Faculty of Integrated Human Studies) ** (Graduate School of Human and Environmental Studies)**

Journal of Material Chemistry, Vol. 6, pp.1195-1198, 1996

$\text{Rb}_{0.5}\text{V}_2\text{O}_5$, an anhydrous phase of the rubidium intercalate, has been synthesized in a hydrothermal $\text{VO}(\text{OH})_2\text{-RbCl}$ system. It crystallizes in the monoclinic system $C2/m$: $a = 11.596(2)$, $b = 3.6908(9)$, $c = 9.723(1)$ Å, $\beta = 100.93(1)^\circ$ and $Z = 4$. A single-crystal study ($R/R_w = 0.069/0.079$) revealed that the V_2O_5 layers are isostructural with those of $\text{K}_{0.5}\text{V}_2\text{O}_5$ in Part 4 which consist of zigzag chains of edge-sharing VO_6 octahedra. The interlayer Rb atom forms an RbO_8 rectangular prism with the apical oxygens of the VO_6 octahedra in contrast to the KO_7 coordination in $\text{K}_{0.5}\text{V}_2\text{O}_5$. $\text{Rb}_{0.5}\text{V}_2\text{O}_5$ With 9.55 Å spacing was oxidized by hydrogen peroxide to a hydrated phase, $\text{Rb}_{0.3}\text{V}_2\text{O}_5 \cdot 0.8\text{H}_2\text{O}$ with 10.85 Å spacing. This compound was reduced by rubidium iodide to a less hydrated phase, $\text{Rb}_{0.4}\text{V}_2\text{O}_5 \cdot 0.5\text{H}_2\text{O}$ with 10.41 Å spacing, rather than to $\text{Rb}_{0.5}\text{V}_2\text{O}_5$. Interlayer sites for monovalent cations in anhydrous phases are suggested to be correlated with cationic sizes and contents.

69: * Synthesis and Crystal Structure of $\sigma\text{-Zn}_{0.25}\text{V}_2\text{O}_5 \cdot \text{H}_2\text{O}$ with a Novel Type of V_2O_5 Layer**Yoshio Oka*, Osamu Tamada**, Takeshi Yao, Naoichi Yamamoto*******(Faculty of Integrated Human Studies) ** (Graduate School of Human and Environmental Studies)**

Journal of Solid State Chemistry, Vol. 126, pp.65-73, 1996.

A new layered vanadium bronze designated as σ -phase $\text{Zn}_{0.25}\text{V}_2\text{O}_5 \cdot \text{H}_2\text{O}$ has been hydrothermally synthesized from ZnCl_2 and $\text{VO}(\text{OH})_2$. A single-crystal study revealed the triclinic system $P\bar{1}$: $a = 10.614(2)$ Å, $b = 8.031(3)$ Å, $c = 10.7688(9)$ Å, $\alpha = 90.65(1)^\circ$, $\beta = 91.14(1)^\circ$, $\gamma = 90.09(2)^\circ$, and $Z = 8$. The structure was solved and refined to $R/R_w = 0.079/0.048$ for 1580 reflections with $I > 3\sigma(I)$, which consists of V_2O_5 layers stacking along the c axis and interstitial hydrated Zn^{2+} ions. The V_2O_5 layer adopts a novel polyhedral framework built up of VO_6 octahedra, VO_5 trigonal bipyramids, and VO_4 tetrahedra. When projected parallel to the ab plane, the V_2O_5 layer is described by the atomic sheet model in a manner similar to the V_2O_5 layer of δ -phase such as $\delta\text{-Ag}_x\text{V}_2\text{O}_5$, that is, a double-sheet type composed of two V_2O_5 sheets facing each other. The interstitial Zn atom forms a ZnO_6 octahedron with two apical oxygens of the VO_4 tetrahedra on opposite sides and with four coplanar water molecules. The

anhydrous σ phase was obtained by heating the hydrate up to 200 °C accompanied by the contraction in layer spacing from 10.76 to 8.92 Å.

70: Novel Method for Zirconium Oxide Synthesis from Aqueous Solution

Takeshi Yao, Takashi Inui, Akira Ariyoshi

Journal of the American Ceramic Society Vol.79, pp.3329-3330, 1996.

A novel method for zirconium oxide crystal synthesis from an aqueous solution at ordinary temperature and pressure has been discovered. Boric acid was added to a sodium hexafluorozirconate solution, fluoride ion was consumed by the formation of BF_4^- complex ion, then the hexafluorozirconate ion was hydrolyzed to zirconium oxide in order to increase the amount of fluoride ion. The formation of zirconium oxide crystal was confirmed by clear X-ray diffraction peaks. This method is promising for preparing zirconium oxide films in various applications.

71: Hydrothermal Synthesis of Hydrous Vanadium Oxide Bronzes $M_x\text{V}_3\text{O}_8(\text{VO})_y \cdot n\text{H}_2\text{O}$ ($M = \text{K, Rb, Ba}$)

Yoshio Oka*, Takeshi Yao, Naoichi Yamamoto, Osamu Tamada****

***(Faculty of Integrated Human Studies) ** (Graduate School of Human and Environmental Studies)**

Materials Research Bulletin, Vol.32, pp.59-66, 1997

Hydrous vanadium (IV, V) oxides containing K or Rb were synthesized by the hydrothermal method from $\text{VOSO}_4\text{-}M_2\text{SO}_4$ ($M = \text{K, Rb}$) solutions. They were found to be isomorphous with previously reported $\text{Ba}_{0.4}\text{V}_3\text{O}_8(\text{VO})_{0.4} \cdot n\text{H}_2\text{O}$, whose structure consists of V_3O_8 layers which are bridged by V-O units (denoted by $(\text{VO})_{0.4}$ in the formula) forming a tunnel-like opening to accommodate hydrous Ba ions. The isomorphous compounds can be formulated by $M_x\text{V}_3\text{O}_8(\text{VO})_y \cdot n\text{H}_2\text{O}$ ($M = \text{K, Rb, Ba}$; $n = 0.6\text{-}0.7$) where x and y show similar values of less than 0.5 as is accounted for by the crystal structure. The formation of this phase seems to be governed by the size of M cation whose ionic radius should lie in a limited range of 1.35 to 1.52 Å. The $\text{V}_3\text{O}_8(\text{VO})_y$ framework structure of a bronze-like type is compared with the V_2O_5 framework of $\beta\text{-}M_x\text{V}_2\text{O}_5$ (bronze) and the V_3O_8 framework of $\text{H}_2\text{V}_3\text{O}_8$.

72: Preparation and Characterization of LaMnO_3 Thin Film Electrode on YSZ

Tsutomu Ioroi*, Zempachi Ogumi*, Zen-ichiro Takehara*, Yoshiharu Uchimoto
***(Graduate School of Engineering)**

Chemistry Letters, pp.949-950, 1996

Dense and thin $\text{LaMnO}_3/\text{YSZ}/\text{La}_{0.85}\text{Sr}_{0.15}\text{MnO}_3$ cell was prepared by CVD- EVD process. The prepared LaMnO_3 film was sufficiently uniform and dense, no pore or crack was observed in the LaMnO_3 film. AC impedance measurements indicated that the electrode interface conductivity was linearly dependent on the electrode surface area. For dense and thin film electrode of LaMnO_3 , oxygen electrochemical reaction proceeded predominantly at the electrode surface region.

73: Preparation and Characteristics of Ni/YSZ Cermet Anodes by Vapor-phase Deposition

Tsutomu Ioroi*, Yoshiharu Uchimoto, Zempachi Ogumi*, Zen-ichiro Takehara*
***(Graduate School of Engineering)**

Denki Kagaku, vol. 64, pp.562-567, 1996

High performance nickel/yttria-stabilized zirconia (Ni/YSZ) anodes were prepared by a novel vapor-phase method. The vapor-deposited Ni/YSZ cermet were prepared by reacting surface-oxidized nickel with zirconium and yttrium chlorides using nickel oxide as an oxygen sources. After the vapor-phase reaction, it was found that nickel grains of the cermets are covered with porous YSZ layer. In the present work, the morphology and polarization behaviors of the vapor-deposited Ni/YSZ cermet anodes were compared with those of the conventional slurry-coated Ni/YSZ cermet. The steady-state polarization and AC complex impedance measurements indicated that the vapor-deposited Ni/YSZ cermets show lower anodic polarization than the cermets prepared by the conventional slurry method. This decrease in the polarization was attributed to an increase of electrochemical active sites, three-phase-boundary, in the vapor-deposited Ni/YSZ cermet anodes.

74: Preparation of Functionally Gradient Fluorocarbon Polymer Films by Plasma Polymerization of NF_3 and Propylene

Akimasa Tasaka*, Akiko Komura*, Yoshiharu Uchimoto, Minoru Inaba, Zempachi Ogumi****

***(Doshisha University) **(Graduate School of Engineering)**

Journal of Polymer Science: Part A: Polymer Chemistry, vol. 34, pp.193-198, 1996

Fluorocarbon polymer films were prepared by plasma polymerization using nitrogen trifluoride and propylene as starting materials. To improve their adhesiveness to substrates, a novel functionally gradient film in which the content of fluorine decreased continuously from the surface to the interior was prepared by changing source gas composition during deposition. This film had a smooth and pinhole-free surface, and had a high contact angle for water drop. In addition, it showed good adhesion to a glass substrate.

75: * Suppression of nonlinear interchange mode by zonal counterstreaming flow generation

A.Takayama, M.Wakatani, H.Sugama (National Institute of Fusion Science)

Physics of Plasmas Vol.3, p.3

Nonlinear evolution of interchange mode produces both vortex flow and shear flow in a scrape-off layer (SOL) plasma with unfavorable magnetic curvature. When the Rayleigh number becomes large, the shear flow exceeds the vortex flow and the zonal counterstreaming flow appears in the perpendicular direction to the ambient magnetic field. Simultaneously, the fluctuation level decreases and the associated cross-field transport becomes almost classical. However, since reduction of the saturation level weakens the shear flow generation, an intermittent oscillatory behavior appears and continues. Transport due to vortex flow measured with a Nusselt number may depend on the Prandtl number for a given Rayleigh number.

76: * ELM modelling based on the nonlinear interchange mode in edge plasma

A. Takayama, M. Wakatani

Plasma Physics and Controlled Fusion Vol.38, p.1411

The nonlinear interchange mode shows an intermittent oscillation and generates a zonal counterstreaming flow when transport due to vortex flow is suppressed. A model of the ELM (edge localized mode) observed in the H- (high- confinement) mode plasma is discussed based on the period of intermittent oscillation depending upon the Rayleigh number.

77: * An optimized plasma shape for magnetic confinement

M.Wakatani, M.Yokoyama

BUTSURI Vol.51, p.102

In order to obtain a "natural shape" of plasma confinement, we find a distorted plasma shape after optimization based on three-dimensional MHD equilibrium calculations. However, this shape has a very simple magnetic spectrum in the non-Euclid Boozer coordinates. Several experimental devices are designed by using this type of approach. (in Japanese)

78: * High Ion Temperature Mode in Heliotron-E

Katsumi Ida (National Institute for Fusion Science), Katsumi Kondo, Kazunobu Nagasaki (Institute for Advanced Energy, Kyoto University), Tadateru Hamada, Shigeru Hidekuma (National Institute for Fusion Science), Fumimichi Sano (Institute for Advanced Energy, Kyoto University), Hideki Zushi, Haruyuki Okada (Institute for Advanced Energy, Kyoto University), Sakae Besshou, Hisamitsu Funaba, Kiyomasa Watanabe (National Institute for Fusion), Tokuhiko Obiki (Institute for Advanced Energy, Kyoto University),

Physical Review Letters.76.(1996) p1268.

A high ion temperature Ti mode is observed for neutral beam heated plasmas in Heliotron E. This high Ti mode plasma is characterized by a peaked ion temperature profile and is associated with a peaked electron density profile produced by neutral beam fueling with low wall recycling. The observed improvement in ion heat transport can be related to the radial electric field shear rather than to the rotation velocity shear in the bulk plasma.

79: * Dipole Moment of the Pfirsch Schluter Current in a Finite Beta Stellarator Plasma on Heliotron E

Sakae Besshou, Norito Fujita, Kenichi Ogata, Katsumi Kondo, Yuuji Kurimoto, Tohru Mizuuchi (Institute of Advanced Energy, Kyoto University), Kazunobu Nagasaki (Institute of Advanced Energy, Kyoto University), Hiroyuki Okada (Institute of Advanced Energy, Kyoto University), Fumimichi Sano (Institute of Advanced Energy, Kyoto University), Hideki Zushi, Tokuhiko Obiki (Institute of Advanced Energy, Kyoto University)

Nuclear Fusion Vol. 37 (1997) p13-18

This paper describes the magnetic determination of the dipole moment of the Pfirsch-Schluter current in a finite-beta stellarator / heliotron plasma. The rotating cos-saddle diagnostic coils and the poloidal flux loops are used to identify the dipole current in a finite-beta toroidal plasma. A typical dipole moment

of the toroidal current in the standard Heliotron E configuration is 0.6 kA.m, when the volume-averaged beta is 0.50% at the magnetic field of 0.94T. The measured equilibrium dipole current is practically proportional to the diamagnetic volume average beta available up to 0.95%. The observed dipole moment of the Pfirsch-Schluter current is compared with the magnetohydrodynamic(MHD) calculation for a finite-beta stellarator plasma.

80: Magnetic Equilibrium Diagnostics in a Finite-Beta Toroidal Helical Plasma on Heliotron E

Sakae Besshou, Norito Fujita, Kenichi Ogata, Katsumi Kondo, Yuuji Kurimoto, Tohru Mizuuchi (Institute of Advanced Energy, Kyoto University), Kazunobu Nagasaki (Institute of Advanced Energy, Kyoto University), Hiroyuki Okada (Institute of Advanced Energy, Kyoto University), Fumimichi Sano (Institute of Advanced Energy, Kyoto University), Hideki Zushi, Tokuhiko Obiki (Institute of Advanced Energy, Kyoto University)

Fusion Engineering and Design, Vol. 34/35 (1997)574

This paper describes magnetic equilibrium diagnostics that are installed both inside and outside the vacuum vessel in the toroidal helical device Heliotron E. These magnetic diagnostics consist of Rogowski coils for plasma currents, a diamagnetic loop with compensation coils, a set of full flux loops, a set of partial saddle loops, modulated Rogowski coils with several harmonics, 2-D array of Bp coils and Rogowski coils for bus lines of helical, auxiliary vertical, and toroidal coils. Up to now we routinely obtain the diamagnetic stored energy, toroidal plasma currents, dipole moment of the Pfirsch-Schluter currents, the toroidal voltage, the finite beta free-boundary plasma shift and poloidal fluxes. We will describe the signals of measured magnetic fluxes, some interpretations for the finite beta equilibrium.

81: D-D Fusion Neutron Measurements in the Beam-Heated Stellarator Deuterium Plasmas on Heliotron E

Etsuro Iki, Sakae Besshou, Kenichi Ogata, Norito Fujita, Yuuji Kurimoto, Katsumi Kondo, Tohru Mizuuchi (Institute of Advanced Energy, Kyoto university), Kazunobu Nagasaki (Institute of Advanced Energy, Kyoto University), Hiroyuki Okada (Institute of Advanced Energy, Kyoto University), Fumimichi Sano (Institute of Advanced Energy, Kyoto University), Hideki Zushi, Tokuhiko Obiki (Institute of Advanced Energy, Kyoto University)

Fusion Engineering and Design, Vol. 34/35 (1997) 589

This paper describes the measurement of D-D fusion neutrons in the toroidal stellarator plasmas on Heliotron E. We used three moderated helium 3 counters and a moderated BF₃ counter. Calibration of neutron detectors was previously done with ²⁵²Cf spontaneous fission neutron source. We describe the measured fusion neutron emissions with several discharge conditions with hydrogen neutral beam injection heating to the deuterium plasmas. The Heliotron E plasmas are usually initiated by electron cyclotron resonance heating at magnetic field 1.9 T without ohmic heating plasma current. We have tried to deduce the central deuterium ion temperature from measured neutron flux and line averaged electron density. We have compared the central ion temperatures by neutron flux, with the passive charge exchanged particle analyses and diamagnetic stored energy. We discuss the possible error sources for the central neutron deduced deuterium temperature.

82: Operation of Thin Metal Foil Bolometer for Radiation Loss Measurement in a Toroidal Plasma on Heliotron E

Sakae Besshou, Sigeyuki Morimoto (Kanazawa Institute of Technology), Norito Fujita, Katsumi Kondo, Yuuji Kurimoto, Tohru Mizuuchi (Institute of Advanced Energy, Kyoto University), Kazunobu Nagasaki (Institute of Advanced Energy, Kyoto University), Hiroyuki Okada (Institute of Advanced Energy, Kyoto University), Fumimichi Sano (Institute of Advanced Energy, Kyoto University), Hideki Zushi, Tokuhiko Obiki (Institute of Advanced Energy, Kyoto University)

Fusion Engineering and Design, Vol. 34/35 (1997) 534

This paper describes the thin metal foil bolometric detector for time-resolved radiation loss measurements in the Heliotron E toroidal plasma confining experiment. The bolometer consists of 10mm or 50mm thick stainless steel radiation absorber, an insulation layer and a nickel resistor pattern. In this report we describe the bolometric detector, its electronics, the construction of array, and installation in the vacuum and high temperature condition in the toroidal plasma devices. We describe the physical principles of detection of the wavelength integrated total radiative loss from plasmas. The detector array consists of wide angle bolometers to monitor the time-resolved total radiative loss power, and a recently tested 17-channel bolometer array camera to measure the profiles of radiative loss. We present typical radiative loss measurement in the helical plasmas on Heliotron E with ECRH and NBI heating.

83: Effect of radial electric field and bulk plasma velocity shear on ion thermal transport in Heliotron-E

Katsumi Ida (National Institute for Fusion Science), Katsumi Kondo, Kazunobu Nagasaki (Institute of Advanced Energy, Kyoto University), Tadateru Hamada, Shigeru Hidekuma (National Institute for Fusion Science), Fumimichi Sano (Institute of Advanced Energy, Kyoto University), Hideki Zushi, Tohru Mizuuchi (Institute of Advanced Energy, Kyoto University), Hiroyuki Okada (Institute of Advanced Energy, Kyoto University), Sakae Besshou, Hisamitsu Funaba, Kiyomasa Watanabe (National Institute for Fusion Science), Tokuhiko Obiki (Institute of Advanced Energy, Kyoto University)

Plasma Physics and Controlled Fusion 38(1996)1433-1437

The effect of radial electric field and velocity shear on thermal transport is studied in Heliotron E. When neutral beams are injected into the target plasma produced by electron cyclotron heating (high Ti mode), or an ice pellet is injected into an NBI plasma (pellet injection mode), the central ion temperature $T_i(0)$ increases in time up to 0.7-0.8 keV. These high Ti plasmas are characterized by a peaked ion temperature profile and associated with a peaked electron density profile produced by neutral beam fueling with low wall recycling, or pellet fueling. The global energy confinement is improved compared with L-mode plasmas by a factor 1.4 for the same line-averaged electron density. The observed improvement in ion heat transport is related to the radial electric field shear rather than to the rotation velocity shear in the bulk plasma.

84: Enhancement and suppression of density fluctuations around electron drift frequency in Heliotron E plasmas measured using CO2 laser phase contrast method

Shinichiro Kado (Interdisciplinary Graduate School of Engineering Science, Kyushu University), Hiroshi Nakatake (Interdisciplinary Graduate School of Engineering Science, Kyushu University), Katsunori Muraoka (Interdisciplinary Graduate School of Engineering Science, Kyushu University), Katsumi Kondo, Fumimichi Sano (Institute of Advanced Energy, Kyoto University), Tohru Mizuuchi (Institute of Advanced Energy, Kyoto University), Sakae Besshou, Hiroyuki Okada (Institute of Advanced Energy, Kyoto University), Kazunobu Nagasaki (Institute of Advanced Energy, Kyoto University), Hisamichi Funaba, Takateru Hamada, Katsumi Ida (National Institute for Fusion Science), Masahiro Wakatani, Tokuhiko Obiki (Institute of Advanced Energy, Kyoto University)

Journal of the Physical Society of Japan vol.65 (1996) 3434-3437

Enhancement and suppression of electron density fluctuations around the electron drift frequency was observed in Heliotron E. This behavior corresponded to changes in the density profiles. Density fluctuations around this frequency were enhanced when the density profile was peaked in the inner region, and suppression was associated with the flattening of the density profile. An examination of

the frequency, wavenumber, and collisionality regimes suggested that the most likely candidate for the instability responsible for driving these fluctuations is the collisionless circulating electron mode.

85: Impurity behavior in Heliotron E plasmas

C.Christou (Max Planck Institute, Germany) Katsumi Kondo, Fumimichi Sano (Institute of Advanced Energy, Kyoto University), Hideki Zushi, Tohru Mizuuchi (Institute of Advanced Energy, Kyoto University), Sakae Besshou, Hiroyuki Okada (Institute of Advanced Energy, Kyoto University), Kazunobu Nagasaki (Institute of Advanced Energy, Kyoto University), Yuji Kurimoto, Hisamichi Funaba, Takateru Hamada, Takeshi Kinoshita, Sinichiro Kado (Interdisciplinary Graduate School of Engineering Science, Kyushu University), Masahiro Wakatani, Tokuhiko Obiki (Institute of Advanced Energy, Kyoto University)

Journal of Electron Spectroscopy and Related Phenomena vol.80 (1996) 271-274

Observations of resonance lines in the 15 to 40 nm spectral range provide useful information regarding the behavior of impurities in a laboratory plasma. Heliotron E emission spectra were recorded using a time-resolved VUV spectroscopy system, and line emission in this range was found to be dominated by impurity radiation from oxygen, carbon, iron and nickel. The magnetic axis of the plasma can be moved relative to the vessel wall, and so a study is presented of the effects of a shift in magnetic axis on the evolution of VUV impurity radiation from different ionic states. Differences in behavior of different states are analysed by the comparison of observed spectra with plasma coronal equilibrium models.

86: Radial profiles of 2p-1s heliumlike oxygen lines measured from the compact helical system using a vacuum crystal spectrometer

Sadatsugu Muto (National Institute for Fusion Science), Shigeru Morita (National Institute for Fusion Science), Katsumi Kondo

Review of Scientific Instruments vol.68(1997) p1039-1042

The vacuum crystal spectrometer (Johann type; RAP crystal) has been designed and developed to measure soft x-ray lines in the vicinity of 2 nm. A photodiode array and a two-stage multichannel plate were used as a detector. Radial profiles of heliumlike oxygen lines were successfully obtained from NBI plasmas in the compact helical system with a spectral resolution of $525(=\lambda/D\lambda)$. The radial profile in the intensity ratio of $Y(3P^1-1S^0)$ to $W(1P^0-1S^0)$ was also obtained. The intensity ratio among $2\ell-1\ell'$ transitions of the heliumlike oxygen are calculated as a function of the electron temperature and the electron temperature profile was obtained from the ratio. The obtained electron temperature was

compared with one from a Thomson scattering measurement. As a result, the comparison showed a good agreement.

87: Comparison of the Calculations of the Stability Properties of a Specific Stellarator Equilibrium with Different MHD Stability Codes

Yuji Nakamura, Taro Matsumoto, Masahiro Wakatani, et al.

Journal of Computational Physics, vol.128, pp.43-57

A Particular configuration of the LHD stellarator with an unusually flat pressure profile has been chosen to be a test case for comparison of the MHD stability property predictions of different three-dimensional and averaged codes for the purpose of code comparison and validation. In particular, two relatively localized instabilities, the fastest growing modes with toroidal mode numbers $n = 2$ and $n = 3$, were studied using several different codes, with the good agreement that has been found providing justification for the use of any of them for equilibria of the type considered.

88: MHD Instabilities in Current Carrying Toroidal Heliotron/Torsatron Plasmas

Taro Matsumoto (Faculty of Engineering, Kyoto University), Yuji Nakamura, Masahiro Wakatani.

Nuclear Fusion, Vol.36, No.11, pp.1571-1582

Current driven ideal MHD instability with $(m,n) = (1,1)$ becomes unstable in a current carrying toroidal heliotron plasma at zero pressure, where $m(n)$ is the poloidal (toroidal) mode number. This result is consistent with the cylindrical plasma approximation under the stellarator expansion. For finite beta current carrying plasmas of Heliotron E with two $\iota = 1$ resonant surfaces or the a highly peaked profile, the current driven $m = 1$ internal kink mode destabilized at the inner $\iota = 1$ surface is gradually changed into the pressure driven $m = 1$ interchange mode localized at the outer $\iota = 1$ surface with an increase of pressure, where ι is the total rotational transform. The growth rate is first increased, then decreased with the increase of pressure, which is correlated with the formation of a magnetic well. In the hollow current case of the Large Helical Device(LHD), there is no purely current driven instability and a specific hollow current profile has a tendency to stabilize the pressure driven interchange modes compared with the currentless case. It is shown that a combination of a positive hollow current with negative peaked current is particularly favourable to the MHD stability of LHD.

89: Improvement of Collisionless Particle Confinement in L=1 Helical Systems

Masayuki Yokoyama, Yuji Nakamura, Masahiro Wakatani, et al.

16th IAEA Fusion Energy Conference (Montreal, 1996) paper IAEA-CN-64/CP-8

Two approaches for improving collisionless particle confinement in L=1 helical systems are shown. One is to select an optimum bumpy field in the coil system composed of a pitch-modulated L=1 helical coil, toroidal coils and poloidal coils. When the sign of bumpy field is opposite to that of L=1 helical field and the magnitudes of both fields are comparable, the configuration with a toroidal ripple comparable to a half of helical ripple seems most effective to suppress the collisionless particle loss. The four period L=1 helical system close to the optimum configuration is discussed. The other is to use the negative pitch modulation for collisionless particle confinement. In the compact L=1 torsatron with seventeen periods, the negative pitch modulation enhances the fraction of passing particle number, simultaneously improves the confinement of trapped particles owing to the significant reduction of the effective toroidal curvature. This also leads to the favorable neoclassical diffusion coefficient.

90: * Control of Mode Locking of Tearing Mode by Lower Hybrid Current Drive and Electron Cyclotron Heating in WT-3

Satoshi Yoshimura*, Yoshio Yoshizawa*, Mitsunari Sukegawa*, Keisa Matsunaga*, Tomoyuki Izuhara*, Akira Yamazaki*, Masahiko Nakamura**, Makoto Asakawa*, Hitoshi Tanaka, Takashi Maekawa, Yasushi Terumichi*

*(Fac. of Science, Kyoto Univ.), **(Osaka Institute of Technology)

Proc. of 1996 Int. Conf. on Plasma Physics, Vol.1, pp.190-193, 1997

In the WT-3 tokamak, saturated MHD oscillations are observed in ohmically heated (OH) plasmas in the range of the safety factor of $q_a = 2.7-3.2$. The internal structure of the mode is investigated by five soft X-ray (SX) cameras by using the computer tomography. It is found that there is an $m=1/n=1$ mode near the plasma center ($r/a \simeq 0.38$) in addition to an $m=2/n=1$ mode in the plasma periphery ($r/a \simeq 0.82$), where m (n) is the poloidal (toroidal) mode number. Both modes are coupled and the whole structure rotates toroidally with the angular frequency of $f \simeq 10$ kHz. When lower hybrid current drive is applied to these OH Plasmas, the rotation frequency begins to decrease and the amplitude slightly increase, and finally a mode locking takes place and a disruption is followed. SX computer tomography shows that the radial width of the $m=2/n=1$ mode steadily increases during mode locking and the $m=1/n=1$ mode grows abruptly just before the disruption. By applying electron cyclotron heating just before the mode locking, both modes are unlocked and the disruption is avoided.

91: * Observation of Sawtooth Crashes Associated with $m=2/n=1$ and $m=3/n=2$ Precursors

Takashi Maekawa, Mitsunari Sukegawa*, Satoshi Yoshimura*, Tomoyuki Izuhara*, Kazuya Uno*, Akira Yamazaki*, Masahiko Nakamura, Makoto Asakawa*, Yasushi Terumichi***

***(Fac. of Science, Kyoto Univ.), **(Osaka Institute of Technology)**

Proc. of the 1996 Int. Conf. on Plasma Physics, Vol.1, pp.538-541, 1997

In the WT-3 tokamak, sawtooth crashes associated with $m=2/n=1$ and $m=3/n=2$ precursors are observed during lower hybrid current drive and electron cyclotron heating for discharges with the safety factor at the limiter being in the range of $q_a = 4 \sim 6$. Only few papers report on sawtooth associated with a precursor with such plural poloidal mode numbers and detailed behavior of such crashes have been unknown. We investigate behavior of the crashes by using soft X-ray (SXR) tomography and compare the results with those with the usual $m=1/n=1$ instabilities in WT-3. Major results are followings. (1) Crashes take place by single $m=2/n=1$ instability, single $m=3/n=2$ instability, and also combined $m=2/n=1$ and $m=3/n=2$ instabilities (2) ΔI_{SX} (SXR intensity before crash - SXR intensity after crash) is small at the plasma core and large at just inside of the $q = 2$ surface in the case of $m=2/n=1$ crashes, while ΔI_{SX} is largest at the core in the case of usual $m=1/n=1$ crashes. (3) Crash times of $m=2/n=1$ crashes are nearly equal to or somewhat longer than those of usual $m=1/n=1$ crashes. (4) The $m=2/n=1$ and $m=3/n=2$ modes remain after the crash.

92: * Localized Plasma Heating Experiments using a Quasi-optical ECH System on the WT-3 Tokamak

Makoto Asakawa*, Tomoyuki Izuhara*, Kazuki Tanabe*, Keisa Tanabe*, Satoshi Yoshimura*, Kazuya Uno*, Akira Yamazaki*, Atsushi Nakayama, Takashi Maekawa, Yasushi Terumichi*

***(Fac. of Science, Kyoto Univ.)**

Proc. of the 1996 Int. Conf. on Plasma Physics, Vol.1, pp.1010-1013, 1997

On the WT-3 tokamak ($R = 65$ cm, $a = 20$ cm), the MHD activities and the sawtooth oscillations were suppressed by the electron cyclotron heating (ECH) using an 56 GHz ECH system if ECH was localized on the rational surfaces such as $q = 1$ and 2. In order to study the effect of localization of ECH on MHD control more extensively, we have installed new ECH system using an 88 GHz gyrotron and a quasi-optical transmission system on WT-3. The beam radius at the focusing point is measured to be 18.5 mm in poloidal direction and 15.5 mm in toroidal direction, being less than the tenth of minor radius of the plasma minor radius. The frequency corresponds to the second harmonic cyclotron frequency near the maximum toroidal field (1.75 T) of WT-3, thus the plasma confinement will be improved compared

with the previous experiments using the 56 GHz system. Preliminary plasma heating experiments have shown that the system can heat the plasma locally.

93: * Polarization of Impurity Emission Lines from a Tokamak Plasma

Takashi Fujimoto*, **Hironori Sahara***, **Tetsuya Kawachi***, **Thomas Kallstenius***, **Motoshi Goto***, **Hiroshi Kawase***, **Takeo Furukubo***, **Takashi Maekawa**, **Yasushi Terumichi****
*(Fac. of Engineering, Kyoto Univ.), ** (Fac. of Science, Kyoto Univ.)

Physical Review E, Vol.54, pp.2240–2243, 1996

The visible–uv spectrometer was equipped with a double refracting calcite plate for the purpose of resolving a spectral line into the two linearly polarized components and observing these simultaneously. Relative intensities of these components have been measured for heliumlike carbon and berylliumlike oxygen impurity lines from the WT–3 tokamak plasma at Kyoto University. In the joule heating mode, for transmission from the joule heating to the lower–hybrid current drive mode, and for application of the electron cyclotron heating, changes in the relative intensities were found, which indicated that these lines were polarized. Implications of the polarization of emission lines from plasma are discussed.

94: * Experiments on Nonneutral Electron and Positron Plasmas in a Potential Well Formed with Multi–Ring–Electrodes

Akihiro Mohri*, **Hitoshi Tanaka**, **Hiroyuki Higaki****, **Youhei Yamazawa****, **Tetsumori Yuyama***, **Toshinori Michishita***
*(Fac. of Integrated Human Studies, Kyoto Univ.), ** (Grad. School of Human and Environmental Studies, Kyoto Univ.)

Proc. of 1996 Int. Conf. on Plasma Physics, Vol.2, pp.2054–2057, 1997

Nonneutral spheroidal plasmas of electrons and positrons were experimentally investigated using developed traps installed with a train of many ring–shaped electrodes (MRE trap). This trap can produce a variety of field configurations. A Configuration compensating image charge effects confined a electron plasma at the longest confinement time of 2600 s. Electrostatic mode frequencies of ($l = 2, m = 0$) and ($3, 0$) was investigated in a wide range of the aspect ratio up to 11 and $T_e \leq 1.5$ eV. Slow positrons produced by combining an efficient photon–positron converter, a LINAC and a Ar solid film remoderator were trapped in a MRE trap, and a positron plasma was formed with the total particle number of 1.5×10^6 .

95: * Effects of ECH on NBI Plasma in Heliotron-E

T. Obiki, F. Sano, K. Kondo, H. Zushi, K. Hanatani, T. Mizuuchi, S. Besshou, H. Okada, K. Nagasaki, M. Wakatani, Y. Nakamura, C. Christou, Y. Ijiri, T. Senju, K. Yaguchi, S. Kobayashi, K. Toshi, K. Sakamoto, Y. Kurimoto, H. Funaba, T. Hamada, S. Sudo, M. Sato, K. Ida, B. J. Peterson, K. Muraoka, S. Kado, H. Sugai, H. Toyoda, K. Sasaki, H. Okura, K. Matsuo

Proc. 16th IAEA Fusion Energy Conference, Montreal, October 7-11, 1996, IAEA-CN-64/C1-3

Propagation and absorption of second harmonic electron cyclotron resonance microwaves are investigated in Heliotron-E. It is experimentally confirmed that the linearly polarized beam should be launched with a proper angle to the sheared field line and cross the resonance layer at the magnetic axis to obtain the best plasma production. The superposition of ECH pulse on NBI plasmas has showed that the ion temperature is dependent on the ECH power deposition profile.

96: Dynamics of Ion Temperature in Heliotron-E

K. Ida (National Institute for Fusion Science), K. Kondo, K. Nagasaki, T. Hamada (Faculty of Engineering, Kyoto University), S. Hidekuma (National Institute for Fusion Science), F. Sano, H. Zushi, T. Mizuuchi, H. Okada, S. Besshou, H. Funaba (Faculty of Engineering, Kyoto University), K. Watanabe (National Institute for Fusion Science), T. Obiki

Proc. 16th IAEA Fusion Energy Conference, Montreal, October 7-11, 1996

Ion temperature dynamics related with the density profile are studied in Heliotron-E plasma. The density profiles can be peaked by the H₂/D₂ pellet injection or flattened by second harmonic electron cyclotron heating (2nd ECH). Higher ion temperature and better ion transport are observed associated with the density peaking, and a large density gradient results in the radial electric field shear. The improvement of ion transport is more related to the radial electric field shear, rather than to the bulk velocity shear.

97: * Effect of Radial Electric Field and Bulk Plasma Velocity Shear on Ion Thermal Transport in Heliotron-E

K. Ida (National Institute for Fusion Science), K. Kondo, K. Nagasaki, T. Hamada (Faculty of Engineering, Kyoto University), S. Hidekuma (National Institute for Fusion Science), F. Sano, H. Zushi, T. Mizuuchi, H. Okada, S. Besshou, H. Funaba (Faculty of Engineering, Kyoto University), K. Watanabe (National Institute for Fusion Science), T. Obiki

Plasma Phys. Control. Fusion 38 (1996) pp.1433-1437

The effect of radial electric field and velocity shear on thermal transport is studied in Heliotron E. When neutral beams are injected into the target plasma produced by electron cyclotron heating (high Ti mode), or an ice pellet is injected into an NBI plasma (pellet injection mode), the central ion temperature $T_i(0)$ increases in time up to 0.7-0.8 keV. These high Ti plasmas are characterized by a peaked ion temperature profile and associated with a peaked electron density profile produced by neutral beam fueling with low wall recycling, or pellet fueling. The global energy confinement is improved compared with L-mode plasmas by a factor 1.4 for the same line-averaged electron density. The observed improvement in ion heat transport is related to the radial electric field shear rather than to the rotation velocity shear in the bulk plasma.

98: * Parameter Study of 106GHz Second Harmonic ECH Plasma in Heliotron-E

K. Nagasaki, H. Zushi, S. Kobayashi (Institute of Advanced Energy, Kyoto University), K. Sakamoto (Institute of Advanced Energy, Kyoto University), F. Sano, K. Kondo, T. Mizuuchi, S. Besshou, H. Okada, C. Christou, Y. Kurimoto, H. Funaba, T. Hamada, T. Obiki, K. Ida (National Institute for Fusion Science), A. Isayama, S. Kado, G. Denisov (Institute of Applied Physics, Russian Academy of Science), A. Goldenberg (Institute of Applied Physics, Russian Academy of Science), V. Kurbatov (Institute of Applied Physics, Russian Academy of Science), V. Orlov (Institute of Applied Physics, Russian Academy of Science)

Proc. 23rd European Physical Society Conference on Control. Fusion and Plasma Physics, Kiev, June 24-28, 1996

106GHz second harmonic ECH experiments have been made in Heliotron-E. Replacing one of the 53GHz ECH systems, a new 106GHz ECH system was introduced using a gyrotron of 0.5MW 0.2sec Gaussian beam output and HE11 waveguide transmission line. The focused Gaussian beam (beam waist, $r=2\text{cm}$) is perpendicularly launched from the outside of the torus. By combining another 106GHz ECH system, the total power of PECH=550kW can be launched into a plasma. According to ray tracing calculations, the single pass absorption of the X-mode is nearly 100% and the power deposition can be localized at the desired resonance region, making it possible to investigate the relation between the plasma profile and the power deposition. We show the experimental results of the 106GHz ECH compared with the previous ECH, and the dependence of plasma parameters on the resonance position and polarization.

99: Study of the Core Particle Confinement during the Transition Phenomenon in the Edge Heating Experiment in Heliotron-E

Y. Kurimoto, H. Zushi, K. Nagasaki, F. Sano, K. Kondo, T. Mizuuchi, S. Besshou, H. Okada, T. Obiki

Proc. 1996 Int. Conf. Plasma Physics, Nagoya (1997) Vol.1 pp.270-273

In the Heliotron-E device, a transition phenomena is observed during the edge heating experiment using 35GHz and 53GHz gyrotrons. The charge exchange flux originated in the core plasma is reduced to 1/5 at the transition. This suggests the reduction of the particle source rate in the core plasma, and a decrease of neutral density is responsible to it. The time needed for the transition for the charge exchange flux is 1-2.5 times longer than that for the $H\alpha$ emission.

100: Ion Transport Analysis of NBI heated Plasma in Heliotron-E

T. Hamada, F. Sano, H. Funaba, K. Ida (National Institute for Fusion Science), K. Watanabe (National Institute for Fusion Science), K. Kondo, T. Mizuuchi, K. Nagasaki, H. Okada, S. Besshou, H. Zushi, K. Hanatani, M. Nakasuga, S. Hidekuma (National Institute for Fusion Science), Y. Kurimoto, T. Kinoshita, S. Kado, T. Senju (Institute of Advanced Energy, Kyoto University), K. Yaguchi (Institute of Advanced Energy, Kyoto University), S. Kobayashi (Institute of Advanced Energy, Kyoto University), K. Toshi (Institute of Advanced Energy, Kyoto University), K. Sakamoto (Institute of Advanced Energy, Kyoto University), Y. Ijiri (Institute of Advanced Energy, Kyoto University), T. Obiki

Proc. 1996 Int. Conf. Plasma Physics, Nagoya (1997) Vol.1 pp.278-281

The multichord charge exchange spectroscopy system has enabled us to obtain ion temperature profile with high spatial resolution. Some improved ion energy confinement states are found which are characterized by a center-peaked ion temperature profile and a peaked electron density profile. On the other hand, the drastic deterioration of the ion energy confinement in the central region is observed during the second harmonic 106GHz ECH overlapping with its resonance being around the center of the plasma column. The behavior ion thermal diffusivity of each state is investigated and compared by transport analysis from experimental data.

101: Electron Thermal Transport Analysis for ECH and NBI Plasmas in Heliotron-E

H. Funaba, H. Okada, F. Sano, K. Watanabe (National Institute for Fusion Science), K. Kondo, K. Nagasaki, K. Hanatani, S. Sudo (National Institute for Fusion Science), K. Ida (National Institute for Fusion Science), T. Mizuuchi, S. Besshou, M. Nakasuga, H. Zushi, Y. Kurimoto, T. Hamada, T. Kinoshita, K. Yaguchi (Institute of Advanced Energy, Kyoto University), K. Toshi (Institute of Advanced Energy, Kyoto University), T. Senju (Institute of Advanced Energy, Kyoto University), S. Kobayashi (Institute of Advanced Energy, Kyoto University), K. Sakamoto (Institute of Advanced Energy, Kyoto University), Y. Ijiri (Institute of Advanced Energy, Kyoto University), M. Wakatani, T. Obiki

Proc. 1996 Int. Conf. Plasma Physics, Nagoya (1997) Vol.1 pp.282-285

The effect of superposing 106GHz ECH to NBI plasmas on electron transport has been studied. The electron thermal diffusivity in NBI+ECH case seems to be almost the same as that in the NBI-only case when we assume the ECH power absorption profile deduced from ECE signals. The difference in the ECH power absorption between ECE-signal measurements and ray tracing calculation is discussed from the view point of electron transport in Heliotron-E.

102: Non-local Response of the Electron Temperature and Longitudinal Propagation of the Plasmoid during Pellet Injection on Heliotron-E

H. Zushi, Y. Kanda, M. Hosotsubo, M. Nakasuga, K. Kondo, S. Sudo (National Institute for Fusion Science), T. Senju (Institute of Advanced Energy, Kyoto University), K. N. Sato (National Institute for Fusion Science), K. Sakamoto (Institute of Advanced Energy, Kyoto University), K. Yaguchi (Institute of Advanced Energy, Kyoto University), Y. Yu. Sergeev (State Technical University of St. Petersburg, Russia), K. V. Khlopenkov (National Institute for Fusion Science), T. Okamoto, Y. Nakamura, M. Wakatani, T. Mizuuchi, H. Okada, K. Nagasaki, F. Sano, T. Obiki

Proc. 1996 Int. Conf. Plasma Physics, Nagoya (1997) Vol.1 pp.362-365

Fast response of the electron temperature to pellet injection is described from the point of view of the global or non-local electron enhanced transport against the local perturbation. The radial extension of the perturbation, enhanced magnetic fluctuations and potential change are discussed.

103: Effects of ECH on Ion Heating during NBI in Heliotron-E

T. Mizuuchi, H. Zushi, K. Nagasaki, K. Kondo, F. Sano, S. Besshou, H. Okada, C. Christou, Y. Ijiri (Institute of Advanced Energy, Kyoto University), T. Senju (Institute of Advanced Energy, Kyoto University), K. Yaguchi (Institute of Advanced Energy, Kyoto University), S. Kobayashi (Institute of Advanced Energy, Kyoto University), K. Toshi (Institute of Advanced Energy, Kyoto University), K. Sakamoto (Institute of Advanced Energy, Kyoto University), S. Sudo (National Institute for Fusion Science), K. Ida (National Institute for Fusion Science), B. J. Peterson (National Institute for Fusion Science), S. Kado, Y. Kurimoto, H. Funaba, T. Hamada, T. Obiki

Proc. 1996 Int. Conf. Plasma Physics, Nagoya (1997) Vol.1 pp.1018-1021

In order to improve ion heating during NBI, the superposition of ECH pulse on NBI plasma has been investigated. Different effects of ECH on the center ion temperature are observed for overlapping of three ECH's with different absorption and resonance mechanisms. The high power ECH overlapping with rather broad power deposition profile elevated T_i above the conventional T_i scaling but reduced it for the overlapping of a center focused ECH case.

104: Li pellet Injection Experiment on Heliotron-E

S. Sudo (National Institute for Fusion Science), K. V. Khlopenkov (National Institute for Fusion Science), K. Kondo, T. Mizuuchi, H. Zushi, F. Sano, H. Okada, S. Besshou, K. Nagasaki, K. Sakamoto (Institute of Advanced Energy, Kyoto University), T. Obiki

Proc. 1996 Int. Conf. Plasma Physics, Nagoya (1997) Vol.1 pp.1282-1285

Li pellet injection on Heliotron-E has provided an interesting feature of pellet ablation and particle transport. The images of the emission intensity of Li I and II are observed, which exhibit the substantial difference of the intensity profiles. The ablation characteristics of the injected Li pellet are presented in both cases of neutral beam injection and electron cyclotron resonance heating.

105: TV Thomson Scattering Measurement in Heliotron-E

H. Okada, H. Funaba, T. Kinoshita, K. Kondo, F. Sano, S. Besshou, T. Mizuuchi, K. Nagasaki, H. Zushi, M. Wakatani, T. Obiki

Proc. 1996 Int. Conf. Plasma Physics, Nagoya (1997) Vol.1 pp.1434-1437

For the local transport analysis, the profile data of plasma temperature and density with sufficient resolution is important. In the Heliotron-E device, Thomson scattering system with photomultiplier tubes and TV camera system has been used for its purpose. For the detector of the TV we selected fast framing camera because the back ground plasma light can be obtained with several hundred nano second interval. The readout gives the flexibility for changing spatial resolution matching the scattering light intensity.

106: Field line measurements in the divertor of Heliotron-E under boronized conditions

**F.Sano, T.Mizuuchi, T.Hamada, H.Funaba, M.Nagasaki, K.Kondo, H.Zushi,
S.Besshou, H.Okada, K.Hamatani, K.Nagasaki, T.Obiki**

J. Nucl. Mater., Vol.241-243, pp. 961-966, 1997

Vacuum magnetic field line structure of Heliotron-E has been studied experimentally with special reference to the edge plasma physics of the helical system(heliotron/torsatron). A new approach for measuring the vacuum impedance between the magnetic surface and the chamber wall under the boronized conditions was attempted in order to extract the detailed field line topology efficiently. Measurements have revealed the position of the experimental last closed surface and the nesting and folding structure of the divertor field lines. In conclusion, an advanced 2D visualization of Heliotron-E divertor field lines was obtained as compared with the previous one using the stainless-steel wall conditions. In addition, the relationship between the edge plasma distribution and the relevant field topology is discussed.

107: Energy confinement scaling from the international stellarator database

U.Stroth*, M.Murakami, R.A.Dory**, H.Yamada***, S.Okamura***, F.Sano,
T.Obiki**

***(Max-Planck-Institut für Plasmaphysik, Germany), **(Oak Ridge National Laboratory,
USA) *** (National Institute for Fusion Science)**

Nuclear Fusion, Vol.36, pp. 1063-1077, 1996

An international stellarator database on global energy confinement is presented. It comprises a total of 859 discharges from the ATF, CHS and Heliotron-E heliotron/torsatrons and the W7-A and W7-AS shearless stellarators. Some design aspects and operation techniques of the different devices are discussed. The data in the database represent electron cyclotron heated(ECH) and neutral beam injection(NBI) heated discharges in the L mode confinement regime. Results from enhanced confinement regimes such as H mode will be reported elsewhere. Regression expressions for the energy confinement time are given for the individual devices, for the subsets of heliotron/torsatrons and shearless stellarators and for the combined dataset. The combined scaling ISS-95 is found to describe satisfactorily a large tokamak L mode

dataset. The aspects of comparing stellarator and tokamak data are discussed on the basis of various scaling expressions. In order to make this database available to interested colleagues, the structure of the database, which is described in detail, is organized in a similar way as the ITER confinement databases.

108: Study of high energy particles produced by ICRF heating in Heliotron-E

H.Okada, T.Mutoh*, M.Okamoto*, M.Ohnishi, H.Zushi, K.Kondo, T.Mizuuchi, S.Besshou, F.Sano, K.Nagasaki, M.Wakatani, T.Obiki

***(National Institute for Fusion Science)**

Nuclear Fusion, Vol.36, pp.465-474, 1996

In ion cyclotron range of frequency(ICRF) heating experiment in Heliotron-E, high energy particle production and confinement were studied. The high energy tail(up to 100 keV) formation of minority protons was clearly observed in a low density plasma experiment. The high energy tail below several tens of kiloelectronvolts was formed within 1ms. The higher energy flux above this range developed within 10 ms. The flux decay time after termination of the ICRF pulse was short compared with the values expected from the collision process. The orbit loss of the accelerated particles is important for estimating the ICRF heating, particularly in helical confinement devices. To analyze the heating and orbit loss mechanism, a Monte Carlo code was used with an ICRF wave acceleration term. The time evolution of the tail formation and its decay resulting from the calculations agreed with the experimental ones. From this analysis, it is clear that the high energy particle production in ICRF experiments in helical confinement systems can be described by RF acceleration, collisional relaxation and orbit loss processes, and also that the orbit loss is not negligible in the ICRF heating of the low density plasmas of Heliotron-E.

109: Impurity behaviour in Heliotron E plasmas

C.Christou, K.Kondo, F.Sano, H.Zushi, T.Mizuuchi, S.Besshou, H.Okada, K.Nagasaki, Y.Kurimoto, H.Funaba, T.Hamada, T.Kinoshita, S.Kado*, M.Wakatani, T.Obiki

***(Interdisciplinary Graduate School of Engineering Science, Kyushu Univ.)**

J. Electron Spectroscopy and Related Phenomena, Vol.80, pp.271-274, 1996

Observations of resonance lines in the 150 to 400Å spectral range provide useful information regarding the behaviour of impurities in a laboratory plasma. Heliotron E emission spectra were recorded using a time-resolved VUV spectroscopy system, and line emission in this range was found to be dominated by impurity radiation from oxygen, carbon, iron and nickel.

The magnetic axis of the plasma can be moved relative to the vessel wall, and so a study is presented of the effects of a shift in magnetic axis on the evolution of VUV impurity radiation from different ionic states. Differences in behaviour of different states are analyzed by the comparison of observed spectra with plasma coronal equilibrium models.

110: Boiling Point of Tetrahalomethanes

Tetsuo Sakka, Yukio Ogata, Matae Iwasaki

J. Fluor. Chem., Vol.76, pp.203-207, 1996

111: Diffusion through a Multilayer and Its Application to Hydrogen Permeation through Nickel Coated Iron

Yukio H. Ogata, Tetsuo Sakka, Masahiro Murata*, Yosohiro Sugie*

***(Himeji Institute of Technology)**

Hydrogen Energy Progress XI : Proceedings of the 11th World Hydrogen Energy Conference, pp.2297-2302, (1996)

Analysis of diffusion phenomena in a multilayer system, which we often encounter in electrochemical systems, comprises certain difficulties. To overcome them, we developed an algorithm using numerical inversion of the Laplace transform of the diffusion equation. This procedure was applied to experimental analysis of hydrogen permeation in an electrochemical testing cell. Hydrogen permeation through a composite layer of nickel coated iron was measured. The coating was performed at one side or both side of the specimen: two- and three-layers, respectively. In the two-layer system, the single layer approximation did not work when the thickness ratio between the coating and the substrate exceeded ca. 5×10^{-4} . On the other hand, the multilayer analysis well reproduced the experimentally obtained permeation current vs. time curve; further, the diffusion coefficient of the coating layer was in agreement with the value of nickel. In the three-layer system, diffusion coefficients obtained for the layers of charging surface and extracting surface were different each other; the cause is considered in connection with the data treatment procedure, effects of the surface or the interface process, deviation from the diffusion-controlled process, and so on.

112: * Mechanism of Protein Solubilization in Sodium Bis(2-ethylhexyl) Sulfosuccinate Water-in-Oil Microemulsion

Kohsaku Kawakami, Makoto Harada, Motonari Adachi, Akihisa Shioi

Colloids and Surfaces, Vol.109, special issue, pp.217-233, 1996.

We selected Δ alpha-chymotrypsinogen A (CTN) as a model protein, and the mechanism for protein solubilization in a sodium bis(2-ethylhexyl) sulfosuccinate (AOT) water-in-oil microemulsion was investigated using the two-phase transfer method. The extraction of CTN by the microemulsion is composed of two processes; a fast extraction and a subsequent slow back-extraction process. The adsorption of AOT onto the surface of CTN through the electrostatic interaction between CTN cations and AOT anions converts CTN from a hydrophilic to a hydrophobic state. This adsorption is responsible for the fast extraction process. The adsorption of AOT due to a hydrophobic interaction with CTN in turn makes the CTN-surface hydrophilic. The slow back-extraction process is attributed to the adsorption due to the latter interaction. The presence of two adsorption modes is ascertained by cation-exchange and hydrophobic-interaction chromatography, and spectroscopic measurements. In the fast extraction stage, CTN is extracted to the microemulsion accompanied with large amount of AOT and water when the CTN-to-AOT mole ratio is comparatively large, suggesting the formation of large clusters composed of many AOT, water and CTN molecules. With a decrease in the ratio, the large cluster is divided into finer aggregates. The distribution of CTN between the microemulsion and the aqueous phase was examined by altering the salinity and organic solvent species of the microemulsion phase in the fast extraction stage. Both effects of the salinity and the solvent species were ascribed to the size effect of the microemulsion droplets. The weak interaction between the microemulsion droplet surface and the tails of the AOT chain adsorbed on the protein plays an essential role in the solubilization of the guest proteins. Since the energy of the droplets

113: * Model for Geometry of Surfactant Assemblies in the Oil-Rich Phase of Winsor II Microemulsions

Akihisa Shioi, Makoto Harada

Journal of Chemical Engineering of Japan, Vol.29, No.1, pp.95-104, 1996.

A model for the relationship between W/O-aggregate geometries and molecular species constituting the aggregates was proposed. The microemulsion phase in equilibrium with an excess aqueous phase was discussed. We restricted the surfactants to ionic ones in which head groups electrostatically interact with each other. The hydrophobic groups were modelled by the density distribution of the chain segments within the surfactant tails in the hydrophobic layer coating the aggregate. The interaction between the hydrophobic groups of surfactants was incorporated based on the excluded volume interaction of the segments. On this basis, we analytically expressed the chemical potentials of the surfactants in terms of microscopic parameters characterizing the nature of the surfactants. Following the thermodynamical equilibrium condition, the surfactant systems were classified into four types: systems forming spherical

aggregates, systems forming cylindrical aggregates, to form aqueous micelles or O/W aggregates and to form no small aggregates. The domain for the four types was drawn on the maps, of which abscissa and ordinate represent the strength of the electrostatic interaction and the length ratio of the hydrophilic/hydrophobic layers, respectively. The packing of the segments within the hydrophobic tails played a key role to determine the aggregates geometry. The predictions by the present model were qualitatively consistent with some experimental observations.

114: Analysis of the Bulk and Surface-Induced Structure of Electrolyte Solutions Using Integral Equation Theories

Masahiro Kinoshita, Daniel. R. Berard (University of British Columbia)

Journal of Computational Physics, Vol.124, No.1, pp.230-241, 1996.

We have developed robust and efficient numerical methods for solving the integral equation theories for electrolyte solutions. These methods are hybrids of Newton-Raphson and Picard iterations and have been obtained as extended versions of the previous methods for pure solvents by solving nontrivial problems posed by the inclusion of ions. Bulk electrolytes and electrolytes near both inert and metallic surfaces are considered. The basic equations previously derived for a one-component fluid near a planar wall are extended to a multicomponent fluid. Analytical expressions for elements of the Jacobian matrices are arranged in compact form. A striking feature of the method for surface problems is that the Jacobian is determined only from bulk properties. A discussion of some special treatments that need to be considered for asymmetrical anions and cations is included. These methods have been demonstrated using the full reference hypernetted-chain theory for various sizes of ions in a wide range of ionic concentrations.

115: * Control of Microstructure Formed by Spinodal Decomposition

スピノーダル分相によって形成される微細構造の制御

Haruhiko Watanabe, Masahiro Kinoshita, Makoto Harada, Akihisa Shioi

Kagaku Kogaku Ronbunshu, Vol.22, No.1, pp.29-41, 1996.

化学工学論文集、22 卷、1 号、29-41 頁、1996 年

Effects of a thermal history on spinodal decomposition structure have been investigated using Langer's theory, the cell dynamical system (CDS) model and Monte Carlo (MC) simulation. Even for nonlinear systems, growth of structure with a particular wave-length in the so-called linear manner is caused by the following operation : Form a structure to some extent at a higher temperature, and then switch the temperature to a lower value and develop the structure further. We may be able to control the microstructure formed so as to gain a sharp wave-length distribution. Effects of a periodic external field introduced have also been examined using MC simulation. The wave-length of decomposition structure in the metastable state established without the field is an important parameter which allows us to determine

the wave-length of the field to be introduced. When the two wave-lengths are of comparable magnitude, control operation is the most successful and the structure is rapidly and notably affected even by a relatively weak field. (in Japanese)

116: * Growth Mechanism of Cadmium Sulfide Ultrafine Particles in Water-in-Oil Microemulsion

Kiyoshi Suzuki, Makoto Harada, Akihisa Shioi

Journal of Chemical Engineering of Japan, Vol.29, No.2, pp.264-276, 1996

The growth mechanism of CdS ultrafine particles in water-in-oil microemulsions was investigated. The growth occurs via a irreversible coagulation process. Its rate constant is dependent on the agglomeration numbers, the rate constant k is about $10^7 \text{ dm}^3 / (\text{mol} \cdot \text{sec})$, It decreases dramatically to about $10^3 / (\text{mol} \cdot \text{sec})$ at a critical agglomeration number n_c followed by a further decrease in k above $2n_c$. This causes sharpening of the size distribution near n_c and $2n_c$. A simple model based on the coagulation process with n -dependent rate constants is proposed, which explains well the experimental results. The effects of initial mixing and feed ratio of Cd^{2+} to S^{2-} are understood well by the proposed model. The relationship between n_c and the stable spramolecules composed of CdS particles was discussed.

117: * Dynamic Behavior and Structure of Concentrated Water-in-Oil Microemulsions in the Sodium Bis(2-ethylhexyl)sulfosuccinate Systems

Ken-ichi Kurumada, Akihisa Shioi, Makoto Harada

The Journal of Physical Chemistry, Vol.100, No.3, pp.1020-1026, 1996.

The dynamical structure are qualitatively estimated by the dynamic light cattering and the rheological measurements for sodium bis(2-ethylhexyl)sulfosuccinate (AOT)/water/n-hexane/sodium chloride systems in the concentrated region up to 50-60 % of the volume fraction of the molecular aggregates. As the volume fraction increases, a very slow mode of relaxation stands out, which is interpreted not by the hindered motions of an individual spherical aggregate but by introducing "clusters" of the aggregates owing to attractive interactions between the aggregates. The effect of the attractive interaction is not negligible only when the volume fraction of the aggregates in the AOT microemulsion is rather high and the average distance between the aggregates is reduced, indicating that the attractive interaction is rather weak. Furthermore, the retardation effect on the decay of the concentration fluctuation due to the attractive interaction is stronger for higher salinity conditions.

118: * X-ray and Light Scattering from Oil-Rich Microemulsions Containing Sodium Bis(2-ethylhexyl) Phosphate**Akihisa Shioi, Makoto Harada, Mitsuru Tanabe**

Langmuir, Vol.12, No.13, pp.3201-3205, 1996

The small angle X-ray scattering intensity was compared with the light scattering intensity in an oil-rich microemulsion composed of sodium bis(2-ethylhexyl) phosphate, which forms cylindrical aggregates. When increasing the surfactant concentration, both intensities were not proportional to each other. This was attributed to the distribution of the refractive indexes of the size-polydisperse aggregates. If the scattering intensity at zero scattering angle of an electromagnetic wave is proportional to the osmotic compressibility of the microemulsion, then the result suggested that the osmotic compressibility evaluated from the electromagnetic wave scattering was dependent on the wavelength. Thus, this nonproportional behavior presents a problem for determining the osmotic compressibility from the scattering experiments.

119: * Bioaffinity Separation of Concanavalin A in Reverse Micellar System Composed of AOT/Butanol or Non-ionic Surfactant**Motonari Adachi, Makoto Harada, Akihisa Shioi, Hiroki Takahashi, Shigeo Katoh**

Journal of Chemical Engineering of Japan, Vol.29, No.6, pp.982-989, 1996

Selective separation of concanavalin A (ConA) using alkylglucoside (AGn) as an affinity ligand was achieved by two different methods in reverse micellar system. The first method used the sodium bis(2-ethylhexyl)sulfosuccinate (AOT)/butanol/iso-octane system, in which ConA extracted effectively when AGn was added to the system but was not extracted at all without AGn. Selective extraction was attained in three steps. In the first step, reverse micelles composed of AOT and alcohol without AGn were used. Proteins extractable to these reverse micelles were removed from the aqueous phase. In the second extraction step, ConA was selectively extracted to the reverse micellar phase with AGn. Backward extraction was successfully using buffer solutions containing glucose. The problem of this method was the precipitation of ConA at the liquid/liquid interface presumably due to the denaturation of ConA by AOT. The second method used the reverse micellar system composed of tetra-oxyethylenedecylether. This reverse micellar system had no ability to extract water-soluble proteins without an affinity ligand, whereas ConA could be extracted selectively with high overall efficiency when AGn was added to the system. Rapid backward extraction was performed using a buffer solution containing glucose or methyl-*alpha*-glucoside by adding ethanol or butanol.

120: Application of the Reference Interaction Site Model Theory to Analysis on Surface-Induced Structure of Water

Masahiro Kinoshita, Fumio Hirata (Institute for Molecular Science)

Journal of Chemical Physics, Vol.104, No.21, pp.8807-8815, 1996.

We consider the extended simple point charge (SPC/E) model water near uncharged and charged macroparticles. It is shown that the size of the macroparticle tested is sufficiently large and it acts in effect as a planar wall. The reference interaction site model (RISM) theory is employed, and a robust and very efficient algorithm has been developed for solving the basic equations. The algorithm is a hybrid of the Picard and Newton-Raphson methods. The Jacobian matrix is just part of the input data and need not be recalculated at all. Sufficiently accurate solutions are obtained in only 7 to 16 iterations. The reduced density profile of oxygen atoms near an uncharged macroparticle indicates significant dewetting and a clear contribution of the ice-like structure. The surface potential calculated is positive but very small. When the macroparticle is charged, the number of water molecules in the close vicinity of the surface increases regardless of the sign of the charge. The interaction between uncharged macroparticles with sufficiently large sizes immersed in pure water is attractive and very strong at small separations. The interaction between negatively charged macroparticles is "more repulsive" than between positively charged macroparticles. On the whole, however, the asymmetry of the SPC/E water in responding to positively and negatively charged surfaces is not high. It has been shown that the results obtained from the RISM theory combined with the SPC/E water are in qualitative accord with those calculated by the reference hypernetted-chain (RHNC) theory for hard spheres with embedded dipoles and tetrahedral quadrupoles, in terms of reduced density profiles, surface potential and macroparticle interactions.

121: Interaction between Macroparticles in Aqueous Electrolytes

Masahiro Kinoshita, Shin-ya Iba, Makoto Harada

Journal of Chemical Physics, Vol.105, No.6, pp.2487-2499, 1996.

We report results of theoretical calculations for the interaction between two isolated, structureless spherical macroparticles immersed in aqueous electrolytes comprising water-like molecules (hard spheres embedded with point dipoles and tetrahedral quadrupoles), 1:1 cations and anions (the diameter of cations is equal to that of anions). The reference hypernetted-chain (RHNC) theory with hard-sphere bridge functions is employed in the calculations. The fluid structure and the potential of mean force scaled by $dS/(\pi dM)$ (dS and dM denote the solvent and macroparticle diameters, respectively) converge to limiting behaviours with increasing dM as long as the surface charge density of the macroparticle is kept constant. The qualitative aspects of the conclusions are not altered even when dM is set at $10dS$.

The interaction between neutral macroparticles in pure water is characterized by strong, short-range attraction. However, a relatively minor, short-range repulsive component is added to the interaction when ions are included in water. On the other hand, the presence of apolar particles in water at a trace concentration leads to considerable enhancement of the attraction. Effects of ionic sizes on the interaction between charged macroparticles are substantially large and opposite to those which would be observed using the primitive model. When the size of counterions is sufficiently large and the ionic concentration is sufficiently high, there is a regime where the interaction between highly like-charged macroparticles is strongly attractive.

122: Interaction between Macroparticles in Lennard-Jones Fluids or in Hard-Sphere Mixtures

Masahiro Kinoshita, Shin-ya Iba, Ken Kuwamoto, Makoto Harada

Journal of Chemical Physics, Vol.105, No.16, pp.7184-7191, 1996.

We report results of numerical analyses on the surface (macroparticle) interactions in simple fluids. The singlet Ornstein-Zernike (OZ) theories with hypernetted-chain (HNC) closures are employed. With no (or very weak) attraction in the surface-fluid interaction u_{MS} , both the interaction ϕ_{MM} and the force f_{MM} between macroparticles in Lennard-Jones fluids are characterized by monotonically decreasing attraction. With increasing attraction in u_{MS} , however, ϕ_{MM} and f_{MM} become more oscillatory. The force between planar Lennard-Jones solids immersed in a Lennard-Jones fluid previously calculated by the grand canonical ensemble Monte Carlo simulation, which oscillates around zero with strong repulsion at small surface-to-surface separations, is well reproduced by our theoretical approach. The previously reported experimental observation that addition of cyclohexane to octamethylcyclotetrasiloxane causes a reduction in the range of the solvation force is well demonstrated by our theoretical calculations on a simple binary mixture of hard spheres with different diameters. Similarly, the model reproduces the observation that at a sufficiently high mole fraction of cyclohexane there is less structure than in either of the pure liquids.

123: Interaction between Macroparticles in a Simple Model System of a Non-Polar Liquid Containing Trace Amounts of Water

Masahiro Kinoshita, Shin-ya Iba, Ken Kuwamoto, Makoto Harada

Journal of Chemical Physics, Vol.105, No.16, pp.7177-7183, 1996.

We report results of numerical analyses on the macroparticle interactions immersed in a simple model system of non-polar liquid containing trace amounts of water. The singlet Ornstein-Zernike approach

with the reference hypernetted-chain closures is employed. Particles of component 1 (water) are characterized by strong attractive interaction among them, those of component 2 (non-polar liquid) are hard spheres, and particles of different components interact through hard-sphere potential. The mole fraction of component 1 x_1 is very small. Beyond $x_1 = x_{1P}$, the mixture cannot exist even in the metastable state with a single phase. Some affinity is considered only between the macroparticle surface and component 1. When the affinity ξ (negative ξ implies repulsion) is increased with fixing x_1 (at a value significantly smaller than x_{1P}) and the macroparticle diameter d_M , the macroparticle interaction ϕ_{MM} shifts to the lower (more attractive) side and eventually becomes extremely long-ranged and divergent. For larger x_1 , the divergence occurs at lower ξ . Whenever ϕ_{MM} becomes divergent, the reduced density profile of component 1 near the surface also becomes extremely long-ranged and divergent. The effects of d_M on ϕ_{MM} is also analyzed. At the stability limit ($x_1 \rightarrow x_{1P}$), the divergences occur irrespective of ξ and d_M , which is consistent with the recent prediction (Attard et al., Phys.Rev.A45, 7621(1992)).

124: * Microemulsions as Liquid Media for Materials Separation

Makoto Harada, Motonari Adachi, Akihisa Shioi, Ken-ichi Kurumada, Kohsaku Kawakami

International Journal of the Society of Materials Engineering for Resources

The functions of the microstructures in water-in-oil microemulsions are elucidated. The electrostatic interaction in the water-pools of the microstructures plays a key role in the solubilization of ionic solutes. A large internal interface of microemulsion contributes to the solubilization of less polar solutes. The curvature of the microstructures affects the local environment of less polar solutes entrapped in the internal interface. For polar macromolecules such as proteins, the microstructures have a function to recognize the size of solutes. The solubilization dynamics was also studied. These knowledge permits tailoring microemulsion for solubilization of solutes and chemical reactions in the microstructures.

125: * Selective Separation of Concanavalin A Using Bioaffinity in Reverse Micellar System

Motonari Adachi, Makoto Harada, Akihisa Shioi, Hiroki Takahashi, Shigeo Katoh

Proceedings of ISEC'96 Vol.2, pp.1393-1398, 1996

Selective separation of a target protein using bioaffinity in reverse micellar system was achieved by two different methods for the extraction of concanavalin A (ConA) using alkylglucoside (AGn) as the affinity ligand. The first method utilized the characteristic behavior of sodium bis(2-ethylhexyl)sulfosuccinate (AOT)/butanol/iso-octane system, i.e., ConA could be extracted effectively when AGn was added as

cosurfactant but was not extracted at all without AGn. The problem of this method was the precipitation of ConA at the liquid/liquid interface presumably due to the denaturation of ConA by AOT. The second method utilized the characteristics of the reverse micellar system composed of non-ionic surfactant, tetraoxyethylenedecylether, i.e., this reverse micellar system had no ability to extract water-soluble proteins without affinity ligand. When AGn was added to this system, ConA could be extracted selectively with high efficiency, and backward extraction could be performed successfully using buffer solution containing glucose or methyl-*alpha*-glucoside by adding ethanol or butanol.

126: * Protein Extraction in Polyoxyethylene Alkyl Ether/AOT Microemulsion Systems

Akihisa Shioi, Makoto Harada, Hiroki Takahashi, Motonari Adachi

Proceedings of ISEC'96, Vol.2, pp.1381-1386, 1996

A method of tailoring water-in-oil microemulsions for protein extraction was proposed. This method is to incorporate an ionic surfactant, AOT, or an affinity ligand surfactant, alkylglucopiranoside (AGn), to the base-microemulsions composed of nonionic surfactants, poly(oxyethylene) alkyl ether (CiEj). The tailored microemulsion with addition of AOT can extract proteins without denaturation of the proteins. The extraction mechanism becomes simple due to restrained of protein denaturation, i.e., the protein are localized in the waterpools of the microemulsion droplets, and the driving force for the extraction is the electrostatic interaction between a protein and the anionic surface of a droplet. The tailored microemulsion with the affinity ligand is effective to the selective separation of proteins.

127: * Catalytic activity of a novel water-soluble cross-linked polymer imprinting by a transition-state analogue for the stereoselective hydrolysis of enantiomeric amino acid esters

Katutosi Ohkubo, Yoshio Funakoshi (kumamoto Univ.), Takashi Sagawa (kumamoto Univ.)

Polymer, 37, 3993 (1996)

A novel water-soluble cross-linked polymer catalyst containing L-histidine and quarternary trimethyl ammonium groups, which was imprinted by a racemic transition-state analogue of phenyl 1-benzyl-oxy-carbonyl-3-methylpentylphosphonate for the hydrolysis of p-nitrophenyl N-(benzyloxycarbonyl)-L (or D)-leucinate (Z-L (or D)-Leu-PNP), exhibited the notable substrate stereospecificity for Z-L-Leu-PNP in the hydrolyses of enantiomeric amino acid PNP esters.

- 128: * The Role of the membrane-assisted hydrophobic interaction between di-, tri-, or tetrapeptide catalysts and amino acid esters in the enhancement of stereoselective hydrolysis reactions.**

Katutoshi Ohkubo, Kennji Urabe (Kumamoto Univ.), Satoshi Usui (Niigata Univ.), Takashi Sagawa (Kumamoto Univ.),

J. Mol. Catal. A: Chemical, 110, L1 (1996).

The 500 MHz ¹H NMR NOESY spectra of membrane-promoted multi-point hydrophobic interactions between peptide catalysts and enantiomeric amino acid esters were detected for clarifying the role of multi-point interactions between the reactants in the highly stereoselective hydrolysis reactions in a vesicular membrane.

- 129: * Novel Photocatalytic Asymmetric-Synthesis of Δ (or Λ)-[Co(acac)₃] (Hacac = Pentane-2,4-dione) from [Co(acac)₂(H₂O)₂] and Hacac with Helical Ruthenium(II) Complexes.**

Katutoshi Ohkubo, Megumi Watanabe (Kumamoto Univ.), Hisashi Ohta (Kumamoto Univ.), Satoshi Usui (Niigata Univ.)

J. Photochem. and Photobiol. A: Chemistry, 95, 231 (1996).

The photocatalytic asymmetrical synthesis of Δ (or Λ)-[Co(acac)₃] (Hacac ; pentane-2,4-dione) from [Co(acac)₂(H₂O)₂] and Hacac was successfully performed with novel helical M(C₃) / Δ -[Ru (Menbpy)₃]²⁺ (Menbpy; 4,4'-bis[(1R, 2S, 5R)-(-)- menthoxycarbonyl]-2,2'-bipyridine).

- 130: * Extremely high stereoselectivity of novel ruthenium(II) complexes for photoinduced reduction of racemic-[Co(acac)₃] (Hacac = Pentane-2,4-dione).**

Katutoshi Ohkubo, Mitsuhiro Fukusima (Kumamoto Univ.), Hisashi Ohta (Kumamoto Univ.), Satoshi Usui (Niigata Univ.)

J. Photochem. and Photobiol. A: Chemistry, 98, 137-140 (1996).

A helical photocatalyst M(C₃)-counterclockwise Δ -[Ru(Menbpy)₃]²⁺ possessing a long lifetime (1500 ns) facilitated reduction of racemic-Co(acac)₃ with extremely high enantiomer rate ratios falling in the range of $k(\Delta)/k(\Lambda) = 14.8$ (in the absence of Hacac) - 91.9 (in the presence of Hacac).

131: * Tryptophan Dioxygenase-like Catalysis of Achiral and Chiral Manganese(II) Porphyrins for Dioxygen-inserted Indole-Ring Opening Reactions.**Takashi Sagawa (Kumamoto Univ.), Katsutoshi Ohkubo**

J. Mol. Cat. A; Chemical (Special Issue on Recent Developments on Biomimetic Oxidation Catalysts), 113, 269-281(1996).

The mimetic tryptophan dioxygenase reaction with tetraphenyl (or 5, 10, 15, 20 α -tetrakis-[o-(L(-)-camphanoylamido)phenyl] porphyrinato-manganese(II), a proximal L-histidine-type N-methylimidazole, and several tryptophan analogues carried ring opening products (53 - 64e.e. of R(-) isomer). The key intermediate was also detected with NMR or with deuterated substrates.

132: Electrochemical behavior of glassy carbon and some metals in a ZnCl_2 -NaCl melt**Yasushi Okano* Akira Katagiri*****(Graduate School of Human and Environmental Studies)**

Proceedings of the Tenth International Symposium on Molten Salts, PV 96-7, pp.244-253, 1996PV 96-7, pp.244-253, 1996

Stability and reactivity of glassy carbon, nickel, platinum, and tungsten in ZnCl_2 -NaCl (60-40 mol%) melt at 450°C were investigated by cyclic voltammetry and constant-potential electrolysis. Glassy carbon was stable in the potential range of 0.23-1.8 V vs. Zn in ZnCl_2 -NaCl(saturated). Nickel was oxidized and partially passivated around 0.8-0.9 V. X-ray diffraction analysis revealed the formation of β_1 -NiZn alloy at 0.3-0.35 V and γ -NiZn alloy at 0.2-0.25 V. Platinum was oxidized and partially passivated around 1.7-1.8 V, formed δ -PtZn alloy at 0.35-0.4 V, γ_1 -PtZn alloy at 0.4 V, and γ -PtZn alloy at 0.2-0.25 V. Voltammograms from a rotating tungsten disk electrode suggested the formation of a poorly soluble compound in an anodic process.

133: * Study on Reactivity Worth of Beryllium by (n,2n) and (γ ,n) Reactions**Tsuyoshi Misawa *, Seiji Shiroya, Keiji Kanda*****(Nagoya Univ.)**

Nucl. Technol., 116[1], 11-20 (1996)

The experiments on the reactivity worth of beryllium metal was performed using the Kyoto University Critical Assembly, and it was analyzed to examine the validity of computational method to treat

(n,2n) reactions in calculation. The experimental results demonstrated that beryllium metal has positive reactivity worth compared with graphite. In the analysis, (n,2n) reactions were treated as modifying scattering cross sections in a transport calculation, whereas, both scattering and absorption cross sections should be modified in a diffusion calculation. The results of calculation for the reactivity worth of beryllium agreed with experimental data within a few percent in the calculated to experimental ratio. Calculated results indicated that (n,2n) reactions of beryllium contribute by about 85 % to the positive reactivity worth compared with graphite in the present experiments at a thermal reactor. Moreover, through the improved neutron and gamma-ray coupled calculation, the effect of (γ , n) reactions of beryllium on reactivity was estimated. It was found that (γ , n) reactions of beryllium can be negligible so far as the present reactivity worth is concerned.

134: * Design Study of Spectrum Shifter Region in Research Reactor by Using the Kyoto University Critical Assembly (KUCA)

Seiji Shiroya, Hironobu Unesaki, Toshikazu Takeda *, Otohiko Aizawa **
 *(Osaka Univ.), ** (Musashi Inst. of Technol.)

Proc. of Intern. Conf. on Neutrons in Res. and Industry, SPIE Vol. 2867, pp. 525-528 (1996)

For the nuclear design of a spectrum-controlled irradiation field in a research reactor, reaction rate distributions of gold, nickel and indium wires were measured in the Kyoto University Critical Assembly in tight-pitch lattice cores of different moderator-to-fuel volume ratios with spectrum shifter regions which consist of beryllium, graphite and aluminum. Spectrum indices were obtained by measuring the cadmium ratio of gold wire and calculating the ratio of reaction rates between gold and nickel wires. The measured data were compared with the results of neutronics calculations which are employed in the neutronics design of the irradiation field.

135: Analysis of Experiment on Temperature Coefficient of Reactivity in Light-Water-Moderated and Heavy-Water-Reflected Cylindrical Core Loaded with Highly-Enriched-Uranium or Medium-Enriched-Uranium Fuel

高濃縮あるいは中濃縮 U 燃料を装荷した軽水減速重水反射型円筒炉心の反応度温度係数実験の解析

Seiji Shiroya, Masaaki Mori, Keiji Kanda

J. Nucl. Sci. Technol., 33[3], 211-219 (1996)

An analysis was performed for the temperature coefficient of reactivity measured in the six types of light-water-moderated and heavy-water-reflected cylindrical cores containing highly-enriched-uranium (HEU) or medium-enriched-uranium (MEU) fuel, which was constructed in the Kyoto University Critical

Assembly (KUCA). The purpose of the present analysis was to reveal a mechanism why a light-water region existed in the core contributes to a large positive temperature effect on reactivity. Therefore, based on the assessment of the computational method to calculate the temperature coefficient of reactivity in a multi-region type core, studies were carried out to examine each effect of three physical processes (Doppler broadening, thermal expansion and thermal neutron spectral shift) on the temperature coefficient and to separate each contribution of the multi-regions to this physical quantity. The measured temperature coefficients were approximately simulated by the calculations using the SRAC code system. The Doppler broadening caused a slightly negative effect in the MEU cores and the thermal expansion a negative effect in all the cores, whereas the thermal neutron spectral shift caused a large positive effect in all the cores. The temperature effect on reactivity in the fuel region was negative, while that in the light-water region existed in the core was positive because of the decrease in neutron absorption due to the thermal expansion and the spectral shift effects, and it became positive in the present core where large light-water regions existed in the core.

136: * Measurement and Analysis of Reaction Rate Distributions in Cores with Spectrum Shifter Region

Seiji Shiroya, Shigekazu Matuura, Hironobu Unesaki, Toshikazu Takeda *, Takanori Kitada *, Otohiko Aizawa **, Keiji Kanda
*(Osaka Univ.), **(Musashi Inst. of Technol.)

Proc. Intern. Conf. on the Physics of Reactors, PHYSOR96, Vol.2, pp.E-219 - E-227 (1996).

For the nuclear design of a spectrum-controlled irradiation field in a research reactor, reaction rate distributions of gold (Au), nickel (Ni) and indium (In) wires were measured in the Kyoto University Critical Assembly (KUCA) by constructing tight-pitch lattice cores of different moderator-to-fuel volume ratios (V_m/V_f), which have different spectrum shifter regions consisting of beryllium (Be), graphite (C) and aluminum (Al). Spectrum indices were obtained by measuring the cadmium (Cd) ratio of Au wire and calculating the ratio of reaction rates between Au and Ni wires. The measured data were compared with the results of neutronics calculations by the SRAC code system which are employed in the neutronics design of the irradiation field.

137: * Calculation of Void Coefficient in HCLWR Cells

Stephane Cathalau*, Hironobu Unesaki, Seiji Shiroya, Otohiko Aizawa**, Toshikazu Takeda***, Franck-Olivier Carre*, Keiji Kanda
*(CEA Cadarache, France), **(Musashi Inst. Tech.), ***(Osaka Univ.)

Proc. Int. Conf. on the Physics of Reactors, PHYSOR96, Vol.2, pp. C-1 - C-10 (1996).

Analysis of the benchmark problems on void coefficient of HCLWR cells have been performed using the Japanese SRAC code system with JENDL-3.2 library and the French APOLLO-2 code with JEF-2.2 library. The benchmark problems have been specified in order to investigate the physical phenomena occurring during the progressive voidage of HCLWR lattices and to evaluate the impact of nuclear data and calculational methods. The discrepancy of k_{∞} and void reactivity values obtained by the two codes have been analyzed, which have been shown to be caused by a complicated balance of both negative and positive components.

138: Measurements of First-Harmonic Eigenvalue Separation in Loosely Coupled-Core Reactor

Kengo Hashimoto*, **Toshikazu Takeda**^{*2}, **Otohiko Aizawa**^{*3}, **Testuo Horiguchi***, **Junji Yamamoto**^{*4}, **Takanori Kitada**^{*2}, **Yoshiki Kato**^{*2}, **Syu Izumi**^{*3}, **Chizuo Mori**^{*5}, **Seiji Shiroya**, **Hironobu Unesaki**

^{*}(Atomic Energy Research Inst., Kinki Univ.), ^{*2}(Osaka Univ.), ^{*3}(Musashi Inst. Tech.), ^{*4}(Setsunan Univ.), ^{*5}(Nagoya Univ.)

Proc. Int. Conf. on the Physics of Reactors, PHYSOR96, Vol.2, pp.E-1171 - E-179 (1996).

The first-harmonic eigenvalue separation of a coupled-core thermal system was experimentally determined by the flux tilt, rod drop and noise-correlation methods. No differences in the eigenvalue separations obtained between measuring techniques could be observed. The separation \$ 0.85 of the present system is comparable to those of large BWR cores.

139: * Study on Reactivity Measurement by the Feynman- α Method

Tsuyoshi Misawa*, **Seiji Shiroya**, **Yoshihiro Yamane***, **Hironobu Unesaki**
^{*}(Nagoya Univ.)

Proc. Int. Conf. on the Physics of Reactors, PHYSOR96, pp. E-228 - E-236 (1996).

The Feynman- α method was applied to measurement of reactivity and the ability of this method for a real-time reactivity monitoring system was assessed. In the experiment, all measured data by BF_3 detectors were stored in a multi-channel scaler controlled by a personal computer, and they were analyzed to obtain prompt neutron decay constant (α) and reactivity with consideration of dead time of detector. It was found that α could be obtained almost in a real-time even for both positive and negative reactivities by the present experimental technique.

140: * Feasibility of High Frame-Rate Neutron Radiography by Using a Steady Thermal Neutron Beam with $10^6\text{n/cm}^2\text{s}$ Flux

$10^6\text{n/cm}^2\text{s}$ の定常熱中性子ビームを用いた中性子ラジオグラフィ高速撮影の可能性

Takashi Hibiki, Kaichiro Mishima

Nucl. Instru. Meth. Phys. Res., A369, 186-194 (1996)

The feasibility of high frame-rate neutron radiography by using a steady thermal neutron flux on the order of $10^6\text{n}/(\text{cm}^2\text{s})$ was investigated and the application of this technique to fluid visualization was examined. The Kyoto University Research Reactor was used as a neutron source. The imaging system for the high frame-rate neutron radiography with the steady thermal neutron beam was constructed by combining a high sensitivity scintillator ${}^6\text{LiF}/\text{ZnS} : \text{Ag}$, a high-speed video which could take images with the light intensity of 1.5 lux at the recording speed of 1000 frames/s and an image booster whose gain was about 100. Visualization of air-water two-phase flows in a rectangular duct with 2.4 mm gap and 40 mm width were successfully performed with the steady thermal neutron beam and this imaging system at the recording speed up to 500 frames/s. The limit of high frame-rate neutron radiography in an ideal system without background radiation such as scattered neutron and with neutron detection efficiency of 100% measurement error of neutrons due to the natural statistics of neutrons in the low neutron flux field. It was shown from this study that the high frame-rate neutron radiography by the steady neutron flux on the order of $10^6\text{n}/(\text{cm}^2\text{s})$ has a good possibility.

141: * Visualization and Measurements of Two-Phase Flow in Metallic Ducts Using Neutrons as Microscopic Probes – (2nd Report, Measurements of Some Flow Characteristics by Image Processing Techniques)

プローブとして中性子を用いた金属管内気液二相流の可視化と計測 – (第2報、画像処理による流動特性計測)

Kaichiro Mishima, Takashi Hibiki

Trans. JSME (Ser.B), 52 [593], 137-144 (1996)

日本機械学会論文集 (B編)、62巻 593号、137-144 (1996)

In order to apply the neutron radiography technique to fluid research, quantitative analyses of high-frame-rate neutron radiographs of air-water flows in a narrow rectangular duct were demonstrated by using image processing techniques. From the geometrical information of the images, the flow regime, bubble rising velocity, water-layer thickness, and interfacial area calculated by multiplying the interfacial length by the channel gap and size distribution of bubbles with diameter greater than 1 mm could be measured by the image processing technique. From the gray levels of the images, the spatial and temporal averaged void fraction and the void profile across the duct could also be measured by the image processing technique. It was clarified that the limited value of the measurable liquid film thickness with the neutron radiography technique was calculated by an error analysis. It was shown quantitatively that the measurement error decreased by integrating the image temporally.

142: * Visualization and Measurement of Two-Phase Flows in Metallic Ducts Using Neutrons as Microscopic Probes – (3rd Report, Quantitative Measurement of Neutron Radiography Image)

プローブとして中性子を用いた金属管内気液二相流の可視化と計測 – (第3報、中性子ラジオグラフィ画像の定量化法)

Takashi Hibiki, Kaichiro Mishima

Trans. JSME (Ser.B), 62[593], 919-926 (1996)

日本機械学会論文集 (B編)、62巻 593号、919-926 (1996)

The quantitative measurement of an image obtained by neutron radiography technique was proposed in order to accurately measure the void fraction of a two-phase flow in a metallic duct. It was shown experimentally that the spatial distribution of the dark-current component was homogeneous and the temporal variation could be ignored. Since the scattered neutrons falling on the image converter could be homogenized by setting the test section at a distance from the converter, it was clarified that the corrections for dark-current and scattered neutrons could be represented by an offset value. It was proposed that the offset value could be determined by using the total macroscopic cross section of the material (Σ -scaling method). By comparing the calculated void fractions with the measured ones obtained by simulating the known void profile using a standard test section, the void fraction could be measured by this method within 2% error. The measurement error was estimated to be up to 10% when no corrections for scattered neutrons were made or no arbitrary offset value was used.

143: * Visualization and Measurements of Two-Phase Flows in Metallic Ducts Using Neutrons as Microscopic Probes – (4th Report, Effect of Image Gray Scale and Pixel Number on Image Quantification)

プローブとして中性子を用いた金属管内気液二相流の可視化と計測 – (第4報、画像定量化に及ぼす階調度および計測画素数の影響)

Takashi Hibiki, Kaichiro Mishima

Trans. JSME (Ser.B), 62[597], 1781-1787 (1996)

日本機械学会論文集 (B編)、62巻 597号、1781-1787 (1996)

A study on the effects of image gray scale and pixel number on image quantification was performed analytically and experimentally in order to establish a method of measuring multiphase flows using neutron radiography. It was found from a simplified model that the resolution of an object thickness to be measured had logarithmic characteristics for the object thickness, and there is a possibility that the measured void fraction in high- and low-void-fraction regions might include large error. It was shown from the numerical analysis that the measurement error would be within 5% except for the annular flow region with the void fraction greater than 90%, when void fraction of an air-water two-phase flow in a channel with the local gap smaller than 9 mm was measured under the condition of the image gray scale=100. It was revealed from a simplified model that the error due to the number of pixels would be within 5% when the number of pixels projecting the object is ten times greater than that projecting the

object boundary.

144: * Quantitative Limits of Thermal and Fluid Phenomena Measurements Using the Neutron Attenuation Characteristics of Materials

物質中の中性子減衰特性を利用した熱流動現象の測定の限界

Kaichiro Mishima, Takashi Hibiki

Exp. Thermal & Fluid Sci., 12, 461-472 (1996)

Temporal and Spatial resolution of the neutron radiographic technique were investigated in order to apply this technique to the visualization and measurement of thermal and fluid phenomena. The temporal resolution of three imaging methods of temporally resolved neutron radiography—static neutron radiography with a pulsed neutron beam and high frame rate neutron radiography with either a pulsed or steady neutron beam—was studied. The temporal resolution was determined by the sensitivity and light decay time of the image detector and statistical variation of neutrons, and the resolution limits of static and dynamic imaging methods were estimated to be a few microseconds and a few hundred microseconds, respectively. By performing an error analysis to calculate the limit value of liquid film thickness that can be measured by neutron radiography, it was determined that the limit value of a rectangular channel gap or round tube diameter should be smaller than 3.25 or 4.00 mm, respectively, for measuring the void fraction of air-water flow within an error of 10% was experimentally confirmed by comparing the void fraction values in a rectangular duct with a 2.4-mm gap obtained by neutron radiography with those obtained by optical and conductance probe methods.

145: * Some Characteristics of Air-Water Two-Phase Flow in Small Diameter Vertical Tubes

垂直細管内空気-水二相流の特性

Kaichiro Mishima, Takashi Hibiki

Int. J. Multiphase Flow, 22[4], 703-712 (1996)

Flow regime, void fraction, rise velocity of slug bubbles, and frictional pressure loss were measured for air-water flows in capillary tubes with inner diameters in the range from 1 to 4 mm. Although some flow regimes peculiar to capillary tubes were observed in addition to commonly observed ones, overall trends of the boundaries between flow regimes were predicted well by Mishima-Ishii's model. The void fraction was correlated well by the drift flux model with a new equation for the distribution parameter as a function of inner diameter. The rise velocity of the slug bubbles was also correlated well by the drift flux equation. The frictional pressure loss was reproduced well by Chisholm's equation with a new equation for Chisholm's parameter C as a function of inner diameter.

146: * Quantitative Limits of Thermal and Fluid Phenomena Measurements Using the Neutron Attenuation Characteristics of Materials Quantitative Method to Measure Void Fraction of two-Phase Flow Using Electronic Imaging with Neutrons

中性子ラジオグラフィ電子撮像法を用いた二相流ボイド率の定量計測法

Kaichiro Mishima, Takashi Hibiki

Nucl. Sci. Eng., 124, 327-338 (1996)

A quantitative method of image processing coupled with the neutron radiography technique is proposed to accurately measure the void fraction of a two-phase flow in a metallic duct. The spatial distribution of the dark current component is experimentally shown to be smooth, and the temporal variation cannot be ignored. Since the neutrons scattered in an object can be smoothed and reduced by setting the test section at a large distance from the converter, it is clarified that the corrections for the dark current and scattered neutrons can be represented by an offset. The offset value can be determined by using the total macroscopic cross section of the object (Σ -scaling method). By comparing the calculated void fractions with the measured ones obtained by simulating the known void profile using a standard test section, the void fraction can be measured by this method within 2% error. The measurement error is estimated to be up to $\sim 10\%$ when no correction for scattered neutrons is made or arbitrary offset values are used.

147: * Approximate Method for Measurement of Phase-Distribution in Multiphase Materials with Small Neutron-Attenuation Using a Neutron Beam as a Probe

中性子をプローブとして用いる中性子減衰係数の小さい多相媒体内の相分布の近似的計測法

Takashi Hibiki, Kaichiro Mishima

Nucl. Instr. Meth. in Phys. Res., A 374, 345-351 (1996)

An approximate method for the quantification of a neutron radiography image was proposed for measuring the phase-distribution of multiphase materials with small neutron-attenuation. Since it is not necessary for this method to put a standard calibration sample in a field of a view, this method has an advantage of measuring the phase-distribution of multiphase materials with unknown internal-structure and neutron-attenuation in the object in an enlarged field of view. Although its application is limited to an object with small neutron-attenuation, it was revealed from a numerical analysis that the approximate method can be applicable to heavy water, liquid sodium and liquid potassium, which are important materials in relation to research on the thermalhydraulics of a nuclear reactor. The validity of the approximate method was also confirmed experimentally by comparing the void fraction of air-water flows in round tubes measured by the approximate method with those by the other more-accurate method.

148: * Visualization and Measurements of Two-Phase Flows in Metallic Ducts Using Neutrons as Microscopic Probes – (5th Report, Void Distribution Measurement Method for Two-Phase Flow in a Round Tube)

プローブとして中性子を用いた金属管内気液二相流の可視化と計測 – (第5報、円管内二相流の半径方向ボイド率分布計測法)

Takashi Hibiki, Kaichiro Mishima

Trans. JSME, 62[600], 3002-3008 (1996)

日本機械学会論文集、62巻600号、3002-3008 (1996)

A method was proposed for measuring the radial void distribution of a two-phase flow in a round tube using neutrons as probes. This method involves (1) assuming an appropriate function which could approximate the radial void distribution, (2) deriving a function to approximate the void distribution projected on a plane perpendicular to the incident neutron beam and along the traverse direction (x -direction) by integrating the function of the radial void distribution, and (3) determining parameters in the function of the radial void distribution by the least squares method. It was shown analytically and experimentally that the effect of scattered neutrons and unparallelness of the incident neutron beam, which might affect the applicability of this method, could be corrected and ignored, respectively, by taking an appropriate distance between the converter and the test section. This method was applied to the measurement of a temporally averaged radial void distribution of an air-water flow in a round tube of 3.90 mm inner diameter. It was revealed that complex void distribution with a saddle-shaped profile could be measured by assuming an appropriate function.

149: * Experimental Study on Critical Heat Flux in Laterally Non-Uniformly Heated Rectangular Channels

横方向に非一様加熱された矩形流路内の限界熱流束に関する実験的研究

Kaichiro Mishima, Takashi Hibiki, Hideaki Nishihara, Toshihiko Motomura*, Tomoo Ohtsuji*, Akira Kurosawa*

***(Kobe University of Mercantile Marine)**

2nd European Thermal-Sciences (EUROTHERM) & 14th UIT National Heat Transfer Conf., Rome, May 29-31, 1996.

The purpose of this study is to collect new experimental data and to obtain better understanding on critical heat flux (CHF) in narrow rectangular channels heated from one lateral side in comparison with that in channels heated from both sides. Four kinds of test sections were used in the experiment, i.e. rectangular channels heated from one side and both sides with gap thickness of 1.0 mm and 2.4 mm. The results indicated that the CHF for a both-side heated channel was close to the prediction based on the critical quality taking account of the effect of unheated wall, while the CHF for a one-side heated channel occurred along the churn to annular flow boundary. This indicates that the liquid interchange between the heated and unheated walls due to the passage of liquid slugs has a significant effect on cooling and rewetting of the heated wall, while the liquid interchange in the annular flow is small. The CHF for

both-sides heated channels were lower at low mass velocities than that for one-side heated channels, if plotted as a function of mass velocity at a given inlet water temperature, but the difference diminished at higher mass velocities. The difference of CHF at low mass velocities could be attributed to the difference in flooding CHF.

150: * High-Frame-Rate Neutron Radioscopy with a Steady Thermal Neutron Beam

定常熱中性子ビームを用いた高速度撮影中性子ラジオグラフィ

Kaichiro Mishima, Takashi Hibiki, Shigenori Fujine, Kenji Yoneda, Keiji Kanda, Hideaki Nishihara, Akira Tsuruno*, Masahito Mastubayashi*

*(Japan Atomic Energy Research Institute)

5th World Conf. on Neutron Radiography, Berlin, June 17-20, 1996.

In this study, a high-frame-rate neutron radioscopy system which makes use of steady thermal neutron beam has been developed to visualize and measure high-speed fluid phenomena. Main features of this system are (1) high-frame-rate (maximum recording speed: 1000 frames/s), (2) long recording time (maximum 21 minutes at 1000 frames/s) and (3) high-sensitivity (minimum gate time 10 μ s). Visualization of air-water two-phase flow in a rectangular duct with 2.4 mm gap and 40 mm width made of aluminum alloy and the behavior of molten metal in heavy water were successfully performed with a steady thermal neutron beam and the present imaging system at frame rates up to 1000 frames/s. The quality of the images obtained from the high-frame-rate neutron radioscopy was good enough to observe the fluid behavior and measure flow characteristics such as flow regimes, bubble rising velocity and void fraction.

151: * Evaluation of Scattered Neutron Component in Thermal Neutron Radiography Image- (Influence of Scattered Neutrons and Unparallelness of Incident Neutron Beam-)

熱中性子ラジオグラフィ画像中の散乱中性子成分の評価 —— 散乱中性子及び入射中性子ビームの平行度の影響 ——

Unesaki Hironobu, Kaichiro Mishima, Takashi Hibiki

5th World Conf. on Neutron Radiography, Berlin, June 17-20, 1996.

Analysis of thermal neutron radiographic images are performed using neutronic methods. Analytical expressions for the behavior of scattered neutron component and image distortions due to the unparallelness of the incident neutron beam are shown. Numerical results are compared with the neutron radiographic images of simple rectangular polystyrene test sections of various thickness. Suggestions for the optimum distance between the test section and the converter has been given.

152: * Verification of Neutron Radioscopic Measurement of Void Fraction by Monte Carlo Simulation

中性子ラジオグラフィを用いたボイド率計測のモンテカルロ・シミュレーションによる検証

Hironobu Unesaki, Kaichiro Mishima, Takashi Hibiki

5th World Conf. Neutron Radiography, Berlin, June 17-20, 1996

Neutron radiographic images have been simulated using the Monte Carlo method to verify the Σ -scaling method used in void fraction measurement of two-phase flow. Continuous energy Monte Carlo code MCNP was used for the accurate treatment of the test section with complex geometry. Radioscopic images of water layer thickness distribution in concentric triple tube test section were successfully reproduced by the Monte Carlo simulation. The simulated images at various distances between the test section and the converter were obtained using an ideal monodirectional (parallel) beam and realistic beam with unparallelness defined by the L/D ration, thus enabling the separate treatment of the unsharpness of the image caused by the scattered neutrons and unparallelness of the incident neutron beam. The treatment of the scattered component and the unparallelness of incident beam employed in the Σ -scaling method was verified to be appropriate through the simulation, which shows that the Σ -scaling method could be successfully adopted for the quantitative measurement of void fraction of two-phase flow.

153: Analytical Study of Two-Phase Flow Pressure-Drop Oscillations in a Vertical Heated Tube

垂直加熱管内の二相流圧力降下振動の解析的研究

Kaichiro Mishima, Jian Zhang, Masatoshi Kureta*, Hideaki Nishihara

***(Japan Atomic Energy Research Institute)**

3rd KSME-JSME Thermal Engineering Conference '96-Kyongju, October 20-23, 1996

第3回日韓熱工学会議、1996年10月20-23日、慶州

This study focuses on the analytical investigation of two-phase flow pressure-drop oscillations in a vertical heated tube with the two-fluid model employed in the computer code MINI-TRAC. The pressure-drop oscillation is an important phenomenon appearing in a two-phase flow channel with compressible volume in the upstream. In the previously obtained experimental data, pressure-drop oscillations with superimposed density wave oscillations have been observed. In the present work, numerical calculations have been carried out to predict the characteristics of the pressure-drop oscillations and the range of the instabilities. It is also an application of the two-fluid model to the analysis of pressure-drop oscillations at a low pressure in a heated channel with a small inner diameter. Good agreement between the simulations and experiments has been obtained.

154: * Visualization and Measurement of Two-Phase Flow by Using Neutron Radiography

中性子ラジオグラフィを用いた二相流の可視化と計測

Kaichiro Mishima, Takashi Hibiki, Hideaki Nishihara

Proc. Japan-US seminar on Two-Phase Flow Dynamics, Fukuoka, July 15-20, 1996

二相流ダイナミクスに関する日米セミナー、1996年7月15-20日、福岡

To apply neutron radiography (NR) technique to fluid research, high frame-rate NR with a steady thermal neutron beam has been developed in the present research program by assembling up-to-date technologies for neutron source, scintillator, high-speed video and image intensifier. This imaging system has many advantages such as a long recording time (up to 21 minutes), high-frame-rate (up to 1000 frames/s) imaging and no need for triggering signal. Visualization of air-water two-phase flow in a metallic duct was performed at the recording speeds of 250, 500 and 100 frames/s. The qualities of those consecutive images were good enough to observe and measure the flow structure and the characteristics. Image processing technique enabled measurements of various flow characteristics, such as flow regimes, rising velocity of bubbles, average void fraction, and void profile. It was confirmed that this new technique may have significant advantages both in visualizing and measuring high-speed fluid phenomena when the other methods such as an optical method and X-ray radiography cannot be applicable.

155: * Dryout in a Boiling Channel under Oscillatory Flow Condition

流動脈動下における沸騰流路のドライアウト

Hisashi Umekawa*1, Mamoru Ozawa*1, Akira Miyazaki*2, Kaichiro Mishima, Takashi Hibiki

***1(Kansai University) *2(Hirakawa Guidom Co.)**

JSME Int. J., (Ser.B), 39[2], 412-418 (1996)

Premature dryout due to flow oscillation is a very important factor in designing boiling systems. The flow oscillation depends, in general, on system size and/or configuration, and therefore the relationship between the premature dryout and the flow oscillation has not been fully understood so far. In this investigation, a CHF experiment in a forced flow boiling channel under the oscillatory flow condition has been conducted. Numerical simulation has also been conducted based on the lumped-parameter model of the boiling channel. The simulation well represents the transient behavior of the dryout under the oscillatory flow condition.

156: Observation of Superstructure on the (0001) Face of C_{70} Single Crystals

L. Jiang, T. Iyoda, N. Kino, K. Kitazawa, K. Hashimoto, and A. Fujishima

Surface Sci., 349, L101-L106 (1996).

A novel superstructure was observed for the first time on the 0001 face of C_{70} single crystal surfaces by atomic force microscopy (AFM). The superstructure was present as parallel fringes along the $[2110]$ direction in AFM images, with a dominant spacing of 27 ± 3 nm and a dominant corrugation height difference of 0.30 ± 0.03 nm. The molecular resolution images obtained on the superstructure indicated a distorted hexagonal arrangement. The observation of the corrugated surface leads us to propose the formation of a periodic array of partial-dislocation lines, which separate two types of alternating strip-like surface regions: one with face-centered cubic (fcc) stacking (ABC or "C" sites) and the other with hexagonal close-packed (hcp) stacking (ABA or "A" sites). The surface molecular dislocation lines occupy bridging (BR) instead of hollow sites (A, C sites).

157: Electrochemical Reduction of CO_2 with High Current Density in a CO_2 + Methanol Medium at Various Metal Electrode

T. Saeki, K. Hashimoto, N. Kimura, K. Omata, and A. Fujishima

J. Electroanal.Chem., 404, 299-302 (1996)

Various metals were used as working electrodes in the electrochemical reduction of highly concentrated CO_2 in a CO_2 + methanol medium. Reduction products were CO, CH_4 , C_2H_4 and methyl formate ($HCOOCH_3$). Methyl formate was formed by the reaction between solvent, methanol, and a CO_2 reduction product, formic acid, which corresponds to formic acid formation in aqueous systems. Basically, most electrodes gave the same principal product both in the present system and in the aqueous system. At W, Ti and Pt electrodes, CO_2 reduction was inefficient. Sn and Pb electrodes were active in formate production. However, CO was formed much more efficiently in the present system than in the aqueous system. It was indicated that Sn and Pb served as electrodes catalyzing formate production, while the supporting electrolyte, tetrabutylammonium cation, promoted CO formation. Electrolysis at Ag, Zn and Pd electrodes yielded CO mainly. Hydrocarbon formation at a Cu electrode was less efficient than in aqueous systems. However, hydrocarbon was formed efficiently at an Ni electrode. These differences in hydrocarbon formation in the present system, in comparison with aqueous systems, could be explained by the balance between hydrogen atom and CO_2 reduction intermediates on the electrode surface.

158: Electrochromic Behavior of Electrodeposited Tungsten Oxide Thin Films

J. N. Yao, P. Chen, and A. Fujishima

J. Electroanal.Chem., 406, 223-226 (1996)

Amorphous tungsten trioxide thin films can be coloured deeply with an optical irradiation of appropriate energy (photochromism) or with an applied electric field (electrochromism). These processes have

received considerable attention because of their potential application in display devices, high-density memory devices, sensor devices and so on. For these purposes, tungsten trioxide films prepared by various physical vapour deposition methods have been investigated. These methods are generally expensive and it is difficult to form large-area films. However, the electrodeposition method is probably the most economical method for making the films in addition to its relative ease in forming large-area films. In a previous publication [11], we studied correlatively the photochromism and electrochromism of the electrodeposited and vacuum deposited molybdenum trioxide films. We found that the electrodeposited molybdenum trioxide films show good photochromic and electrochromic properties. In the present work, we extend our correlation study to the electrochromism of the electrodeposited and vacuum deposited tungsten trioxide films.

159: Two-Dimensional Surface-Enhanced Raman Imaging of a Roughened Silver Electrode

X. M. Yang, K. Ajito, D. A. Tryk, K. Hashimoto, and A. Fujishima

Surface with Adsorbed Pyridine and Comparison with AFM Images *J. Phys. Chem.*,
100 (18), 7293-7297 (1996)

Raman Scattered light from pyridine adsorbed on an electrochemically roughened silver electrode surface was used to image the two-dimensional surface morphology with a spatial resolution of $1 \mu\text{m}$. The images showed that the spatial distribution and intensity of the surface-enhanced Raman scattered (SERS) light intensity varied to a significant extent over the electrode surface and revealed apparent surface features, specifically, ridges and domes with dimensions on the order of $10 \mu\text{m}$. Atomic force microscopic images also showed similar structures. In addition, the AFM images showed that smaller surface features, on the order of $1-3 \mu\text{m}$, were associated with brighter areas in the SERS images. However, the difference in SERS intensities for bright vs dark areas was at most a factor of ~ 6 , indicating that, even in the dark areas, there was significant surface enhancement. Consistent with this result is the fact that, at still higher magnification, the AFM images in different areas of the electrode showed very similar surface structure, consisting of silver particles with diameters in the range 50-400 nm.

160: Strong Magnetocrystalline Anisotropy in MnTPP-TCNE Charge Transfer Complex

K. Nagai, T. Iyoda, A. Fujishima, and K. Hashimoto

Chem. Lett., 591-592 (1996).

Magnetic properties of one-dimensional charge transfer complex between manganese meso-tetraphenylporphyrin (MnTPP) and tetracyanoethylene (TCNE) were investigated as its plate crystals. Strong magnetocrystalline anisotropy was observed in the field and the temperature dependences of magnetization.

Magnetic phase transition was observed at 24 K and 27 K under 0.5 T of magnetic field along a- and b-axis, and c-axis, respectively. Either temperature was higher than that (18 K) of powder sample reported previously.

161: Photoinduced Magnetization of a Cobalt-Iron Cyanide

O. Sato, T. Iyoda, A. Fujishima, and K. Hashimoto

Science, 272, 704-705 (1996).

Photoinduced magnetization was observed in a Prussian blue analog, $K_{0.2}Co_{1.4}[Fe(CN)_6]6.9H_2O$. An increase in the critical temperature from 16 to 19 kelvin was observed as a result of red light illumination. Moreover, the magnetization in the ferrimagnetic region below 16 kelvin was substantially increased after illumination and could be restored almost to its original level by thermal treatment. These effects are thought to be caused by an internal photochemical redox reaction. Furthermore, blue light illumination could be used to partly remove the enhancement of the magnetization. Such control over magnetic properties by optical stimuli may have application in magneto-optical devices.

162: An Efficient TiO_2 Thin-Film Photocatalyst: Photocatalytic Properties in Gas-Phase Acetaldehyde Degradation

I. Sopyan, M. Watanabe, S. Murasawa, K. Hashimoto, and A. Fujishima

J. Photochem. Photobiol.A: Chem., 98, 79-86 (1996).

A semitransparent TiO_2 film with extraordinarily high photocatalytic activity was prepared on a glass substrate by sintering a TiO_2 sol at 450 C. Crystallographic analysis by X-ray diffraction and Raman spectroscopy showed that the film was purely anatase. The photocatalytic properties of the film were investigated by measuring the photodegradative oxidation of gaseous acetaldehyde at various concentrations under strong and weak UV light in radiation conditions. The photocatalytic activity of the film was higher than that of one of the most active commercial TiO_2 powders, Degussa P- 25. The kinetics of acetaldehyde degradation as catalyzed by the TiO_2 film as well as by p-25 powder were analyzed in terms of the Langmuir- Hinshelwood model. It is shown that the number of adsorption sites per unit true surface area is larger with the TiO_2 film, as analyzed in the powder form, than with P-25 powder. Meanwhile, the first-order reaction rate constant is also much larger with the film than with P-25 powder. Moreover, under most experimental conditions, particularly with high concentrations of acetaldehyde and weak UV illumination intensity, the quantum efficiency was found to exceed 100 % on an absorbed-photon basis, assuming that only photo-generated holes play a major role in the reaction. This leads to the conclusion that the photodegradative oxidation of acetaldehyde is not mediated solely

by hydroxyl radicals, generated via hole capture by surface hydroxyl ions or water molecules, but also by photocatalytically generated superoxide ion, which can be generated by the reduction of adsorbed oxygen with photogenerated electrons.

**163: Syntheses and Magnetic Properties of Dye Included Organometallic Magnets:
DAMS[MCr(ox)3]**

Z. Gu, O. Sato, T. Iyoda, K. Hashimoto, and A. Fujishima

Mol. Cryst. Liq. Cryst., 286, 147-152 (1996).

A series of dye-included metal complex-based magnets, DAMS[MCr(ox)3] (DAMS⁺ = 4-[2-(4-dimethylaminophenyl)ethenyl]-1-methylpyridinium cation; M²⁺ = Mn²⁺, Fe²⁺, Ni²⁺; ox²⁻ = Oxalate Ion), were synthesized. In these compounds different kinds of metal cations are bridged to each other by ox²⁻ ions. The compounds have a layered-structure and molecules of DAMS⁺ are enclathrated between the layers. Field-cooled magnetization (FCM) measurement showed that these compounds exhibit magnetic phase transition at 10K, 14K, and 18K respectively.

**164: Molecular Arrangement in an Azobenzene-Terminated Self-Assembled Monolayer
Film**

R. Wang, T. Iyoda, L. Jiang, K. Hashimoto, and A. Fujishima

Chem. Lett., 1005-1006 (1996).

An azobenzene-functionalized material was used to perform comparative investigation of molecular arrangements in self-assembled monolayer film and in crystalline state. By the means of atomic force microscopy and absorption spectroscopy, a unique herringbone structure was revealed in the densely packed self-assembled monolayer film.

165: A Film-Type Photocatalyst Incorporating Highly Active TiO₂ Powder and Fluorescein Binder: Photocatalytic Activity and Long-Term Stability

I. Sopyan, M. Watanabe, S. Murasawa, K. Hashimoto, and A. Fujishima

J. Electroanal. Chem., 415, 183-186 (1996).

In the present work, a novel TiO₂ film which is consistent with this strategy has been developed. The TiO₂ film photocatalyst has been prepared by incorporating extremely active TiO₂ particles into a paint-like sol which includes a fluoropolymer resin and an organotitanium coupling agent. Curing of the film spread on substrates was carried out by drying at the relatively low temperature of 120°C. Through this procedure, a polymer-bonded TiO₂ film with a high TiO₂ concentration (90 vol%) was obtained. The film was then examined for its photocatalytic activity in terms of the degradation of gaseous acetaldehyde, as well as its long-term stability under prolonged illumination.

166: Surface-Enhanced Raman Scattering Imaging of Photopatterned Self-Assembled Monolayers

X. M. Yang, D. A. Tryk, K. Ajito, K. Hashimoto, and A. Fujishima

Langmuir, 12 (23), 5525-5527 (1996).

A nonroughened evaporated silver film was used as a substrate for a self-assembled monolayer of p-nitrothiophenol, which was then subjected to UV photopatterning. The photopattern was imaged using surface-enhanced Raman scattering (SERS). To our knowledge, this is the first report of the use of SERS to image a patterned monolayer. Although the nature of the photoproduct is uncertain, it is probable that it is predominantly the azobenzene species.

167: Molecular-Level Design of a Photoinduced Magnetic Spin Coupling System: Nickel Nitroprusside

Z. Z. Gu, O. Sato, T. Iyoda, K. Hashimoto, and A. Fujishima

J. Phys. Chem., 100 (47), 18289-18291 (1996).

Rational design of a magnetic material (nickel nitroprusside) at the molecular level allowed switching of a spin coupling by means of photoinduced metal to ligand charge transfer (MLCT). Before irradiation, spins on Ni²⁺ are in a disordered state. An illumination at 375 nm induces a MLCT from Fe to NO and forms new spins on Fe and NO. The newly appearing spin on Fe orders the spins on the nearest Ni²⁺ ions around Fe. In other words, one MLCT aligns five spin sources resulting in the formation of magnetic clusters with $s = 5$. Furthermore, such a photoinduced spin ordering can be randomized by thermal treatment.

168: Atomic Force Microscopy and Kelvin Probe Force Microscopy Evidence of Local Structural Inhomogeneity and Nonuniform Dopant Distribution in Conducting Polybithiophene

O. A. Semenikhin, L. Jiang, T. Iyoda, K. Hashimoto, and A. Fujishima

J. Phys. Chem., 100 (48), 18603-18606 (1996).

Direct evidence of local structural inhomogeneity and nonuniform doping-level distribution in conducting polymer film has been obtained using Kelvin probe force microscopy (KFM) and atomic force microscopy (AFM). The KFM data suggests that the polymer consists of grains that constantly differ in work function and thus in the dopant concentration from the grain peripheral regions. For the as-grown polymer, most of the doping charge is located at the grain tops, whereas the electrochemically doped polymer features relatively higher doped grain periphery and less doped grain tops. The AFM study reveals two different kinds of the polymer molecular structure dependent on whether the image was taken at the top of a grain or the grain periphery. This result confirms the inherent inhomogeneity of conducting polymers demonstrated with KFM.

169: Micropattern Formation on ZnO Films Using a Photodissolution Reaction

M. Futsuhara, K. Yoshioka, Y. Ishida, O. Takai, K. Hashimoto, and A. Fujishima

J. Electrochem. Soc., 143 (11), 3743-3746 (1996).

Micropattern formation on ZnO thin films has been carried out using a photodissolution reaction. ZnO thin films were prepared on glass and on transparent, conductive SnO₂-coated glass by spray Pyrolysis. The dissolution rates of the ZnO films were measured under illumination (v_{light}) and in the dark (v_{dark}) under various conditions. The v_{light} and v_{dark} values were determined by measuring the zinc content in the ZnO film before and after the dissolution reaction using x-ray fluorescence spectroscopy. The dissolution rate became larger under UV illumination under various conditions. Both v_{dark} and v_{light} depended strongly on the pH value of the electrolyte solution and the bias voltage. The best conditions to form the ZnO film micropattern were determined by measuring both v_{light} and v_{dark} . Under the best conditions, a micropattern was obtained on the ZnO thin films on SnO₂-coated glass substrates under illumination through a photomask. The linewidth of the micropattern can be as low as about 130 μm .

170: An Electrochemical Study of Some Spirobenzopyran Derivatives in Dimethylformamide

J. F. Zhi, R. Baba, and A. Fujishima

Ber. Bunsenges. Phys. Chem., 100 (11), 1802-1807 (1996).

The electrochemical behavior of spirobenzopyran derivatives with substituted groups of OCH₃, Br and NO₂ in the benzopyran ring and the indoline ring has been studied by cyclic voltammetry and spectro-electrochemistry in a dimethylformamide (DMF) solvent at a platinum electrode. The six spirobenzopyran derivatives studied can be divided into two groups according to the presence or the absence of a nitro group substituted in the benzopyran ring. In the potential range of - 1.8 V to + 1.0 V (vs. Ag QRE), neither redox reactivity nor reversible color changes were observed for those derivatives without a substituted nitro group, while the nitro-substituted spirobenzopyrans exhibited appreciable redox behavior and the electrochromism corresponding to the redox reaction of the nitro group. In addition, an irreversible oxidation wave observed at about +1.3 V (vs. Ag QRE) for all the derivatives studied (except SP-18) was assigned to the oxidation of the nitrogen atom in indoline moiety. These oxidation wave potentials of the nitrogen atom are linear with the Hammett values $\Sigma\sigma^*$ of the substituted group, and thus suggest that a significant electron-induced interaction existed between the benzopyran and the indoline ring in the spirobenzopyran molecule.

171: Surface Enhanced Raman Imaging of a Patterned Self-Assembled Monolayer Formed by Microcontact Printing on a Silver Film

X. M. Yang, D. A. Tryk, K. Hashimoto, and A. Fujishima

Appl. Phys. Lett., 69 (26), 4020-4022 (1996).

The surface enhanced Raman scattering effect was used in conjunction with a micro-Raman system to produce an image of a pattern, on an evaporated silver surface, formed by microcontact printing of p-nitrothiophenol (PNTP). This surface is characterized by roughness on the scale of 50- 100 nm. It was confirmed that this type of printing technique forms a self-assembled monolayer with PNTP. Even without roughening of the silver surface, the surface enhancement provided a high contrast image. The resolution of the resulting image was approximately 1 μm .

172: Electrochemical Syntheses and Electrochromic Properties of Chromium Cyanide Magnetic Thin Films

O. Sato, Z. Gu, H. Etoh, J. Ichiyanagi, T. Iyoda, A. Fujishima, and K. Hashimoto

Chem. Lett., 37-38, (1997).

Electrochemical preparation method and electrochromic properties of the mixed valence chromium cyanide thin film, which is one of the ferrimagnet with highest critical temperature (T_c) among molecule-based magnets, were described. The difference in the ability of the ligand substitution reaction between Cr^{II} and Cr^{III} was utilized to synthesize the Prussian blue analogs. The obtained magnetic material exhibited excellent electrochromic properties. This indicates the compound has a potential for future display devices, as well as tunable molecule-based magnetic devices.

**173: Tuning of Superexchange Couplings in a Molecule-Based Ferro-ferrimagnet:
($\text{Ni}_{1-x}\text{Mn}_{1-x}$) $1.5[\text{Cr}^{\text{III}}(\text{CN})_6]$**

S. Ohkoshi, O. Sato, T. Iyoda, A. Fujishima, and K. Hashimoto

Inorg. Chem., **36** (3), 268-269 (1997).

In the last few years, there has been considerable interest in the preparation of molecular magnets with high Curie temperature (T_c). One of the advantages of molecular and metal complex-based magnets is that novel functions, for example, control of the magnetic properties via external stimuli, can be incorporated through proper design of the electronic properties. We recently reported the first examples of T_c control, via electrochemical and optical stimuli using Prussian blue analogs.

**174: Photoinduced Magnetic Pole Inversion in a Ferro-ferrimagnet :
($\text{Fe}_{0.40}\text{Mn}_{0.60}$) $1.5\text{Cr}^{\text{III}}(\text{CN})_6$**

S. Ohkoshi, S. Yorozu, O. Sato, T. Iyoda, A. Fujishima, and K. Hashimoto

Appl. Phys. Lett., **70** (8), 1040-1042 (1997).

175: Photoelectrorheology of TiO_2 Nanoparticle Suspensions

Y. Komoda, Tata N. Rao, and A. Fujishima

Langmuir, **13**, (6), 1371-1373. (1997).

The electrorheological properties of a TiO₂ (anatase) particle suspension in silicone oil were found to undergo changes during illumination, including an increased electrorheological effect, i.e., increased viscosity upon illumination. The increased viscosity is due to the polarization of photoinduced charge carriers under the influence of the imposed electric field. A small photocurrent was observed, which can be attributed to photoelectrophoretic conduction and leakage of photogenerated charge through field-induced columns. Microscopic observation carried out under stationary conditions showed an increase in the number of field-induced columns upon illumination, consistent with increased viscosity.

176: Photoeffects on Electrorheological Properties of TiO₂ Particle Suspensions

T. N. Rao, Y. Komoda, N. Sakai, and A. Fujishima

Chem. Lett., 307-308 (1997).

The electrorheological (ER) effect of TiO₂/silicone oil fluids was investigated under illumination. Two types of commercial TiO₂ powders showed opposite photoeffects on the ER properties. While the photoinduced increase in the ER effect for the first type arises from the polarization of photogenerated charges, the decrease in the effect of the latter type appears to be due to photoelectrophoresis, which may be facilitated by effects associated with the large surface area and high water content.

177: * Electrochemistry of Diamond

A. Fujishima

2nd Japan-Italy Electrochemical Seminar (Shinjyuku, Tokyo, Japan, 11/7-9, 1996)

178: Self-Cleaning and Anti-bacterial Functions of Various TiO₂ Coated and Containing Materials

K. Hashimoto, A. Fujishima

The Electrochemical Society, (Los Angeles, U.S.A., 5/5-10, 1996)

- 179: * **The Kinetic Study of Photocatalysis Using TiO₂ Thin Film Under Weak UV Light**

K. Hashimoto, Y. Ohko, M. Watanabe, A. Fujishima

The Electrochemical Society, (Los Angeles , U.S.A, 5/5-10, 1996)

- 180: * **Reaction Mechanism and New Materials for Photocatalysis**

A. Fujishima

Asian Photochemistry Conference (Hong Kong, 6/23-26, 1996)

- 181: * **Electrochemistry and Photoelectrochemistry of Diamond**

A. Fujishima, K. Hashimoto, L. Boonma and T. Yano

First Spanish/Japanese Conference on Fundamentals and Applications of Molecular Functional Electrodes and Materials (Madrid, Spain, 6/3-6, 1996)

- 182: * **TiO₂ Photocatalysis : Reaction Mechanisms and Real Applications**

A. Fujishima

Eleventh International Conference on Photochemical Conversion and Storage of Solar Energy (IPS-11) (Bangalore, India,7/28-8/2,1996)

- 183: * **Photoelectrochemistry of TiO₂ Particle Suspensions**

Hisao Yanagi, Yoshihiro Ohoka, Takashi Hishiki, Katsuhiko Ajito, and Akira Fujishima

Eleventh International Conference on Photochemical Conversion and Storage of Solar Energy (Bangalore, India, 7/28-8/2, 1996) akira-fu@fchem.t.u-tokyo.ac.jp

184: * Recent Progresses in TiO₂ Photocatalysis

Akira. Fujishima

TiO₂ Photocatalytic Purification and Treatment of Water and Air (Chincinnati, Ohio, U.S.A., 10/26-29, 1996)

185: * Photo-Induced Super-Hydrophile Property of TiO₂ Coated Materials : Novel Phenomenon in Photocatalysis

K. Hashimoto, A. Fujishima, and T. Watanabe

TiO₂ Photocatalytic Purification and Treatment of Water and Air (Chincinnati, Ohio, U.S.A., 10/26-29, 1996)

186: * Anti-Fog Glass and Mirror Utilizing Super-Hydrophilic TiO₂ Photocatalysis

T. Watanabe, M. Shimohigoshi, E. Kojima, K. Norimoto, A. Kitamura, K. Hashimoto, and A. Fujishima

TiO₂ Photocatalytic Purification and Treatment of Water and Air (Chincinnati, Ohio, U.S.A., 10/26-29, 1996)

187: * Dependence of Product Distribution on TiO₂ Surface Characters : Photocatalytic Decomposition of Gaseous Acetaldehyde

T. Noguchi, K. Hashimoto, and A. Fujishima

TiO₂ Photocatalytic Purification and Treatment of Water and Air (Chincinnati, Ohio, U.S.A., 10/26-29, 1996)

- 188: * **Reproducibility of Supported TiO₂ Films on Pyrex and Soda Line Glass in Photocatalytic Degradation of Formic Acid for 50 Days**

D. H. Kim, T. Iyoda, K. Hashimoto, A. Fujishima, and D. Y. Weon

TiO₂ Photocatalytic Purification and Treatment of Water and Air (Chincinnati, Ohio, U.S.A., 10/26-29, (1996) akira-fu@fchem.t.u-tokyo.ac.jp)

- 189: * **Self-Cleaning Building Materials Utilizing Super-Hydrophilic TiO₂ Photocatalysis**

T. Watanabe, M. Shimohigoshi, M. Machida, M. Chikuni, R. Kojo, K. Hashimoto, and A. Fujishima

TiO₂ Photocatalytic Purification and Treatment of Water and Air (Chincinnati, Ohio, U.S.A., 10/26-29, (1996))

- 190: * **Water Purification Using Immobilized Titanium Dioxide: Adsorbent Effect on Photocatalysis**

S. Fujita, T. Iyoda, K. Hashimoto, and A. Fujishima

TiO₂ Photocatalytic Purification and Treatment of Water and Air (Chincinnati, Ohio, U.S.A., 10/26-29, (1996))

- 191: * **Interfacial Photochemical Reactions**

A. Fujishima

Workshop on Photoresponsive Materials (Catalina Island, California, U.S.A., November 3-8, 1996)

192: * Optically Tunable Molecule-Based Magnets

T. Iyoda, O. Sato, S. Ohkoshi, K.Nagai, A. Fujishima and K. Hashimoto

Workshop on Photoresponsive Materials(Catalina Island, California,U.S.A, November 3-8, 1996)

193: * New Challenges in Photofunctional Systems

A. Fujishima

Seventh International Symposium on Electrochemistry(Tainan, Taiwan, R.O.C, 11/20-24, 1996)

194: * The Diamond Surface-A New Type of Electrochemical Reaction Site

A. Fujishima

Seventh International Symposium on Electrochemistry(Tainan, Taiwan, R.O.C, 11/20-24, 1996)

195: * New Challenges in Photofunctional Systems

A. Fujishima

4th China-Japan Bilateral Symposium on Intelligent Electrophotonic Materials and Molecular Electronic (Nanjing,P.R.China,11/ 17-18,1996)

196: * A Drastic Change in Magnetic Hysteresis Loop by Photo-Induced Spin-Flopping in MnTetOPP-TCNE Charge Transfer Salt

K. Nagai , T. Iyoda, A. Fujishima, and K.Hashimoto

4th China-Japan Bilateral Symposium on Intelligent Electrophotonic Materials and Molecular Electronic (Nanjing,P.R.China,11/ 17-18,1996)

197: * Optical Control of Magnetic Properties in Molecule-Based Magnets

K. Hashimoto, O. Sato, S. Ohkoshi, K. Nagai, Z -Z Gu, T. Iyoda, and A. Fujishima

4th China-Japan Bilateral Symposium on Intelligent Electrophotonic Materials and Molecular Electronic (Nanjing,P.R.China,11/ 17-18,1996)

198: * Magnetic Properties of Functional Prussian Blue Derivatives

Z. -Z. Gu, O. Sato, T. Iyoda, K. Hashimoto, and A. Fujishima

4th China-Japan Bilateral Symposium on Intelligent Electrophotonic Materials and Molecular Electronic (Nanjing,P.R.China,11/ 17-18,1996)

199: * In Situ Observasion of a Thin Film TiO₂ Photocatalyst Surface using a Holographic Method

N. Kakimi, R. Baba, and A. Fujishima

4th China-Japan Bilateral Symposium on Intelligent Electrophotonic Materials and Molecular Electronic (Nanjing,P.R.China,11/ 17-18,1996)

200: * Electrostatic cis-trans Isomerization of Azobenzene Derivatives in Langmuir-Blodgett Films

H. Hagiwara, D.A. Tryk, K. Hashimoto, and A. Fujishima

4th China-Japan Bilateral Symposium on Intelligent Electrophotonic Materials and Molecular Electronic (Nanjing,P.R.China,11/ 17-18,1996)

201: * Photo-Induced Magnetization of Cobalt Iron Cyanide

T. Takebuta, O. Sato, Y. Einaga, T. Iyoda, T. Matsumoto, K. Hashimoto, and A. Fujishima

4th China-Japan Bilateral Symposium on Intelligent Electrophotonic Materials and Molecular Electronic (Nanjing,P.R.China,11/ 17-18,1996)

202: * Band to Band Excitation of p-type Diamond Thin Films by Short-Wavelength UV Illumination

L. Boonma, T. Yano, D.A. Tryk, K. Hashimoto, and A. Fujishima

4th China-Japan Bilateral Symposium on Intelligent Electrophotonic Materials and Molecular Electronic (Nanjing,P.R.China,11/ 17-18,1996)(English)

203: * Photoelectrorheology of TiO₂ Particle Suspensions

Y. Komoda, N. Sakai, Tata N. Rao, and A. Fujishima

4th China-Japan Bilateral Symposium on Intelligent Electrophotonic Materials and Molecular Electronic (Nanjing,P.R.China,11/ 17-18,1996)(English)

204: * Electrochemistry of Conducting B-Doped Diamond Electrodes

A. Fujishima, K. Hashimoto, D. A. Tryk, Tata N. Rao, T. Yano, M. Shimanuki, H. Hagiwara, Z. Wu, and E. Popa

The International Mini-Symposium on Diamond Electrochemistry and Related Topics(12/18-19, 1996.Sanjyoukaikan, The University of Tokyo)

- 205: * Photoelectrochemical Studies of P-Type Semiconducting Diamond Electrodes using Excimer Laser Illumination**

L. Boonma, T. Yano, D. A. Tryk, Tata N. Rao, K. Hashimoto, and A. Fujishima

The International Mini-Symposium on Diamond Electrochemistry and Related Topics(12/18-19, 1996.Sanjyoukaikan, The University of Tokyo)(English)

- 206: * Scanning Probe Microscopic Study of Diamond Film Surfaces as Organic Electroluminescence(EL)and Electrochemical Electrodes**

T. Miyatani, T. Kato, K. Hashimoto, A. Fujishima, and M. Fujihira

The International Mini-Symposium on Diamond Electrochemistry and Related Topics(12/18-19, 1996.Sanjyoukaikan, The University of Tokyo)

- 207: * Electrochemical Responce of Diamonds in Aqueous Electrolytic Solution Containing Ce^{3+} Ions**

Y. Maeda,K. Hashimoto, and A.Fujishima

The International Mini-Symposium on Diamond Electrochemistry and Related Topics(12/18-19, 1996.Sanjyoukaikan, The University of Tokyo)

III Department of Energy Conversion Science

(エネルギー変換科学専攻)

208: * Analysis of Stability of a Two-Dimensional Jet with Density Variation

密度変化のある二次元噴流の安定性解析

Makoto Ikegami, Hiroshi Kawanabe, Masahiro Shioji

Trans. JSME(B), Vol. 62, No. 594, pp. 783-786, Feb. 1996

日本機械学会論文集(B編), 62巻594号, 783-786頁, 1996年2月

The flow instability of a jet diffusion flame was investigated based on a linearized stability theory. The equation of disturbance was solved numerically for a two-dimensional parallel flow with density variation. Results show that the existence of a hot layer at the jet boundary makes the flow more stable, increasing the critical wave number and critical Reynolds number at which turbulence neither grows nor declines. The increase of the critical wave number is due mainly to the interaction between the flow and density gradient, and the local change of the viscous dissipation increases the critical Reynolds number, thereby leading to a wider stability limit. (in Japanese)

209: * Formation of Turbulent Eddies in Jet Diffusion Flames

Makoto Ikegami, Masahiro Shioji, Hiroshi Kawanabe, Koji Yamane*

(* Department of Mechanical Systems Engineering, The University of Shiga Prefecture)

JSME International Journal, Ser.B, Vol.39, No.2, pp.433-439, 1996

The transition from laminar to turbulent mode of an ethylene jet flame was investigated using the two-dimensional instantaneous photography of turbulent eddies by a laser-light sheeting method. Observations were made of the eddies around the break point in the fuel flow and the flame. The results show that in the laminar region the fuel flow is curved due to instability in the shear layer, whereas the outer soot layer has little curvature because of the high viscosity in the hot layer. In the transient region, eddies generated in the fuel flow deform the outer soot layer. Numerical calculations were performed to predict fluid motions due to interaction between density and pressure gradients in the flame boundary. The results show that the pressure gradient in a medium of varying density generates the vorticity along the flame. Deformation and stretching of the flame boundary take place once the vorticity becomes stronger than the dissipation due to viscosity.

210: * Reduced Initial Injection Rate and Pilot Injection at a Spool Acceleration Type Injection System

スプール加速式燃料噴射における初期噴射率抑制および先立ち噴射

Koji Yamane*, Makoto Ikegami, Koichiro Nakatani, Shotaro Tanaka, Kenichi Sakagoshi

(* Department of Mechanical Systems Engineering, The University of Shiga Prefecture)

Trans. JSAE, Vol.27, No.3, pp.47-52, July 1996

自動車技術会研究論文集, Vol.27, No.3, pp.47-52, 1996年7月

In diesel engines, pilot injection or reduced initial injection rate with high-pressure injection has a high potential to reduce particulate, NO_x and noise emissions, simultaneously. In this study, methods of pilot injection and reduction of initial injection rate were developed for KD-3 injection system which relies on spool acceleration and oil-hammering in the injection pipeline. A pilot injection can be achieved by using either a fuel spill path in a plunger body or extending pre-lift of spool. An alternative method is the staged motion of the spool by dual input pulses to electromagnetic pilot valve. Computer simulation and bench tests of injection system were carried out. (in Japanese)

211: * Fuel Injection Rate Shaping and Its Effect on Exhaust Emissions in a Direct-Injection Diesel Engine Using a Spool Acceleration Type Injection System

Makoto Ikegami, Koichiro Nakatani, Shotaro Tanaka, Koji Yamane*

(* Department of Mechanical Systems Engineering, The University of Shiga Prefecture)

SAE Technical Paper 970347, pp. 163-174, 1996

In diesel engines, pilot injections and injections at a reduced initial injection rate with high-pressure fuel injection have a potential to reduce particulate, NO_x and noise emissions simultaneously. For this reason, various shaping methods of injection rate waveform have been proposed. The present authors also propose such a high-pressure injection system with variable injection rate that relies on spool acceleration and oil-hammering in the injection pipeline. This paper first describes the injection rate shaping, including injections with pilot and reduced initial injection rate, and elucidates their effects on reducing exhaust and noise emissions. A pilot injection can be achieved by either installing a fuel spill path in a plunger body or elongating prelift of the spool. Computer simulations and bench tests of such injection systems show that pilot injection quantity is small enough and the pilot injection pressure is much lower than that of the main part of the injection. To reveal the effect of fuel injection rate on exhaust and noise emissions, experiments were carried out on a high-speed direct-injection diesel engine having a high-swirl deep-bowl combustion chamber. The results show that reduction of initial injection rate and pilot injection lowers both the exhaust NO_x concentration and the noise emission, and that smoke is significantly reduced

by increasing the average injection rate. This characteristic is remarkable at lower engine speeds and scarcely depends on a nozzle orifice diameter.

212: * Effects of Heat Release Rate on NO_x Time History in Diesel Combustion

ディーゼル燃焼における熱発生率経過が NO_x 濃度履歴に及ぼす影響

Takuji Ishiyama, Kei Miwa^{*1}, Satoru Watabe^{*2}, M.Higashida^{*1}

(*1 The University of Tokushima, *2 Kawasaki Heavy Ind.)

Trans. JSME(B), Vol. 62, No. 598, pp. 2521-2527, 1996

日本機械学会論文集 (B 編), 62 巻 598 号, 2521-2527 頁, 1996 年

For determining the optimum combination of combustion control techniques to reduce NO_x emission from diesel engines, it is important to clarify the effects of each techniques not only on the NO_x emission but also on its time history during combustion. In this paper, NO_x concentration in the combustion chamber of a rapid compression machine has been measured by using a total gas sampling method. In order to elucidate the relation between NO_x history and heat release rate, compressed air temperature, nozzle hole size and air motion are varied to control the heat release process. The results show that NO_x emission is not solely dependent upon initial combustion. Air utilization in the main diffusive combustion phase has great influence on NO_x formation and its decay. NO_x formation is accelerated by activation of the initial stage of the main combustion when using a nozzle with small holes. (in Japanese)

213: Simultaneous Reduction of Particulates and Nitrogen Oxides in the Unsteady Turbulent Diffusion Combustion

Masahiro Shioji, Makoto Ikegami, Koji Yamane*

(*Dept of Mechanical Systems Engineering, The University of Shiga Prefecture)

Thermal Science & Engineering, Vol.4, No.1, pp.25-30, 1996

This paper outlines the strategies for simultaneous reduction of particulates and nitrogen oxides in a diesel engine. Especially, two concepts are proposed for suppressing NO_x formation in the case of pressurized injection; one is the injection-pressure control and the selection of nozzle-orifice diameter. Furthermore, the homogeneous and lean combustion at an elevated injection-pressure with a smaller nozzle-orifice is assessed by the observations of soot clouds that are formed in flames.

214: * Gas-Flow Measurements in a Jet Using Cross Correlation of Particle Images

粒子画像の相互相関を用いた噴流内ガス流動計測

Makoto Ikegami, Masahiro Shioji, Hiroshi Kawanabe, Tohru Yamaguchi*

(*Yanmar Diesel C.C.)

Trans. JSME(B), Vol. 62, No. 593, pp. 297-303, Jan. 1996

日本機械学会論文集 (B 編), 62 巻 593 号, 297-303 頁, 1996 年 1 月

Particle image velocimetry (PIV) for measuring velocity vectors in a turbulent flow is developed based on high-speed photographs obtained by means of a laser light-sheeting method. The velocity vector is estimated by calculating a two dimensional cross-correlation coefficient between two photos which have a small time interval. Characteristics of turbulent eddies in a nitrogen jet are clarified from the obtained vorticity distribution, and from the distributions of strain rate and divergence which are calculated from the velocity distribution. In addition, the accuracy of PIV is assessed using the simulated image. The result shows that to suppress an error due to appearance and disappearance of particles, it is necessary to distribute particles uniformly in the test section, whereas to suppress an error due to random motions and rotational motions, it is necessary to distribute the particle heterogeneously. (in Japanese)

215: * Production and Destruction of Nitrogen Oxides in the Dilution Process of Fuel-Rich Burnt Gases

過濃燃焼ガスの希薄化過程における窒素酸化物の生成と分解

Masahiro Shioji, Osamu Yamada*¹, Makoto Ikegami, Koji Yamane*²

(*1 Yanmar Diesel C.C., *2 Dept of Mechanical Systems Engineering, The University of Shiga Prefecture)

Trans. JSME(B), Vol.62, No.603, pp.3982-3987, Nov. 1996

日本機械学会論文集 (B 編), 62 巻 603 号, 3982-3987 頁, 1996 年 11 月

Production and destruction of nitrogen oxides in the dilution process of fuel-rich burnt gases are investigated based on detailed chemical kinetics. From the analysis of combustion processes with mixing of methane-air fuel-rich burnt gas and air, it is shown that fast mixing due to strong turbulence enables a great deal reduction in NO_x concentration, and that a further reduction cannot be achieved for a rich mixture of equivalence ratio higher than 1.2. The NO production rates of elementary reactions indicate that NO is formed by the destruction of HNO at low NO concentration and is deoxidized into HNO at high NO concentration. It is also shown that NO_x concentration can be halved if the temperature decreases with the volume expansion in a high-speed piston-engine motion prior to the heat release due to dilution. Furthermore, the effect of temperature fluctuation on the dilution path is discussed from the practical point of view for reducing NO_x in two-stage combustion. (in Japanese)

216: Effects of Shock Waves on Living Tissue Cell (Red Blood Cell) (Damage of Red Blood Cell and Mathematical Analysis of Deformation Model Using Spherical Shell Filled with Liquid)

衝撃波の生体組織細胞（赤血球）に及ぼす影響（赤血球損傷と球殻内部液体モデルによる数理解析）

Masaaki Tamagawa, Keiichiroh Yoshida*¹, Teruaki Akamatsu*²

(*1 Denso Co Ltd., *2 Dept. of Mech. Eng., Kyoto Univ.)

Transactions of the Japan Society of Mechanical Engineers, Vol.62, No.594, Ser.B,
pp.613-619, 1996

日本機械学会論文集, 62 卷, 594 号, B 編, 613-619 頁, 1996 年

This paper describes damage to living tissue cells induced by plane shock waves. It is an effective method for sensing injury to living tissue cells using pseudo-living cells. In this study, micro-capsules are used to estimate the degree of damage when subjected to shock waves. Mathematical models that can analyze displacement of living tissue cells and pressure in fluid when subjected to shock waves are evaluated. An elastic spherical shell, the dynamic properties of the living tissue cells (red blood cells and micro-capsules) are obtained. The results show that damage to living tissue cells depends on (1)the elastic modulus of the cell, (2)the bulk modulus of intracellular material and (3)the thickness of cell membrane. (in Japanese)

217: * Prediction of Hemolysis Tendency by Shear Stress in a Pipe Orifice Blood Flow

オリフィス管内せん断血流の溶血特性予測

Masaaki Tamagawa, Keijiroh Saitoh^{*1}, Teruaki Akamatsu^{*2}

(*1 Mitsubishi Heavy Industry Co. Ltd., *2 Dept. of Mech. Eng., Kyoto Univ.)

Transactions of the Japan Society of Mechanical Engineers, Vol.62, No.597, Ser.B,
pp.1747-1753, 1996

日本機械学会論文集, 62 卷, 597 号, B 編, 1747-1753 頁, 1996 年

This paper describes methods of predicting hemolysis induced by turbulent shear stress (Reynolds stress) in simplified pipe orifice flow. In a centrifugal blood pump, serious hemolysis occurs at the impeller or the casing edge. The turbulent shear stress computed using a low-Reynolds number k-e model near the edge proves to be several hundred times the laminar shear stress that obtained from a conventional hemolysis test using viscometer. Then the threshold of turbulent shear stress for hemolysis is determined by comparing with that obtained in hemolysis experiments of pipe orifice blood flow. (in Japanese)

218: Experimental and Mathematical Model of Living Tissue Cell Damage Induced by Plane Shock Waves

Masaaki Tamagawa, Teruaki Akamatsu^{*1}, Keiichiroh Yoshida^{*2}

(*1 Dept. of Mech. Eng., Kyoto Univ., *2 Denso Co Ltd.)

Proc. of the 20th Int. Symp. on Shock Waves, Vol.II, pp.1649-1654, Pasadena, USA,
1996

This paper describes a model of living tissue cell damage induced by plane shock waves. In this study, red blood cells and micro capsules are damaged by incident plane shock waves, and then evaluated to estimate the degree of damage by shock wave. Mathematical models of this damage are analyzed, and

the results show that cell damage depends on (1)elastic modulus of cells, (2) bulk modulus of cells, and (3) width of cell membrane.

219: * Prediction of Hemolysis by Shear Orifice Flow

Masaaki Tamagawa, Keijiroh Saitoh^{*1}, Teruaki Akamatsu^{*2}

(*1 Mistubishi Haevy Industry Co. Ltd., *2 Dept. of Mech. Eng., Kyoto Univ.)

Artificial Organs, Vol.20, No.6, pp.553-559, 1996

This study proposes a method of predicting hemolysis induced by turbulent shear stress (Reynolds stress) in a simplified orifice pipe flow. In developing centrifugal blood pumps, there has been a serious problem with hemolysis at the impeller or casing edge: because of flow separation and turbulence in these regions. In the present study, hemolysis caused by turbulent shear stress must occur at high shear stress levels in regions near the edge of an orifice pipe flow. We have computed turbulent shear flow using the low-Reynolds number k-e model. We found that the computed turbulent shear stress near the edge was several hundreds times that of the laminar shear stress (molecular shear stress). The peak turbulent shear stress is much greater than that obtained in conventional hemolysis testing using a viscometer apparatus. Thus, these high turbulent shear stress should not be ignored in estimating hemolysis in this blood flow. Using an integrated power by shear force, it is optimal to determine the threshold of the turbulent shear stress by comparing computed stress levels with those of hemolysis experiments of pipe orifice blood flow

220: * Effects of Shock Waves on Living Tissues (Numerical Analysis of a Propagating Pressure Wave toward Living Tissue)

Masaaki Tamagawa, Teruaki Akamatsu*

(* Dept. of Mech. Eng., Kyoto Univ.)

JSME Int. J., Ser.B, Vol.39, No.4, p.714-720, 1996

This paper describes pressure wave analysis in order to examine the effects of shock waves on living tissues. From the comparison of displacements of living tissue models by FEM with that obtained by experiments, dynamic properties of living tissue (rat's kidney) are determined. Using these properties of the living tissues in shock compression (solid-state equation), the flow fields in two layers that consist of air and the living tissue, and in three layers that consist of air, water, and the living tissues are numerically obtained. It is found that the incident time derivative of pressure in the living tissue is smaller than that of pressure in air and water. Hence, the effects of the living tissue depends on the relaxation of pressure waves and duration of exposure.

221: * Coupled Solid-Liquid Analysis for Viscoplastic Body with Moving Boundary Caused by Melting/Solidification (Ist Report, Modeling and Fundamental/Finite Element Equations)

溶融・凝固による移動境界問題の粘塑性構成式を用いた固相 - 液相の達成解析 (第 1 報, 問題のモデル化と基礎式, 有限要素式)

Atsushi Sakuma*, Tatsuo Inoue

(* Department of Mechanical Eng., Yamaguchi Univ.)

Trans. Japan Society of Mechanical Engineers, Ser.A, Vol.62, No.596, pp.1025-1031, 1996

日本機械学会論文集 (A 編), 62 巻, 596 号, 1025-1031 頁, 1996 年 4 月

Formulation of conservation laws of mass, momentum and energy for the region with moving interface between a solid and a liquid is described in the first part of the paper. Here, jump conditions of velocity, stress and heat flux on the interface are applied to give the fundamental equations including the Stefan condition relevant to the analysis of some problems incorporating melting/solidification. Discretized finite element equations for the analysis of temperature, stress/strain and melting/solidification in the course of welding are formulated using the thermo-elastio-viscoplastic constitutive equation. (in Japanese)

222: * Coupled Solid-Liquid Analysis for Viscoplastic Body with Moving Boundary Caused by Melting/Solidification (2nd Report, Application to the Simulation of Welding Process)

溶融・凝固による移動境界問題の粘塑性構成式を用いた固相 - 液相の達成解析 (第 2 報, 溶接過程のシミュレーションへの適用)

Atsushi Sakuma*, Tatsuo Inoue

(* Department of Mechanical Eng., Yamaguchi Univ.)

Tans. Japan Society of Mechanical Engineers, Ser.A, Vol.62, No.596, pp.1032-1037, 1996

日本機械学会論文集 (A 編), 62 巻, 596 号, 1032-1037 頁, 1996 年 4 月

Fundamental and finite element equations developed in the previous paper by the present authors considering the effect of a moving interface between solid and liquid are applied to the simulation of the butt welding process of plates with heat input from the electrode. Here, the analysis is carried out for half the crosssection of the plate and the plane strain condition is assumed for stress analysis. The variations in the mode of deformation, velocity, temperature and stress fields are presented, where the emphasis is placed on the effect of the molten pool. The simulated results show that the proposed method is applicable to a practical welding process. (in Japanese)

223: Metallo-Thermo-Mechanical Simulation of Quenching-Tempering Process Based on Metallo-Thermo-Mechanics

変態 - 熱 - 力学に基づく焼入れ・焼もどし過程のシミュレーションとその検証

Dong-Ying Ju* Masato Sahashi, Takahiro Ohmori, Tatsuo Inoue
(* Department of Mechanical Eng., Saitama Institute of Technology)

J. Society of Materials Science, Japan, Vol.45, No.6, pp.643-649, June, 1996

材料, 45 卷, 6 号, 643-649 頁, 1995 年 6 月

This paper is concerned with the metallo-thermo-mechanical simulation considering the interaction among phase transformation, temperature and stress/strain by the finite element technique for a quenching-tempering process. Here, a method for evaluating the change of volume fraction due to phase transformation, controlled by a diffusion mechanism in the heating process before quenching and tempering process, is presented. Some results of simulation for the ring shaped model of a carbon steel are compared with the experimental data to verify the analytical results and discussions are also given on the operatin conditions in the quenching-tempering process. (in Japanese)

224: Computer Simulation of Residual Stresses, Distortion and Structural Change in the Course of Scanning Induction Hardening

Fumiaki Ikuta*¹, Kyozo Arimoto*², Tatsuo Inoue
(*1 Nuturen Co., *2 CTRC Research Institute)

Proc. 2nd International Conference on Quenching and Control of Distortion, Cleveland, pp.259-265, 1996

Simulated results of structural change residual stresses and distortion are presented for carbon steel cylinder in the scanning-type induction hardening process by a CAE system "HEARTS (HEAt tReAtment Simulation system)". The system HEARTS has been developed to simulate heat treatment processes based on "metallo-thermo-mechanics" available for describing the coupling effect between metallurgical change due to phase transformation, temperature and inelastic stress/strain. A steel cylinder is treated as an axisymmetric model with scanning internal heat generation and convection boundary. The results under different scanning velocity and magnitude of the heat source from induction coil are compared with experimental data of distortions, volume fraction of metallic phases as well as residual stresses.

225: Simulation and Experimental Verification of Induction Hardening Process for Some Kinds of Steel

Kyozo Arimoto*, Tatsuo Inoue
(* CRC Reserach Institute, Co.)

Proc. 3rd Asia-Pacific Symposium on Avdances in Engineering Plasticity and its Applications, Hiroshima, pp.55-62, 1996

Developing strategy and structure of a program "HEARTS (HEAt tReaTment Simulation system)" by the finite element method is presented in this paper, which is relevant to simulating heat treatment processes associated with phase transformation. The governing theory adopted in the program is based on "metallo-thermo-mechanics" developed by one of the authors to describe the coupling effect between metallurgical change due to phase transformation, temperature and inelastic stress/strain. Simulated results on carbon content, temperature, structural change and stress/strain during heat treatment process of an engineering component are illustrated by use of the program combined with available prepost processor.

226: Development Strategy of CAE System HEARTS and Some Results of Heat Treatment Simulation of Steel

Kyozo Arimoto*, Tatsuo Inoue
(* CRC Research Institute, Co.)

Proc. 3rd Asia-Pacific Symposium on Advances in Engineering Plasticity and its Applications, Hiroshima, pp.647-652, 1996

Developing strategy and structure of a program "HEARTS (HEAt tReaTment Simulation system)" by the finite element method is presented in this paper, which is relevant to simulating heat treatment processes associated with phase transformation. The governing theory adopted in the program is based on "metallo-thermo-mechanics" developed by one of the authors to describe the coupling effect between metallurgical change due to phase transformation, temperature and inelastic stress/strain. Simulated results on carbon content, temperature, structural change and stress/strain during heat treatment process of an engineering component are illustrated by use of the program combined with available prepost processor.

227: Identification of Heat Transfer Coefficient of Quenching Media

熱処理用冷却剤の熱伝達率の同定

Hideo Kanamori*, Nakamura Eiichi*, Hitishi uchida*, Ichiro Koyama*, Tatsuo Inoue
(* Idemitsu Kosan Co.)

Journal of the Japan Society of Heat Treatment, Vol.36, No.5, pp.390-396, December 1996

熱処理, 36 卷, 5 号, 390-396 頁, 1996 年 12 月

Based on the fundamental theory of metallo-thermo-mechanics incorporated with phase transformation proposed by one of the authors, a finite element CAE system program for the simulation of the quenching process has been developed. In order to obtain the accurate results of the simulation, it is necessary to identify the value of the heat transfer coefficient of the quenchants to be used. In this paper, a method to identify the heat transfer coefficient depending on temperature from the cooling curve for a cylinder made of silver (JIS K 2242) is prescribed. The solution of heat conduction equation of the cylinder

immersed in the stationary quenchant is applied to determine the heat transfer coefficient by the inverse method. From the data thus obtained, temperature dependence of the heat transfer coefficient is clearly observed, and the value shows the difference between film and nucleate boiling as well as convection for some kinds of quenchants. (in Japanese)

228: Metallo-Thermo-Mechanical Simulation of Centrifugal Casting Process of Multi-layer Roll

Dong-Ying Ju*, Tatsuo Inoue
(* Saitama Institute of Technology)

Material Science Research International, Vol.2, No.1, pp.18-25, 1996

The paper motivates to simulate temperature, solidification mode and stress in a multi-layer roll during centrifugal casting process, where the boundary of liquid phase grows and the interface between liquid and solid phase moves. A set of coupled equations of heat conduction, stress/strain and solidification is given in the framework of metallo-thermo-mechanics proposed by the authors, and the method of numerical calculation by the finite element method considering such feature of growing boundary and moving interface as well as the effect of multi-layer is proposed. The validity of the calculated results is discussed in comparison with the experimental data, and the effect of material property in each layer and boundary condition on the simulated results of temperature, solidification mode and residual stresses in the roll is evaluated.

229: Simulation of Damaging Interface between Matrix and Reinforcement in Metal Matrix Composite

Mamoru Mizuno*, Tatsuo Inoue
(* Nagoya University)

Proc. 3rd Asia-Pacific Symposium on Advances in Engineering Plasticity and its Applications, Hiroshima, pp.321-326, 1996

Damaging process under creep condition on the interface between Al matrix and SiC whisker aligned unidirectionally is simulated by use of the finite element method. In the simulation, a unit cell model is employed in order to estimate damage and stress development in the vicinity of the whisker. Aluminum matrix is considered as an elastoplastic material, while the whisker is assumed to be elastic. Debonding on the interface is simulated by a local approach in the framework of continuum mechanics. Mode of damaging in the vicinity of the whisker within the matrix is evaluated as an axisymmetric and plane strain conditions. The difference in damage development between both conditions is discussed.

230: Finite Element Analysis of Solidification Process Based on Integral Penalty Method

Shoji Imatani, Teru Nakata*, Katsuhiko Yamaguchi*

(* Kyoto Institute of Technology)

Proceedings of the 3rd Asia-Pacific Symposium on Advances in Engineering Plasticity and its Applications, pp.635-640, 1996

An analytical method for solving the Stefan problem is proposed, based on the integral penalty method which is an alternative approach to the conventional scheme based on the mixture theory. The general frame of the Stefan problem is firstly discussed from the viewpoint of spatial coordinate system. The finite element equation is then formulated in one dimensional state, and analyses are carried out to examine the validity of the proposed method. It is shown that the numerical result agrees well with the exact solution when adopting a particular value as the penalty number. A simple two dimensional example is analyzed, taking account of the thermo-viscous flow. Well acceptable results concerning the variation of phase boundary are obtained through the series of simulation.

231: Investigation on Variation of Drawability of Laminated Sheet Metals Using FEM Simulations

Junhua Liu*, Katsuhiko Yamaguchi*, Shoji Imatani, Norio Takakura*

(* Kyoto Institute of Technology)

Advanced Technology of Plasticity 1996, Vol.2, pp.699-702, 1996

Drawability is investigated using a rigid-plastic finite element simulation. The U-bending test is carried out to evaluate the effects of material combinations, thickness ratio and setting condition of the sheet blank. The results of the FEM simulation show that the limiting drawing ratio (LDR) is larger when the sheet with a higher flow stress (harder layer) is set at the punch side for a given thickness ratio. These results can also be estimated by the Y-value, a parameter which stands for the difference between the maximum punch load and the bending resistance in the U-bending-stretching test. The LDR increases with increasing thickness of the harder sheet layer for a given material combination. The variation of the LDR with the thickness ratio and setting condition of laminated sheet blank can be explained based on the thickness strain distributions of the drawn cups.

232: * Effect of Strain Rate on Compaction Characteristics of Iron Powders

Fu-Shi Jan*, Katsuhiko Yamaguchi*, Shoji Imatani, Norio Takakura*

(* Kyoto Institute of Technology)

Advanced Technology of Plasticity 1996, Vol.2, pp.1007-1010, 1996

The effect of strain rate on compaction pressure, density of green compact and frictional coefficient between die wall and powders is examined for the closed-die compaction of iron powders. It is shown that the axial and lateral stresses increase with increasing compacting speed and this appreciably contributes to the production of green compact with larger height-to-diameter ratio and uniform density. It is also shown that the frictional coefficient between die wall and powders and the material parameters in the conventional constitutive models are hardly affected by the compacting speed, i.e. the strain rate.

233: Generation of Various Curves and Slitting of Aluminium Thin Sheet along the Curves

曲線の創成と極薄板の曲線スリッティング加工

Norio Takakura*, Nobuhiko Shirakawa*, Shoji Imatani, Katsuhiko Yamaguchi*

(* Kyoto Institute of Technology)

Journal of the Japan Society for Technology of Plasticity, Vol.37, No.430, pp.1155-1161, 1996

塑性と加工, 37巻, 430号, 1155-1161頁, 1996年

A new method is proposed for curvilinear slitting or cutting of thin sheet materials, in which a rolling mill and piano wires are used, as a versatile cutting device and tool. Various curves can be generated at the roll entrance using a computer-controlled guide. The relationship between the movement of the guide at the roll entrance and the generated curve at the roll exit is derived geometrically. The results show that the slitting of an aluminium sheet with 0.1 mm thickness can be carried out using a wire with diameter equal to or slightly larger than the thickness of the sheet. The quality of the edge of the slitted sheet depends on the shape of wire, but it should be emphasized that there is no burr at the slitted edge. It is also shown that not only curvilinear slitting but also other types of figures can be easily achieved using this new method. (in Japanese)

234: * On the Use of Piezoelectric Films for Determination of Plane Stress Distribution

Shiro Biwa*, Keisuke Katsumi*, Eiji Matsumoto, Toshinobu Shibata*

(* Graduate School of Engineering, Kyoto University)

Advanced Technologies for Clean Environment, Vol.2, pp.133-140, 1996

The objective of the present study is to exploit the feasibility of the use of a piezoelectric polymer film to evaluate in-plane stress and strain distributions in structural components. In contrast to ordinary use of piezoelectric films as strain and strain-rate sensors detecting electric charges and currents through electrodes, the proposed strategy consists of measuring the distribution of electric potentials induced in the piezoelectric film mounted on the surface of a structural component in loading. The stress and

strain distributions can be subsequently determined from the measured potentials taking into account the piezoelectric coupling in the film material. As an illustrative example, thin films of polarized polyvinylidene fluoride (PVDF) are mounted on a holed elastic plate subjected to in-plane compressive loading, and the induced potential distribution was measured on the film surface by an electrostatic voltmeter of non-contact type. It is then demonstrated that the determined stress distributions are in fair conformity with those analytically predicted.

235: * Inversion Scattering in Finite Space Domain

Tomas Novotny*, Eiji Matsumoto, Toshinobu Shibata*
(* Graduate School of Engineering, Kyoto University)

Journal of the Acoustical Society of America, Vol.100, No.6, pp.3600-3606, 1996

The general integral representation of scattered acoustic field with arbitrary boundary conditions is introduced. Assuming weakness of the scatterer, two linearized methods for the recovery of object's shape and position are derived and briefly discussed. The methods are applied to one- and two-dimensional problems in order to compare them with the standard use of the first Born approximation (1BA). By presenting the numerical examples, this paper discusses the influence of the power spectrum of the incident pulse on exactness of the recovered object, the influence of "weakness" of scatterer and comparison of proposed methods to 1BA.

236: * Analysis of Bias-Type Actuator Using Shape Memory Alloy Based on Its Thermo-mechanical Constitutive Description

Shiro Biwa*¹, Kenichi Yamada*², Eiji Matsumoto, Toshinobu Shibata*¹
(*¹ Graduate School of Engineering, Kyoto University, *² Kawasaki Heavy Industries, Ltd.)

JSME International Journal, Series A, Vol.39, No.4, pp.526-532, 1996

Dynamic behaviour of a bias-type actuator using Ti-Ni shape memory alloy is examined theoretically as well as experimentally. The constitutive and the heat equations for the shape memory alloy, derived in the framework of continuum thermomechanics with phase transformation taken into account, are employed to describe the response of the considered actuator to applied electric input varying in time. Material parameters in the constitutive model adopted are determined from uniaxial loading-unloading tests at different temperatures. An experimental setup of the actuator, consisting of a shape memory alloy wire and a bias spring connected serially, is also manufactured, and the response of the actuator to cyclic electric input is measured. The experimental results obtained are compared with the predictions of the

analytical model, which proves promising to describe the behaviour of the actuator very well in terms of its dependence on various factors such as the rigidity of the bias spring, as well as the magnitude and the period of cyclic input.

237: * Rate-Dependence in One-Dimensional Magnetization

一次元磁化過程における速度依存性

Shusuke Nishimura*, **Atsushi Matsumoto***, **Eiji Matsumoto**, **Toshinobu Shibata***
(* Graduate School of Engineering, Kyoto University)

Journal of the Japan Society of Applied Electromagnetics and Mechanics, Vol.4, No.4,
pp.43-46, 1996

日本 AEM 学会誌, Vol.4, No.4, 43-46 頁, 1996 年

This paper deals with the expressions of the dynamic relation between the magnetization and the magnetic field in ferromagnetic materials. It includes the exchange energy and the rate of the magnetization and the magnetic field in a one-dimensional linear constitutive equation. Then the distribution of the magnetization becomes inhomogeneous due to the effect of the exchange energy and there exists the magnetic aftereffect from the rate dependence of the constitutive equation. The theoretical results are compared with the dynamic magnetization of carbon steel to determine the constitutive parameters. (in Japanese)

238: * Determination of Plane Stress Distribution by Potential Measurements of Surface-Mounted Piezoelectric Film

Shiro Biwa*, **Keisuke Katsumi***, **Eiji Matsumoto**, **Toshinobu Shibata***
(* Graduate School of Engineering, Kyoto University)

Proceedings of the Russian-Japanese Joint Seminar on the Physics and Modeling of
Intelligent Materials and Their Applications, pp.171-178, 1996

The use of piezoelectric films to evaluate in-plane stress distributions in structural components is examined. Electric potentials induced in the surface-mounted piezoelectric film are directly measured in loading, and converted into stress distributions accounting for the piezoelectricity of the film. Stress concentration near a hole in a compressed plate is demonstrated using polarized polyvinylidene fluoride (PVDF) thin films.

239: * Magnetostriction and Magnetoacoustic Emission of Ferromagnetic Material under Stress

Eiji Matsumoto

Interdisciplinary Applied Electromagnetics, A. Gottvald and I. Zemanek editors,
pp.120-129,1996

The mechanical and the magnetic constitutive equations are derived from a continuum theory of deformable ferromagnetic materials. When such a material is subjected to the magnetic field and the stress, the H-M relation and the magnetostriction depend on the deformation and the stress. When the magnetic field changes in time, acoustic waves are generated due to discontinuous movement of domain walls during magnetization. Since the magnetic properties are influenced by the deformation, so is the count of the magnetoacoustic emission. Experimental result on low-carbon steel is presented and analyzed on the basis of the obtained theoretical result. It is also shown that magnetostriction and magnetoacoustic emission can be applied to nondestructive measurement of applied stress.

240: * Mechanical Properties of Borosilicate Glass Coated with Alumina by Sputtering Process

Toshihiko Hoshide, Kenji Hayashi, Takahiro Saito, Kazumitsu Katsuki, Tatsuo Inoue

Mater. Sci. Res. Inter., Vol.2, No.1, pp.33-38, 1996

The borosilicate glass was coated with alumina ceramics by a radio-frequency (RF) magnetron sputtering method under various conditions. Mechanical properties of coated materials were investigated with respect to the sputtering condition. The hardness of alumina coating film was measured by using a dynamic microhardness tester. The film hardness was larger in thicker films and/or in films produced under a higher RF output. The hardness of film produced in every condition was superior to that of glass substrate. The scatter in the hardness of a thicker film was larger than that of a thinner film. The three-point bending test of coated materials and the glass substrate was also conducted. As for the coated material with the same film thickness, the bending strength improved with increasing the RF output. In the case of a lower RF output, the bending strength of some coated materials became less than that of the glass substrate. The dynamics of rigid spheres was adopted in modeling the present sputtering process, and the simulation based on the model was carried out. The apparent density of particles in simulated coating film explained qualitatively the dependence of the hardness on the RF output, which was observed experimentally.

241: Fatigue Life Evaluation of Notched Components under Combined Axial-Torsional Loading

Tatsuo Inoue, Toshihiko Hoshide, Eisaku Kakiuchi

Multiaxial Fatigue and Design, ESIS 21, pp.301-313, 1996

A procedure to evaluate the subsequent life after an initial fatigue stage, specified by a distribution of small cracks, was proposed for a notched component subjected to cyclic combined axial-torsional loading. Distributed cracks at the initial stage were modeled as straight-line cracks by using an image-processing technique. The algorithm for the analysis of crack growth after the initial stage was constructed by taking account of both modes of the propagation as a single crack and the coalescence between propagating cracks. Fatigue tests under combined axial-torsional loading with constant and variable amplitudes were conducted using cylindrical specimens with circumferential blunt notches. The dependence of fatigue life and cracking morphology on loading pattern was clarified experimentally. When compared with the same value of the equivalent plastic strain range, the fatigue life became longer with increasing shear components in the stress state, with no significant difference between two loading patterns of constant and variable stress amplitudes. The fatigue life defined by the formation of cracks with a specific length was evaluated based on the proposed procedure. The predicted life almost coincided with the experimental data. Cracking morphology was also simulated by using the present model to show a good agreement with that observed experimentally.

242: * Cost Analysis of IDLT Reactors Using the ARIES Code

Yuichi Ogawa*, Nobuyuki Inoue
(* Tokyo Univ.)

J. of Plasma and Fusion Research 72, pp.953-959, 1996

We analyzed the Cost Of Electricity (COE) for an Inductively Long-pulse Tokamak (IDLT) reactor with the ARIES system code, and compared with a conventional pulsed tokamak reactor PULSAR-II design. To obtain ultra-long pulse operation for up to ~8 hours using only an inductive current drive, the major radius of the IDLT reactor should be increased up to ~10 m, while that of PULSAR-II is ~8 m with a pulse length of ~2 hours. In addition, the IDLT reactor has no energy storage system to compensate an electric power during dwell periods. It was found that the COE of IDLT reactor is 7% more than that of PULSAR-II, although the major radius is different between IDLT and PULSAR-II. This is because the fatigue problem is mitigated due to the reduction of the operation cycle number, and the power supply system is lightened due to the slow start-up of the plasma current. We should also remark that the maintenance scheme should be reconsidered in the IDLT reactor, because a single radial movement of blanket modules employed in the PULSAR design is difficult in large aspect-ratio devices such as IDLT reactor.

243: An Equilibrium in Negative Hydrogen Ion Production Process Related to the Sheet Plasma Experiment

Kouichi Jimbo

J. Phys. Soc. Jpn., Vol.65, pp.2455-2458, 1996

In the sheet plasma experiment, plasma potentials decreased but negative hydrogen ion currents increased toward the outside. The negative hydrogen ions are pushed inside by the electric field and are not coming out from the plasma unless an equilibrium exists somehow. A relation between negative hydrogen ion currents and plasma potentials is well explained by the one-dimensional Saha equation, from which the electron temperature 1.3eV is obtained. This value is very close to the electron temperature 1eV of the Langmuir method. A reasonable negative hydrogen ion density is also calculated from the equation. We conclude that electrons, hydrogen atoms and negative hydrogen ions are in equilibrium.

244: * Preliminary Studies of Inertial-Electrostatic Confinement Fusion Experiments

Yasushi Yamamoto, Masami Ohnishi, Kiyoshi Yoshikawa, Hisayuki Toku, Mitsunori Hasegawa, Takashi Matsuo

Fusion Technology, Vol.30, pp.1332-1336, 1996

Preliminary inertial-electrostatic confinement fusion experiments have been carried out using hydrogen gas, and measurements of the light from a plasma core were made. The life time of charged particles in gridded IECF configuration is found to be longer than in the conventional spherical electrode discharges. The light intensity is found to be proportional to about 2/3 power of the input power.

245: Direct Energy Conversion from Spent Electron Beam in High-Power CW Klystrons

Kai Masuda, Kiyoshi Yoshikawa, Masami Ohnishi, Yasushi Yamamoto, Masaaki Sobajima

Fusion Technology, Vol.30, pp.805-809, 1996

Design of a multi-stage depressed collector for a 1.2MW L-band CW klystron was accomplished by use of numerical simulations. To obtain information on spent electrons (i.e. input condition for collector design), a klystron simulation code was newly developed.

246: First-Principles Calculation of Oxygen Adsorption on Zr(0001): Possible Site Occupation between the Second and the Third Layer

Masahiro Yamamoto, C. T. Chan^{*1}, K. M. Ho^{*2}, Shizuo Naito
(*1 HKUST, Hong Kong, *2 Ames Lab-USDOE, USA)

Phys. Rev. B, Vol.54, 14111, 1996

The oxygen adsorption on the Zr(0001) surface is studied using first-principles total-energy and force calculations. We calculated the atomic structure, heat of adsorption, work function and electronic structure for oxygen occupying various surface and subsurface sites for both the Zr(0001)-(1×1)-O and Zr(0001)-(2×1)-O system. We found that the energetically most favorable occupation sites for oxygen are the octahedral sites between the second and the third layer. The change in the work function induced by oxygen adsorption depends strongly on the position of the adsorbed oxygen atoms and the calculated change of work function at the energetically most favorable site is consistent with previous experiments. Large difference in the electronic structure between the overlayer and subsurface adsorption is also found.

247: First-Principles Calculation of the Longitudinal Phonon in the Surface Normal Direction of Zirconium(0001) Slab: Localization Mode at the Subsurface

Masahiro Yamamoto, C. T. Chan^{*1}, K. M. Ho^{*2}, Shizuo Naito
(*1 HKUST, Hong Kong, *2 Ames Lab-USDOE, USA)

Phys. Rev. B, Vol.53, 13772, 1996

The energies and amplitudes of the longitudinal vibrational mode in the surface normal [0001] direction of the fully-relaxed zirconium slab with (0001) surface are calculated with force constants determined from first-principles total-energy and force calculations. A subsurface vibrational mode with frequency above the bulk continuum is found. We attribute the origin of this mode to the hardness of the force constant between the surface and the second layer.

248: Measurements of Young's Modulus and the Modulus of Rigidity of the Solid Solution of Hydrogen in Zirconium between 300 and 1300 K

Yuh Ashida^{*1}, Masahiro Yamamoto, Shizuo Naito, Mahito Mabuchi^{*2}, Tomoyasu Hashino^{*3}

(*1 now Fuji Electric Co., *2 now Niihama National College of Technology, *3 now Chubu Univ.)

J. Appl. Phys., Vol.80, 3254, 1996

Young's modulus (E) and the modulus of rigidity (G) have been measured for zirconium between 300 and 1300 K and for zirconium hydrides ZrH_x ($0 < x < 0.9$) at 941 and 1001 K, using an apparatus capable of making *in situ* measurements of them under an ultra-high-vacuum condition. Values of E and G have been obtained from resonance frequencies for bending and torsion vibrations of a polycrystalline zirconium wire. As the temperature increases, E and G of zirconium decrease in the α phase of an hcp structure and in the β phase of a bcc structure with an abrupt decrease at the $\alpha \rightarrow \beta$ transition temperature 1135 K. As the hydrogen concentration increases, E and G of ZrH_x decrease in the α phase and increases in the β phase.

249: Calculation of Lindgård and Mouritsen's Free Energy Using Recently Measured Moduli of Elasticity for Hydrogen in Zirconium

Yuh Ashida^{*1}, Masahiro Yamamoto, Shizuo Naito, Mahito Mabuchi^{*2}, Tomoyasu Hashino^{*3}

(*1 now Fuji Electric Co., *2 now Niihama National College of Technology, *3 now Chubu Univ.)

J. Appl. Phys., Vol.80, 3259, 1996

The Young's modulus E and the modulus of rigidity G were measured for Zr as a function of temperature between 300 and 1300K and for ZrH_x ($0 \leq x < 0.9$) as a function of hydrogen concentration at 941 and 1001K in the previous paper. The abrupt change of the observed G for Zr at a critical temperature determines all the unknown coefficients of the free energy (LM free energy) derived by Lindgård and Mouritsen, who discussed the structural phase transition between the α (a hexagonal closed packed structure) and the β (a body centered cubic structure) phases in a Landau theory [Phys. Rev. Lett. **57**, 2458 (1986)]. LM free energy is modified so as to include effects of interstitial hydrogen atoms at low hydrogen concentration. A modified LM free energy which represents the transition from the α to the β phases through the $\alpha + \beta$ phase is obtained by introducing an order parameter proportional to hydrogen concentration. The order parameter multiplied by a lattice constant is the displacement between the position of Zr atom in the α phase and its respective position in the β phase.

250: Diffusion of Hydrogen in Titanium, $Ti_{88}Al_{12}$ and Ti_3Al

Toshiyuki Miyoshi^{*1}, Shizuo Naito, Masahiro Yamamoto, Minoru Doi^{*2}, Masao Kimura^{*3}

(*1 now Murata Mfg. Co., *2 Nagoya Institute of Technology, *3 Nippon Steel Corporation)

J. Chem. Soc. Faraday Trans., Vol.92, 483, 1996

Diffusion coefficients for hydrogen in titanium, its alloy $\text{Ti}_{88}\text{Al}_{12}$ and intermetallics Ti_3Al have been measured in the temperature range 873-1298 K. It has been found that the activation energy for diffusion in Ti_3Al (0.84 eV) is nearly twice that in titanium (0.45 eV), and in $\text{Ti}_{88}\text{Al}_{12}$ (0.57 eV) it is closer to that in titanium than to that in Ti_3Al . The prefactor of the diffusion coefficient has been found to increase as the aluminium content increases. The activation energy and prefactor obtained for Ti_3Al are shown to be explained by the presence of ordered aluminium atoms in Ti_3Al as well as by the large difference in the heats of solution of hydrogen in titanium and aluminium. The diffusion coefficient of $\text{Ti}_{88}\text{Al}_{12}$ is modelled, assuming distributions of the prefactor and activation energy resulting from the disordered aluminium atoms.

251: Isotope Effect in the Diffusion of Hydrogen and Deuterium in Titanium, $\text{Ti}_{88}\text{Al}_{12}$ and Ti_3Al

Shizuo Naito, Masahiro Yamamoto, Toshiyuki Miyoshi^{*1}, Mahito Mabuchi^{*2}, Minoru Doi^{*3}, Masao Kimura^{*4}

(*1 now Murata Mfg. Co., *2 Niihama National College of Technology, *3 Nagoya Institute of Technology, *4 Nippon Steel Corporation)

J. Chem. Soc. Faraday Trans., Vol.92, 3407, 1996

Diffusion coefficients of hydrogen and deuterium in titanium, titanium-aluminium alloy $\text{Ti}_{88}\text{Al}_{12}$ and intermetallic Ti_3Al have been measured in the temperature range 873-1298 K. Activation energy for diffusion has been found to be almost the same for hydrogen and deuterium and to increase, as the aluminium content in the metals increases, from *ca.* 0.44 eV for titanium to *ca.* 0.85 eV for Ti_3Al . The ratio of the measured diffusion coefficient of deuterium to that of hydrogen also increases from the classical value $1/\sqrt{2}$ for titanium to *ca.* 0.8 for Ti_3Al . An application of the classical rate theory to the measured ratio shows that hydrogen atom at the saddle point of the diffusion path is more tightly bound to the metal atoms and has a larger vibration energy in Ti_3Al than in titanium.

252: Formation of Singlet Oxygen Photosensitized by Aromatic Amino Acids in Aqueous Solutions

Okiyasu Shimizu^{*1}, Jun Watanabe^{*1}, Keiichi Imakubo^{*2}, Shizuo Naito

(*1 Nagoya City University, *2 Nagoya University)

Chem. Lett., 203, 1997

Spectral and kinetic evidences are provided for the formation of singlet oxygen photosensitized by aromatic acids in air-saturated water. Irradiation of these solutions at 266 nm induces infrared luminescence

with a time-resolved spectrum peaking at 1270 nm and a lifetime characteristic of singlet oxygen. In the cases of tryptophan, tyrosine and phenylalanine, the radiative lifetime are $3.32 \pm 0.01 \mu\text{s}$, $3.94 \pm 0.04 \mu\text{s}$ and $3.72 \pm 0.01 \mu\text{s}$, respectively.

253: Vibrational Properties of a Polycrystalline Titanium Surface Studied by Electron Energy-Loss Fine Structure (EELFS) Analysis

Mitsunori Kurahashi^{*1}, Masahiro Yamamoto, Mahito Mabuchi^{*2}, Shizuo Naito
(*1 now National Research Institute for Metals, *2 Niihama National College of Technology)

J. Surf. Anal., Vol.3, 451, 1997

We have measured the electron energy loss fine structure (EELFS) of a polycrystalline titanium surface in reflection mode for electron beams at different angles to the normal of the surface. From the analysis of the temperature dependence of the EELFS spectra, we have shown that the mean square relative displacement of the titanium atoms is particularly large on the surface layer and is estimated to be more than twice that for bulk. This result is consistent with the reported result of LEED measurements.

IV Department of Energy Science and Technology

(エネルギー応用科学専攻)

254: * First Principles Molecular Orbital Calculation of Electron Energy Loss Near Edge Structures of α -quartz

I. Tanaka, H. Adachi

J. Phys. D. 29 1725-1729

We report results of first-principle molecular orbital calculations using the discrete-variational (DV)- $X\alpha$ method on a model cluster of α -quartz, $(\text{Si}_5\text{O}_{16})^{12-}$. Self-consistent calculations of the cluster which include a half-filled core-hole, i.e., at Slater's transition state, are made in order to evaluate the effect arising from the presence of a core-hole associated with the electron energy-loss process. The presence of a half-filled Si-2p core-hole does not change the unoccupied Si-3s/3d partial density of states (PDOS) significantly. On the other hand, a remarkable core-hole effect appears on O-2p PDOS when a half-filled O-1s hole is introduced. The calculated PDOSes at the transition states are in good agreement with the electron energy-loss near edge structures (ELNES) at both Si- L_{23} edge and O-K edge. Absolute transition energies at both edges are also reproduced to within an error of 3 eV when the spin-polarization during the transition is taken into account. The photoabsorption cross sections (PACS) are calculated from first principles and are compared with the PDOS for the corresponding electric dipole transitions. The difference between the PACS and the PDOS is found to be small at both the ground state and the Slater's transition state in the present calculation.

255: * Chemical Bonding of Transition Metal Disilicides

N. Takao, I. Tanaka, H. Adachi

Intermetallics, 4 supplement 1 S113-S118.

First principles molecular orbital calculations of 3d and 4d transition-metal (TM or M) disilicides are conducted using model clusters composed of nearly 20 atoms with special interests on their chemical bondings. M is positively, and Si is negatively charged for early TM-disilicides. The direction of charge transfer changes in between Fe and Co in the 3d TM-disilicides. The net charge of M decreases almost linearly with the increase of atomic number except for Sc_3Si_5 (defective ScSi_2). The bond overlap population between M-Si decreases and Si-Si increases with rising atomic number of M. Energy distribution of Si-3s and 3p components is found to play important roles for magnitude of both Si-Si and M-Si bonds. The Si-Si bond strength in Sc_3Si_5 is exceptionally strong among these disilicides. Results for 4d-TM

disilicides in regards to net charge and bond overlap population are qualitatively the same as that of 3d TM-disilicides.

256: * Electronic States of F-Centers in Alkali Halide Crystals

K. Matsunaga, N. Narita, I. Tanaka, H. Adachi

J. Phys. Soc. Jpn. 65, (1996) 2564-70.

The electronic states of F-centers in alkali halides with NaCl-type structure have been investigated using the discrete variational (DV) $X\alpha$ cluster method. The electronic transition accompanied by optical absorption is examined on the basis of Slater's transition state concept. The photo-absorption energies of F-centers computed for the compounds with relatively small anions agree well with experimental data, but those for iodides and bromides exhibit much lower values than the observed values. We have also investigated the change in the absorption energy by the atom displacement. By the inward displacement of 1st neighbor cations, the absorption energies are decreased to approach the experimental values. The relaxation of the 1st neighbors estimated from the computation exhibits fairly small values in fluorides, while large values in iodides and bromides. The effect of lattice relaxation around an F-center is discussed in connection with the bonding nature of the F-center level.

257: * Structure and Chemistry of Intergranular Films in Ca-doped Si_3N_4

H. Gu*, X. Pan*, I. Tanaka, R.M. Cannon, M.J. Hoffmann*, H. Müllejans*, M. Rühle***

***(MPI, Stuttgart, Germany), **(LBL, UCB, USA)**

Mater. Sci. Forum, 207-209, pp.729-732

Intergranular amorphous films at grain boundaries (GB) in Si_3N_4 ceramics doped with 0, 80, 220 and 450 ppm of calcia were investigated by high resolution transmission electron microscopy (HRTEM) and spatially-resolved electron energy-loss spectroscopy (EELS). The observed film thicknesses are consistent with previous observations. Ca additives segregated at GB films, but not at the large triple pockets. EELS revealed the presence of N in the GB films. It is suggested that N is introduced into the GB films by Ca segregation. Electron energy-loss near-edge structure (ELNES) analysis indicates the presence of $\text{Si}(\text{O},\text{N})_4$ tetrahedra in the GB films.

258: * Electronic Structures of Ln^{3+} - α -Sialons with Correlations to Solubility and Solution Effects

T. Nakayasu, T. Yamada, I. Tanaka, H. Adachi and S. Goto

J. Am. Ceram.Soc., 79, 2527-2532

First principles molecular orbital calculations using discrete-variational (DV)- $X\alpha$ method are made on model clusters of α - Si_3N_4 and its solid solutions with lanthanide elements, which occupy interstitial sites in the structure. The formula is $\text{Ln}_x\text{Si}_{12-4.5x}\text{Al}_{4.5x}\text{O}_{1.5x}\text{N}_{16-1.5x}$, ($\text{Ln} = \text{La, Nd, Gd, Dy, Ho, Er, Tm, Yb}$), i.e., $\text{Ln}\alpha$ -sialon solid solution. Covalent bond strength between Si and N, evaluated by overlap population, is found to increase due to the presence of trivalent charges at interstitial sites. When a Ln^{3+} ion is present, antibondings occurs between Ln orbitals and N/Si orbitals, and depends significantly on the ionic radius of Ln^{3+} . The total overlap population for the whole cluster is determined by the balance of 1)Si-N bond reinforcement and 2)Ln-N/Si antibonding. Good correlation between maximum solubility and the total overlap population for the whole cluster is demonstrated for the first time.

259: * Calculation of Core-Hole Excitonic Features on Al- L_{23} edge X-Ray Absorption Spectra of α - Al_2O_3

Isao Tanaka and Hirohiko Adachi

Phys. Rev. B., 54, 4604-4608

We carry out first principles molecular orbital calculations for model clusters composed of 21 to 41 atoms with and without inclusion of a core-hole. The strongest peak that appear near the Al- L_{23} edge X-ray absorption spectrum and electron energy-loss spectrum of α - Al_2O_3 is found to originate from the presence of a core-hole. Such an effect is less significant in MgO and α -quartz (SiO_2). The cation-cation overlap population in the lowest unoccupied molecular orbital (LUMO) is found to be exceptionally strong at one of the Al-Al bonds in α - Al_2O_3 because of its short Al-Al bond-length. The LUMO strongly localizes when the core-hole is introduced.

260: * Electronic States and Chemical Bondings of an Interstitial Cation in Ionic Compounds AgCl and NaCl

K. Matsunaga, I. Tanaka and H. Adachi

J. Phys. Soc. Jpn., 65, 3582-3590

We have performed the electronic structure calculation of an interstitial cationic defect in AgCl and NaCl crystals, using the DV-X α molecular orbital method. Ag-4d orbitals are well admixed with Cl-3p orbitals in the valence band, and the electronic structure of AgCl is quite different from that of NaCl. The cation-anion covalent bonding in AgCl is stronger than that in NaCl. In addition, it is found that an interstitial Ag has a considerably strong covalent bonding with its surrounding Ag because of the interaction between Ag-4d orbits. Such a covalent bonding between Ag ions is likely to play an important role for the stabilization of an interstitial Ag in AgCl.

261: * Growth Mechanism of BaTiO₃ Thin Film by Theoretical Calculation of Electronic Structure

Y-S. Kang, I. Tanaka, H. Adachi and S-J. Park

J. Japan Appl. Phys. Part 2 35[12A] L1614-L1617

The surface electronic structure of BaTiO₃ and the adsorption of oxygen ion have been calculated using the DV-X α cluster method. We use the concept of embedded clusters to model the BaTiO₃ (001) surface, and O²⁻ adsorption and Ba²⁺ coadsorption on the surface. We calculate the valence electronic states for the surface and those involved in adsorption. Using Mulliken's population analysis it is found that the adsorption of oxygen ion on the surface weakens the covalent bonds between Ti and O in the BaTiO₃ substrate. In contrast, oxygen ion O²⁻ ion. The present results indicate that epitaxial BaTiO₃ thin films can be grown by simultaneous adsorption of groups of ions which have overall charge neutrality.

262: * Effects of Solute Atoms on the Chemical Bonding of Fe₃C (cementites)

M. Mizuno, I. Tanaka and H. Adachi

Phil. Mag. B, 75, 237-248

First principles molecular orbital calculations for Fe₃C (cementite) containing solute atoms have been made by the use of the discrete-variational (DV) X α method. Metal-metal (M-M) bonds around solute atoms show strong dependence on the atomic number of solute atoms, but metal-C (M-C) bonds are nearly constant irrespective of the solute atoms. Overlap population diagrams show that the Fermi level in pure Fe₃C lies in the anti-bonding band of the M-M bonding. The solute atoms induce the anti-bonding band to shift, thus the M-M bonds around the solute atoms are changed. The change of the magnitude of the M-M bonds with solute atoms is in good agreement with the variation of Vickers hardness of the Fe₃C solid solutions. Since the M-M bond is dominant between (001) planes in Fe₃C, it

is natural that the M-M bond strength shows strong effects on the hardness which is mainly determined by the (001) slip. The present result is contrary to the previous views: it has been believed that the M-C bond strength rather than the M-M bond determines the hardness of the Fe_3C solid solutions.

263: * Dopant modified local chemical bonding at a grain boundary in SrTiO_3

I. Tanaka, T. Nakajima, J. Kawai, H. Adachi, H. Gu and M. Ruhle

Phil. Mag. Lett. 75, 21-27

Chemical bonding at a grain boundary of an Fe^{3+} -doped SrTiO_3 bicrystal has been determined by a combination of spatially resolved electron energy-loss spectroscopy and a first-principles molecular-orbital calculation. The near-edge structure of the O-K edge spectrum on the boundary shows that the manner of the TiO_6 linkage is different from that in the bulk SrTiO_3 : The linkage changes locally from a corner-sharing to an edge-sharing configuration contemporary with the removal of Sr^{2+} ions from the boundary. This type of theoretical calculation is demonstrated to be a powerful tool to for analysing the ELNES spectra without preconceived models.

264: Estimation of Kapitza Conductance Effect on Steady and Transient Boiling Heat Transfer in He I based on Kapitza Conductance Results in He II

Masahiro Shiotsu, Koichi Hata*, Yuto Takeuchi*, Katsuhiko Hama*, Akira Sakurai**

***(Inst. of Advanced Energy, Kyoto Univ.) **(Future Energy Research Assoc.)**

Cryogenics, Vol.36, pp. 197-202, 1996

Kapitza conductance in steady and transient boiling heat transfer on a horizontal 0.2 mm diameter test wire was estimated based on the measured Kapitza conductance value for the same surface in He II. The He II experiments performed are for liquid temperature ranging from 1.8 to 2.1 K under atmospheric pressure, and the He I experiments of the steady and transient heat transfer caused by exponential heat inputs are for the periods ranging from 0.2 ms to 10 s under saturated conditions at liquid temperature ranging from 2.2 to 4.2 K, and subcooled conditions for the subcooling of 1.0 and 2.0 K at atmospheric pressure. The Kapitza conductance in He I is higher for higher saturation temperature but little dependent upon heat flux, liquid subcooling, and heat input increasing rate. The temperature drop due to the Kapitza conductance for the wall superheat becomes more significant with the increase in heat flux and in saturation temperature. It was confirmed that the Kapitza conductance in He I can be estimated correctly based on the Kapitza conductance value for the same surface in He II.

265: Boiling Phenomena due to Quasi-steadily and Rapidly Increasing Heat Inputs in LN₂ and LHe I**Akira Sakurai*, Masahiro Shiotsu, Koichi Hata*******(Future Energy Research Assoc.) **(Inst. of Advanced Energy, Kyoto Univ.)**

Cryogenics, Vol.36, pp.189-196, 1996

The dynamic boiling process on a horizontal wire in LN₂ and LHe I caused by an exponentially increasing heat input was investigated for a wide range of exponential period and pressure. The main problem is that there are no active cavities on the wire surface for initial boiling in the liquids; the transition from a single-phase non-boiling regime to film boiling was observed at certain conditions. The heat transfer processes due to increasing heat inputs with increasing rates ranging from quasi-steady to rapidly increasing ones in LN₂ were classified into three types for the pressures. The dynamic boiling process in LHe I due to a rapidly increasing heat input corresponds to Type 3 process in LN₂ including semi-direct transition. The lower limit temperature of boiling initiation on the wire surface due to a quasi-steadily increasing heat input is clearly lower than the homogeneous spontaneous nucleation temperature corresponding to the pressure. Liquid superheat close to the solid surface in LHe I was evaluated from the wire surface temperature, taking off the temperature drop due to Kapitza resistance. The initial boiling temperature due to quasi-steady heat input in saturated LN₂ and LHe I agreed with the values derived from the theoretical model based on the heterogeneous spontaneous nucleation in flooded cavities on the solid surface.

266: * Transient Heat Transfer from a Horizontal Wire in Subcooled He II at Atmospheric Pressure for a Wide Range of Wire Diameter**Masahiro Shiotsu, Koichi Hata*, Akira Sakurai*******(Inst. of Advanced Energy, Kyoto Univ.) **(Future Energy Research Assoc.)**

Advances in Cryogenic Engineering, Vol.41, pp.241-248, 1996

Transient heat transfer caused by large stepwise heat inputs to a horizontal wire in subcooled He II at atmospheric pressure was measured for the wire diameter of 0.08, 0.2, 0.5 and 0.7 mm. Liquid temperatures tested were 1.8, 1.9, 2.0 and 2.1 K. The steady-state critical heat flux which is dependent on liquid temperature and wire diameter was well expressed by the authors' correlation based on Gorter-Mellink equations. The lifetime of quasi-steady Kapitza conductance state, which corresponds to that of a certain point on the extrapolation of steady-state Kapitza conductance curve, was systematically measured on the wires: the quasi-steady state rapidly changes to film boiling regime at the end of the lifetime. The lifetime at an excess heat flux beyond steady-state critical heat flux, is longer for a larger diameter wire, though the steady-state critical heat flux is lower. Excessive heat flux beyond steady-state

critical heat flux, when integrated from the time that the heat flux reaches the steady-state critical heat flux to the end of the quasi-steady state lifetime is almost constant and it is independent of the step heights and of the initial waveform during the rise time to the step height. A correlation for the average integrated value was given as a function of the wire radius and bulk liquid temperature. The lifetimes for the ideal step heat inputs (rise time = 0) are given from the correlation.

267: Incipient Boiling Superheats and Critical Heat Fluxes due to Increasing Heat Inputs in Subcooled He I at Various Pressures

Akira Sakurai*, Masahiro Shiotsu, Koichi Hata**

***(Future Energy Research Assoc.) **(Inst. of Advanced Energy, Kyoto Univ.)**

Advances in Cryogenic Engineering, Vol. 41, pp.203-210, 1996

Dynamic boiling heat transfer processes on a 0.2 mm diam. horizontal wire due to exponentially increasing heat inputs, $Q_0 e^{t/\tau}$, with the periods, τ , from 0.2 ms to 25 s in subcooled He I at pressures of atmospheric, 142 kPa and 196 kPa were investigated to clarify the effect of liquid subcooling on the incipient boiling superheat and critical heat flux. The steady-state critical heat fluxes for the subcoolings ranging from 0 K to around 2.5 K at atmospheric pressure, 142 kPa and 196 kPa were obtained for the heat input with a period of around 20 s; almost data obtained did not agree with the values derived from the existing correlation based on hydrodynamic instability model. An empirical correlation was given. The liquid temperature close to the test wire surface, T_{lw} , is given as the difference between the wire surface temperature and the temperature corresponding to the Kapitza resistance: the Kapitza conductance was estimated based on that experimentally obtained for the same test wire in He II. It was confirmed that the boiling incipience caused by a heat input over the range from quasi-steadily increasing one to rapidly increasing one occurs due to the heterogeneous spontaneous nucleation, HSN, at the T_{lw} lower than the corresponding theoretical value of homogeneous spontaneous nucleation temperature. The correlations for critical heat flux at which the transition to film boiling occurs due to the HSN in originally flooded cavities on the wire surface were given for the wide ranges of exponential periods, τ , pressures and subcoolings.

268: Pool Boiling Critical Heat Flux on a Horizontal Cylinder in Subcooled Water for Wide Ranges of Subcooling and Pressure and Its Mechanism

Akira Sakurai*, Masahiro Shiotsu, Katsuya Fukuda**

***(Future Energy Research Assoc.) **(Kobe Univ. of Mercantile Marine)**

ASME HTD-Vol.326, Vol. 4, pp.93-104, 1996

Pool boiling critical heat fluxes (CHF) on a 1.2 mm diameter horizontal cylinder in water were measured for subcoolings from zero to 180 K at pressures from atmospheric to about 2 MPa. The CHF's for the subcoolings lower than around 40 K were clearly dependent on the pressure. On the other hand, those for the subcoolings larger than about 40 K were almost independent of the pressure except those for the pressures lower than around 200 kPa. Although the CHF values for the very narrow range of subcoolings below 20 K almost agree with the corresponding values obtained from the existing CHF correlations given by Kutateladze and Zuber based on the hydrodynamic instability, other CHF data obtained did not agree with the corresponding values. The values derived from the modified Kutateladze correlation, which was given by the authors taking into account the nonlinear effect of subcooling, agree with the CHF's for all the subcoolings at pressures below around 200 kPa, and with those for the subcoolings lower than around 40 K at pressures higher than the value. The empirical equation for the CHF's being independent of pressures for higher subcoolings at higher pressures was presented. The trend of CHF for high subcoolings suggests that there exists another mechanism of heat transfer crisis at CHF different from that applicable for the low subcoolings. The mechanism for high subcoolings at high pressures was suggested to be that based on the spontaneous nucleation in originally flooded cavities on the heater surface in fully developed nucleate boiling regime.

269: Experimental Study on Measurement of Damping Coefficient of Power System by Use of SMES

超伝導エネルギー貯蔵装置による電力システムの制動係数の測定

Yasuyuki Shirai, Tanzo Nitta*, Kazuhiko Shimoda

*The University of Tokyo

IEEJ Vol.116-B. No.9, September, 1996, pp.1039-1045

電気学会論文誌 Vol.116-B. No.9, September, 1996, pp.1039-1045

In this paper, a new application of Superconducting Magnetic Energy Storage (SMES) for diagnosis of power systems is proposed. Basic experiments for measurement of damping coefficient of power systems by use of SMES are carried out in an experimental system with a small generator, artificial transmission lines and a small SMES. The SMES gives small power disturbances to the power system without affecting operating conditions of the power system. The small power oscillations in the power system due to continuous power disturbances generated by SMES are observed. The relations among the damping coefficient, the power disturbances and the power change of SMES are discussed for one-machine infinite-bus system. The damping coefficients of the power system are obtained by investigating the oscillations due to the sinusoidal power change of SMES. The possibility of estimation of the steady state power system stability by monitoring the damping coefficients of the operated power system by use of SMES can be shown experimentally. (in Japanese)

270: A Method of Simulation for Power System Characteristics including Superconducting Generator with High Response Excitation

速応励磁形超電導発電機の電力系統特性解析シミュレーション法

Tanzo Nitta*, Yasuyuki Shirai, Katsunori Ooba

*** The University of Tokyo**

IEEEJ Vol.116-B, No.11, November, 1996, pp.1347-1353

電気学会論文誌 Vol.116-B, No.11, November, 1996, pp.1347-1353

A method of simulation for power system characteristics including a superconducting generator with high response excitation is proposed in this paper. The magnetic energy in the field winding of a superconducting generator (SCG) is much more than that of a conventional generator (CG), because magnetic flux in SCG almost is in air but that in CG almost is in iron core. Then, the power of exciter for SCG at the flux change by AVR is much more than that for CG. Therefore, the power of exciter must be taken into account for analyses of power systems including SCG with high response excitation. The exciter contains thyristorized converters which generate harmonics currents. The commutations of the thyristors must be taken into account. By conventional methods of simulation, one simulation code must be made for one power system, and another one for another one. This paper describes a simulation code flexible for various power systems. In the code, the system is divided into two parts. One is for the field winding circuit and the other is for the power system. They are linked in the magnetic couplings of the transformer of exciter and the magnetic coupling between the armature winding and the field one of SCG. This paper shows the comparison of the simulation results with the experimental one, too. (in Japanese)

271: Evaluation of Steady State Stability of Electric Power System by Use of Superconducting Magnet Energy Storage

超電導エネルギー貯蔵装置による電力システムの定態安定度の把握

Tanzo Nitta*, Yasuyuki Shirai, Yukikazu Ito

*** The University of Tokyo**

IEEEJ Vol.116-B, No.6, June, 1996, pp.678-684.

電気学会論文誌 Vol.116-B, No.6, June, 1996, pp.678-684.

In this paper, a new application of Superconducting Magnetic Energy Storage (SMES) for diagnosis of power systems is proposed. Basic experiments for diagnosis of power systems by use of SMES were carried out by use of small generators, artificial transmission lines and a small SMES. The SMES gives small power disturbances to the power system without affecting operating conditions of the power system. The small power oscillations in the power system due to continuous power disturbances generated by SMES are observed. The relations between the power disturbances and the power change of SMES are discussed. Natural frequencies of the power system are obtained by investigating the oscillations due to the sinusoidal power change of SMES. The relations between the natural frequencies and the steady state stability of the power system are discussed, too. The possibility of estimation of the steady state power system stability by monitoring the natural frequencies of the operated power system by use of SMES can be shown experimentally. (in Japanese)

272: On-line Measurement of Eigen-Frequencies of Power Systems by Use of SMES

Hajime Miyauchi*, Takashi Hiyama*, Yasuyuki Shirai, Tanzo Nitta**

*Kumamoto University, **The University of Tokyo

Proc. of 12th Power System Computation Conference, pp.895-900, August, 1996

It is useful for power system operators to grasp the system conditions on line. A new application of Superconducting Magnetic Energy Storage (SMES) for diagnosis of power systems were proposed. Basic experiments were carried out for on-line measurement of eigen-frequency of one or two machines infinite bus system by use of a small SMES. As the SMES has an ability of power source of quick response, it can give continuous power disturbances of arbitrary patterns to the power system without changing the operating conditions of the system. The response of power system for the continuous power disturbances by SMES were measured and analyzed to obtain eigen-frequencies. In this paper, we apply this method to multi-machine systems, which have several eigen-frequencies. The possibility of on-line measurement of eigen-frequencies of multi-machine systems by use of SMES can be shown by simulation studies.

273: A New Power Supply for Superconducting Pulse Magnet by Use of Energy Transfer Circuit

Yasuyuki Shirai, Tanzo Nitta*

*The University of Tokyo

Proc. of 7th International Power Electronics & Motion Control Conference, Vol.3, pp.660-664, Sept. 1996

Energy transfer circuits of inverter converter bridges (ICB) between two superconducting magnets have been proposed, discussed and tested. We have studied on power supplies for superconducting magnets which consists of a small power converter, a superconducting magnet for an energy storage, and the ICB energy transfer circuit. We derived analytical solutions on the basic characteristics of ICB energy transfer circuits. From the analytical solutions, a new control method of ICB energy transfer circuit to reduce voltage ripples across a load superconducting magnet was proposed and discussed. In this paper, the power supply of the proposed type which was designed and made is shown. The basic characteristics and the control methods of the test system are explained briefly. The results of fundamental tests are shown and discussed. Availabilities of the proposed control method were confirmed by the experimental studies.

274: * Removal of Antimony by Volatilization from Industrial Copper Matte and White Metal

銅溶錬マットおよび白皮からのアンチモンの揮発除去

Toshio Oishi*, Motohiro Horiguchi*, Yoichi Kawasaki*, Katsutoshi Ono
 (*Kansai Univ.)

Journal of The Mining and Materials Processing Institute of Japan , Vol. 112, No. 1, pp. 61-65, 1996

資源と素材, 112 巻, 1 号, 61-65 頁, 1996 年

Removal of antimony by volatilization from an industrial copper matte or white metal was carried out at 1523 K. The experimental conditions favored to the effective removal of antimony was selected from the thermodynamic considerations. H₂S gas was used as a bubbling gas to increase the partial pressure of sulfur and simultaneously the activity coefficient of antimony in the melt. The antimony concentration both in the matte and white metal were effectively lowered by bubbling 10 % H₂S -Ar mixed gas into the melt under a reducing atmosphere. In the case of matte, for example, antimony was removed from 2000 mass ppm to a level of 10 mass ppm in 3.6 ks at a gas flow rate of 8.3 cc/s. (in Japanese)

275: Elimination of Copper from Molten Steel by Ammonia Gas Blowing

アンモニアガスによる溶鋼の脱銅

Toshitsugu Hidani, Koji Takemura, Ryosuke O. Suzuki, Katsutoshi Ono

Tetsu-to-Hagane, Vol. 82, No.2, pp. 135-140, 1996

鉄と鋼, 82 巻, 2 号, 135-140 頁, 1996

Based on the finding that blowing of NH₃ gas onto molten pure copper at atmospheric pressure causes its evaporation of enormously high rate, attempts have been made on elimination of copper dissolved in molten steel by NH₃ gas blowing under reduced pressure. The decuprization experiments have been conducted to measure the rate at which the copper level in the molten steel is reduced by using a vacuum induction furnace and blowing NH₃ gas through a vertical water-cooled copper nozzle. For comparison, the rate of copper elimination from a small molten steel droplet has also been determined. From these experiments the rate constant for copper elimination from a flat and smooth surface of molten steel was the order of $2 \times 10^{-3} \text{ m} \cdot \text{min}^{-1}$ at 1900 K and the pressure range of 100 to 10000 Pa. Because the boiling phenomena are accompanied by an immense increase in the surface area from which volatile species are able to evaporate, NH₃ gas blowing may be useful to reduce the decuprization time. Nitrogen concentration in the molten steel increases with increasing the flow rate of NH₃ gas. It was reduced down to the initial level by vacuum degassing after stopping NH₃ gas blowing. (in Japanese)

276: Quantitative SIMS Analysis of Trace Metallic Impurities in High Purity Copper

SIMSによる高純度銅中の微量不純物の定量分析

Hiroyuki T. Takeshita, Takuya Kagawa, Ryosuke O. Suzuki, Toshio Oishi*, Katsutoshi Ono

(*Kansai Univ.)

J. Japan Inst. Metals, Vol. 60, No.3, pp. 290-294, 1996

日本金属学会誌, 60 卷, 3 号, 290-294 頁, 1996 年

Quantitative analysis of trace amounts of dominant impurities in copper, Ag, Fe, Ni and Pb, were studied using secondary ion mass spectrometry (SIMS). Based on the survey of the secondary ions species, which disturbed the detection of atomic ions of impurities, the removal of these disturbance is proposed as the two methods; applying the high resolution of mass spectrometry, and calculating the isotopic abundance. The precision, detection limit and relative sensitivity factor were experimentally discussed to establish the reliable quantitative SIMS analysis at the local area of high purity copper.

277: Quantitative SIMS Analysis of Mo in Ti-Dilute Mo Alloys Using Isotopic Abundance

同位体分離法による Ti-希薄 Mo 合金中の Mo の SIMS 定量分析

Yuichiro Sudo, Hiroyuki T. Takeshita, Ryosuke O. Suzuki, Yoichi Tomii, Katsutoshi Ono

J. Japan Inst. Metals, Vol. 60, No.4, pp. 406-411, 1996

日本金属学会誌, 60 卷, 4 号, 406-411 頁, 1996 年

For the application of SIMS (Secondary Ion Mass Spectrometry) to quantitative analysis for the dilute element in metallic alloys, it is indispensable to eliminate the disturbance which is counted with the secondary ions of the dilute element. Ti_2^+ ions from the Ti matrix overlap the Mo^+ ions from the Ti-dilute Mo alloys. However, a conventional SIMS could not be applied to separate Ti_2^+ ions either by its high resolution mass analysis or by the separation based on the energy profiles. Since the secondary ion intensities of Mo^+ and Ti_2^+ are proportional to their isotopic abundances, the secondary ion intensity of Mo^+ can be calculated and separated from the measured intensity. Using the ion intensity of $^{92}Mo^+$ or $^{100}Mo^+$ after the disturbance elimination and the normalization, a good linear relationship for the quantitative Mo analysis was obtained in the range of 766 mass ppm to 2.31 mass% Mo. The lower quantitative limit is evaluated to be 80 mass ppm due to the improved preciseness. (in Japanese)

278: Electrochemical deoxidation of yttrium-oxygen solid solutions

T.H.Okabe*, T.N.Deura, T.Oishi, K.Ono and D.R.Sadoway***

(*Dept. of Materials Science and Engineering, MIT, **Kansai Univ.)

J. Alloys and Compounds, Vol. 237, pp. 150-154, 1996.

Oxygen was removed from yttrium by an electrochemical method in which the metal is made the cathode in a cell consisting of a carbon anode and molten $CaCl_2$ electrolyte. At 1223K yttrium containing 5700 ppm oxygen was deoxidized down to less than 100 ppm. The method can be used to deoxidize other highly reactive metals. Furthermore, in principle it should be possible to remove other impurities besides oxygen.

279: Removal of copper from steel scraps by NH₃ gas

アンモニアによる鉄スクラップからの銅の除去

Ryosuke O. Suzuki, Toshitsugu Hidani, Koji Takemura, Katsutoshi Ono

Metals and Technology, pp. 55–66, August, 1996.

金属, 8月臨時増刊号, 55–66頁, 1996年

A concept for copper removal from the molten steel was proposed to recycle the car scraps to a fresh steel sheet suitable to a new car body. Evaporation of copper by blowing NH₃ gas onto molten pure copper was found and shown visually by the laser-light sheet method. This evaporation rate was significantly larger than the theoretical maximum evaporation rate under the vacuum, and several possible mechanisms were discussed in detail. The copper removal from the molten steel was confirmed experimentally by blowing of NH₃ under the reduced pressure. This decuprization was ten times faster than the vacuum degassing. The industrial applicability and efficiency were simulated and discussed. (in Japanese)

280: Thermodynamic Properties of Oxygen in Yttrium-Oxygen Solid Solutions**T.H.Okabe*, T.N.Deura, T.Oishi**, K.Ono and D.R.Sadoway***

(*Dept. of Materials Science and Engineering, MIT, **Kansai Univ.)

Metall. Trans. B, Vol. 27, pp. 841–847, October, 1996.

The oxygen potential in yttrium–oxygen(Y–O) solid solutions was measured by equilibration with titanium–oxygen(Ti–O) solid solutions. Yttrium and titanium samples were immersed in calcium–saturated CaCl₂ melts at temperatures between 1108 and 1438K, and oxygen levels in the two metals were measured. With the Ti–O system acting as a reference, oxygen potentials in Y–O solid solutions were determined. By this technique, it was possible to make reliable measurements of extremely low oxygen potentials(as low as 10⁻⁴⁴ atm at 1273K), far beyond the range of solid oxide electrolyte sensors.

281: * Removal of Antimony by Volatilization from Industrial Copper Matte and White Metal**Toshio OISHI*, Motohiro HORIGUCHI*, Yoichi KAWASAKI* and Katsutoshi ONO**

(*Kansai Univ.)

Metallurgical Review of MMIJ, Vol. 13, No.2, pp. 14-23, December, 1996.

Removal of antimony by volatilization from industrial copper matte or white metal was carried out at 1523 K. Experimental conditions favoring the effective removal of antimony were based on the thermody-

namic data. H₂S gas was used to simultaneously increase the partial pressure of sulfur and the activity coefficient of antimony in the melt. The antimony concentrations both in matte and white metal were effectively lowered by bubbling 10 % H₂S -Ar mixed gas into the melt under an atmosphere of reduced pressure. For example, antimony in matte was reduced from 2000 mass ppm to a level of 10 mass ppm in 3.6 ks at a gas flow rate of 8.3 cc/s.

282: Iron-Based Element for Low Temperature Thermoelectric Generator

低温用鉄系熱電変換素子

Katsutoshi ONO, Ryosuke O. SUZUKI, Ryoichi NAKAHASHI and Masahiro SHODA

Tetsu-to-Hagane, Vol. 83, No. 2, pp. 157-161, 1997.

鉄と鋼, 83 巻, 2 号, 157-161 頁, 1997 年

Direct conversion of low temperature waste heat source into electrical energy with thermoelements is an interesting and challenging problem. In this study, the thermocouple consisting of a junction between Fe and Fe-7~12mass%Al alloy has been developed. The uni-couple exhibits the power of 40 μ V/K at room temperature which is equivalent to that for the junction between Cu and Constantan. The iron and iron-aluminum alloy may be of great significance as materials for low temperature thermoelectric energy conversion because of their abundant production. Electric power generating facility using the iron and iron-based devices may have definite advantages: It has no moving parts and requires very little attention. It cannot wear out. Therefore, the determining factor of the possible use of thermoelectric generator is its efficiency. So, the latter half of this paper has been focused on the possibility to convert low temperature heat source into useful power with high efficiency. Recovery of electricity was discussed on the basis of a thermoelectric generator of the heat exchanger type in which the heat transferred by conduction through a energy panel consisted of a series of thermoelectric elements is accumulated in the air circulating as coolant and recycled as a heat source for the use to a subsequent thermoelectric panel. (in Japanese)

283: Removal of oxygen and nitrogen from niobium by external gettering

Yong Hwan Kim, Ryosuke O. Suzuki, Hiroshi Numakura*, Hirobumi Wada*, and Katsutoshi Ono

(*Dept. of Materials Science and Technology, Kyoto Univ.)

J. Alloys and Compounds, vol. 248, pp. 251-258, 1997.

External gettering has a potential to remove interstitial gaseous impurities from solid niobium (Nb) even below 1500K. The oxygen concentration in the deposit and the Nb bulk is evaluated by a combination of material thermodynamics and mass balance. The removal of oxygen and nitrogen was experimentally studied by using Ti, Y, Zr, Al and Si. Titanium deposited smoothly on the Nb surface in vacuum, and

absorbed the gaseous impurities most efficiently. By applying Ti as an external getter on commercial Nb at 1463K, the residual resistivity ratio reached 780. The oxygen distribution was calculated by combining thermodynamics and diffusion data. The experimental deoxidation rate was found to be slower than the calculated value. This may be attributed to the slow growth of the deposited layer, its morphology, and the interdiffused Ti-Nb alloy layer.

284: * Chemical potentials of the components in the system $\text{CaO} + \text{P}_2\text{O}_5 + \text{FeO}$

H. Hoshino and M. Iwase

Metallurgical Transactions, vol.27B, 1996, pp.595.603

Emf measurements were conducted with solid oxide galvanic cell of the type;
 $\text{Mo} / \text{Mo} + \text{MoO}_2 / \text{ZrO}_2(\text{MgO}) / \text{Fe}(\text{s}) + \text{Fe}_x\text{O}(\text{in slag}) / \text{Ag} / \text{Fe}$
 at 1673 K in order to obtain the activities of Fe_xO in $\text{CaO} + \text{P}_2\text{O}_5 + \text{Fe}_x\text{O}$ ternary slags. By using the Gibbs-Duhem integration, the activities of P_2O_5 and CaO were also obtained.

285: Oxidation-reduction equilibrium of $\text{Cu}^{2+}/\text{Cu}^+$ in binary alkaline sulfate melts

T. Yamamoto. N. Yamano-uchi, M. Tamura and M. Iwase

Metallurgical Transactions, vol.27B, 1996, pp.385/392

Red-ox equilibrium for $\text{Cu}^+/\text{Cu}^{2+}$ couple in binary alkaline sulfate melts ($\text{Li}_2\text{SO}_4 + \text{Na}_2\text{SO}_4$, $\text{Li}_2\text{SO}_4 + \text{K}_2\text{SO}_4$, $\text{Li}_2\text{SO}_4 + \text{Rb}_2\text{SO}_4$, $\text{Li}_2\text{SO}_4 + \text{Cs}_2\text{SO}_4$) were determined at temperatures between 973 and 1073 K by equilibrating these melts with gas mixtures of $\text{Ar} + \text{O}_2 + \text{SO}_2$. The red-ox equilibrium could be well interpreted by average ionic radii of alkaline metals.

286: * Chemical potentials of oxygen for mixtures of $\text{CaO} + \text{Ca}_4\text{P}_2\text{O}_9 + (\text{CaO} + \text{P}_2\text{O}_5 + \text{FeO})$ melts and $\text{Ca}_4\text{P}_2\text{O}_9 + \text{Ca}_3\text{P}_2\text{O}_8 + (\text{CaO} + \text{P}_2\text{O}_5 + \text{FeO})$ melts

H. Hoshino and M. Iwase

Metallurgical Transactions, vol.27B, 1996, pp.375/378

An electrochemical technique was employed for the determinations of the chemical potentials of three-phase assemblages of $C + C_4P + L$ and $C_4P + C_3P + L$ at temperatures between 1250 and 1450 °C, where $C = CaO$, $C_4P = 4CaO.P_2O_5$, $C_3P = 3CaO.P_2O_5$ and $L =$ ternary melts of $CaO + P_2O_5 + FeO$

287: * An automatic equipment for determinations of the FeO activity - laboratory and in-plant applications

M. Iwase

Proceedings of 5th International Conference on Molten Slags, Fluxes and Salts, held at Sydney, January 6-8, 1997.

The study of chemical reactions of liquid steel and molten slag involves a complex slag system of at least eight important components, i.e., CaO , MgO , MnO , FeO , SiO_2 , Al_2O_3 , P_2O_5 , CaF_2 , and often a number of others such as Na_2O , TiO_2 , Cr_2O_3 , CaS and so on. One of the greatest obstacles to the application of physico-chemical principles to the elucidation of slag-metal and slag-gas reactions is a lack of knowledge of the activities of reacting species. Since, iron oxide in slag participates in numerous reactions between metal, slag and gas, the evaluation of the activities of ferrous oxide should be first considered. Since 1940's, a number of experimental determinations of the activities of ferrous oxide have been conducted). Because of such concerted efforts of many laboratories during the five decades, approximately two thousand data were obtained for the FeO activities, while there are many duplicate measurements. Our knowledge of the activities of FeO is, nevertheless, still far from satisfaction. The present paper is aimed at documenting development of an automatic facility which allows the FeO activities in metallurgical slags at any given composition to be determined within 5 minutes, and the in-plant application of this system.

288: Depression of vaporization of melts formed during the immobilization of high level nuclear waste by the addition of P_2O_5

M. Iwase, H. Watanabe, J. Ouchi and K. Kawamura

Radioactive Waste Management and Environmental Restrtaion, vol.20,1995, pp.61/71.

Vaporization from melts consisting of Glass frit and High-Level Nuclear Waste (HLW) was investigated by using candidate glass frit PF798 and simulated HLW of Power Reactor and Nuclear Fuel Development Corporation, in order to test the feasibility of depressing the vaporization by the addition of P_2O_5 into the melts. By adding P_2O_5 at a rate of 1 wt.%, vaporization could be depressed by a factor of 1/5.

289: A Thermodynamic study of the system $\text{CaO} + \text{Al}_2\text{O}_3 + \text{FeO}$ at 1673 K**V. Espejo and M. Iwase**

Metallurgical Transactions, vol.26B, 1995, pp.257/261.

Electrochemical measurements of the solid-oxide galvanic cell;
 $\text{Mo} / \text{Mo} + \text{MoO}_2 / \text{ZrO}_2(\text{MgO}) / (\text{CaO} + \text{Al}_2\text{O}_3 + \text{Fe}_x\text{O}) + \text{Fe(s)} + \text{Ag} / \text{Fe}$
have been conducted at 1673 K in order to obtain the activities of Fe_xO in $\text{CaO} + \text{Al}_2\text{O}_3 + \text{Fe}_x\text{O}$ slags. By using the activity data for Fe_xO the iso-thermal section of the phase diagram for the system $\text{CaO} + \text{Al}_2\text{O}_3 + \text{Fe}_x\text{O}$ was derived.

290: Activity of phosphorous in liquid Ni + P alloys saturated with solid nickel**R. Kawabata and M. Iwase**

Metallurgical Transactions, vol.26B, 1995, pp.783/787.

By employing an electrochemical technique incorporating magnesia-stabilized zirconia electrolyte, the activities of phosphorous in liquid Ni + P alloys saturated with solid nickel were determined at temperatures between 1477 K and 1663 K. The activities of phosphorus referred to gaseous diatomic phosphorous at 1 atm pressure, a_P , could be expressed by analytical formulas;

291: Solubilities of CO_2 in candidate glasses for nuclear waste immobilization part 2, a summary for binary alkali silicate and borates**K. Haba, H. Watanabe M. Iwase, O. Oh-uchi and K. Kawamura**

Glass Technology, vol.36, 1995, pp.84/88.

Solubilities of carbon dioxide in candidate glasses used for immobilization of nuclearwaster were determined by employing a gravimetric technique for better understanding of the subject glass. This article summarises the authors results for silicate and borate melts.

292: Solubility of molybdenum in liquid tin

R. Kawabata, M. Myochin and M. Iwase

Metallurgical Transactions, vol.26B, 1995, pp.654/655.

Solubilities of molybdenum in liquid tin were determined at temperatures between 1000 and 1450 °C by employing a conventional sampling technique.

293: New nitriding technologies of steel utilizing thermal decomposition of CaCN_2 and its characteristics

CaCN₂の熱分解を利用した鋼の新しい窒化処理技術とその特徴

H. Fujita, O. Kudo, M. Furuya, M. Iwase and M. Tokizane

Heat Treatment vol.35, 1995, pp.349/358.

熱処理 35 巻、1995、pp.349/358.

An overview is given on the recent progress of the steel-nitriding based upon an application of CaCN_2 . A thermodynamic analysis revealed that the chemical potentials of the mixture $\text{CaCN}_2 + \text{CaO} + \text{CaC}_2$ would be high enough to form solid solution of Fe-N at temperatures below 700 K. (in Japanese)

294: * Thermodynamics of oxygen behaviour in cobalt-nickel alloys

Mansour Soltanieh, Alex Mclean and M. Iwase

Steel research., vol.68, 1997, pp.149/153.

In this study the concentration and chemical potential of oxygen in liquid Co-Ni alloys equilibrated with Co-Ni-aluminate spinel solid solutions and alumina have been determined at 1773, 1823 and 1873 K as a function of nickel concentration. The oxygen content of the melt has been measured by suction sampling and inert gas fusion analysis. The corresponding oxygen partial pressures have been determined with solid state cell, $\text{Mo} / \text{Mo} + \text{MoO}_2 / \text{ZrO}_2(\text{MgO}) / \text{Co-Ni melts} + \text{Al}_2\text{O}_3 + (\text{Co-Ni})\text{OAl}_2\text{O}_3 / \text{Mo}$. The effect of nickel on the activity coefficient of oxygen in Co-Ni alloys has been determined.

295: A Solid State Sensor for The Determination of Silicon in High-Carbon Ferrochromium Melts

K. Gomyo, L. R. Nelson, Y. Shin-ya, A. McLean and M. Iwase

Scandinavian Journal of Metallurgy, vol.25, 1996, pp.193/198

A three-phase zirconia electrolyte, which consists of cubic ZrO_2 -MgO solid solution, monoclinic ZrO_2 and Mg_2SiO_4 , was used to construct a solid state electrochemical sensor for the rapid determinations of silicon activities in ferrochromium melts. The performance of the cell; Mo + MoO_2 / three-phase zirconia electrolyte / ferrochromium was tested with ferrochromium melts at temperatures between 1860 and 1990 K. Upon immersion in the molten alloys, the cell showed stable emf's within 10 to 15 seconds, and the silicon levels could be determined within a standard deviation of ± 0.09 % Si.

296: * Refining of ferrous scrap intermingled with copper by using molten aluminium

Masanori Iwase

Steelmaking Conference Proceedings, 1966, vol.79, pp.633/642.

A new approach for the removal of copper from solid ferrous scrap has been proposed by the present authors. With this process, solid ferrous scrap intermingled with pure copper is brought into contact with molten aluminum, which dissolved copper preferentially, and is recovered as Al + Cu alloys. After a duration of 30 minutes at temperatures between 963 K and 1223 K, steel scrap is removed from the bath, resulting in being free of copper contamination.

297: * Distribution equilibria of the metallic elements and boron between Si based liquid alloys and $CaO-Al_2O_3-SiO_2$ fluxes

Si 基溶融合金と $CaO-Al_2O_3-SiO_2$ 系フラックス間の金属元素およびボロンの分配平衡

Hiroyasu Fujiwara, Liang Jin Yuan, Kenshirou Miyata, Eiji Ichise and Ryotatsu Otsuka*

(* Showa Aluminum Corp.)

J. Japan Inst. Metals, vol.60, No.1, (1996), pp.65-71

日本金属学会誌, vol.60, No.1, (1996), pp.65-71

Flux treatment is one of the effective methods in refining of metallurgical grade silicon to sollar grade. However, if the process is carried out under low oxygen potential, the components in the flux will be reduced to the metallic phase. In this study, the distribution of the metallic elements and boron between Si based liquid alloys and $CaO+Al_2O_3+SiO_2$ fluxes satulated with alumina or calcium-aluminates are investigated at 1873 K. Aluminum and calcium concentrations in silicon alloy can be related to the flux composition. When the $XSiO_2/(XSiO_2+XCaO)$ ratio in flux varies from 0.25 to 0.87, [mass%Al] and [mass%Ca] increase from 0.4 and 0.02 to 10 and 8 mass %, respectively. Equilibrium distribution ratio

of Boron: $(\text{mass}\%B)/[\text{mass}\%B]$ is about unity in the composition range investigated, and shows a peak value at $X\text{SiO}_2/(X\text{SiO}_2+X\text{CaO}) = 0.67$. (in japanese)

298: * Reducing Removal of Phosphorous from Calcium Containing Silicon Alloys

Hiroyasu Fujiwara, Jin Yuan Liang, Kotaro Takeuchi and Eiji Ichise

Materials transactions, JIM, vol.37, (1996), No.4, pp.923-926

Distribution equilibrium of phosphorous between silicon based alloys and $\text{CaO} + \text{Al}_2\text{O}_3 + \text{SiO}_2$ fluxes saturated with Al_2O_3 or calcium-aluminates was investigated at 1873 K. It was found that almost all the phosphorous in flux exist as phosphide ion: P^{3-} in the experimental composition range. Distribution ratio of phosphorous between metal and flux: L_P can be related to the flux composition. When the $X\text{CaO} / (X\text{CaO} + X\text{SiO}_2)$ ratio in flux increases from 0.38 to 0.85, $\log L_P$ increases from -2 to 0.4. These experimental results suggest that the dephosphorization reaction expressed as: $\text{P}(\text{in Si}) + (3/2) \text{O}^{2-}(\text{in Flux}) = \text{P}^{3-}(\text{in Flux}) + (3/4) \text{O}_2(\text{g})$ can proceed at the silicon refining by flux treatment and that the phosphorous removal process becomes more effective if the process is carried out under the conditions of high basicity, low oxygen potential, and high temperature.

299: Application of a Florescent Technique to the Study of the Weathering Process

Takashi Nishiyama, Hiromu Kusuda

Engineering Geology, 42, pp.247-253, 1996

Processes and rates of weathering in representative tuff obtained from a Green Tuff region were directly examined using a new fluorescent approach. This approach was developed to visualize microscopically the microcracks and micropores that contribute to deterioration. The following observations were made. Progression of tuff weathering is caused by a delicate balance between chemical alteration and physical disintegration. Weathering occurs in many hidden microcracks and micropores not detected under natural light, but which can be clearly visualized under ultraviolet light. Water pathways, such as microcracks and cavities, accelerated the chemical alteration by increasing the effective surface area of rocks in contact with water. As the reaction proceeds, the constituent materials loosen and alteration products become widespread in the matrix. Secondary amorphous to poorly crystallized materials, such as iron hydroxide and aluminosilicate, precipitate on the fracture surfaces, slowing the progress of weathering. At the ultimate stage of weathering in tuff, all cracks and most of the micropores are filled with secondary materials. These observation on a microscopic scale during tuff weathering agree with the assessment of weathering obtained by measuring porosity, P-wave velocity and tensile strength.

300: Pre processing Using Fluorescent Paint in Visual Recognition and Image Analysis - Extraction and Evaluation of the Vein by Image Processing -

蛍光塗料を用いた前処理による画像認識と解析— 画像処理による鉱脈の抽出と解析例 —

Hiromu Kusuda, Takashi Nishiyama

Shigen-to-Sozai, Vol.112, pp.589-592, 1996

資源と素材, 112, pp.589-592, 1996

Image processing is rapidly becoming popular in applied geology. However, it is often difficult to extract the object from other parts by image processing. In order to facilitate visual recognition, pre-processing before image input is useful. Therefore, the object is coated with the fluorescent paint on the photograph, and then examined under ultraviolet ray. The technique is effective for image processing because obtained images display a great difference in both brightness and color between objects and other parts. Three images were obtained by a CCD camera using optical filters (red, green and blue filter), and processed in several steps, including image sharpening, thresholding, and inter-picture operation. The gold vein in the Hishikari Mine were examined through the method described above. The gold veins in the mine were classified as three types (network veins, a banded vein, and complex veins with the different vein widths from the geological point of view). They demonstrate that all types of veins can be extracted practically from the host rock. The ore grade can accurately and easily be calculated by image analysis combined with chemical analysis.

301: Trends and Short-Term Prospects for Copper Demand

Takashi Nishiyama

Nonrenewable Resources, Vol.5, No.3, pp.155-168, 1996

In recent years, the rate of consumption of minerals and energy has been increasing. Herein, a few fundamental components of mineral consumption including population growth, rising standard of living, advances in technology, and economic growth are analyzed. Copper is one of the best resources for illustration the growth of metal consumption and components of that growth because statistical data for copper are quite comprehensive. Among the various factors examined, an index of rising standards of living is the significant factors explaining growth of copper consumption.

302: The Borehole Television System by the Fluorescent Method

蛍光法とボアホールテレビジョンシステムを用いた孔壁の割れ目の抽出

Takashi Nishiyama, Hiromu Kusuda, Youquing Chen, Michinao Terada*, Seiji Ebisu*, Kenji Hagimori*

*(Okumura Co.)

Journal of the Japan Society of Engineering Geology, 36-6, pp.442-447, 1996

応用地質、36巻6号、pp.442-447, 1996

It is very difficult to identify microcracks and pore spaces using conventional borehole television systems, because there are no characteristic differences in microcracks from other materials of rocks. We applied the fluorescent technique to the borehole television system to examine microcracks and pore spaces. Many hidden microcracks and pore spaces which were not recognized by conventional systems were visualized.

303: * An Application of Computer Graphic Simulation of Changes at Stone-Quarrying Sites

碎石場の開発における景観シミュレーションの適用

Toshihide Ito*, Hiromu Kusuda, Takashi Nisiyama

***(Kansai Univ.)**

建設用原材料, Vol.6, No.2, pp.7-15, 1996

Computer graphic simulation is quite useful in obtaining basic data concerning future changes in the scene which is caused by stone quarrying. We examined simulation changes in landscape caused by crushed stone quarrying. Montage and perspective projections were used to depict the color and other features of the surface of mountains, the course of tree planting on the pit face and the features of a newly developed pit face. A wireframe model was used to predict changes in the geographical features of quarries on the basis of existing stone-quarrying plants. By combining these techniques, we devised a method for editing two-dimensional still pictures, obtained from video tapes, from various angles. Still images of the current scene and the predicted future scene were made while gradually changing the angle of view.

304: * Theoretical Analysis for Non-Equilibrium Flow Fields with Transitional Process from Two-Phase to Three-Phase Mixtures by Injecting Air Halfway into a Lifting Pipe – (Fundamental study on lifting system for mining marine mineral resources (3rd Report)–)

揚鉱管途中の空気注入による2相流から3相流への遷移を含めた非平衡な流れ場の理論解析 (エアリフト方式による深海底資源の揚鉱システムの基礎的研究 (第3報) –)

Natsuo Hatta, Hitoshi Fujimoto

J. Mining and Materials Processing Institute of Japan, Vol.112, No.2, pp81-88, 1996

資源と素材, Vol.112, No.2, pp.81-88, 1996

This paper treats theoretical analyses to predict the steady flow characteristics of multiphase mixture in an air lifting pipe. When slurries containing solid particles such as manganese nodules are lifted from the deep-sea bed to the sea surface by an air lift pump, gas phase is injected halfway into a lifting pipe with a very large length ranging from the sea floor of about 5,000 m in depth to the sea surface. Here,

the case is treated where slurries are the solid particles-sea water two-phase mixture before the position of the gas injection and the air-solid particles-sea water three-phase mixture after that. Some numerical experiments are performed using a set of five equations in the two-phase region and a set of eight equations in the three-phase region for determining the flow properties. By comparing the non-equilibrium solutions with the numerical results of the case where the three-phase flow is assumed to be in velocity equilibrium, it is numerically shown that the equilibrium solution gives a threshold of the highest possible solid-phase mass flux on condition that both the gas-phase and liquid-phase mass fluxes are kept constant. (in Japanese)

305: * Deformation and Rebounding Processes of a Water Droplet Impinging on a Flat Surface Above Leidenfrost Temperature

Hitoshi Fujimoto, Natsuo Hatta

Trans. ASME, J. Fluids Engineering, Vol.118, pp.142-149, 1996

This paper treats numerical analyses of the deformation and rebounding processes of a water droplet impinging on a flat solid surface above the Leidenfrost temperature with a speed in the order of a few [m/s], as well as the flow field inside the droplet. These calculations were performed using the MAC-type solution method to solve a finite differencing approximation of the axisymmetric Navier-Stokes equations governing incompressible fluid flows. Also, the whole dynamic process of a droplet from the moment of collision with a hot surface including the rebound from it was recorded by using a video camera equipped with a macro lens. First, the water film formed by the droplet impinging on the surface spreads radially in a fairly thin discoid-like shape until it reaches a maximum. Next, the water film begins to recoil backwards towards the center and the recoiling process continues to occur owing to the surface tension effect at the periphery. Subsequently, the center part of the liquid drop begins to elongate upwards and the liquid near the top of the drop pulls up the lower part of the remaining liquid. Finally, a vertical ring structure appearing at the bottom of the elongated droplet induces the rotative motion in such a way as to form the rising flow and the droplet rebounds from the surface as a bowling pin-shaped mass. The numerical model to predict the deformation and rebounding processes was build up by accounting for the presence of viscous and surface tension effects. The numerical results obtained by the model were compared with the experimental data and discussed from a practical point of view.

306: * Nonsteady Behaviour of a Free Surface Configuration and Velocity Distribution in a Flow Field of Molten Steel in a Mold

溶鋼の鑄型内流動における自由表面形状と流速の非定常挙動

Natsuo Hatta, Takashi Fukui, Yoshio Nakajima*, Jun-ji Ikeda*

***(Kure Works, Nisshin Steel Co., Ltd.)**

Tetsu to Hagane, Vol.82, No.4, pp.285-290, 1996

鉄と鋼, Vol.82, No.4, pp.285-290, 1996

This paper treats numerical analyses of the flow structure of molten steel in a mold, focusing upon the unsteady behaviour of the free surface profile and velocity. These calculations were performed using the MAC-type solution method to solve a finite differencing approximation of the three-dimensional Navier-Stokes equations governing incompressible fluid flow. Here, the nonsteady body-fitted coordinate system was used so that the uppermost surface coordinate of the computational domain fits the free surface boundary in the physical space and therefore the mesh system is renewed at each computational time step. Also, the experimental study was undertaken to measure the surface velocity distribution, using water instead of molten steel. It was found that the numerical time-averaged surface velocity distribution is fairly in good agreement with experimental data. According to the results obtained by the present mathematical model, the flow field in a mold, including the free surface configuration and velocity, has been clarified to locally and temporarily fluctuate in somewhat a periodic manner. The effect to the casting speed and the kind of immersion nozzle on the flow structure of molten steel is estimated and discussed from a practical standpoint. (in Japanese)

307: * Prediction of Forming Limit in Axisymmetric Deep Drawing of Steel/Aluminium Alloy Laminated Sheets Using a Simple Criterion for Ductile Fracture

簡易延性破壊条件式を用いた鋼/アルミニウム合金積層板の円筒深絞り加工における成形限界予測

Hirohiko Takuda, Ken-ichiro Mori*, Tomoyuki Hirose, Natsuo Hatta

*(Osaka University)

J. Japan Society for Technology of Plasticity, Vol.37, No.424, pp509-514, 1996

塑性と加工, Vol.37, No.424, pp.509-514, 1996

Deep drawing process of laminated sheets composed of mild steel and various aluminium alloy sheets are simulated by the rigid-plastic finite element method. From the stress and strain histories of elements in each layer calculated by the finite element simulation, the fracture initiation site and the forming limit are predicted using the ductile fracture criterion. The predictions so obtained are compared with experimental observations. The results show that the ductile fracture criterion is useful to predict fracture initiation in forming of laminated composite sheets. Furthermore, it is found that the drawability is improved by setting the mild steel sheet on the punch side for the case of aluminium alloy sheet with comparatively high ductility, and by sandwiching the aluminium alloy sheet with the mild steel sheets for the case of low ductility. (in Japanese)

308: * Prediction of Forming Limit in Deep Drawing by Combination of Finite Element Simulation and Criterion for Ductile Fracture

Ken-ichiro Mori*, Hirohiko Takuda

*(Osaka University)

Trans. NAMRI/SME, Vol.24, pp.143-148, 1996

To predict forming limits in a wide range of sheet metals, a criterion for ductile fracture is combined with the finite element simulation. From the histories of stress and strain in each element calculated by the finite element simulation, the critical stroke and the fracture initiation site are predicted by the use of the criterion. The prediction by the ductile fracture criterion is applied to calculate limiting drawing ratios in axisymmetric deep drawing of aluminum alloy and mild steel sheets. Material constants in the ductile fracture criterion are determined from uniaxial and plane-strain tension tests of the sheets. The predicted limiting drawing ratios are in good agreement with the experimental ones, even in no appearance of localized necking such as aluminum alloy sheets with low ductility. It is shown that the fracture initiation site is changed by the amount of ductility, i.e., near the punch corner in the cup wall for mild steel and commercially pure aluminum sheets with high ductility and near the die corner for aluminum alloy sheets with low ductility.

309: * Prediction of Forming Limit in Deep Drawing of Fe/Al Laminated Composite Sheets Using Ductile Fracture Criterion

Hirohiko Takuda, Ken-ichiro Mori*, Hitoshi Fujimoto, Natsuo Hatta
***(Osaka University)**

J. Materials Processing Technology, Vol.60, pp.291-296, 1996

A criterion for ductile fracture is applied to the prediction of fracture in deep drawing processes of the laminates composed of mild steel and various aluminium alloy sheets, using the local stress and strain histories calculated by the rigid-plastic finite element simulation. The predictions are compared with experimental observations. The results exhibit that various types of fracture initiations in deep drawing of the laminated composite sheets are successfully predicted. Furthermore, it is numerically as well as experimentally shown that the drawability of the aluminium alloy sheets can be improved by laminating with the steel sheets.

310: * Finite Element Simulation of Redrawing Processes with Ductile Fracture Criterion

Hirohiko Takuda, Ken-ichiro Mori*, Akihiro Jinno, Natsuo Hatta
***(Osaka University)**

Proc. of the Asia-Pacific Symposium on Advances in Engineering Plasticity and Its Applications – AEPA'96, pp.691-696, 1996

A recently proposed method using the ductile fracture criterion is applied to the prediction of forming

limit in redrawing processes. Axisymmetric deep drawing and redrawing processes of various aluminium alloy sheets are simulated by the rigid-plastic finite element method. The calculated histories of stress and strain are substituted into the ductile fracture criterion, so that the fracture initiation site and the critical stroke are predicted. From the numerical experiments the total limiting drawing ratios are evaluated for various redrawing conditions. The results show that the fracture initiation site is dependent on the degree of ductility. The optimal redrawing conditions are discussed from the viewpoint of the improvement in limiting drawing ratio, not only for the aluminium alloy sheet with high ductility, but also for the sheet with low ductility.

311: * Experimental Study of Deformation Process of a Water Droplet Impinging on Polished and Rough Surfaces Heated to above the Leidenfrost Temperature

表面粗さの異なる加熱金属平面に衝突する微小液滴の変形挙動特性

Hitoshi Fujimoto, Takashi Fukui, Natsuo Hatta

Tetsu to Hagane, Vol.82, No.12, pp.975-980, 1996

鉄と鋼, Vol.82, No.12, pp.975-980, 1996

This paper treats the comparison of the deformation process of a water droplet impinging upon a hot polished (smooth) surface with that upon a hot oxide scaled (rough) surface. The surface whose material is SUS304 stainless steel, has been heated to 773 K for both the smooth and rough cases and a water droplet diameter has ranged between 0.3 mm to 0.7 mm. The rough surface has been made artificially by rapid-quenching the impingement side of the test surface piece, which has been heated to 1273 K in a furnace for about three hours, by water spraying. Thereby, the so-called oxide film has been formed on the surface. The droplet deformation process has been measured for the two cases where the droplet is struck on the smooth and rough surfaces, keeping the other experimental conditions constant. The deformation process has been found to be significantly different between the smooth and rough cases. The irregularity of the droplet configuration on the rough surface has been found to occur even in a short time after collision and to be amplified as the droplet deformation proceeds. For various Weber numbers, it has been found that the time needed for a droplet to reach a maximum diameter on surfaces can not be arranged as a function of the Weber number alone. Again, the difference between the smooth and rough cases becomes remarkable with increasing the Weber number. (in Japanese)

312: * Deformation Process of a Droplet Impinging on a Hot Oxide-Scaled Surface above the Leidenfrost Temperature

Natsuo Hatta, Hitoshi Fujimoto, Hirohiko Takuda

Steel research, Vol.68, No.1, pp.15-19, 1997

This paper is concerned with the collision dynamics of a water droplet impinging on a hot surface heated to above the Leidenfrost temperature, focusing upon the case where the impingement side is rough (oxide-scaled) with an oxide film. The rough surface has been artificially made by rapidly quenching as-rolled stainless steel by water spraying, after it has been heated to 1273 K in a furnace. A sequence of photographs showing the progressive stages of droplet deformation have been taken on several Weber number conditions. It has been found that the droplet configuration is not axially symmetric around the initial impact point even at an early stage immediately after collision and that the irregularity of the droplet configuration is amplified as the droplet deformation proceeds. With increasing Weber number, the irregularity has been seen to be more remarkable in the later stage and finally the droplet breaks up into some parts. Therefore, the critical Weber number to specify whether or not the droplet is disintegrated on the rough surface has been found to become small compared with the smooth surface case.

313: * Effect of Pressure Drop Owing to Friction between Pipe Inner Wall and Water on Non-equilibrium Flow Fields in an Air-lifting Pipe – (Fundamental study on lifting system for mining marine mineral resources–)

管摩擦が鉛直管内における非平衡流動と揚鉱特性に及ぼす効果 (一エアリフト方式による深海底資源の揚鉱システムの基礎的研究一)

Hitoshi Fujimoto, Makoto Isobe, Takashi Fukui, Natsuo Hatta

J. Mining and Materials Processing Institute of Japan, Vol.113, No.2, pp.133-139, 1997

資源と素材, Vol.113, No.2, pp.133-139, 1997

The present paper is concerned with a theoretical analysis of the steady characteristics of an air-lift pump system for conveying the marine mineral resources from the deep-sea bed to the sea surface. Here, the effect of pressure drop owing to the friction between the fluid and the inner wall of the pipe is taken into consideration. Some numerical experiments have been carried out using a set of five equations in the solid-liquid two-phase region and a set of eight equations in the solid-gas-liquid three-phase region for determining the non-equilibrium flow properties. In particular, the influence of the pipe diameter as well as the liquid-phase velocity on the solid-phase mass flux to be lifted has been examined from a numerical point of view. It has been quantitatively demonstrated how the mass flux of mineral ores decreases because the pressure drop due to the wall friction becomes more remarkable as the liquid-phase velocity is higher and the pipe diameter is selected to be smaller. Again, the critical condition whether or not solid particles can be lifted has been indicated with the liquid-phase velocity and the pipe diameter as parameters. Such important problems are described in detail. (in Japanese)

314: * A Study on Recycling of Disposal Consumer Electronic Goods

Y. Nakahiro, H. b. Kamarudin, Y. Fukunaka, E. Kusaka, M. Niinae and K. Takahashi

Proc. of the 6th JSPS-UCC Seminar on Integrated Engineering, p.1-9, 1996

Disposal substrate taken out from the consumer electronics goods or disposed PWB (Print Wiring Board) materials were crushed, sieved and magnetically separated. Sample was dissolved into aqua regia and analyzed with an atomic absorption method. Au, Ag and Cd were not detected. Copper content and distribution ratio in -20+35 mesh fraction were 45.5% and 41.5%, respectively. Non-magnetic particles of -20+35 mesh were processed with a Wilfley table. The effect of flow rate of water and the table frequency were significant to effectively separate the non-magnetic particles into concentrate, middling and tailing. Concentrate shows apparently metallic reflection. The copper content and distribution ratio were improved to be 70% and 90%, respectively.

315: A Study on Recovery of Valuable Metals from Auto Shredded Dust

Y. Nakahiro, K. Takahashi, Y. Fukunaka, J. Yamamoto and E. Kusaka

Proc. of the 3rd International Symposium on East Asian Resources Recycling Technology, p. 283-291, 1996

As a part of the studies on the recovery of valuable metals such as iron and copper from the industrial waste, the feasibility of magnetic and gravity separation to upgrading the ash supplied from the fluidized bed combustion furnace have been investigated. In recovering copper from the bottom ash, a hand sorting operation with the help of a ferrite magnet having a magnetic field strength of 1400 gauss could assist the following gravity separation using a Wilfley table. It can be concluded that the upgrading the bottom ash is possible when the magnetic and gravity separation is effectively combined and that by optimizing the table operating conditions, such as water flow rate and stroke frequency, the table concentrate consisting of 88% Cu and more can be obtained with a copper recovery more than 94%.

316: * The Role of Hydrolyzed Metal Cations in the Liquid-Liquid Extraction of Ultrafine Silica with Dodecyl Sulfate

E. Kusaka, Y. Kamata, Y. Fukunaka and Y. Nakahiro

Minerals Engineering, Volume 10, Number 2, pp. 155-162, (1997)

As part of fundamental studies on the recovery of fine particles, ultrafine silica was liquid-liquid extracted with anionic collector, sodium dodecyl sulfate (SDS). Isooctane and water were used as the two liquid phases. The pH dependence of the recovery level of the silica was determined in the absence and presence of metal salts, such as Fe(III), Al(III) and La(III), for physicochemical interpretation on the role of the hydrolyzed metal species during the anionic liquid-liquid extraction of the silica fines. The

results showed that the silica could not be recovered without the metal salts while the addition of the metal salt led to a significant increase in recovery in a certain pH range. Comparison of these results and the distribution diagrams of the metal species indicated that the increase in recovery is in line with the formation of metal hydroxides, hydroxo complexes and precipitates. Also, the minimum extraction edges of the silica in terms of pH were correlated to the residual concentration of the respective metal species in the water phase; the hydroxo complexes that form prior to the precipitation pH were the species responsible for the silica activation as well.

317: Flotation Separation of Plastics Using Selective Depressants

J. Shibata*, S. Matsumoto*, H. Yamamoto*, E. Kusaka and Pradip

International Journal of Mineral Processing, Volume 48, pp. 127-134, (1996)

Four important plastics, namely polyvinyl chloride (PVC), polycarbonates (PC), poly acetal (POM) and polyphenylene ether (PPE) were successfully separated from their synthetic mixtures using common wetting agents like sodium ligninsulfonate, tannic acid, Aerosol OT and saponin. The efficient flotation separation amongst these naturally hydrophobic polymers could be attributed to the selective reduction in hydrophobicity (measured as the drop in contact angle) as a consequence of surfactant adsorption. The relative order of floatability measured with the help of column flotation experiments in the presence of various depressants selected for this study was found to be $PPE > POM > PC > PVC$, a trend consistent with the critical surface tension values determined for these solids except PPE. A flowsheet was developed on the basis of flotation results. It was possible to accomplish almost a perfect separation using the proposed flowsheet involving heavy media separation followed by flotation in two stages.

318: * Mass Transfer Rate in Powder Injection

K. Koyama, T. Ogino, Y. Fukunaka and Z. Asaki

Metallurgical Review of MMIJ, 13, pp.49-61(1996)

A mixed CO_2-N_2 gas was injected into an aqueous NaOH solution with acrylic resin particles of 0.19, 0.55 and 1.12mm in average diameters, and the absorption rate of CO_2 gas was measured. It was observed that a cavity was formed on the liquid surface and the plume, where gas and particles penetrates into the liquid, was formed below the cavity. The overall rate of absorption of CO_2 gas into the NaOH solution was controlled by mass transfer, and the value of the overall mass transfer parameter, AK_0 , varied in the range from 30 to $100cm^3s^{-1}$. CO_2 gas is absorbed in both the cavity and the plume. The ratio of CO_2 gas absorption in the plume region to that at the cavity ranged from 0.3 to 1.9 and the ratio increased with the increase in the particle diameter and with the decrease in gas velocity.

319: Electrodeposition of Copper under Microgravity

Y. Fukunaka, K. Okano, Y. Tomii, Z. Asaki, and K. Kuribayashi(ISAS)

Proc. of the 3rd Symp. on "Electrochemically Deposited Thin Films", Ed. by M.Paunovic and D.A.Scherson, The Electrochemical Society, Vol.96-19, pp.136-147 (1997)

Copper was electrodeposited from 0.9M CuSO₄ aqueous solution for 8 seconds during a free fall experiment in a drop shaft. A horizontally-orientated quasi two-dimensional electrolytic cell, in which a 200 μ m thick electrolyte layer was sandwiched by two sheets of slide glass, fell in the shaft. Electrolysis was conducted at constant current densities from 0.05 to 0.3A cm⁻², and the potential difference between electrodes was simultaneously monitored. A common-path microscopic interferometer was installed in the capsule. The time variation of interference fringe pattern, corresponding to the concentration profile due to the ionic mass transfer rate accompanied with copper electrodeposition, was measured in-situ around the periphery of a 1-mm-dia circular cathode. The morphology of copper electrodeposited under microgravity conditions was compared with that obtained in a ground-level experiment. The development of diffusion layer thickness measured by the intereferometer increased with the square root of time during the 8s experiment. The transient diffusion model combined with the migration effect reasonably explained the development of diffusion layer thickness. Calculated surface concentrations corresponded with the measured time variation of potential difference between electrodes. Under the gravitational field, the radius of annular interference fringe pattern developed at a rate much faster than that under microgravity, beginning 1 or 3 s after initiation of electrodeposition. Natural convection was evident in the ground-level experiment, even using such a shallow electrolyte layer. Under microgravity, lower-index planes preferentially grew to form a fewer number of larger grains, even though electrodeposition was conducted at 0.05 to 0.3 A cm⁻² only for 8 s.

320: Ionic Mass Transfer Rate Associated with Electrodeposition of CdTe Film

Y. Fukunaka, S. Izuo, Z. Asaki and Y. Nakahiro

Proc. of the 3rd Symp. on "Electrochemically Deposited Thin Films", Ed. by M.Paunovic and D.A.Scherson, The Electrochemical Society, Vol.96-19, pp.103-114 (1997)

CdTe film was potentiostatically electrodeposited on a rotating disk electrode in aqueous solution. The effects of overpotential, pH and sometimes HTeO²⁺ concentration or temperature to the film composition and microstructure were examined. At 80 °C, CdTe compound semiconductor film with preferentially grown (111) plane was electrodeposited in electrolyte adjusted to pH=1 and 1.5. A significantly induced codeposition phenomena on Cd was observed at pH=1 and 60 °C. HTeO²⁺ ion at the cathode surface hindered the hydrogen gas bubble evolution rate. From the experimental results, a

phenomenological similarity between the alloy electrodeposition of metal/metalloid and metal/chalcogen system was noticed. The adsorption mechanism applied to amorphous film formation mechanism of metal/metalloid system was also adopted. The composition of electrodeposited CdTe film was reasonably explained with the calculated surface concentration of HTeO^{2+} ion.

321: Observation of Electrochemical Interfacial Phenomena under Microgravity

Y. Fukunaka and Y. Nakahiro

DENKI KAGAKU, 65, pp.170-174(1997)

The ionic mass transfer rate associated with natural convection caused by the electrochemical reaction at the electrode has been studied with the laser interferometry technique. The surface concentration of metal cation can be calculated from the boundary layer theory, as long as the hydrogen gas bubble is not evolved. The coupling phenomena between the ionic mass transfer rate and the morphology of electrodeposited film has been considered. As an idealistic case, the experiment without the induction of natural convection has been proposed. The duration time of electrodeposition under microgravity level is limited to less than 10 second, even the largest drop shaft is utilized. The development of Ag^+ ion concentration around a 1mm diameter circular cathode immersed in AgNO_3 solution was in-situ measured with interferometer. The experimental results were reasonably compared with the transient diffusion model. The previous works on the electrochemical interfacial phenomena under microgravity were also reviewed.

322: * Adsorption of Inorganic Depressants on Synthesized Diamond and Graphite

N. Ishida, D. Mwaipopo, E. Kusaka, M. Niinae, Y. Fukunaka and Y. Nakahiro

J. of the Mining and Materials Processing Institute of Japan, 113, 269-273(1997)

The adsorption phenomena of sodium pyrophosphate and sodium silicate were studied on synthesized diamond and unreacted graphite. Both depressants adsorbed on diamond surface, while they were rarely onto unreacted graphite. It suggests that the diamond surface adsorbed with depressant becomes hydrophilic to depress the floatation of diamond. The adsorption isotherm curves were also measured to estimate the differential heat of adsorption. They were between the typical values corresponding to physical and chemical adsorption. The dependency of adsorption density for these depressants on pH showed as follows: primary adsorption species was $\text{HP}_2\text{O}_7^{3-}$ and adsorption isotherm equation was of Langmuir type for sodium pyrophosphate, while it was $\text{SiO}(\text{OH})_3^-$ and Freundlich type for sodium silicate.

- 323: * S=1/2 quantum spin-gap in 1-D antiferromagnet with bond alternation: NMR study of $\text{CuCl}_2(\gamma\text{-picoline})_2$**

Meiro CHIBA, Takeji KUBO*, Yoshitami AJIRO and Takayuki ASANO ****

*** Nara University of Education, ** Department of Applied Physics, Fukkui University**

Czech. J. Phys. 46, Supplement, 1971-1972 (1996)

Proton NMR experiment has been performed in $\text{CuCl}_2(\gamma\text{-picoline})_2$ up to 9 T for the study of S = 1/2 quantum spin-gap in the one-dimensional antiferromagnet (1-D AF) with bond alternation. It is shown that the proton NMR spectrum as well as the proton spin-lattice relaxation is characterized by the singlet-ground-state. Furthermore, NMR results suggest the existence of the paramagnetic spin around the end of the finite chain.

- 324: * Effect of Spin Correlation on ^{133}Cs Nuclear Magnetic Relaxation in Singlet Ground State System CsFeCl_3**

M. Toda*, T. Sadakane*, T. Goto*, M. Chiba and K. Adachi* * Graduate School of Human Environmental Studies, Kyoto University ** Kobe Tokiwa Junior College**

Czech. J. Phys. 46, Supplement, 2087-2088 (1996)

To study correlation in singlet ground state system CsFeCl_3 , we have measured the temperature dependence of the nuclear spin lattice relaxation time T_1 of ^{133}Cs in the field range up to the critical field 7.5 T (H//c-axis). In low fields T_1^{-1} exhibits remarkable temperature dependence, which is essentially expressed by an activation-type equation with the gap energy between the ground- and first-excited-state. The comparison of temperature dependence between the results above and below 5 T is discussed and two model is discussed respectively.

- 325: * ^{59}Co NMR in Stacked Triangular Lattice Antiferromagnet CsCoBr_3**

T. Kubo*, M. Uyeda*, H. Marutani*, M. Chiba

Czech. J. Phys. 46, Supplement, 2049-2050 (1996)

From ^{59}Co NMR at 484.5 MHz in Ising-like antiferromagnet CsCoBr_3 in the low temperature phase, we found the antiparallel coupling Co^{2+} spins along the c-axis together with the pseudo-field effect. The

zero-field spectra, however, including a weak component besides the main lines suggest that sublattice canting in CsCoBr₃ unlike the ferrimagnetic structure in CsCoCl₃.

326: * Reports on Quantum Spin Effect Contributed to LT21: NMR Study on Quantum Spin-Gap and Magnetic Frustration

Meiro CHIBA

Research Report of I.A.E. No.6 (1996)

Three original reports of NMR experiment on the quantum spin effect in low dimensional antiferromagnets will be contributed to the coming LT21 (International Conference on Low Temperature Physics, Prague, 8 - 14 August, 1996). The first two reports are devoted to the quantum spin-gap: the one is the spin-gap in CuCl₂(γ -picoline)₂ one-dimensional S = 1/2 antiferromagnet with bond alternation due to the many body quantum spin effect, and the other is the quantum spin-gap due to the single ion anisotropy in CsFeCl₃. The third report is the subject on three-dimensional order under the magnetic frustration in triangular-lattice antiferromagnet CsCoBr₃. The essential points on these experimental works are reviewed.

327: Materials Studies for Fusion Reactors - with the Emphasis on Radiation Damage Studies-

Akira Kohyama

2nd Japan-Central Europe Joint Workshop on Modelling of Materials and Combustion, 1996

Research and development programs on fusion reactor materials in Japan have been promoted mainly by universities, Japan Atomic Energy Research Institute (JAERI) and National Research Institute for Metals (NRIM) under a task sharing scheme.

The University activities on fusion materials became active and gradually organized in the 1970s and the Special Research Project on Nuclear Fusion supported by Monbusho (FY 1980-1989) was the first large scale coordinated joint research among Japanese universities. During this period, from FY 1982-1986, Japan/US Joint Project on utilization of RTNS- was completed successfully for providing extremely useful data on radiation damage produced by 14MeV neutrons. Since 1987, The Japan/US Collaboration in Fundamental studies of irradiation effects in fusion materials utilizing fission reactors (FFTF/MOTA Collaboration) has started as an eight year termed project. The phase- program of the US/Japan collaboration was initiated in April 1995 under the title of "Dynamic Behavior of Fusion Materials and Their Response to Variable and Complex Environments".

The Japanese current activities and future trends contain many of the world wide common interests.

Further promotion of international collaboration on these common issues is quite important and essential for fusion research heading for the near-term ITER and long-term DEMO and Power Reactors.

328: A modeling of radiation induced microstructural evolution under applied stress in austenitic alloys

Hiroyasu Tanigawa, Akira Kohyama

Journal of Nuclear Materials, 233, p.p. 80-84, 1996

Effects of applied stress on early stages of interstitial type Frank loop evolution were investigated by both numerical calculation and irradiation experiments. The final objective of this research is to propose a comprehensive model of complex stress effects on microstructural evolution under various conditions. In the experimental part of this work, the microstructural analysis revealed that the differences in resolved normal stress caused those in the nucleation rates of Frank loops on 111 crystallographic family planes, and that with increasing external applied stress the total nucleation rate of Frank loops was increased. A numerical calculation was carried out primarily to evaluate the validity of models of stress effects on nucleation processes of Frank loop evolution. The calculation stands on rate equations which describe evolution of point defects, small point defect clusters and Frank loops. The rate equations of Frank loop evolution were formulated for 111 planes, considering effects of resolved normal stress to clustering processes of small point defects and growth processes of Frank loops, separately. The experimental results and the predictions from the numerical calculation qualitatively coincided with each other, but the result suggested that the present model need to be improved by including cascade effects to make it more realistic.

329: Elastic FEM Analysis of Fiber Push-Out Test for C/C Composites

Hisashi Seeizawa *, Akira Kohyama, Kenichiro Watanabe *, Teruo Kishi *, Shinji Sato *, * (The University of Tokyo)

Materials Transactions, JIM, Vol. 37, pp. 409-413, 1996

To study mechanical properties of fiber, matrix and their interface in C/C composites, fiber push-out test has been carried out. Where, to decompose the deformation, measured from indenter displacement, into local deformation is essential for mechanistic understandings. But up to now, there has been no systematic study on this effect. In this study, as the preliminary analysis of the push-out test, the push-out tests with variety of groove width on specimen holder were performed and the elastic deformations of specimen under these tests were analyzed with a finite-element method (FEM). Materials used were unidirectionally reinforced C/C composites. Fiber push-out tests were carried out by utilizing dynamic

ultra micro indentation test machine. For the cases of 20 and 100 mm groove, plateaus which indicate the occurrence of fiber push-out could be seen in Load-displacement curves (indentation curves) and there was a difference in the duration of plateau. On the other hand, for all the cases, any difference can not be seen before plateaus. Now by using axis symmetrical FEM model, elastic deformation of C/C composites before push-out was calculated. From the results of calculation, the effect of groove width on indentation curves within elastic regime was considered to be little. But there was a large difference in the distribution of the stress transverse to carbon fiber direction on fiber-matrix interface between 20 and 100 mm, and this was considered to be the origin of the difference of the dilation of plateau.

330: NIFS Information Network for Fusion Engineering Research in Japanese Universities

Chusei Namba*, Akira Kohyama, Yutai Katoh *National Institute for Fusion Science,

Journal of Nuclear Materials, 233-237, 1029-1034

The characteristics of defect production and effective flux of freely migrating point defects under cascade damage conditions are among the key issues to assess the materials behavior under fusion environment by mechanistic modeling. In this paper, using a rate theory model of point defect and cluster evolution combined with results from molecular dynamics simulations, issues on characterizing cascade-induced defect production by microstructural analysis are discussed. In particular, determination of cascade vacancy cluster configuration, surviving defect production efficiency and cascade-interaction volume is attempted by analyzing temperature dependence of swelling rate and loop growth rate in austenitic steels and model alloys.

331: * Temperature Dependence of Young's Modulus And Internal Friction on SiC/SiC Composites

A.Kohyama, S.Hisashi (University of Tokyo), S.Sato (University of Tokyo)

IEA International Workshop on SiC/SiC Ceramic Composites for Fusion Structural Applications, pp. 171-173, 1996

As a result of R & D efforts for silicon carbide (SiC) fibers, newly developed SiC fibers offer excellent resistance to high temperature, superior mechanical properties at high temperature and good stability to irradiation damages. So SiC fiber reinforced ceramic composites (SiC composites) are the most promising candidates as high heat flux component materials, where temperature dependence of mechanical properties is important baseline properties. In this research, as the first study of SiC composites, temperature dependence of Young's modulus and internal friction on SiC composites reinforced with newly developed SiC fibers was precisely measured.

332: * In-Situ Observation Fracture Process and Microstructural Analysis of SiC/SiC Composites

S.Sato (University of Tokyo), A.Kohyama, T.Suzuki (University of Tokyo)

IEA International Workshop on SiC/SiC Ceramic Composites for Fusion Structural Applications, pp. 165-169, 1996

There have been many efforts to correlate mechanical properties of composite materials with deformation and fracture behaviors, but they are still insufficient to understand even qualitatively. In many cases, especially for the cases of ceramics composites, varieties of fracture behaviors have been observed in, so-called, the identical materials. This is due to the complex and heterogeneous microstructure of CMCs (ceramics matrix composites) with many pores, cavities, cracks and interfacial defects. It is still impossible to control the structure and properties of CMCs sufficient to identify them as the identical materials. Therefore, Japanese working group on SiC/SiC for fusion materials has been working on a round robin test material of Hi-Nicalon fiber reinforced SiC/SiC made by Ube Industries(1). The objective of this study is to obtain fundamental information about fracture behaviors of SiC/SiC composite material with carbon coated Hi-Nicalon and CVI-SiC matrix. In this study, fracture process was inspected "in-situ" using three point bending test apparatus with video microscope(2). In order to see the effect of surface cracks introduced during specimen cut-out and preparation processes, some specimens have been applied CVD-SiC coating.

333: Preparation of High-Purity SiCf/SiC Composites

T.Noda (National Research Institute for Metals), H.Araki (National Research Institute for Metals), A.Kohyama

IEA International Workshop on SiC/SiC Ceramic Composites for Fusion Structural Applications, pp. 31-34, 1996

Microstructures, mechanical properties, and purities of UD SiCf/SiC composites prepared with Nicalon SiC fibers containing oxygen of 12.3 and 0.5 respectively, using chemical vapor infiltration process have been studied. The composites show that favorable mechanical properties and a purity better than 99.99% large weight loss mainly due to deoxidation resulting the degradation of the composites was observed for the Nicalon SiC fiber/SiC composite(SiCf/SiC) above around 1700K, while Hi-Nicalon fiber composite(Hi-SiCf-SiC) kept the fibrous structure even at 2273K. The decomposition of Nicalon SiC fibers can be explained by the evaporation of SiO. The induced activation analysis for the composites which was assumed to be used as a first wall showed that the dose rate decreases by 5-6 orders magnitude after several days cooling.

334: Tandem Electron Beam Welding for Maintenance of Nuclear Fusion and Fission Reactors

A.Kohyama, N.Abe (Osaka University), M.Tomie (Kinki University), B.Shaojun (Beijing Polytechnic University), T.Suzuki

Proceedings of the 6th International Symposium of Japan Welding Society, Vol.2, pp. 477-482, 1996

As the important part of the life extension program for nuclear fission reactors and that of the maintenance scheme of blanket of fusion reactors, repair welding technique of neutron damaged materials is recognized to be one of the most urgent subjects to be established. This work provides the potentiality and the critical issues of "Tandem electron beam welding technique" when it is applied to heavily neutron damaged materials. Where mechanical property degradation due to the displacement damage and helium production from (n, a) reaction makes it very difficult to produce sound welded joint.

This paper presents the preliminary results to see the elementary characteristics of the welded joints produced by Tandem electron beam welding technique. Not only for the stainless steel nor high-nickel alloys, also for stainless steel to high-nickel alloy welded joints were studied. The tandem electron beam welding was done at JWRI, Osaka University. By optimizing the drilling effect from the leading electron beam and the weld defect suppression effect from the secondary electron beam, weld defect free welded joints were obtained with the excellent joint strength and ductility. The weld bead shape and penetration characteristics are also provided. The present results are quite promising to apply "Tandem e

335: A Modeling of Radiation Induced Microstructural Evolution Under Applied Stress in Austenitic Alloys

H.Tanigawa, Y.Katoh, A.Kohyama

Journal of Nuclear Materials, No.239, pp. 80-84, 1996

Effects of applied stress on nucleation process of interstitial type Frank loop evolution have been investigated by both numerical calculation and irradiation experiments. The final objective of this research is to propose a comprehensive model of complex stress effects on microstructural evolution under various condition.

In the experimental part of this work, tension specimens of Fe-15Cr-20Ni ternary alloy (solution annealed) and single crystal SUS316 were irradiated by 4 MeV nickel ions up to 0.5 dpa, under nominal tensile stresses of 0, 35, and 70 MPa, i.e., approximately 0, 1/3 and 2/3 of the yield stress, respectively. The irradiation temperature were 623K, 673K and 723K, and dose rate were 1×10^{-3} and 1×10^{-4} dpa/s. The microstructural analysis revealed that the Frank loop nucleation rates on 111 family planes increased as the magnitude of resolved normal stress increased.

A numerical calculation has been carried out to evaluate the validity of the model of stress effects on nucleation process of Frank loop evolution. The calculation stands on rate equations which describe evolution of point defects, small points defect clusters, Frank loops and network dislocation. The rate equations of Frank loop evolution were formulated for 111 family planes, considering effects of resolved normal stress to clustering processes of small point defects and growth processes of Frank loops, separately. In the equations, the interstitial clustering and dissociation rate constants, the unfaulting fraction of Frank loops were supposed to be dependent on the applied stress. The propriety of the model will be discussed with the experimental results.

336: Effect of Heat Treatment Temperature on Interfacial Mechanical Properties of C/C Composites by means of Micro-Indentation Test

S.Sato (University of Tokyo), K.Watanabe (University of Tokyo), H.Serizawa (University of Tokyo), K.Hamada (University of Tokyo), A.Kohyama

Microstructures and Functions of Materials, pp. 157-160, 1996

Effects of heat treatment temperature (HTT) on interfacial microstructure and interfacial mechanical properties of carbon/carbon (C/C) composites are investigated. Formation and/or growth of graphite layers adjacent to fiber-matrix interface were detected by transmission electron microscopy (TEM). Ultra micro indentation test technique was developed and was applied to C/C composites and fiber push out tests were also carried out. In case of fiber push out, the indentation curve showed a plateau which was interpreted to correspond with fiber push out. Interfacial sliding strength, evaluated from the load at the plateau, was increased with increasing HTT above 2000 K. Also, the effects of irradiations on those characteristics are provided and discussed.

337: Blanket Design Using FLiBe in Helical-type Fusion Reactor FFHR

A.Sagara (National Institute for Fusion Science), O.Motojima (National Institute for Fusion Science), O.Mitarai (Kyushu Tokai University), S.Imagawa (National Institute for Fusion Science), K.Watanabe (National Institute for Fusion Science), H.Yamanishi (National Institute for Fusion Science), H.Chikaraishi (National Institute for Fusion Science), A.Kohyama, H.Matsu (Tohoku University), T.Muroga (National Institute for Fusion Science), N.Noda (National Institute for Fusion Science), T.Noda (National Research Institute for Materials), N.Ohyabu (National Institute for Fusion Science), T.Satow (National Institute for Fusion Science), A.A.Shishkin (Kharkov Physics and Technology Institute, Ukraine), S.Tanaka (University of Tokyo), T.Terai (University of Tokyo), K.Yamazaki (National Institute for Fusion Science), J.Yamamoto (National Institute for Fusion Science), FFHR Group

Journal of Nuclear Materials, 1996

The blanket design for Force-Free Helical reactor, FFHR, is presented, which is a demo-relevant heliotron-type D-T fusion reactor based on the first all- superconducting-coils device, LHD (Large Helical Device) under construction in NIFS at present. For the goal of a self-ignited reactor of 3GW thermal output, the design parameters at the first stage for concept definition of FFHR have been investigated. The main feature of FFHR is force-free-like configuration of helical coils, which makes it possible to simplify the coil supporting structure and to use high magnetic field instead of high plasma beta. The other feature is the selection of molten-salt FliBe as a self-cooling tritium breeder from the main reason of safety owing to low tritium inventory, low reactivity with air and water, low pressure operation and low MHD resistance compatible with a high magnetic field. In particular, as common issues in fusion reactors, the FliBe blanket system in FFHR is expressed in detail by showing engineering possibilities to overcome key issues on tritium permeation, material corrosion, heat transfer, operation pressure, etc. The basic design for maintenance and repair of the blanket is also discussed.

338: Effect of Heat Treatment Temperature on Young's Modulus and Microstructure of C/C Composites

S.Tato*, H.Serizawa*, A.Kohyama, H.Tsunakawa*, S.Kagaya**, *(The University of Tokyo), **(Haruna Engineering Co., Ltd.)

Microstructures and Functions of Materials, pp. 129-132, 1996

As one of the most important mechanical properties of C/C composites for high temperature structural applications, temperature dependences of Young's modulus were precisely studied in a vibration method from room temperature up to 1373 K. Materials used were two kinds of unidirectional C/C composites, where the variables were microstructure of carbon fibers in C/C composites and heat treatment temperature of C/C composites. The temperature dependences of Young's modulus showed positive and negative trends reflecting microstructure changes of carbon fibers by heat treatments. Also, the graphitization effects of carbon fibers on the temperature dependences are presented quantitatively.

339: Design Assessment of Heliotron Reactor

K.Yamazaki (National Institute for Fusion Science), A.Sagara (National Institute for Fusion Science), O.Motojima (National Institute for Fusion Science), M.Fujiwara (National Institute for Fusion Science), T.Amano (National Institute for Fusion Science), H.Chikaraishi (National Institute for Fusion Science), S.Imagawa (National Institute for Fusion Science), T.Muroga (National Institute for Fusion Science), N.Noda (National Institute for Fusion Science), N.Ohyabu (National Institute for Fusion Science), T.Satow (National Institute for Fusion Science), J.F.Wang (National Institute for Fusion Science), K.Y.Watanabe (National Institute for Fusion Science), J.Yamamoto (National Institute for Fusion Science), H.Yamanishi (National Institute for Fusion Science), A.Kohyama, H.Matsui (Tohoku University), O.Mitarai (Kyusyu Tokai University), T.Noda (National Research Institute for Metals), A.A.Shishkin (NSC Kharkov Physics and Technology Institute, Ukraine), S.Tanaka (University of Tokyo), T.Terai (University of Tokyo)

Research Report NIFS Series, No.447, 1996

Helical reactor designs are studied based on the physics and engineering concept of the Large Helical Device (LHD) which is characterized by two advantages; efficient closed helical divertor and simplified continuous-coil system.

Firstly, optimization studies of $l=2$ conventional LHD-type Reactors (LHD-R) have been carried out. One-point plasma modelling in addition to 3D- equilibrium/1D-transport analysis clarified the D-T ignition condition. An accessible design window for reactor parameters is found using physics and engineering constraints. The cost estimation suggests the importance of the compact design to reduce the cost of electricity.

Secondly, a new reactor design candidate, Modular, Heliotron Reactor (MHR) is proposed focusing on the advantage of efficient helical divertor compatible with modular helical coil system. The special coil winding system permits the appropriate coil gap for reactor module maintenance, and leads to the compatibility between the good plasma confinement and the efficient helical divertor configuration. Two MHR design options are selected based on the LHD-R system analysis.

Thirdly, based on the advantage of the simplified continuous-coil design, a high-field Force-Free Helical Reactor (FFHR), is proposed for the reduction of the electrom-magnetic force by adopting $l=3$ force-free-like continuous-coil system. The molten-salt FLiBe, LiF-BeF₂, is selected in FFHR as the self-cooling tritium breeder from the view-point of safety and the compatibility with high magnetic field design.

340: Low Activation Ferritic and Martensitic Steels Development for Fusion Reactors

A.Kohyama, A.Hishinuma (Tokai Establishment, JAERI), D.S.Gelles (Battelle Pacific Northwest National Laboratory), R.L.Klueh (Oak Ridge National Laboratory), W.Dietz (EC/DGXII/Fusion Program), K.Ehrlich (Forschungszentrum)

16th IAEA Fusion Energy Conference, 1996

The development of low-activation ferritic/martensitic steels is a key to the achievement of nuclear fusion as a safe, environmentally attractive and economically competitive energy source. The Japanese and the European Fusion Materials programs have put low-activation ferritic and martensitic steels R & D at the highest priority for a demonstration reactor (DEMO) and the beyond. An international collaborative test program on low-activation ferritic/martensitic steels for fusion is in progress as an activity of the International Energy Agency (IEA) fusion materials working group. The objective of the test program is to verify the feasibility of using ferritic/martensitic steels for fusion by an extensive test program covering the most relevant technical issues for the qualification of a material for a nuclear application. The development of a comprehensive data base on the representative industrially processed reduced- activation steels of type 8-9Cr-2WVTa is underway for providing designers a preliminary set of material data within about 3 years for the mechanical design of components, e.g. for DEMO relevant blanket modules to be tested in the International Thermonuclear Experimental Reactor (ITER). Knowledge on the current limitations of low-activation ferritic steels for application in advanced fusion systems is reviewed and future prospects are defined.

341: Current Status of Materials Research for Nuclear Fusion Reactors

A.Kohyama, H.Matsui (Tohoku University), A.Hishinuma (Tokai Establishment, Japan Atomic Energy Research Institute),

10th Pacific Basin Nuclear Conference, Vol. 1, pp. 883-890, 1996

The characteristic features of materials research for fusion reactors are briefly reviewed along the R & D scenarios of nuclear fusion reactors. Followed to a brief overview of fusion materials, R & D strategies of structural materials are provided. Materials issues and the current status of materials R & D activities, for "ITER" and other near term machines, are introduced. As one of the two major materials R & D paths, materials for DEMOs and other long term fusion reactors are briefly introduced together with the current status of R & D activities, both domestic and international.

342: Status of Silicon Carbide Composites for Fusion

L.L.Snead, R.H.Jones, A.Kohyama

Journal of Nuclear Materials, No. 233-237, PP. 26-36, 1996

Silicon carbide composites are currently being investigated as potential fusion energy materials in the United States, the European Community and Japan. This paper presents an overview of some of the

recent issues regarding the use of this low activation material including the radiation performance of present day materials and the direction towards the development of radiation hardened SiC composites.

343: Rate Theory Modeling of Defect Evolution Under Cascade Damage Conditions: The Influences of Vacancy-type Cascade Remnants on Defect Evolution

Y.Katoh, T.Muroga (National Institute for Fusion Science), A.Kohyama

Journal of Nuclear Materials, No. 233-237, PP. 1022-1028, 1996

Recent computational and experimental studies have confirmed that high energy cascades produce clustered defects of both vacancy- and interstitial-types as well as isolated point defects. However, the production probability, configuration, stability and other characteristics of the cascade clusters are not well understood in spite of the fact that clustered defect production would substantially affect the irradiation-induced microstructures and the consequent property changes in a certain range of temperatures and displacement rates. In this work, a model of point defect and cluster evolution in irradiated materials under cascade damage conditions was developed by combining conventional reaction rate theory and results from the latest molecular dynamics simulation studies. This paper provides a description of the model and a model-based fundamental investigation of the influence of configuration, production efficiency and the initial size distribution of cascade-produced vacancy clusters.

344: NIFS Information Network for Fusion Engineering Research in Japanese Universities

C.Namba (National Institute for Fusion Science), A.Kohyama, Y.Katoh

Journal of Nuclear Materials, No. 233-237, PP. 1612-1616, 1996

Networking of research organizations, personnel and information is underway in order to organize nation-wide interdisciplinary research activities in fusion engineering in Japan. The National Institute for Fusion Science, established in 1989, is steering this effort by cooperating with other universities and national institutes operated by the Ministry of Education, Science and Culture (Monbusho), as the first designated center-of-excellence institute in the field of fusion research. The role of information networking in the entire networking effort and examples of information network services for fusion engineering research activities are presented, with the emphasis on those for materials science and engineering.

345: Effect of Heat Treatment Temperature on Young's Modulus and Microstructure of C/C Composites

S.Sato (University of Tokyo), H.Serizawa (University of Tokyo), A.Kohyama, H.Tsunakawa (University of Tokyo), S.Kagaya (Haruna Engineering Co., Ltd.)

Microstructures and Functions of Materials, pp. 129-132, 1996

As one of the most important basic mechanical properties of advanced C/C composites for high temperature structural applications, temperature dependence of Young's modulus were precisely studied in a vacuum with a lateral vibration method from room temperature up to 1373 K. Materials used were two kinds of unidirectional C/C composites, where the variables were microstructure of carbon fibers in C/C composites and heat treatment temperature of C/Cs. The temperature dependences of Young's modulus showed positive and negative trends reflecting microstructure changes of carbon fibers by heat treatments. Also, the graphitization effects of carbon fibers on the temperature dependences are presented quantitatively.

346: Evaluation of Interfacial Shear Strength of C/C Composites by means of Micro-Indentation Test

K.Watanabe (University of Tokyo), S.Sato (University of Tokyo), H.Serizawa (University of Tokyo), A.Kohyama, T.Kishi (University of Tokyo)

Materials Transactions, JIM, No. 37, pp. 1161-1165, 1996

Micro indentation test technique was applied to evaluate interfacial shear strength of uni-directional C/C composites, and the effectiveness of this method was discussed. Interfacial sliding was detected in the load - displacement of indenter curve (indentation curve) , and push-in and/or push- out fibers were observed. From the load displacement information of the micro indentation test, interfacial shear strength in C/C composites was defined. At lower Heat treatment temperature (HTT) than 2000K, almost no temperature dependence can be recognized. At higher HTT, however, interfacial shear strength was increased with increasing HTT, which was supposed to be effected by the growth of graphite layer and increment residual compressive stress to fiber.

347: In-situ Observation of Compressive Fracture Processes in Flat Woven Carbon Fabric Reinforced Carbon Composite Materials

平織炭素繊維強化型炭素マトリックス複合材料の圧縮破壊過程における“その場”観察

炭素 (1996) No. 173, pp. 161-167

There have been many efforts to correlate mechanical properties of composite materials with deformation and fracture behaviors, but they are still insufficient to understand even qualitatively. In many cases, especially for the cases of ceramics composites, varieties of fracture behaviors have been observed in, so-called, the identical materials. This is due to the complex and heterogeneous microstructure of CMCs (ceramics matrix composites) with many pores, cavities, cracks and interfacial defects.

It is still impossible to control the structure and properties of CMCs sufficient to identify them as the identical materials. Therefore, Japanese working group on SiC/SiC made by Ube Industries.

The objective of this study is to obtain fundamental information about fracture behaviors of SiC/SiC composite material with carbon coated Hi-Nicalon and CVI-SiC matrix. In this study, fracture process was inspected "in-site" using three point bending test apparatus with video microscope. In order to see the effect of surface cracks introduced during specimen cut-out and preparation processes, some specimens have been applied CVD-SiC coating.

C. Review Articles

C. 総説

Chapter 3

Review Articles

I Department of Socio-Environmental Energy Science

(エネルギー社会・環境科学専攻)

1: Pursuit of Happiness

大学院エネルギー科学研究科の創設

Hideo Shingu

ふえらむ Vol.2 (1997) 113-120

2: The Problem of Energy and Environment -Pursuit of Happiness-

エネルギー・環境問題-人間の幸福から考える-

Hideo Shingu

エネルギー・資源 Vol18 (1997) 1-8

3: Application of Virtual Reality for Nuclear Engineering

人工現実感（バーチャルリアリティ）の原子力工学への適用

Hidekazu YOSHIKAWA, Tetsuo TEZUKA, Makoto TAKAHASHI, Shogo FUKUSHIMA

Journal of Atomic Energy Society of Japan, Vol.38, No.9, pp.737-745 (1996)

日本原子力学会誌、Vol. 38, No. 9, 737~745頁 (1996)

Virtual Reality (VR) technology has been progressing very rapidly, and it has been widely recognized as a new technology to broaden the capability of innovative human interfaces. In the former part of this review, the authors first start a general overview on what the VR is like, and then they explain the basic technology of VR both on its hardware and software, VR technology with network environment, and finally, physiological effects of VR to human. In the latter part of this review, the authors proceed to the extensive research reviews on the ongoing works both inland and abroad, with respect to the various application of VR technology in the field of nuclear engineering, in which the authors also introduces their own works of VR applications. The authors conclude that the plausible areas of VR application in the nuclear engineering are the VR applications to (i)the formation of cooperative system design work environment using VR and internet, (ii)remote control of robotics systems in hazardous environment, (iii)development of training systems for personnels both for plant operation and maintenance work, and (iv)scientific visualization of basic physical principles of nuclear engineering, as a useful education tool both in the courses of junior or high schools and university level.

4: Chemical Composition of Atmospheric Aerosols, and Their Sources and Generation Mechanism

大気圏エアロゾルの化学組成と発生機構、発生源

Mikio Kasahara

J. Aerosol Research, Japan, Vol.12, pp.120-126, 1996

エアロゾル研究, Vol.12, pp.120-126, 1996

The atmospheric aerosols have different characteristics according to differences of their generating and growing processes. The characteristics of atmospheric aerosol are described by a number of physical and chemical factors. The most important factors are concentration, size and chemical composition. Chemical composition gives a lot of information about the sources of atmospheric aerosols and also the transformation processes of gaseous and aerosol pollutants in the atmosphere. In this article, the following topics were reviewed and discussed; (1) Physical and chemical factors of atmospheric aerosols and chemical characteristics, (2) Generation of aerosol particles and their mechanisms, (3) Secondary particle formation from gaseous pollutants in the atmosphere, (4) Source contribution analysis using chemical composition of aerosol particles. (in Japanese)

5: Current Status and Key Issues of Nuclear Liability Regime

原子力損害賠償制度の現況と課題

Kenkichi Hirose, Keiji Kanda

J. At. Energy Soc. Japan, Vol.39, pp.28-40, 1997

日本原子力学会誌、第39巻、第1号、28頁－40頁、1997年

Nuclear liability regime has been established from the beginning of the nuclear power industry. The first nuclear accident with major transboundary consequences occurred at Chernobyl, and led to reexamination

of the nuclear liability regime. Current status and key issues of the national and international nuclear liability regime are reviewed. (in Japanese)

6: Reforming the Social Regulation of Japan

今後の社会的規制の在り方について

Hiroshi Yamagata*, Keiji Kanda, Hisaji Shimizu** *(MITI) **(Yokohama National Univ.)

安全工学、第36巻、第1号、2頁-9頁、1997年

Japanese Government made more stringent standards and strict control systems of the social regulation, that is the health, safety, and environmental regulation, every time an accident occurred. The Citizens and the industries have accepted it because it has contributed to make the safe society and develop the industries. Nevertheless, now, the strict control systems make the Japanese economy and society inefficient. The social regulation of Japan must be reformed. The selfresponsibility of the private sector should be established and the regulation by the government should be necessary and sufficient. The rational safety level should be achieved by an efficient manner, for example, an insurance system. Compensation should be made swiftly and sufficiently. Finally, international harmonization of the social regulation should be needed. (in Japanese)

7: Current Topics of BWR Nuclear Thermal Hydraulic Stability: Regional stability and activities in design and operation

BWR 核熱水力安定性に関する最近の話題：領域安定性および設計・運転面での取組み

Takafumi Anegawa*, Akitoshi Hotta**, Shigeo Ebata***, Yasunori Bessho, Katsuhiro Tsuda****

*(Tokyo Electric Power Co.), **(Toden Software, Inc.), ***(Toshiba, Ltd.), ****(Genshi Nenryo Kogyo, Ltd.)

J. Atomic Energy Soc., Jpn., Vol.38, No.5, pp.12-20, 1996

日本原子力学会誌, Vol.38, No.5, pp.12-20, 1996

Nuclear-thermal-hydraulic instability is peculiar to Boiling Water Reactors, in which boiling two-phase flow is used as a coolant, and, therefore, is used to explain its causes and mechanism. The basic analytical model for the total core instability had been established and its result had been used to evaluate core regional instability since then. Recently, much effort is made to the direct evaluation of core regional instability. We have developed the direct analytical method of core regional instability in the frequency domain and have successfully applied to commercial BWRs. In the paper, the direct analytical method of core regional instability in the frequency domain is explained and is reviewed with application results, also with current topics of total core instability and regional instability and with activities in design and operation to further improve commercial BWR stability.

II Department of Fundamental Energy Science

(エネルギー基礎科学専攻)

8: Crystal Chemistry on the Cation Sites of Oxide Spinels

陽イオンサイトから見たスピネル型酸化物

Takeshi Yao

Journal of the Materials Science Society of Japan, Vol. 33, pp.13-18, 1996

材料化学、Vol. 33, pp.13-18, 1996

The structure of oxide spinels can be described as a close-packed cubic arrangement of oxide ions with one-eighth of the tetrahedral holes (the tetrahedral sites) and one-half of the octahedral holes (the octahedral sites) filled with cations. The cation distribution between the tetrahedral site and octahedral site is mainly determined by the electrostatic energy consisting of Madelung energy and repulsion energy, crystal-field stabilization energy due to the *d*-orbital splitting and the polarization energy of the oxide ion induced by the surrounding cations. In the spinel structure, superstructure formation is possible, if the sublattices are occupied by more than one kind of cations. X-ray crystallography, especially powder X-ray Rietveld analysis is useful for cation distribution analysis. When the crystal contains plural number of cations with similar atomic scattering factor each other, EXAFS analysis is effective. Studies of LiMn_2O_4 and $\text{Li}_{4/3}\text{Ti}_{5/3}\text{O}_4$ as the material of rechargeable lithium battery were presented.

9: Overview of Heliotron E results

M. Wakatani, S.Sudo(National Institute for Fusion Science)

Plasma Physics and Controlled Fusion Vol.38, p.937

Theoretical characteristics of Heliotron E are summarized in section 2. Initial experiments in 1980-3 were mainly for studying ohmically heated plasmas. Topics relating to current-carrying plasmas are reviewed in section 3. In Helitron E the first currentless plasma was produced by ECRH using a gyrotron with a frequency of 28 GHz in 1982. Then the gyrotron frequency was increased to 53 GHz to produce higher density currentless plasmas. After NBI heating of the target plasma produced by ECRH was successful, currentless plasmas were studied intensively in Heliotron E. In section 4 the production and heating of currentless plasmas by ECRH, NBI and ion cyclotron range of frequency (ICRF) are summarized. MHD properties of currentless Heliotron E plasmas are summarized in section 5. Confinement and transport are discussed for ECRH, NBI and ICRF plasmas in section 6. Characteristics of edge plasma and plasma-wall interaction in Heliotron E are summarized in section 7. Configuration improvement and future direction based on Heliotron E results are discussed in section 8.

10: Infrared spectroscopy of hydrogen in porous silicon

多孔質シリコン中の水素の赤外分光

Yukio Ogata

Hyomen-Kagaku, vol.17, pp.27-33, 1996

表面科学、17 巻、27-33 頁、1996

When a silicon wafer is anodized in hydrofluoric solution under some conditions, a porous layer is formed on the surface. There are some studies utilizing the porous structure for applications to the formation of insulating layers, heterojunctions, electronic devices, and so on. Since the photoluminescence from this material at ambient temperature was reported in 1990, the porous silicon has attracted much attention to many researchers. Most of the studies are concentrated to the elucidation of the luminescent mechanism and the development of luminescent devices. This interesting material is characterized by the porous structure of nanometer size and the presence of hydrogen. In the present review, the history of the researches is reviewed; then some results of hydrogen environment in the porous silicon layer revealed by vibrational analyses using infrared spectrometry and quantum chemistry. (in Japanese)

11: Present Status and Future Prospect of Research Reactors

研究用原子炉の現状と将来

Yutaka Maeda (Res.Reactor Inst., Kyoto Univ.), Seiji Shiroya, et al.

J. At. Energy Soc. of Japan, 38[11], 870-891 (1996)

日本原子力学会誌、38[11], 870-891 (1996)

Research reactors have been utilized for the research and development of nuclear science in Japan, ever since the first research reactor in Japan, JRR-1, attained its criticality in 1957. These reactors have been contributing to the promotion of various scientific studies through the application of neutrons. In the present issue, the present status and future prospect of research reactors are described from a synthetic view point of the generation and application of 'controlled neutrons'.

12: Development of High Frame-Rate Neutron Radiography and Its Application to Fluid Measurement

中性子ラジオグラフィ高速度撮像法の開発と流体計測への応用

Takashi Hibiki, Kaichiro Mishima

Radiation, 22[1], 35-42, 1996

放射線、22 巻 1 号、35-42 頁、1996 年

Development of a high-frame-rate neutron radiography (HFRNR) technique has been indispensable to apply the neutron radiography technique to visualize and measure high-speed transient phenomena.

Since the advent of high-flux research reactors, not only the HFRNR with a pulsed neutron beam but also the HFRNR with a steady neutron beam has been developed recently. In this review paper, a guideline to construct an imaging system and a temporal-resolution limit of the HFRNR are presented. The recent progress and the prospects for the HFRNR are also summarized.

13: Electrochemistry and Photoelectrochemistry of Diamond

A. Fujishima, K. Hashimoto, L. Boonma and T. Yano

First Spanish/Japanese Conference on Fundamentals and Applications of Molecular

14: TiO₂ Photocatalysis : Reaction Mechanisms and Real Applications

A. Fujishima

Eleventh International Conference on Photochemical Conversion and Storage of Solar Energy

15: Photoelectrochemistry of TiO₂ Particle Suspensions

Hisao Yanagi, Yoshihiro Ohoka, Takashi Hishiki, Katsuhiko Ajito, and Akira Fujishima

Eleventh International Conference on Photochemical Conversion and Storage of Solar Energy

16: Recent Progresses in TiO₂ Photocatalysis

Akira. Fujishima

TiO₂ Photocatalytic Purification and Treatment of Water and Air

17: Photo-Induced Super-Hydrophile Property of TiO₂ Coated Materials : Novel Phenomenon in Photocatalysis

K. Hashimoto, A. Fujishima, and T. Watanabe

TiO₂ Photocatalytic Purification and Treatment of Water and Air

18: TiO₂ Photocatalysis in Action

光触媒が活躍する

Y. Kikuchi, A. Fujishima

Finechemical, 25 (8), p.6-11 (1996).

化学工業, 12月号, 9-14 (1995).

19: Photocatalytic Ceramic Tile

光触媒が活躍開始 ——タイルの場合——

K. Hashimoto, A. Fujishima

Kagaku to Kougyou, 49 (6), p.764-767(1996)

化学と工業, 49 (6), 764-767 (1996).

20: Techniques for Ultra Thin Film Using Ultrafine Particles

超微粒子の薄膜化技術

T. Miwa, A. Fujishima

Finechemical, 25(12), p.5-12(1996).

ファインケミカル, 25 (12), 5-12 (1996).

21: Self-Cleaning Material Using Light - A New Application of TiO₂ -

光が当たるときれいになる材料 ——酸化チタン光触媒の新しい応用——

K. Hashimoto, A. Fujishima

Gendai Kagaku, 1996(8), p.23-28

現代化学, 8月号, 23-28 (1996).

22: New Trends in TiO₂ Photocatalysis

酸化チタン光触媒の新しい流れ

A. Fujishima

Kankyō Kanri, 32 (8), p.909-914, (1996).

環境管理, 32 (8), 909-914 (1996).

23: Frontiers in Photocatalytic Materials

光触媒材料の最前線

A. Fujishima

Kagaku Kougaku, 60 (9), p.648-650(1996).

化学工学, 60 (9), 648-650 (1996).

24: Role of Oxygen for Photocatalysis

光触媒反応における酸素の関わり

K. Ikeda, K. Hashimoto, A. Fujishima

Kou Kagaku, 22, p.54-58(1996)

光化学, 22, 54-58 (1996).

25: Semiconductor Photoelectrode and Photocatalysis

半導体光電極, 光触媒反応

K. Hashimoto, A. Fujishima

Ceramics, 31(10), p.815-820 (1996).

セラミックス, 31 (10), 815-820 (1996).

26: Photocatalysis for Self-Cleaning and Sterilizing Effects

防汚・殺菌効果の光触媒

A. Fujishima

Sentannkagakujitenn Sec.9-3, p.392-395 (1996)

先端材料事典, V. 光機能性無機材料, 第9章3

27: TiO₂ Photocatalysis Remarkable for Antibacterial and Self-Cleaning Effects

抗菌性、セルフクリーニング効果の著しい酸化チタン光触媒

A. Fujishima

Almiproducts, 79(2), p.14 - 17 (1997)

アルミプロダクツ, 79 (2), 14-17 (1997).

28: Water Treatment Using TiO₂ Photocatalyst

酸化チタン光触媒による水処理

A. Fujishima

Shigen kannkyo taisaku, 33(3), p.241 - 245 (1997)

資源環境対策, 33 (3), 241-245 (1997).

29: Electrorheology and Photoelectrochemistry

電気粘性効果と光電気化学

Y. Komoda, A. Fujishima

Koukagaku, 24, p.32-39 (1997)

光化学・24・32-39 (1997).

We have recently become interested in photo-effects in conjunction with electrorheology. This new field, which we have termed "photoelectro-rheology", is based on changes in the properties of electrorheological (ER) fluids under illumination. Such fluids typically consist of suspensions of semiconducting particles in insulating fluids. Photoelectrorheological effects involve photoelectrochemical and photoelectrophoretic phenomena. We review the previous literature in this area as well as our recent work using TiO₂ fine particles. Examples of possible applications of photoelectrorheological effects include the photo-control

of ER fluids, display devices, and as a possible method for characterizing semiconductor particles. (in Japanese)

III Department of Energy Conversion Science

(エネルギー変換科学専攻)

30: Problems of Diesel Engine Combustion

ディーゼルエンジン燃焼の課題

Makoto Ikegami

Combustion Science and Technology (Japan), Vol.3, pp.151-157, 1996

燃焼の科学と技術, Vol.3, pp.151-157, 1996

This paper reviews recent advancement of combustion technologies for diesel engines and the related matters, paying special attention to the abatement of air-pollutant emissions such as particulate matter and nitrogen oxides. First discussed are the significance and roles of high-pressure injection, enhancement of turbulence in the later burning stages, gaseous flows, geometries of combustion chamber, indirect injection and so forth. Also, various methods of after-treatment for reducing the emissions are reviewed; they include oxidation and deNO_x catalysts, particulate filter and exhaust gas recirculation. In addition, the fuel properties required for a cleaner exhaust are discussed briefly. (in Japanese)

31: Current Status of Automotive Technology and Environmental Protection

自動車技術及び環境保全技術の現状

Makoto Ikegami

NGV, No.29, pp.4-7, 1996

NGV, No.29, pp.4-7, 1996

This article first discusses how far the characteristics of a vehicle and the power train may affect fuel economy and tailpipe pollutant emission. Emphasis is placed on the necessity of reducing the powertrain loss and the vehicular weight so as to attain a better fuel economy. Also, discussed is the abatement of air-pollutant emission for conventional power plants, such as spark-ignition engine and diesel engine. A higher potential of vehicles fueled by alternative fuels is also mentioned from the viewpoint of emission control. (in Japanese)

32: Role of Turbulence in Diesel Combustion

ディーゼル燃焼における乱流の役割

Makoto Ikegami

JSAE of Japan, Vol.50, No.9, pp.3-5, 1996

自動車技術, Vol.50, No.9, pp.3-5, 1996

Based on the studies performed by the present author, the importance of in-cylinder turbulence and the turbulence mixing are discussed as one of essential driving forces of the diesel combustion process. A stochastic model on this line was advocated by the author, and it may successfully describe what goes on in the non-premixed burning stage during combustion. Explanations are also made for the background of the stochastic model, together with the related matters, such as sources of turbulence, spray, and flame spreading. (in Japanese)

33: Scientific Exchange Programme on Integrated Engineering

Makoto Ikegami

Advanced Technologies for Clean Environment Proc. of the 6th JSPS-VCC Seminar on Integrated Engineering, pp.1-6, 1996

The JSPS-VCC and JSPS-NUS Scientific Exchange Programmes on Integrated Engineering are reviewed. After short explanations of their history and backgrounds, recent cooperative research projects and the outcome are outlined. It is emphasized that these two programmes have played important roles not only in exchanging scientific knowledge and views required to advance engineering and technologies, but also deepening mutual understanding between respective countries. Finally, the future scope of the exchange programmes is discussed.

34: Simulation of Engine Combustion

エンジン燃焼のシミュレーション

Makoto Ikegami

Motoring, No.4, pp.5-6, March, 1997

モーターリンク, No.4, pp.5-6, 1997年3月

Recent progress of computational fluid dynamic calculation methods enables us to simulate what takes place during combustion in the cylinder in internal combustion engines. In the computer simulation, it is especially important to establish submodels that may correctly describe turbulence, mixture formation, chemical reactions, combustion and heat transfer to and/or from cylinder walls, in order to achieve fast and efficient but accurate results of the computer simulation. In addition, the future direction of simulation of the in-cylinder combustion is suggested. (in Japanese)

35: Sheet Metal Forming Simulation System Using Finite Element Method

板成形 FEM シミュレーションシステム

Shoji Imatani, Susumu Takahashi*

(* Nissan Motors Co.)

Journal of the Japan Society for Technology of Plasticity, Vol.37, No.421, pp.160-165,
1996

塑性と加工, 37 卷, 421 号, 160-165 頁, 1996

Recent development in finite element simulation system in terms of sheet metal forming process is discussed. One of the main topics in the first part is the practical utilization of FEM systems in the design and production process of automobile parts. The strategy of computer-integrated design is shown and the role of FEM simulation is discussed from the viewpoint of cost performance in manufacturing process. The modelling technology of sheet metal and die tool into finite element mesh is also discussed. The second part describes some theoretical issues in FEM. Since sheet metals are characterized by "thin" three dimensional bodies, special consideration must be taken into account. Some of the techniques to overcome these difficulties are shown in the paper, and further developments in modelling the materials as well as the frictions are also reviewed. (in Japanese)

36: Speed Change of Waves Due to Stress and Damage in High-Polymer Composite

高分子複合材料中の応力と損傷による音速変化

Eiji Matsumoto

Ultrasonic Technology, Vol.9, No.1, pp.28-32, 1997

超音波 TECHNO, 9 卷, 1 号, pp.28-32, 1997

This paper considers the relation between the damage and the speed change of ultrasonic waves in a short fiber reinforced high-polymer composite. The speed of a wave depends nonlinearly on the applied stress due to the strong nonlinear elasticity of the high-polymer matrix. When a cyclic load is applied to the composite, the speed of the wave depends also on the number of the cycles due to the accumulation of damage. A damage parameter is introduced to describe the irreversible speed change, and a viscoacoustoelasticity law with damage is derived. The law enables us to evaluate the extent of the damage during cyclic loading by measuring the speed change of ultrasonic waves. (in Japanese)

37: Strength Characteristics of Structural Ceramics

Toshihiko Hoshide

Mater. Sci. Res. Inter., Vol.2, No.4, pp.220-228, 1996

In structural ceramics, a remarkable scatter of strength is observed due to brittle behavior in deformation and flaws unavoidably formed during material processing. Therefore, information on strength characteristics of ceramics is required for the mechanical design in their applications to high-performance

components. In the present paper, the strength properties of typical ceramics are reviewed from statistical aspects, especially. As for the static strength, general features of ceramic strength are first outlined, and then several factors affecting strength, such as environments, specimen geometry, stress state and machining, are described. The fatigue strength is reviewed in two categories of the static and cyclic fatigue. As one of screening procedures to exclude components with a lower strength, the proof testing in ceramics is described and problems in the testing are also mentioned.

IV Department of Energy Science and Technology

(エネルギー応用科学専攻)

38: Electron Energy Loss Spectroscopy

電子エネルギー損失分光法

Isao Tanaka

Bunseki (1997) 190

ぶんせき (1997) 190

With recent improvement of high spatial resolution analytical electron microscopy, electron energy-loss spectroscopy (EELS) is challenging to obtain spectra with single atomic column resolution. Since the near edge-structure of EELS (ELNES) conveys information on chemical bonding from the illuminated area, one can expect to identify the local chemical environment of atomic-sized imperfections, such as interfaces, directly by experiments. Since major features of the ELNES can be ascribed to electronic dipole transitions from core orbitals to unoccupied band, accurate electronic calculations of the unoccupied band are necessary in order to interpret the experimental spectra. We found that our first principle molecular orbital calculations by discrete variational (DV) $X\alpha$ method using model clusters provide quantitatively reliable reproduction of experimental spectra in the range of ~ 30 eV from the conduction band-edge for various compounds. A brief introduction to the computational method, followed by a detailed explanation of the origin of spectral features of ELNES obtained for some oxides is given. (in Japanese)

39: Electronic structures of metal-oxides by DV- $X\alpha$ cluster calculations

DV- $X\alpha$ 法による酸化物のクラスター計算

Isao TANAKA, Katsuyuki MATSUNAGA, Masataka MIZUNO, Fumiyasu OBA, Hirohiko ADACHI

New Ceramics (1997) 10 17-24

ニューセラミックス (1997) 10 17-24.

Current activities on first principles calculations of metal oxides by means of DV- $X\alpha$ molecular orbital calculations in the authors' lab. are reviewed. (in Japanese)

40: Ferrors scrap - an overview with a particular emphasis on the removal of copper

鉄スクラップの現状と脱銅法

Masanori Iwase

Metals and Technology 1996, no.8, pp.43/54.

金属 1996 NO.8 , pp.43/54

An overview is given on the current status of ferrous scrap with a particular emphasis on the potential technology for the removal of copper from solid ferrous scrap.

41: Development of Deep Sea Minerals from the Viepoint of Social Engineering of Resources

資源社会論から見た深海底鉱物資源

Takashi Nishiyama

Energy and Resources, Vol.17, No.1, pp.73-79, 1996

エネルギー資源、Vol.17, No.1, pp.73-79, 1996

42: Hydrodynamic Examinations and Problems on Lifting Characteristics of Manganese Nodules by Air-Lift Pump System

マンガン団塊揚鉱システムの流体力学的検討と問題点

Natsuo Hatta

Energy and Resources, Vol.17, No.1, pp.50-56, 1996

エネルギー・資源, Vol.17, No.1, pp.50-56, 1996

This review paper treats hydrodynamic examinations and problems on lifting characteristics of manganese nodules by air-lift pump system. Manganese nodules were known to exist at the bottom of many of the world's oceans as early as the 1870s. Interest was rekindled in the 1960s when it appeared that the world would need new sources of nickel to supply the increasing demand for jet engines, magnets and high quality stainless steel for corrosion resistance. Air-lift pumps are regarded as one of the most convenient means of lifting these manganese nodules from the deep sea bed of about 5000 m to the sea surface. However, it is very difficult to clearly understand the operation performance of air lift pump, since the experimental results so far obtained in this area are not always systematic and consistent. On the other hand, the theoretical approaches have been made by many researchers and are based upon a momentum balance, an empirical correlation, a power balance and a multi fluid model. The present situations of these investigations, involving the present author's one, are summarized from an experimental as well as theoretical point of view. (in Japanese)

- 43: **Summary and Conclusions of the Discussion Session (ch. A.Kohyama) on "Joining SiC/SiC Composites"**

A.Kohyama

IEA International Workshop on SiC/SiC Ceramic Composites for Fusion Structural Applications, pp. 119, 1996

- 44: **Dedign Studies of Helical Reactor FFHR (1) - Overview of FFHR Dedign**
ヘリカル炉 **FFHR** 設計研究 (1)、設計の概要

- 45: **Dedign Studies of Helical Reactor FFHR (6) - Overview of FFHR Dedign**
ヘリカル炉 **FFHR** 設計研究 (6)、材料システム

日本原子力学会年会、1996

D. Books

D. 著書

Chapter 4

Books

1: Challenges to Japan

日本の難問—閉塞の日本と勃興のアジアー

Takamitsu Sawa .

佐和隆光

Nihon Keizai Shimbun, Inc. . : 日本経済新聞社

1997 / 03 / 13 published

2: Wood-Plastic Combination, in "The Handbook of New Woody Materials"

木材・プラスチック複合化、"木質新素材ハンドブック"

Shiro Saka .

坂 志朗

Gihodo Shuppan Co., Ltd. . : 技報堂出版株式会社

1996 / 05 / 30 published

A review was made of the chemical processing of wood with plastics in manufacturing so-called WPC (wood plastic composites). The followings are the subjects described; woody raw materials, plastics and manufacturing process for the WPC, methods of chemicals to be penetrated and their polymerizing process, the evaluation in chemical penetration and polymerization, and characteristics of the WPC and its topochemistry for enhancing the wood properties.

3: Wood-Inorganic Composites, in "The Handbook of New Woody Materials"

木材・無機質複合化、木質新素材ハンドブック

Shiro Saka .

坂 志朗

Gihodo Shuppan Co., Ltd. . : 技報堂出版株式会社

1996 / 05 / 30 published

Several approaches for wood property enhancement by wood-inorganic modification were briefly reviewed, and topics on wood-inorganic composites as prepared with several metal alkoxides by the sol-gel process were summarized on a relation between the composite properties and a distribution of inorganic substances. Particularly, the topochemistry of wood was emphasized on its property enhancement by inorganic modification in dimensional stability, termite resistance and fire-resistance.

4: Butterflies and Environments

チョウと環境

Shiro Saka .

坂 志朗

Kinki Chemical Society . : (社)近畿化学協会

1997 / 03 / 01 published

The earth environments are discussed in a viewpoint of butterfly ecology; a relation between the global warming due to carbon dioxide emission from fossil resources and subtropical butterflies expanding toward the north was introduced as one of the evidence for the worldwide warming. Also emphasized was a variation of the wing marks caused perhaps by their life adjustment as their distribution was expanded to the northern regions in our country. Also introduced were the tree species as foodplants of butterflies which the author has collected from the fields and planted in his garden. Finally, it was emphasized that the human beings should consider themselves only *Homo sapiens* in ecosystems, and that when they reconstruct their environments in their society, a selection of trees planted in the city should be made so as to reward not only the human beings but also ecosystems.

5: Wood Is Environmentally Friendly

木は環境にやさしい

Shiro Saka .

坂 志朗

1996 / 07 / 22 published

Wood as biomass renewable resources has been playing important roles in developing a human culture. This is because wood is natural composite materials and appropriate for adjusting our life environments. In this paper, therefore, characteristic features of wood as environmentally friendly materials were discussed from chemical, physical and biological viewpoints. Additionally, in comparison with fossil resources of petroleum or coal, a significance of this clean and renewable biomass resources was discussed against global warming of our environments. Also described was a potential of wood for developing "superwood" as environmentally friendly materials.

6: Proceedings of Cognitive Systems Engineering in Process Control: CSEPC 96

Hidekazu YOSHIKAWA, Erik HOLLNAGEL* *(OECD Halden Reactor Project) .

Technical Committee on Man-Machine Systems, Atomic Energy Society of Japan, and Graduate School of Energy Science, Kyoto University . :

1996 / 11 / 12 published

A new research area of Cognitive Systems Engineering (CSE) has emerged since 1982, in order to meet the growing need for methods and models that could be used to improve the analysis and understanding of man-machine systems in complex, dynamic environment. The research field of CSE highlights the problems of human cognitives and the related systemization, from the viewpoint of human factors in process controls ranging from power engineering, to aviation and to tele-communication, etc. The first International Conference on Cognitive Systems Engineering in Process Control 1996 (CSEPC96) was took place in Kyoto, in November 12 -15, 1996, to reflect the rapid emergence and the developments of the CSE-related activities in East Asian countries, especially in Japan and South Korea. There were more than 80 scientists and engineers around the world attended at the CSEPC96 conference, presented their papers and discussed with each other on the recent progress on their works. In this Proceedings of CSEPC96, as many as forty technical papers were compiled in accordance to the following four research topics of (i)joint systems which deal with performance prediction and evaluation, system simulation model, human-machine cooperation, and models of cognition, (ii)use of tools which deals with support systems, interface of designing, and new technology, (iii)coping with complexity which deals with the problems of individual and crew performance and automation and human-centered design, and (iv)data, models and experience with respects to field studies and simulator studies.

7: Energy-Resources Handbook: 7-1 A Survey of Energy System Models - Their Roles in Energy-Systems Study-

エネルギー・資源ハンドブック（分担執筆） 7編1章 エネルギーシステムモデルの役割と開発事例

Tetsuo Tezuka .

手塚哲央

Ohmsha . : オーム社

1996 / 11 / 30 published

Energy System model is defined as the model that can evaluate the relation between energy system and energy-related technology. This kind of model can be classified into two categories, i.e., simulation type and optimization type. These two types of models have completely different features which, however, compensate each other. Which type of model should be used depends on what result we want to obtain by using the model. Energy system model research started with oil shock that has changed the way of thinking about energy all over the world. And then, the target of the model development changed according to the change of the concerns of each times. This article summarizes the history of the development of energy-system model, and some typical models are also outlined with the key points of the model utilization.

8: Cancer Neutron Capture Therapy

癌の中性子捕捉療法

Yutaka Mishima*, *(Mishima Institute for Dermatological Research) .

三嶋 豊*、*（三嶋皮膚科学研究所）

Plenum Press, New York, USA . :

1996 / / published

Kanda's Papers: 1. Effect of intratumoral injection of ^{10}B -immunoliposome on BNCT for growth inhibition of human pancreatic cancer grafts in nude mice. 2. Procedures for the medical application of research reactors. 3. Physics of boron neutron capture therapy in Japan. 4. Remodeling of the heavy-water facility of the Kyoto University Reactor for epithermal and thermal neutrons. 5. The utilization of hyper-thermal neutrons for neutron capture therapy. 6. Calculated electron spectra for gadolinium neutron capture therapy. 7. BNCT of malignant melanoma-Radiobiological analysis and data comparison with conventional radiotherapy. 8. Assessment of photon contributions in gadolinium neutron capture reactions - A preliminary study.

9: Electrochemical Technology (-Inovation and New Developments-)

N. Masuko, T. Osaka , Y. Ito eds. .

Kodansha & Gordon and Breach Publishers . :

1996 / / published

In recent decades the electronic industry has undergone a rapid evolution towards microscale

**10: Intoroduction to Fluorine Chemistry(-Fundamentals and Experiments-) Inorganic,
Chapter 3 1.3.2 S₂O₆F₂**

フッ素化学入門 (－基礎と実験法－) 無機化学編、第3章 1.3.2 S₂O₆F₂

Rika Hagiwara .
萩原理加

Nikkan Kogyo Shimbun Co., Ltd. . : 日刊工業新聞社

1997 / 03 / 01 published

Preparation, physical and chemical properties of peroxydisulfuryl difluoride, S₂O₆F₂ are described. A convenient preparative method in the laboratory starting from xenon difluoride and fluorosulfonic acid are described in detail. (in Japanese)

**11: Intoroduction to Fluorine Chemistry(-Fundamentals and Experiments-) Inorganic,
Chapter 3 2.1 Fluorides and fluorocomplexes of silver**

フッ素化学入門 (－基礎と実験法－) 無機化学編 第3章 2.1 銀のフッ化物、フルオロ錯体

Rika Hagiwara .
萩原理加

Nikkan Kogyo Shimbun Co., Ltd. . : 日刊工業新聞社

1997 / 03 / 01 published

Preparative methods, physical and chemical properties of all the binary fluorides of silver are described in detail. Preparative, structural and chemical aspects of the complexes of silver(II) fluorocations and silver (II, III) fluoroanions are comprehensively reviewed. (in Japanese)

12: Microstructures and Functions of Matter

物質における微細構造と機能

Makoto Harada (Ed.) .

原田 誠 (編者)

The Society of Chemical Engineers Japan . : 化学工学会

1996 / 02 / 22 published

In this series, rapid communication of recent research works in chemical engineering field were compiled for the formation of self-organised microstructure and its function, by focussing on amphiphilic molecular systems, polymer and membrane systems, particulate system, inorganic reaction media, and clusters near critical point. The methodology concerned with microstructure formation by cooperative motion of molecules were also reviewed.

13: Microstructures and Functions of Matter

物質における微細構造と機能

Makoto Harada (Ed.) .

原田 誠 (編者)

The Society of Chemical Engineers Japan . : 化学工学会

1996 / 02 / 22 published

In this series, rapid communication of recent research works in chemical engineering field were compiled for the formation of self-organised microstructure and its function, by focussing on amphiphilic molecular systems, polymer and membrane systems, particulate system, inorganic reaction media, and clusters near critical point. The methodology concerned with microstructure formation by cooperative motion of molecules were also reviewed.

14: Photocatalysts for anti-pollution and sterilization

防汚・殺菌効果の光触媒 先端材料事典, 第9章3節

藤嶋 昭

.: 光機能性無機材料

1996 / / published

15: Corrosion of iron

鉄の腐食

藤嶋 昭

.: 丸善出版

1996 / / published

16: Photo Clean Revolution

光クリーン革命 酸化チタン光触媒が活躍する

藤嶋 昭、橋本和仁、渡部俊也

.: シーエムシー出版

1997 / / published

17: Corrosion of Iron

鉄の腐食実験で学ぶ化学の世界 2 物質の変化

藤嶋 昭

.: 丸善出版

1996 / / published

18: Photo Clean Revolution

光クリーン革命 酸化チタン光触媒が活躍する

藤嶋 昭、橋本和仁、渡部俊也

.: シーエムシー出版

1997 / / published

This is a guide of photocatalytic TiO₂. (In Japanese)

19: Combustion in Internal Combustion Engines

内燃機関の燃焼

Makoto Ikegami .

池上 詢 (共著)

.: (社)日本伝熱学会編 (黒崎晏夫監修), エネルギー新技術体系, エヌ・ティー・エス, p105-115.

1996 / 08 / published

Fundamentals and recent progress in the combustion science and technologies of reciprocating internal combustion engines are given with special regard to fuel economy and environmental protection. For the spark-ignition engine, the in-cylinder turbulence and its effect on the flame propagation are described in depth. Also, explanations are made for the formation and destruction of air pollutants, such as unburned hydrocarbons and nitrogen oxides. For the diesel combustion, roles of spray, mixture formation, ignition delay, the subsequent rapid burning and non- premixed burning are mentioned, together with formation of pollutants such as nitrogen oxides and particulate matter. (in Japanese)

20: Metals Resources, Smelting and Recycling

金属の資源・製錬・リサイクル

西山 孝 (共著:長井 寿 編著)

.: 化学工業日報社

1996 / 07 / 24 published

21: "Infrared Semiconductor Laser by Means of J x H Force Excitation of Holeds" Elec (Amazing Light, A Volume Dedicated to Charles Hard Townes on His 80th Birthday, ed. R. Y. Chiao, Springer, New York, 1996) pp.497-505.

T. Morimoto. M. Chiba and G. Kido .

Springer, New York . :

1996 / / published

List of Academic Staff

教官名簿

Chapter 5

List of Academic Staff

March 31, 1997

Department of Socio-Environmental Energy Science

PROFESSORS:

SHINGU, Hideo	SAWA, Takamitsu	SAKA, Shiro
YOSHIKAWA Hidekazu	KAWAHARA, Mikio	KANDA, Keiji
NISHIHARA Hideaki	KAYA, yoichi (Visiting P)	

ASSOCIATE PROFESSORS:

ISHIHARA, Keiichi	OOTUKI, Toru	NAGATA, Yutaka
KAWAMOTO, Haruo	TEZUKA, Tetsuo	TOHNO, Susumu
NAKAGOME, Yoshihiro	BESSHO, Yasunori (Visiting AP)	

INSTRUCTORS:

SHIMODA, Hiroshi	YAMAMOTO, Kouhei	ONO, Koichi
FUJINE, Shigenori	TAKEUCHI, Takayuki	HAYASHI, Masatoshi

Department of Fundamental Energy Science

PROFESSORS:

ITOH, Yasuhiko	Yoshida, Katsukuni	YAO, Takeshi
FUJISHIMA, Akira (Visiting P)	WAKATANI, Masahiro	KONDO, Katsumi
MAEKAWA, Takashi	OBIKI, Tokuhiro	SANO, Fumimichi
OGATA, Yukio	HARADA, Makoto	OHKUBO, Taketoshi
KATAGIRI, Akira	SHIROYA, Seiji	MISHIMA, Kaichiro

ASSOCIATE PROFESSORS:

HAGIWARA, Rika	ITOH, Sumiko	TOMII, Yochi
UCHIMOTO, Yoshiharu	YOSHIDA, Zensho	ZUSHI, Hideki
NAKAMURA, Yuji	TANAKA, Hitoshi	MIZUUCHI, Tohru
HANATANI, Kiyoshi	KINOSHITA, Masahiro	

LECTURERS:

ADACHI, Motonari

INSTRUCTORS:

TADA, Masayuki

NAGASAKI, Kazunobu

SHIOI, Akihisa

KOBAYASHI, Keiji

NAKASUGA, Masahiko

OKADA, Hiroyuki

HARADA, Toshio

UNESAKI, Hironobu

BESSHOU, Sakae

SAKKA Tetsuo

MIZUTANI, Yasuo

HIBIKI, Takashi

Department of Energy Conversion Science**PROFESSORS:**

IKEGAMI, Makoto

MATSUMOTO, Eiji

ECHIGO, Ryozo (Visiting
P)

SHIOJI, Masahiro

INOUE, Nobuyuki

IKEUCHI, Kenji (Visiting
P)

INOUE, Tatsuo

YOSHIKAWA, Kiyoshi

ASSOCIATE PROFESSORS:

ISHIYAMA, Takuji

OHNISHI, Masami

IMATANI, Shoji

NAITO, Shizuo

HOSHIDE, Toshihiko

LECTURERS:

TAMAGAWA, Masaaki

INSTRUCTORS:

KAWANABE, Hiroshi

YAMAMOTO, Masahiro

JINBO, Kouichi

YAMAMOTO, Yasushi

Department of Energy Science and Technology**PROFESSORS:**

NOZAWA, Hiroshi

IWASE, Masanori

NAKAHIRO, Yoshitaka

SHIOTSU, Masahiro

NISHIYAMA, Takashi

KOHYAMA, Akira

ONO, Katsutoshi

HATTA, Natsuo

Jaroslav Sestak (Visiting
P)**ASSOCIATE PROFESSORS:**

TANAKA, Isao

FUJIWARA, Hiroyasu

FUKUNAKA, Yasuhiro

SHIRAI, Yasuyuki

KUSUDA, Hiromu

CHIBA, Meiro

SUZUKI, Ryosuke

TAKUDA, Hirohiko

KATOH, Yutai

INSTRUCTORS:

UEDA, Yukitomi

YAMAMOTO, Masao

FUJIMOTO, Hitoshi

TAKEUCHI, Yuuto

KUSAKA, Eishi

HATA, Koichi

エネルギー科学研究科教官名簿

1997/03/31 現在

エネルギー社会環境専攻

教授:

新宮秀夫	佐和隆光	坂 志朗	吉川榮和
笠原三起夫	神田啓治	西原英晃	茅 陽一(客員)

助教授:

石原慶一	大槻 徹	永田 豊	河本晴雄
手塚哲央	東野 達	中込良廣	別所泰典(客員)

助手:

下田 宏	山本浩平	小野光一	藤根成勲
武内孝之	林 正俊		

エネルギー基礎科学専攻

教授:

伊藤靖彦	吉田起國	八尾 健	藤島昭(客員)
若谷誠宏	近藤克己	前川 孝	大引得弘
佐野史道	尾形幸生	原田 誠	大久保捷敏
片桐 晃	代谷誠治	三島嘉一郎	

助教授:

萩原理加	伊藤澄子	富井洋一	内本喜晴
吉田善章(客員)	関子秀樹	中村祐司	田中 仁
水内 亨	花谷 清	木下正弘	

講師:

足立基斎

助手:

多田正行	中須賀正彦	別生 榮	長崎百伸
岡田浩之	作花哲夫	塩井章久	原田敏夫
水谷保男	小林圭二	宇根崎博信	日引 俊

エネルギー変換科学専攻

教授:

池上 詢	塩路昌宏	井上達雄	松本英治
井上信幸	吉川 潔	越後亮三(客員)	池内建二(客員)

助教授:

石山拓二	今谷勝次	星出敏彦	大西正視
内藤静雄			

講師:

玉川雅章

助手:

川那辺洋	神保光一	山本 靖	山本雅博
------	------	------	------

エネルギー応用科学専攻

教授:

野澤 博	塩津正博	小野勝敏	岩瀬正則
西山 孝	八田夏夫	中廣吉孝	香山 晃
Jaroslav Sestak(客員)			

助教授:

田中 功	白井康之	鈴木亮輔	藤原弘康
楠田 啓	宅田裕彦	福中康博	千葉明朗
加藤雄大			

助手:

植田幸富	藤本 仁	日下英史	山本正雄
竹内右人	畑 幸一		

平成 9 年 11 月 30 日 印刷

平成 9 年 12 月 1 日 発行

編集兼
発行者 京都市左京区吉田本町

京都大学エネルギー科学研究科

代表者 新宮秀夫

印刷所 (有) 津田印刷
京都市左京区岩倉中大鷲町 14